An Engineering Geological Investigation Into Pit Slope Stability At Macraes Gold Mine, Macraes Flat, Otago, New Zealand.

A thesis submitted in partial fulfilment
of the requirements for the degree of
Master of Science in Engineering Geology
at the University of Canterbury
by **Aaron P. Chapple**

University of Canterbury,
Christchurch,
New Zealand,
1998.

FRONTISPIECE: View overlooking Round Hill Pit, the largest of the 3 current pits operating at Macraes Gold Mine

ABSTRACT

Macraes Gold Mine at Macraes Flat is located approximately 60km north-west of Dunedin, and is currently the largest producer of gold in New Zealand. Open-pit mining currently takes place in the three large pits of Round Hill, Southern and Innes Mills along the Hyde-Macraes Shear Zone (HMSZ) which is the source of gold mineralisation. This study is an engineering geological investigation into pit slope stability at Macraes. Pit slope stability is an integral part of open-pit mining since slopes should be as steep as possible to minimise waste material which needs to be removed, yet shallow enough to minimise potential hazards to personnel and equipment below pit slopes.

Joints at Macraes are characterised by high friction angles (45-55°)as a result of roughness/waviness along the joint surface at low normal stresses. Geotechnical testing of fault gouge, and back analysis of fault controlled failures, shows much lower shear strengths for faults (c=0 kPa, ϕ=6-14°) than those previously assumed for the mine (c.f. c=10-14 kPa, ϕ=15-17°), with the small discrepancies (≈8°) between laboratory test results (5°) and back analysis results (13°) being attributed to both the removal of coarser material from laboratory samples and surface roughness/waviness, which would otherwise increase the friction. X-ray diffraction analysis shows a dominance of interlayered swelling chlorite/smectite in clay fraction of fault gouge which will heave when water is present increasing the instability of pit slopes.

Intact rock strength testing on schist from the mine shows much lower strengths (4.8 - 61.2 MPa) for the material than previously determined at other project locations in Otago (c.f. 29 - 86MPa). Pelitic schist at the mine appears to be stronger than psammitic schist which was unexpected and contrasts with previous testing in Otago. The higher strengths of pelitic schist may reflect annealing processes associated with mineralisation of the HMSZ, but has not been fully investigated.

Two structural domains can be recognised at the mine which are controlled by the Hanging Wall Shear (HWS) of the HMSZ. The rock mass above the HWS is dominantly psammitic and is referred to as the Hanging Wall Zone Domain (HWZD), while the rock mass below the HWS is dominantly pelitic and referred to as the Ore Zone Domain (OZD). Three joint sets and five fault sets are recognised in the HWZD, while in the OZD the same three joint sets as for the HWZD are recognised, but only four of the fault sets are present.

A standard recording sheet for pit slope failures is developed to assist engineering geological investigations by recording the relevant information in a consistent format. Such a sheet forms the basis for a pit slope failure database, ensures consistency in recording and provides records of failure for assessments of failure development with time.

Failures at Macraes are classified according to the geometry of the failure surface and the types of discontinuities controlling failure as: high angle planar, low angle block, toppling, joint-joint wedge, joint-fault wedge, and fault-fault wedge. High groundwater pressures, and lower shear strength material than previously assumed, are interpreted as major factors in driving pit slope failures at Macraes, and horizontal drainage is recommended as the most effective method in preventing future pit slope failures.

Two large pit slope failures, RH27 (volume = 900m^3) & RH28 (volume =450 000m^3), located on the north wall of Round Hill Pit occurring prior to this project, are mapped in detail at scales of 1:500 and 1:800 with failure mechanisms interpreted. RH27 is a complex wedge failure formed between the Slip 27 fault and a westerly dipping joint set. RH28 is a large wedge failure formed between two faults plunging at low angles (≈3°) out of the pit slope and driven by high water pressures along a fault set parallel to the pit slope. The stability of RH27 and RH28 is determined, and future development and implications to mining operations assessed.

Thirteen types of failure are predicted to occur at Macraes based upon the integration of hydrological influences, strength properties, rock mass structure, and calibration with those failures observed at Macraes to date. Kinematic models for these thirteen failure models have been constructed to assist in recognition of these predicted failure modes in the field.

Prediction of pit slope failures should be based on sound monitoring and management of recognised active failures, and should include: visual inspections and photography, movement monitoring, hydrologic monitoring and warning monitoring, so that the hazards and adverse effects associated with unexpected slope failure movements are minimised.

TABLE OF CONTENTS

LIST OF FIGURES

Number *Page*

LIST OF TABLES

LIST OF SHEETS IN MAP VOLUME

CHAPTER 1: INTRODUCTION

1.1 BACKGROUND

Pit slope stability is an important feature of any mining operation. However there is a fundamental difference between slopes designed for permanent civil engineering ventures and those for mines. Generally in civil engineering projects failures of slopes are unacceptable and may have severe consequences, whilst there is much greater flexibility when considering the stability of working pit slopes (Anon., 1994). Both the orientation and sequence of extraction of working slopes can be adjusted to take into account slope stability and while instability of pit slopes is undesirable some can usually be tolerated; since access to the area by personnel and equipment can be restricted, exposure of the working slopes to failure is usually for a limited time, and the consequences of failure are much easier to control at a mine.

Another factor that must be considered in the excavation of pit slopes is the profile of the slope. Slopes should be as steep as possible and consistent with safety in order to minimise the volume of material to be removed and increase profits (Bell, 1987). The profile (and associated stability) of pit slopes will not only be controlled by these economic factors but also significantly influenced by many geological factors at the site.

Together with my supervisor David Bell, I approached Macraes Mining Company Ltd (MMCL) in September 1995 about the possibility of researching a project looking at pit slope stability at their Macraes Flat East Otago mine. This project was given approval by Macraes in January 1996 and work commenced in the following month.

Macraes Mining Company Ltd (MMCL) mine in east Otago is currently the largest gold mining operation in New Zealand. Open-pit mining is currently undertaken in three different pits (Round Hill, Southern and Innes Mills), although several new pits are possible in the future. Two large failures (failures RH27 and RH28) had occurred on the northern wall of Round Hill Pit prior to this project. During the initial months of the project it also became apparent that the main tailings dam abutment to Round Hill pit was also experiencing some movement, although this was excluded from this project. Not only do these large pit slope failures represent a significant hazard to personnel and equipment at the mine, but the economic losses associated with such failures of the pit slope could be substantial.

Current production at the mine is approximately 3Mt a year (mill feed), although recent plans to upscale production to 9Mt a year have been considered. This planned increase in production along with the larger slope failures mentioned above have increased the need to understand the factors and mechanisms of pit slope failures at Macraes. Increases in production will invariably mean the development of pits at faster rates, in turn increasing the likelihood of failures being generated and the increased risk for adverse effects.

1.2 THESIS OBJECTIVES

The principal objectives of this thesis consist of five interrelated parts:

1. To carry out geotechnical testing to determine relevant geotechnical parameters for the Macraes open-pit mine site. Strength testing of intact rock and fault gouge gives quantitative data which may be used for stability analyses. Quantitative determination of strength parameters may be also be used for rock mass characterisation.
2. Assessment of structural domains at Macraes. The orientations of structures in rock masses is one of the most important features in the assessment of the stability of rock slopes. By working out mean orientations for different structural features it is possible to predict failure types kinematically.
3. Collation of pit slope failures to date at Macraes Gold Mine in a consistent format. By constructing a standard recording sheet for pit slope failures at Macraes, failures may be more easily compared for the development of failure models at the mine.
4. Analysis of Round Hill Pit failures RH27 and RH28, and to provide geotechnical input data to assist in the design of possible remedial measures. Detailed engineering geological mapping of failures RH27 and RH28 was undertaken so that failure models for these could be constructed, for stability assessment so that the most effective remedial measures can be assessed.
5. The construction of an integrated rock mass model(s) for pit slope failures at the Macraes open-pit mine site. The compilation and integration of all of the above information allows predictive models for failures to be developed at the mine. Predictive models may help reduce any adverse effects that could be associated with unexpected pit slope failures

1.3 STUDY AREA

1.3.1 Site Location

The study area (Figure 1-1) is located approximately 3km north-east from Macraes Flat (latitude 45° 23'S, longitude 170° 26'E) and approximately 60km north-west of Dunedin at around 520m above sea level. The field area covers about 2½km^2 and encompasses the three current operating pits of: Round Hill Pit, Southern Pit and Innes Mills Pit. The predominant focus throughout most of this thesis centres around the northern wall of Round Hill Pit, which currently contains two of the largest pit slope failures at the mine (failures RH27 & RH28).

1.3.2 Mining History

Gold in the Macraes Flat area was first discovered by alluvial prospectors in 1862 and a flourishing canvas town was soon established. As late as 1936 a company using electric-powered methods obtained 1,654oz (51.4kg) of alluvial gold on the formerly worked over alluvial gold area at Macraes Flat (Wood, 1970). The first gold bearing quartz lodes were not found in the area until 1866, although little gold was won from these reefs and mining activity ceased in 1868.

Reefs were first discovered at Golden Point and Round Hill in 1889. From 1890 to 1930 an estimated 15 000 ounces (466.5kg) of gold at 4.7g/t and 1 000 tons of scheelite were recovered from underground mining at Golden Point, Deepdell, Maritana and open pit mining at Round Hill (Williamson, 1939). Underground mining didn't commence at Round Hill until 1932, and from then until 1936 a total of 3374 tons of ore were treated for the recovery of 981 ounces (30.5kg) of gold. These four mines were spaced over a distance of about 2km and worked parts of what is now referred to as the Round Hill-Golden Point lode system (a part of the Hyde Macraes Shear Zone). Mining ceased for the duration of World War II, after which sporadic mining continued until 1954 (Lee *et. al.*, 1989).

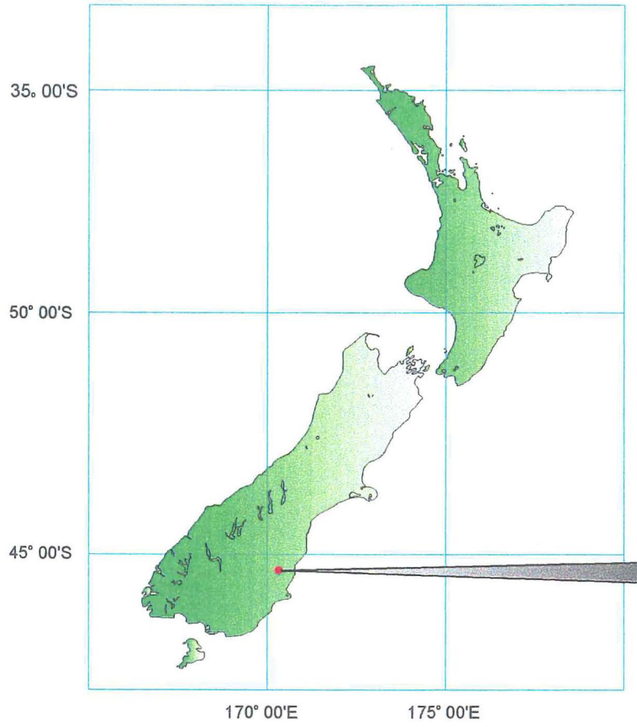

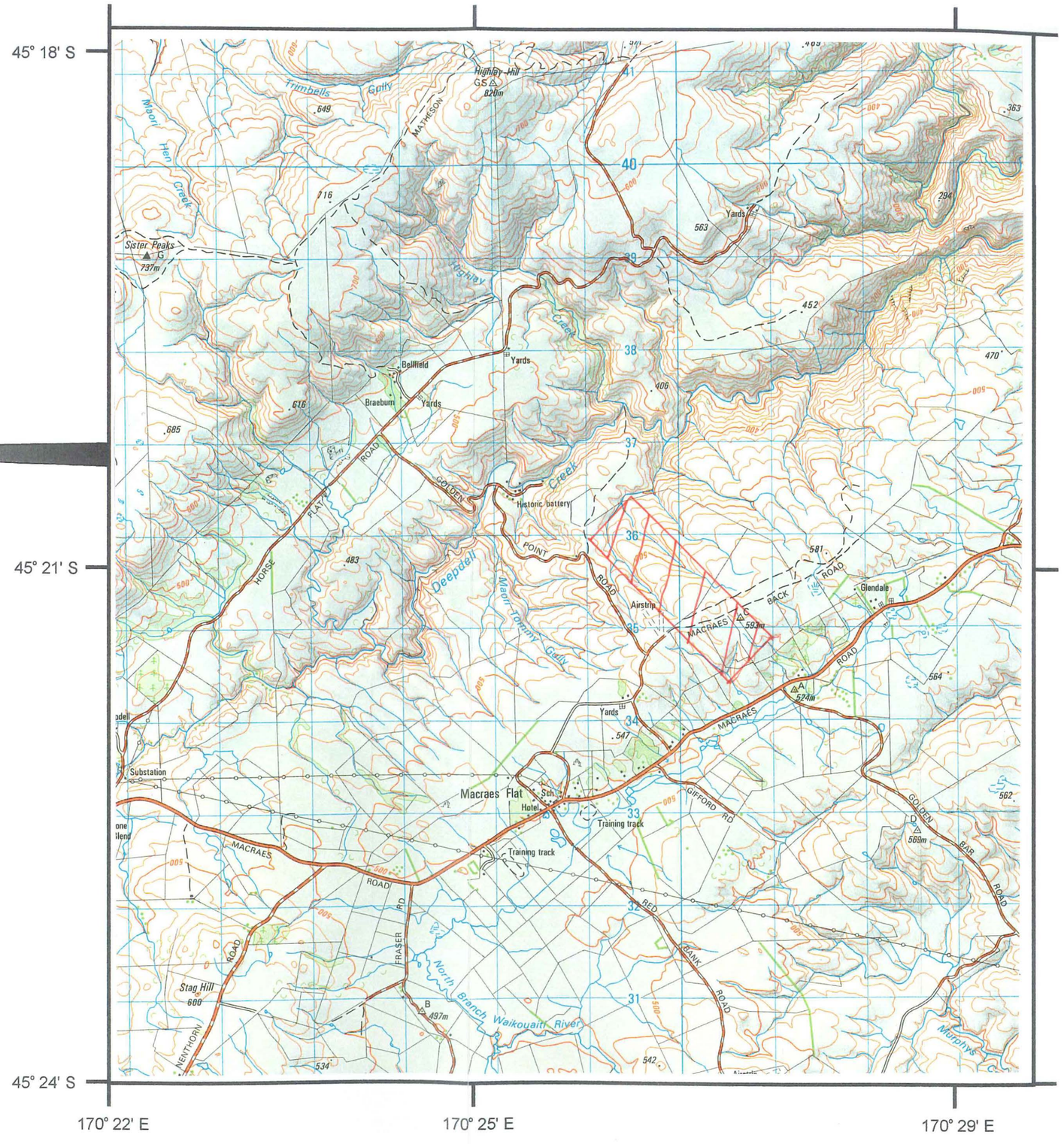

Figure 1-1: Location of the field area. (Sourced from: Department of Land and Survey Information, 1:50 000, NZMS260 - I42, Dunback).

1.3.3 Current Mining Activities

With three current operating pits; Round Hill, Southern and Innes Mills, MMCL are currently the biggest producer of gold in New Zealand. Mining activities occur Monday to Saturday dayshift, and Monday to Friday nightshift. The production figures for the 1996 financial year are presented in Table 1-1. Mining operations are presently contracted out to Eltin Limited of Australia and gold is processed using a carbon in leach system with waste tailings being pumped and stored behind a large tailings dam in Maori Tommy Gully. The overall layout of the mine site is depicted in Figure 1-2.

Table 1-1: Production details for 12 month period at the Macraes Gold Mine to the end of 1996 financial year (Macraes Mining Company Limited Annual Report 1996).

Waste Mined (bank cubic metres)	Ore Mined (tonnes)	Mill Feed (dry milled tonnes)	Gold Produced (fine ounces)	Ore mined grade (grams/tonne)	Resources (million ounces	Reserves (million ounces
6 778 335	3 514 877	3 019 377	116 365	1.75	4.0	1.8

Macraes Mine operates on its own co-ordinate system known as Macraes Mine grid (MMG). MMG was first developed so that the strike of the shear zone is rotated around to trend north-south instead of north-west south-east under New Zealand Map Grid (NZMG). MMG can be calculated by rotating NZMG 45° clockwise about the origin point 286492.55E, 750046.90N and subtracting 21599.23E, 736549.36N which gives corresponding MMG value of 70501.32E, 13497.54N. **It should be clearly noted at this stage that <u>ALL</u> directions given throughout this project are in terms of MMG in Dip/DipDir. (##/###) or Trend/Plunge (###/##), unless otherwise specified.** Since the information from this project is intended for use at the Macraes mine, it seemed appropriate to quote directions in terms of MMG so that no later conversion is required which may result in errors. To convert directions in this thesis back to NZMG true north then 45° needs to be added to the dip direction.

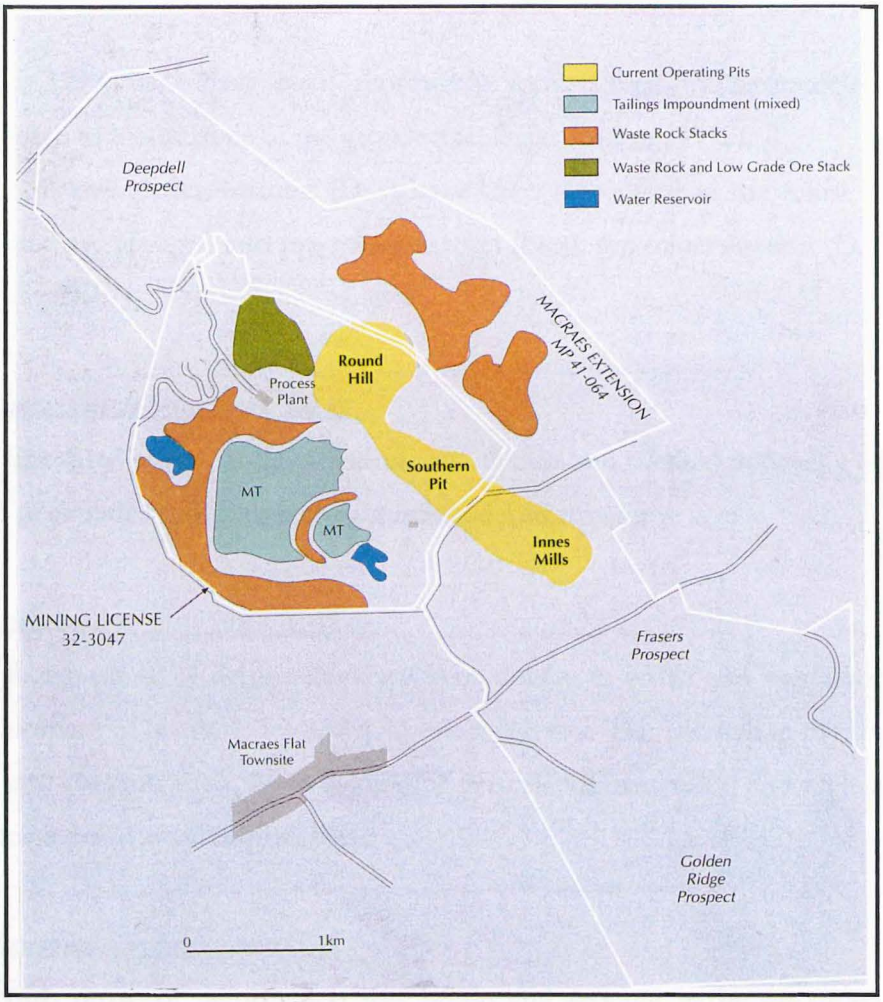

Figure 1-2: Macraes Gold Mine operations layout (MMCL Annual Report 1996).

1.4 GEOLOGICAL SETTING

1.4.1 Regional Geological Setting

Located within the Upper Palaeozoic to Lower Mesozoic Haast Schist Group, the regional geology of the study area (Figure 1-3) is depicted on both the 1:250 000 scale NZ Geological Map Sheet 23 - Oamaru (Mutch, 1963), and the new 1:500 000 scale NZ Geological Map 7- "Geology of the Otago Schist and Adjacent Rocks" (Mortimer, 1993). The Haast schist group consists of a complexly deformed sequence of psammitic and pelitic schists with subordinate metabasite (greenschist), and minor chert and marble horizons (Coombs et. al., 1976; McKeag *et. al.*, 1989). The schists were probably formed by tectonic amalgamation of the Caples, Aspiring and Torlesse terranes during the Rangitata Orogeny

(Braithwaite, 1989), and have been thoroughly recrystallised to Textural zone 4, and metamorphosed to biotite zone of the green schist facies (Bishop, 1972).

Five phases of deformation (D_{1-5}) have been recognised in the schist by previous workers. These are grouped into pre-mineralisation (D_{1-3}), syn-mineralisation (D_4), and post-mineralisation (D_5).

1. Pre-Mineralisation Structures (D_{1-3})

   The first three phases of deformation were ductile and resulted in development of low angle penetrative foliations and tight isoclinal fold structures.

2. Syn-Mineralisation Structures (D4):

   The fourth phase of deformation was semi-ductile to brittle and was associated with development of quartz lodes and gold mineralisation. This resulted in the formation of kink and chevron folds, open folding of pre-existing structures, and high-angle faults and fractures of small displacement.

3. Post-Mineralisation Structures (D_5)

   The fifth phase of deformation was brittle and thought to be associated with the Kaikoura Orogeny (uplift of the schists) during the Late Tertiary movement on the Alpine Fault. This has resulted in high angle reverse and normal faults, some of which have significant displacement and produced the present characteristic basin and range province of the Haast Schist. Post mineralisation structures at Macraes include NE dipping (NZMG) normal faults within the Intra-shear pelite and SW dipping (NZMG) imbricate thrusts above the Macraes Hanging Wall Shear. The development of these structures is kinematically compatible with normal movement on the Hyde Macraes Shear Zone and is related to mid Cretaceous break up of Gondwanaland in the SW Pacific (Angus, 1992).

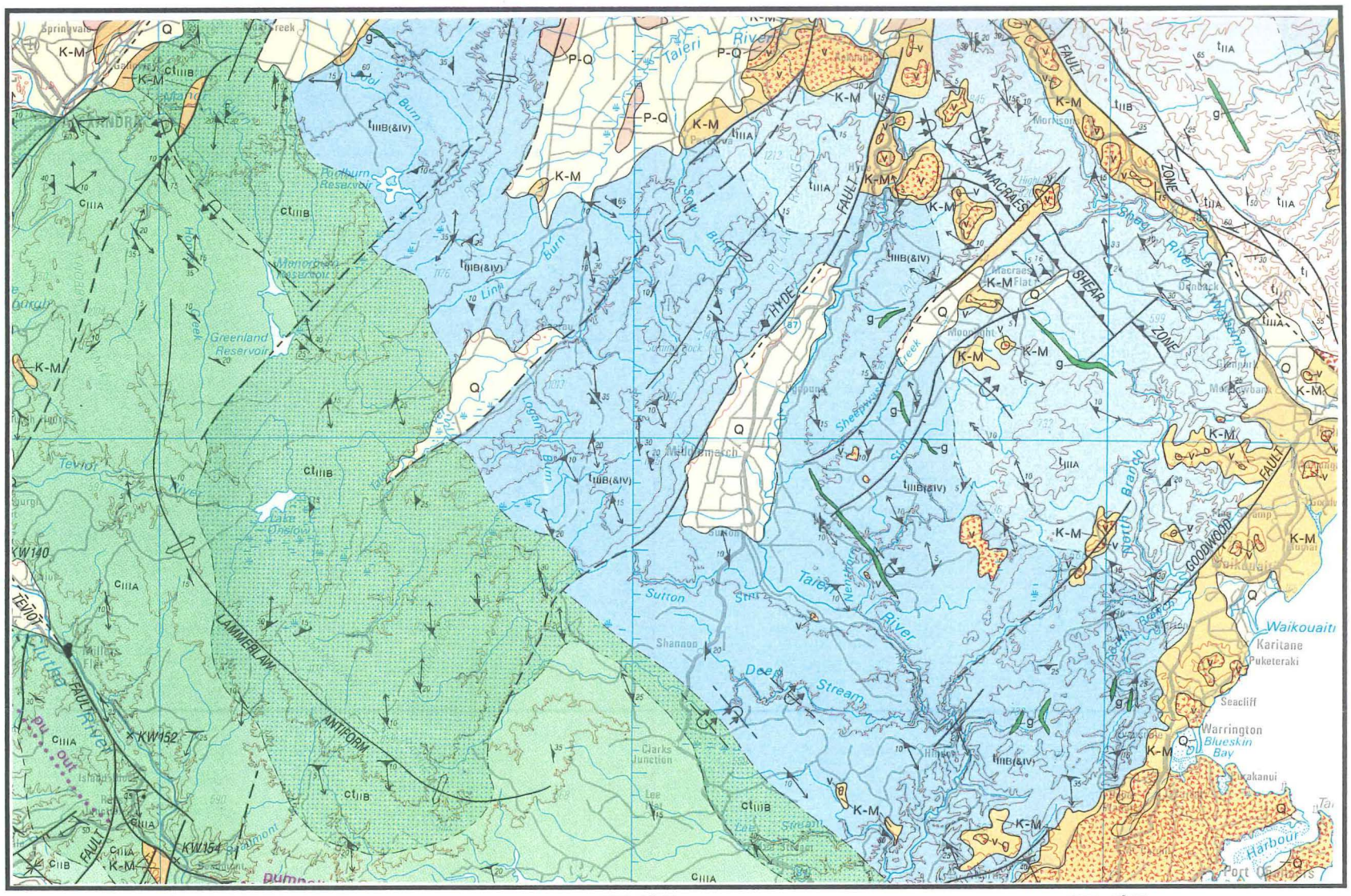

GEOLOGICAL LEGEND

Alluvial and glacial outwash deposits. — Q — QUATERNARY (Wanganui-Hawera Series)

REGIONAL UNCONFORMITY

Weathered, slightly warped and faulted piedmont gravels (Maori Bottom & Prospect formations, Clydevale and Gore Piedmont gravels, Schoolhouse Fanglomerate, Kurow Group). — P-Q — PLIOCENE-LOWER QUATERNARY (Taranaki Series)

REGIONAL UNCONFORMITY

Marine, estuarine, deltaic, and fluvial strata in west and Central Otago (Manuherikia Group, Bobs Cove Beds), Southland (Gore Lignite Measures, Annick Group, Waiau Group) and east Otago and South Canterbury (Taratu, Wangaloa, Ngarara, Green Island, Burnside, Amuri, Concord, Weka Pass, Bluecliffs, Southburn, Blue Spur Conglomerate, and Whiterock formations and their equivalents [Carter 1988]). v = intercalated mafic volcanic rocks (Dunedin Volcanic Complex, Waipiata, Deborah, and Waiareka volcanics). — K-M, v — LATE CRETACEOUS-MIOCENE (Mata-Southland Series)

REGIONAL UNCONFORMITY

Non-marine conglomerate and breccia (Shag Point Group, Kyeburn Formation, Henley Breccia). — mK — MIDDLE CRETACEOUS (Clarence-Raukumara Series)

REGIONAL UNCONFORMITY

WESTERN PROVINCE[1] — EASTERN PROVINCE

MEDIAN TECTONIC LINE — LETHAM FAULT — HILLFOOT FAULT — LIVINGSTONE FAULT

OTAGO SCHIST

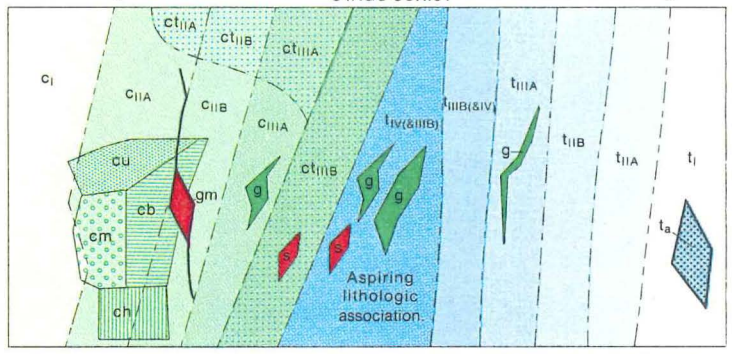

EARLY CRETACEOUS
JURASSIC
TRIASSIC
PERMIAN
CARBONIFEROUS

DARRAN COMPLEX, MACKAY INTRUSIVES, LARGS TERRANE

Leucogabbro, diorite, granite, granophyre, migmatite, biotite gneiss, andesite, tuff & breccia (Darran Leucogabbro, Nurse, Glade, and Hut Plutonic suites, Hollyford Gabbroic Suite, Mistake Diorite, Gunn Dolerite. Largs terrane). Sandstone of Martins Bay Formation north-west of Alpine Fault.

BROOK STREET TERRANE

Basalt, augite porphyry, andesite, diorite, minor ultramafic rocks, volcanic breccia and greywacke (Plato terrane, Eglinton Volcanics, Skippers Group, Takitimu Group).

MURIHIKU TERRANE

Sandstone, siltstone, argillite, tuff and minor conglomerate (Murihiku Supergroup).

MAITAI TERRANE

mt = gabbro, altered mafic volcanic rocks, volcanic breccia, limestone, sandstone, siltstone and argillite (Maitai Group, part of Humboldt Group, part of Dun Mountain Ophiolite Belt).
mu = ultramafic rocks, serpentinite and serpentinite-matrix mélange (part of Humboldt Group and Dun Mountain Ophiolite Belt)

CAPLES TERRANE, TORLESSE TERRANE, AND OTAGO SCHIST[2]

CAPLES TERRANE (c). In tz I, dominantly grey-green volcaniclastic sandstone, siltstone and argillite with subordinate conglomerate, chert, volcanic rocks, and limestone. Schistose equivalents occur in tz IIA-IIIB. West of Lake Wakatipu, the Caples terrane has been subdivided into the Harris Saddle Formation and West Burn Semischist (ch); Momus Sandstone and Mount Campbell Formation (cm); Bold Peak Formation (cb); Upper Peak, Kays Creek, and Cosmos formations (cu); Greenstone Mélange (gm) .

TORLESSE TERRANE (t). In tz I, dominantly grey quartzofeldspathic sandstone, siltstone and argillite with subordinate conglomerate, chert, volcanic rocks and limestone, mainly of Rakaia subterrane. ta = Akatarawa subterrane. Schistose equivalents occur in tz IIA-IV. Tz IV of the Torlesse terrane as shown on this map broadly coincides with the Aspiring lithologic association of Craw (1984).

UNDIFFERENTIATED CAPLES OR TORLESSE TERRANE (ct). Includes wedge-shaped area in southeasternmost Caples terrane containing schist geochemically similar to Torlesse terrane rocks; lenses of lower textural grade Caples-like schist in tz IV Torlesse schist, and zone of uncertainty of position of terrane boundary proposed by Mortimer and Roser (1992)

DIFFERENTIATED LITHOLOGIES[4]
Greenschist (g), serpentinite, talc schist, and tremolite schist (s)

TEXTURAL ZONES (tz) (Bishop 1972) Characteristics of schist derived from psammitic protoliths (original sandstone):

- I: Indurated, nonfoliated medium-grained sandstone.
- IIA: Slightly foliated metasandstone with widely spaced cleavage.
- IIB: Penetratively and well foliated semischist.
- IIIA: Strongly foliated schist with segregation lamellae 1-10mm long.
- IIIB: As for IIIA, but segregation lamellae >10mm and < 2mm thick.
- IV: As for IIIA, but segregation lamellae > 2mm thick.

Figure 1-3: 1:500 000 regional geological map for the study area. Structural symbols given on next page. (Sourced from: Mortimer, 1993)

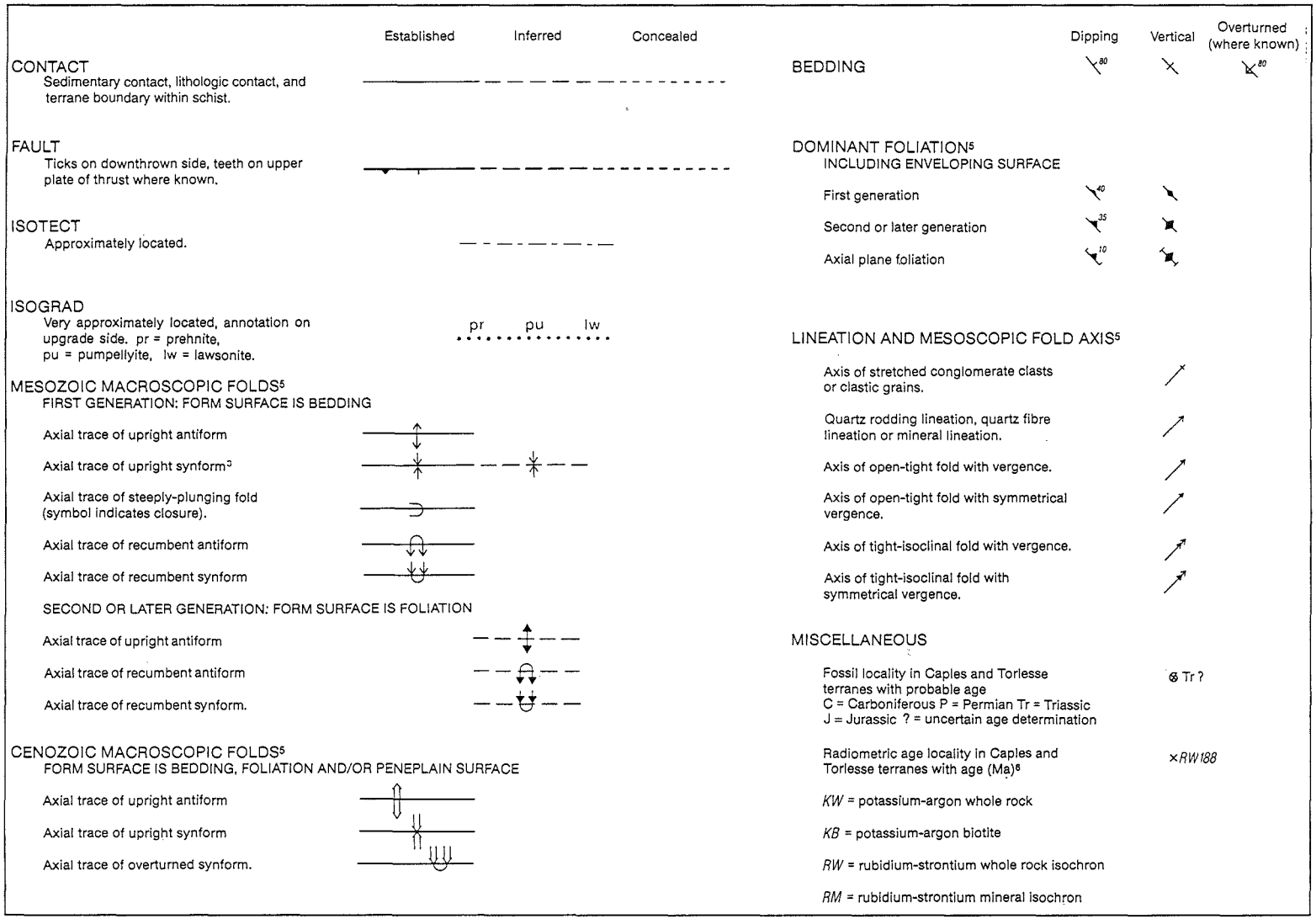

Figure 1-4: Geological Symbols for map of regional geology (figure 1-3).

Winsor (1991b) established a relation between low-angle shear zones and folds in the schist. North-dipping shears are often subparallel to F_3 axial planes, with south-dipping mesoshears present as an antithetic set. Thrusting was initiated on the shear zones after F_3 folding and accompanied continued regional compression.

The Otago schist zone is also cut by numerous gold-bearing quartz veins formed from metamorphic fluids during the Cretaceous-Tertiary uplift of the belt (Henley et. al., 1976; Norris and Henley, 1976; Paterson, 1982, 1986; McKeag and Craw, 1989). A prominent suite of these Au-bearing quartz veins is found in the Hyde-Macraes Shear Zone (Teagle et. al., 1990).

1.4.2 The Hyde-Macraes Shear Zone (HMSZ)

Extending for approximately 25km along strike the HMSZ is the most extensive low angle mineralised shear known in Otago (Craw and Norris, 1988) (Figure 1-3; Figure 1-5). Between Round Hill and Golden Point the HMSZ is located on the lower limb of an inclined F_3 macroscopic fold but transects the fold further to the north and indicates that the HMSZ post dates the F_3 structure, although it is subparallel to S2, a shallow, north-dipping penetrative cleavage (Winsor, 1991a). The shear zone is offset in several places by north-easterly (NZMG) trending faults, thought to have resulted from extensional tectonics during the Tertiary (Figure 1-5).

The shear HMSZ has well-defined upper (Hanging Wall Shear) and lower (Footwall Shear) faults, separated by a zone (5 - 140m thick) of variably faulted and folded graphitic schist (McKeag et. al., 1989). Above the shear zone is a strongly banded, well foliated, psammitic schist containing 2 to 5mm thick quartz albite laminae and synmetamorphic veins and darker micaceous chlorite-muscovite layers. Below the shear zone is a highly folded (in a ductile manner) quartz-rich psammitic schist with visible development of a sub-horizontal second foliation in the micaceous horizons (Teagle *et. al.*, 1990).

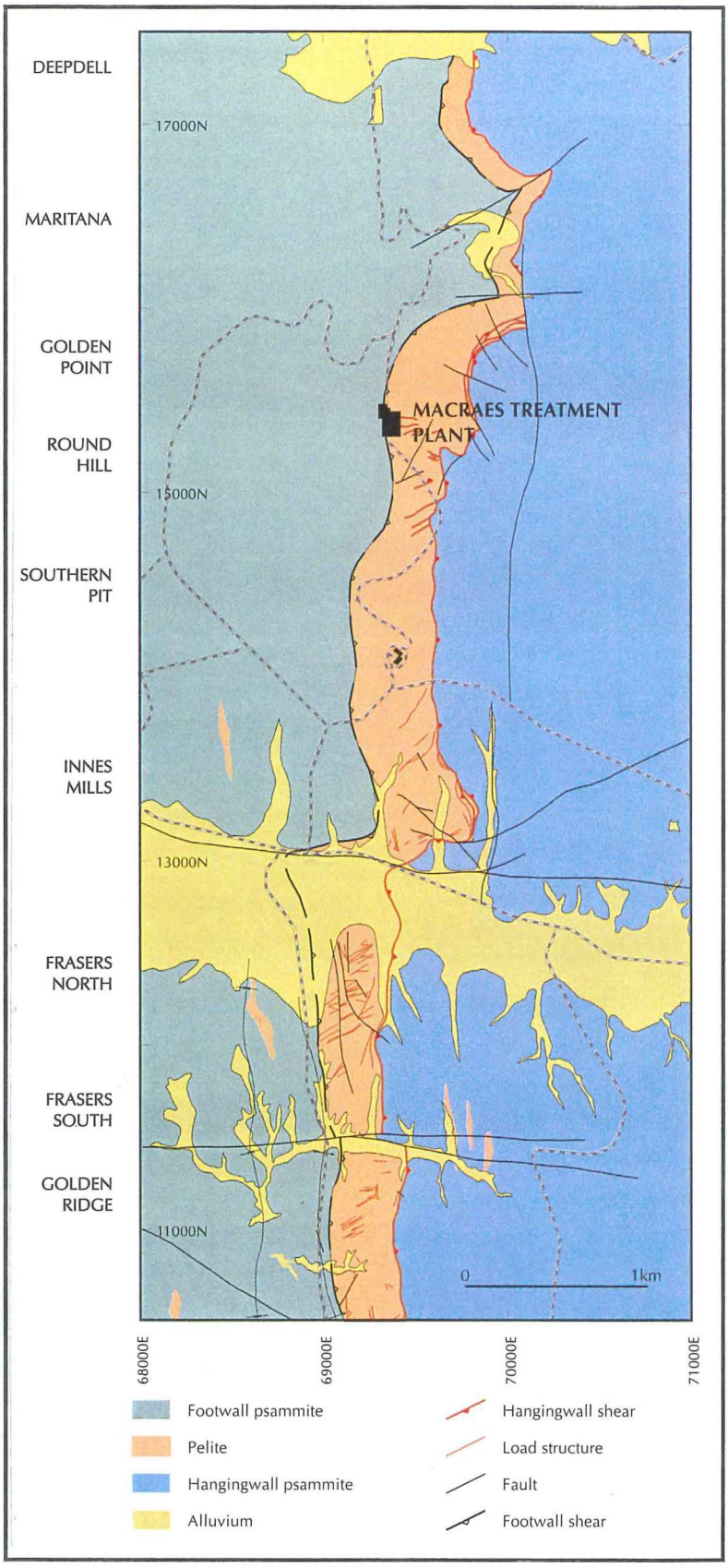

Figure 1-5: Map of geology of Hyde-Macraes Shear Zone in MMG. Note the offset of the shear zone in places by easterly trending faults as discussed by Windsor 1991a. (MMCL Annual Report 1996).

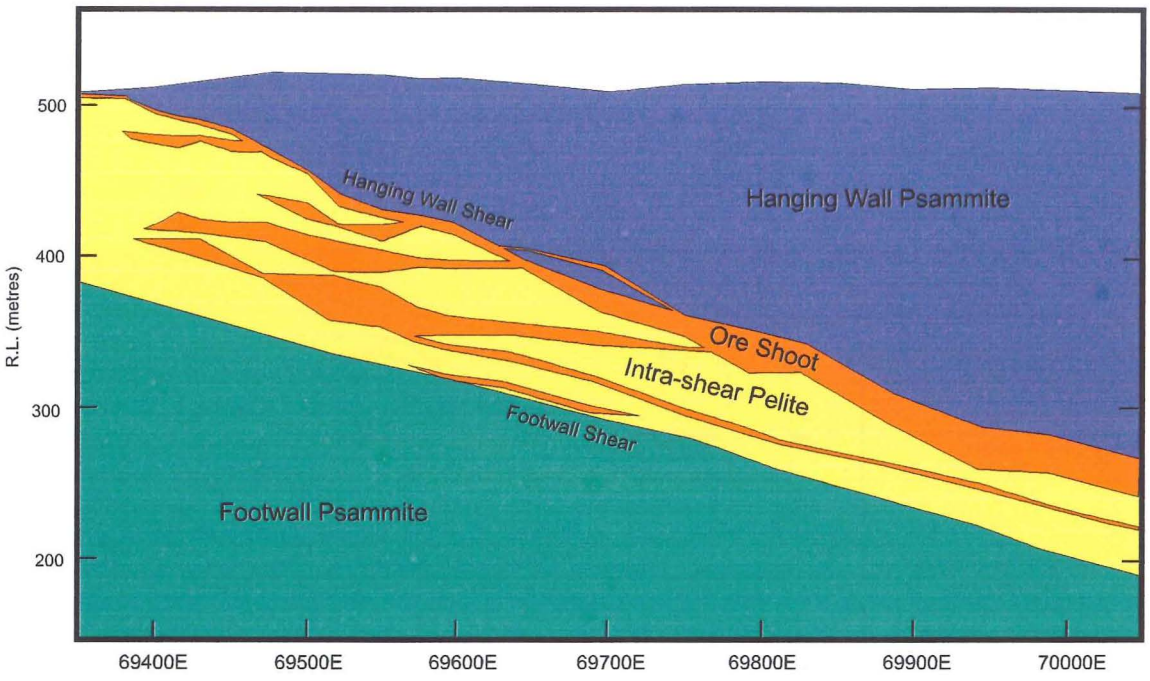

Figure 1-6: Cross section of the Hyde-Macraes Shear Zone illustrating the general geology of the Macraes Shear Zone at the proposed Frasers North Prospect section 12425N (*after* MMCL Annual Report 1996).

The Hanging Wall Shear (HWS), which defines the top of the HMSZ, is located between the contact of the Upper Psammite and the Intra-shear pelite (Figure 1-6), and is exposed in all the pits, while the Footwall Shear is not generally exposed in the pits. Figure 1-7 shows the HWS is generally uniform in attitude with an average orientation of around 18/090. The shear rock comprises dark fine grained micaceous graphitic schist with a strongly developed shear fabric (Angus, 1992).

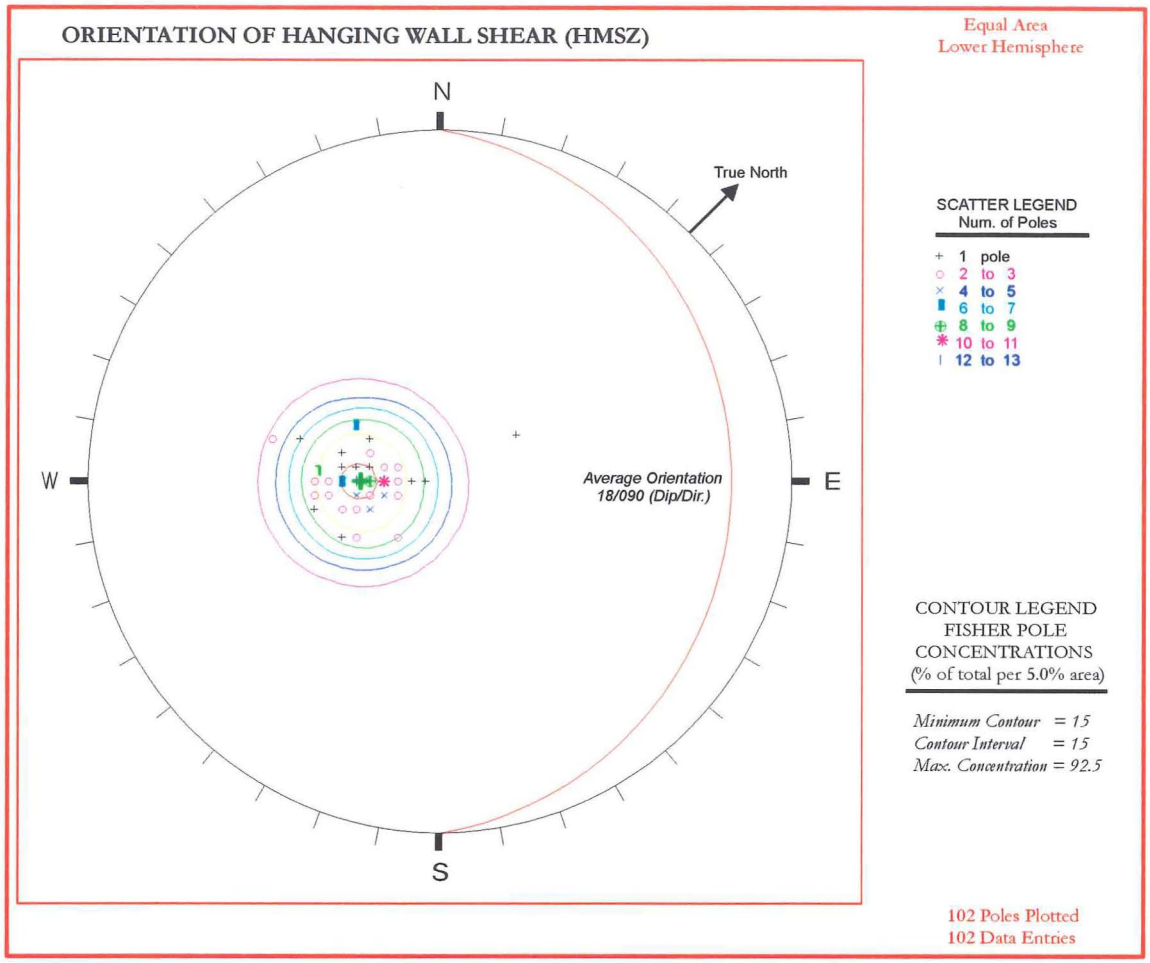

Figure 1-7 : Average orientation (MMG) of Hanging Wall Shear for the Hyde-Macraes Shear Zone at the Macraes mine site (*data sourced from* 'Macraes Geotechnical database')

Gold mineralisation is widespread throughout the HMSZ and has been extensively studied (Craw and Norris, 1991; Teagle et al., 1990; McKeag et al., 1989; Henley et al., 1976). Batt and Robinson (1986 in: Lee, 1987) have described three styles of mineralisation in the Macraes Shear Zone.

1. Lode shears: High strain shear zones which comprise lode quartz veins; strongly silicified and mineralised cataclastic to mylonitic shears generally concordant with the lode system; and strongly deformed stockwork zones.
2. Low strain stockwork zones with greater than three volume percent of high angle discordant mineralised veins; and
3. Disseminated sulphide and weak stockwork (less than three volume percent) mineralisation.

1.5 PREVIOUS GEOTECHNICAL WORK

The majority of previous work relevant to this project is contained within proprietary documents held at the mine site. It must be noted however that no real geotechnical work had been carried out by staff at Macraes prior to this project, with the majority of work having been undertaken by both Australian and New Zealand private consulting firms.

The main works carried out by these private consulting firms and relevant to this project are as follows:

- Coffey Partners International Pty. Ltd - Main reports are: "Assessment of pit slope design" (May 1992); "Site visit and Geotechnical Review" (October 1993); and "Slope Monitoring Programme" (December 1992)
- Pells Sullivan and Meynink Pty. Ltd. - Pit slope design investigation, and workers Bertuzzi, Eggers and Sullivan have undertaken work associated with failures RH27 & RH28 and the current tailings dam movement.
- Woodward-Clyde Ltd (1997). - have recently undertaken work associated with the main tailings dam movement as well as geotechnical investigations associated with the suitable locations for a new tailings dam.
- Works Consultancy Services (1996) - uniaxial compressive strength testing on schist core, direct shear testing on fault gouge, and ring shear testing on fault gouge. Most of this testing is associated with movement of the main tailings dam.
- Riddolls and Grocott Ltd. (1997) - Review of schist and fault gouge strength properties at Macraes.

1.6 THESIS ORGANISATION

Following this introductory chapter, Chapter 2 discusses the geotechnical investigations undertaken during this thesis and assesses strength parameters for schist and fault gouge at the mine site. Chapter 3 consists of structural domain interpretation at the mine from the geotechnical database of wall mapping data, collected during the previous five years of current mining operations. Chapter 4 comprises both the compilation of the pit slope failure database for the development of pit slope failure models at the mine, and examines two current large pit slope failures (failures RH27 & RH28) in Round Hill Pit. Chapter 5

integrates the information from Chapters 2-4 into a predictive rock mass model for the mine site. By integrating all of the studies in this project it is possible to develop predictive models for slope failures at the mine, which can be used in the future to both predict failures prior to the event and assist in the implementation of remedial measures for failures that do occur. Finally Chapter 6 summarises and concludes on the aspects covered by this thesis and makes recommendations for further work.

CHAPTER 2 : ENGINEERING GEOLOGICAL AND GEOTECHNICAL INVESTIGATIONS

2.1 INTRODUCTION

The investigative procedures used in this study follow the methodology developed by Bell and Pettinga (1983) and focuses on the operation/maintenance phase (Table 2-1). The principal aims of this engineering geological investigation have been to provide geotechnical input data for the interpretation of pit slope failures (RH27 & RH28) in Round Hill Pit, and the compilation of all available information into integrated pit slope failure models for the mine site (see Chapter 4). The results of this investigation are to assist in the long term performance of the mine site by the integration of the available information into predictive rock mass models for pit slope failures at the mine.

Table 2-1: Site investigation stages and objectives (Bell and Pettinga, 1983).

	PROJECT STAGE	SITE INVESTIGATION OBJECTIVES
I	PRE-FEASIBILITY and/or FEASIBILITY	selection of a geotechnically suitable site (or sites) assessment of the environmental impact of the project
	⇓	
II	DESIGN	design and specification of foundations and associated earthworks, and of compatible engineering structures design of temporary engineering works to permit project construction
	⇓	
III	CONSTRUCTION	construction monitoring to confirm satisfactory design performance of the structure construction logging to provide a record of foundation conditions for future reference
	⇓	
IV	OPERATION and/or MAINTENANCE	investigation of existing engineering structures to evaluate safety or long-term performance design and implementation of remedial works as required

The principal engineering geological and geotechnical aspects of this thesis are therefore:

1. Engineering geological mapping of selected failures for the construction of failure models (Chapter 4).
2. Laboratory testing of intact rock and fault 'gouge' material collected during the field studies part of this project for the provision of geotechnical input data (Section 2.3). This data may then be used for the strength characterisation of these materials and to assist in interpretations of pit slope stability.
3. Desktop investigations involving: the assessment of structural data into structural domains for the mine (Chapter 3); integration of available data into a database for failure models (Chapter 4); and the construction of predictive rock mass models for the Macraes mine (Chapter 5).

2.2 FIELD INVESTIGATION PROGRAMME

2.2.2 Engineering Geological Mapping

Engineering geological mapping of pit slope failures was undertaken between February 1996 and June 1996. During this period 9 new failures were observed at the mine site and later interpreted in terms of failure mechanisms (Map Sheet 7; see Chapter 4). Aside from these new failures, engineering geological mapping focused primarily on the two large failures RH27 (Map Sheet 8) and RH28 (Map Sheet 9) located on the north-eastern and northern walls respectively of Round Hill Pit. Mapping identified geomorphic features such as tension cracks and scarps related to current active movement, and detailed structural information for discontinuities in the rock mass was recorded for interpretation of the structure of the northern wall, Round Hill Pit. The main structural features controlling failure were identified and compared with those determined by structural domain analysis (Chapter 3). Selected fault gouge and intact rock samples were also collected during mapping for later strength determination.

2.2.3 Hydrological Investigations

a) Rainfall Data

Central Otago has one of the driest climates in New Zealand, with records kept at the mine site showing an average annual precipitation of 650mm/yr. Rainfall data is collected on a daily basis at the mine site by mine staff, and is presently available for the years 1991 and 1993-1996 (Appendix B1). Snowfall is of relatively common occurrence at the mine during the winter months, although monitoring records make no distinction between snow and rain as forms of precipitation. Rainfall records for the mine are therefore presently very limited which restricts present interpretations.

Monthly rainfall figures collected to date at the mine site are presented in Figure 2-1. Records show that the months of November through March are typically the wettest months, while April through October generally form the driest months at the mine site. When precipitation does occur it is typically less than 30mm/day, and very rarely greater than 50mm/day.

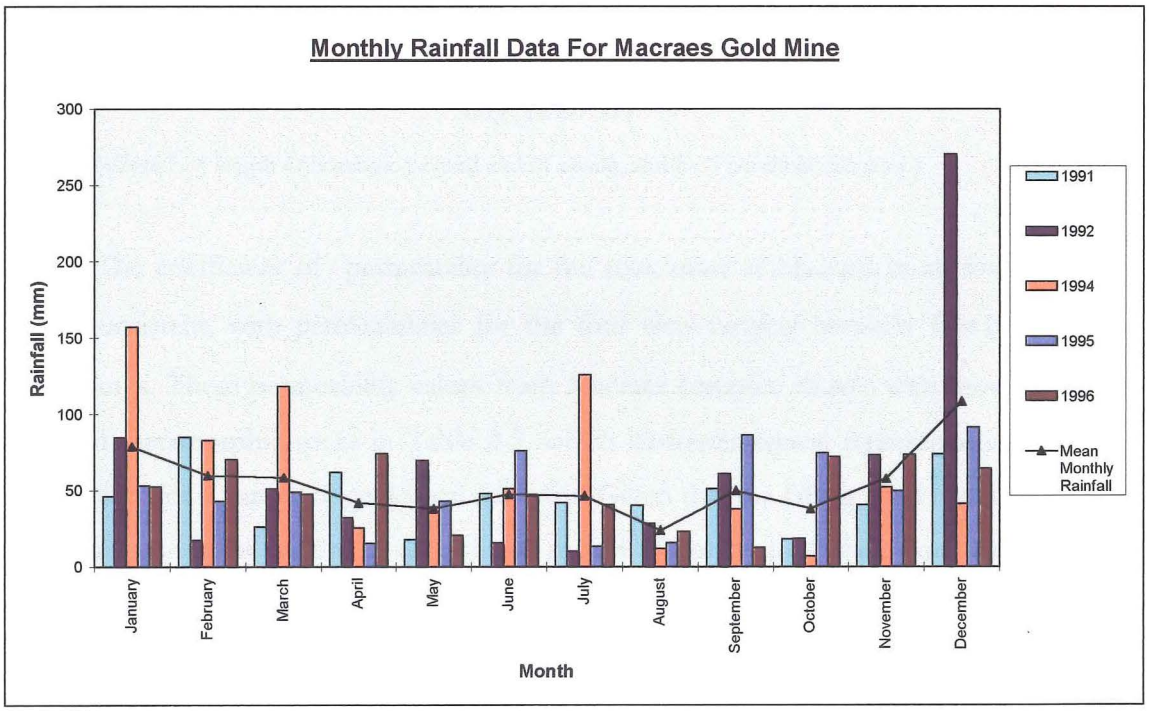

Figure 2-1: Monthly rainfall at Macraes Flat mine site for years 1991, 1993-1996. Average monthly rainfall for these years is represented by solid black line.

The influence of precipitation on inducing surficial pit slope failures (<5m deep) at the mine is supported by the failure database (Chapter 4). Charts of precipitation and failure dates show that surficial pit slope failures at Macraes characteristically occur within 24 - 48 hours following precipitation.

b) Permeability Data

The results of four falling head permeability tests undertaken at the mine site by Macraes staff prior to commencement of this thesis were available. Tests were carried out on piezometers SP9, SP10, SP11, and SP12 and the results are presented in Appendix B2.

In the falling head test water is poured into a vertical bore hole and the time taken for the water level to fall to its original level is determined. The coefficient of permeability (K) for falling head tests in saturated ground is then calculated as follows (Hoek and Bray, 1981):

$$K = \frac{A}{F(t_2 - t_1)} \times \log_e \frac{H_1}{H_2}$$

where A = cross-sectional area of the water column

H_1 = water level in the borehole at time t_1

H_2 = water level in the borehole at time t_2

F = the shape correction factor = $\dfrac{2\pi L}{Log_e(2L/D)}$

(where L = length of borehole beyond end of casing, and D = borehole diameter.)

The coefficient of permeability for the rock mass at Macraes in all four tests was highly consistent, with permeabilities for the four tests ranging between 1.0×10^{-7}m/s and 8.4×10^{-8}m/s. These permeability values from Macraes compare closely with those given for fractured metamorphic rocks in Table 2-2, which illustrates typical representative values of permeability for a variety of geological materials. Given that the falling head test is calculating permeabilities for the rock mass (both intact rock + discontinuities) then from Table 2-2 it is reasonable to conclude that permeabilities along discontinuities will be reasonably high ($K\approx10^{-4}$m/s or higher), but low through intact schist ($K\approx10^{-10}$ or less).

Table 2-2: Representative values of hydraulic conductivity for various rock types (*after* Domenico and Schwartz, 1990).

Material	Hydraulic conductivity (m/sec)
SEDIMENTARY	
Gravel	$3 \times 10^{-4} \rightarrow 3 \times 10^{-2}$
Coarse Sand	$9 \times 10^{-7} \rightarrow 6 \times 10^{-3}$
Medium Sand	$9 \times 10^{-7} \rightarrow 5 \times 10^{-4}$
Fine Sand	$2 \times 10^{-7} \rightarrow 2 \times 10^{-4}$
Silt, loess	$1 \times 10^{-9} \rightarrow 2 \times 10^{-5}$
Clay	$1 \times 10^{-11} \rightarrow 4.7 \times 10^{-9}$
CRYSTALLINE ROCKS	
Fractured igneous and metamorphic rock	$8 \times 10^{-9} \rightarrow 3 \times 10^{-4}$
Unfractured igneous and metamorphic rocks	$3 \times 10^{-14} \rightarrow 2 \times 10^{-10}$

c) Piezometric Data

Piezometric data serves a number of purposes in terms of pit slope stability during the operation of the mine. Piezometric data allows assessment of groundwater levels at different sites around the pit, and areas of higher groundwater pressures may be identified. Areas of higher groundwater pressures may then be either assessed for wall stability, or monitored to assess the effectiveness of installed horizontal drainage. Further, the monitoring of piezometers allows for the interpretation of the relationship between rainfall and groundwater response.

Piezometric information is available from a number of open stand pipes located around the mine site, however recording intervals are often both widely and irregularly spaced, meaning the interpretation of relationships between rainfall and groundwater response is difficult. Interpretation of piezometric records (Figure 2-2) suggests that the lag time, or time from peak precipitation to peak piezometric response is generally in the order of one to two weeks (although it is difficult to determine accurately with the variability in recording intervals). This lag time will be dependent on a number of factors such as antecedent rainfall history, snow melt etc. It is therefore recommended that piezometric data is recorded daily to allow better interpretations. The greater lag time between rainfall and piezometric response (1 - 2 weeks), compared to the rainfall and surficial pit slope failures (24 hours) is merely a reflection of the greater distance through which water has to permeate to effect piezometric levels.

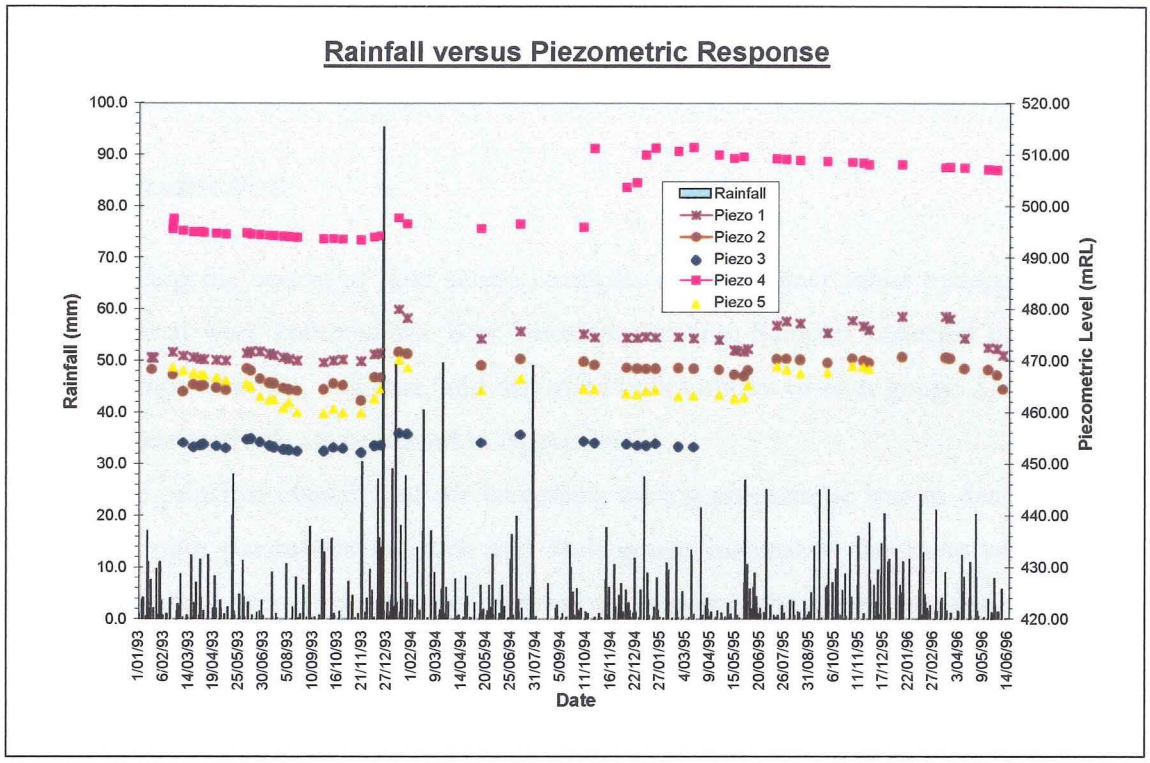

Figure 2-2: Precipitation versus piezometric response for Macraes Mine Piezometers 1-5. Lag time from peak rainfall generally appears to be between one and two weeks although this will vary depending on antecedent precipitation conditions (*sourced from* Macraes mine file).

The implications of lag times in the order of one to two weeks between rainfall events and deeper groundwater response has major implications for the larger deeper seated failures driven by groundwater pressures, like RH28 (Section 4.4.2). Acceleration of movement rates on failures like RH28, are not likely to reach their maximum until one to two weeks following precipitation when the groundwater response is highest. Once again this will be dependent on the antecedent rainfall history, etc., in the area.

2.3 LABORATORY INVESTIGATIONS

2.3.1 Introduction

During the course of field studies, samples of both intact schist material and fault gouge material were collected for later laboratory testing. Samples collected consisted of irregular lumps of schist, drill core, and disturbed bulk samples of fault gouge. Details of the laboratory test methods are presented in Appendix C.

The principal objective of the laboratory testing programme was to determine site-specific strength parameters for rock and fault gouge material at the mine site, and the influence of these strength parameters on pit slope failures at the mine. Quantitative strength data serves to complement strength data derived from other sources such as back analysis (Chapter 4; Appendix F7), and can also be assessed and used for the development of predictive rock mass models for pit slope failures at the mine (Chapter 5). The testing programme can be subdivided into:

1. Testing of intact rock (Point load strength testing, Uniaxial compressive strength testing), which is important when considering those failures that involve breakage through intact rock before shear failure develops.
2. Testing of fault gouge infill material (Ring shear testing, X-ray diffraction analysis), which is an important parameter when considering fault controlled pit slope failures because failure is more likely to occur along the fault than through intact rock material.

While ideally it would have been desirable to carry out shear strength testing on joints, no facilities or equipment were available that allowed this testing to be undertaken.

2.3.2 Uniaxial Compressive Strength Testing

a) Introduction

Uniaxial compressive strength (UCS) testing was undertaken on schist core from the mine site to ascertain peak strengths for intact rock. Strengths were also correlated with point load strengths to determine a site specific correlation factor for the conversion of $Is_{(50)}$ point load index values to UCS (see Section 2.3.3). Strain measurements on core were not

conducted during testing due to the tight time constraints imposed by the civil engineering laboratory being refurbished.

UCS testing was conducted on 20 samples collected from four diamond drill holes (DDG31; DDG33; DDG34; and DDG35) around the mine site. Storage conditions for the core at the mine meant that samples were not at their natural moisture content when collected, so strength versus natural moisture content could not be determined. Given that almost all pit slope failures observed during field studies occurred following rainfall, it was decided that the samples should be tested in a fully saturated condition. Samples were immersed in a water bath under vacuum for 3 hours and the core was then permitted to surface dry at air temperature prior to the onset of loading by the testing equipment.

UCS testing was carried out in accordance with the ISRM 'suggested methods' (Brown, 1981; see Appendix C2). Preparation of core samples for testing was undertaken in the Department of Geological Sciences', Engineering Geology laboratory. The limited height adjustment of the grinding equipment prevented the larger PQ (83mm) core being cut to the recommended length/diameter (L/D) ratio of 2.5 - 3.0. The L/D ratio of this larger size core instead ranged between 1.94 and 2.11.

Samples were tested on one of the University of Canterbury, Civil Engineering Department's concrete testing machines with specimens loaded at the suggested rate of 0.5MPa/s (Brown, 1981). This rate of loading was found to be too rapid for the schist core, inducing failure in less than a minute. Subsequently failure loading was reduced to 0.1MPa so that failure was generated somewhere between 5 and 10 minutes as specified by the ISRM. The uniaxial compressive strength is calculated as the peak load divided by the original cross-sectional area of the core and given in units of MPa.

Cores were tested at different foliation (schistosity) angles where the foliation angle (β) specified corresponds to the angle between the loading direction (σ_1) and the schistosity in the core (Figure 2-5). For example a foliation angle of 0° corresponds to schistosity being parallel to the core axis (and parallel to the loading direction), while 90° corresponds to schistosity orientated perpendicular to the core axis (and perpendicular to the loading direction).

b) Results

All core tested during this project behaved in a brittle manner and failed by one or a combination of the modes described by Hawkes and Mellor (1970):

1. Cataclasis → General internal crumbling of the test specimen by formation of multiple cracks in the direction of the applied load
2. Axial Cleavage → Vertical splitting of the test specimen in which one or more major cracks split the test specimen along the loading direction
3. Shear → Shearing of the test specimen along a single oblique plane (which may or may not be controlled by schistosity).

The only previous UCS testing available for the mine site was that by Woodward Clyde (1997) where strengths on 11 samples of "unweathered grey schist" were measured ranging between 5.9 MPa and 39.2 MPa, with an average strength of 22 MPa.

A summary of the UCS test results is presented in Table 2-3 and photographic records of the core samples prior to and after testing are presented in Appendix C2. During preparation of the core, three of the samples (AP/UCS 5, AP/UCS 10 & AP/UCS 20) broke along schistosity indicating the weak fissile nature of the rock parallel to schistosity.

Table 2-3 shows that peak schist strengths from UCS testing during this study ranged between 4.8 MPa and 61.2 MPa, with an average calculated strength of 23.7 MPa. Saturated densities for the schist core samples tested here ranged between 2 679 kg/m^3 and 2 854 kg/m^3, with an average saturated density of 2 723 kg/m^3. UCS versus foliation angle for the different lithotypes tested here, combined with the results of UCS testing undertaken by Woodward Clyde Ltd (1997) on grey schist, are presented in Figure 2-3.

Table 2-3: Uniaxial compressive strength test results.

Sample No.	*Length (mm)*	*Upper Core Diameter (mm)*	*Lower Core Diameter (mm)*	*Average Core Diameter (mm)*	*Cross-sectional Area (mm^2)*	*L/D Ratio*	*Volume (mm^3)*	*Saturated Weight (g)*	*Saturated Density (kg/m^3)*	*Angle of Foliation[1] (β)*	*Load at Failure (kN)*	*UCS (MPa)*	*[Corrected UCS[2] to L/D=2 (MPa)]*	*Description of Core*	*Failure Description*
AP UCS 1	172.3	83.0	82.8	82.9	5398	2.08	930003	2523	2 713	75°	275	**50.9**	**[51.2]**	Unweathered, dark greenish-grey, strong , semi-psammite, containing two bands of pelitic schist.	Combined cataclasis/cleavage. Dominant fractures are a conjugate set orientated at 35° either side of σ_1. Also axial fracture at top of core along quartz vein.
AP UCS 2	160.6	83.0	82.9	83.0	5404	1.94	867897	2325	2 679	80°	191	**35.3**	**35.2**	Unweathered, grey, semi-pelite schist containing fine limonite bands parallel to foliation	Combined cataclasis/cleavage. Dominant fracture lies 35° from σ_1. Fractures parallel to foliation also present
AP UCS 3	174.1	83.0	82.9	83.0	5404	2.10	940852	2566	2 728	70°	110	**20.4**	**[20.5]**	Unweathered, greenish grey, slightly contorted psammite schist.	Combined cataclasis/cleavage. Failure changes from a conjugate set of fractures laying 20° either side of σ_1, which join and form single axial stepped fracture at other end of core. Crushing is present in the transition zone between these two fracture types.
AP UCS 4	171.3	83.0	82.9	83.0	5404	2.07	925721	2576	2 783	remnant @20°?	94	**17.4**	**[17.5]**	Unweathered, yellowish-white to black, cataclastic schist containing some remnant structures orientated at 70°	Cataclastic. Lots of fracturing and crushing at top end of core.
AP UCS 5	CORE BROKEN WHILE CUTTING DURING SAMPLE PREPARATION														
AP UCS 6	174.6	82.9	83.0	83.0	5404	2.10	943554	2543	2 695	80°	47	**8.7**	**[8.8]**	Unweathered, dark greenish-grey, semi-psammite schist; contains annealed fractures at 30° and quartz veins at ≈70°	Shear. Failure formed along single fracture plane at 45° from σ_1 stress direction.
AP UCS 7	175.2	82.9	82.9	82.9	5398	2.11	945656	2561	2 708	70°	186	**34.5**	**[34.7]**	Unweathered, grey, semi-pelite schist; cut by two sets of quartz veins at 30° and 55°	Combined cataclasis/cleavage. Failure formed by a combination of fractures along foliation and quartz veins (55°) and newly formed fractures through intact material at 35° from σ_1.
AP UCS 8	175.6	83.1	83.1	83.1	5424	2.11	952394	2566	2 694	80°	156	**29.5**	**[29.0]**	Unweathered, dark grey, pelite schist; containing quartz veins at 45°.	Shear. Failure formed along single plane 40° from σ_1 stress direction.
AP UCS 9	171.6	83.2	83.0	83.1	5424	2.06	930699	2510	2 697	30°	26	**4.8**	**[4.8]**	Unweathered, grey, semi-pelite schist; core slightly contorted at one end (refer photo)	Shear. Failure formed along single plane concordant with foliation.
AP UCS 10	CORE BROKEN WHILE CUTTING DURING SAMPLE PREPARATION														
AP UCS 11	172.6	82.8	83.0	82.9	5398	2.08	931622	2504	2 688	remnant @20°?	84	**15.6**	**[15.6]**	Unweathered, foliated, greyish black cataclasite schist cut by large quartz vein. (NB chips in end of core corresponding to about 2cm loss in surface area)	Combined shear/cataclasis. Shear failure formed along remanent foliation with cataclastic failure at top of core.
APUCS 12	165.7	83.1	83.1	83.1	5424	1.99	898699	2447	2 723	-	160	**29.5**	**[29.5]**	Greyish black structureless, cataclastic schist; containing annealed fracture at 40°.	Combined cataclasis/cleavage. Conical type failure with disintegration of centre of core into fine material .
AP UCS 13	167.0	60.8	60.9	60.9	2908	2.74	485655	1347	2 773	75°	178	**61.2**	**[63.4]**	Unweathered, dark grey, pelite schist; containing some discrete quartz veins at 80°.	Combined shear/axial. Shear failure formed at 45° to σ_1 stress direction, with axial fracture passing through top of core which is terminated against shear fracture.
AP UCS 14	150.8	60.9	61.2	61.1	2927	2.47	441431	1260	2 854	25°	53	**18.1**	**[18.5]**	Unweathered, grey, pelite schist	Shear. Failure fracture formed along foliation
AP UCS 15	171.5	60.9	60.9	60.9	2913	2.82	499561	1363	2 729	≈40°	29	**10.0**	**[10.3]**	Unweathered, slightly contorted, greenish-grey, psammite schist	Stepped shear. Stepped shear failure cutting across foliation with general trend 30° from σ_1.
AP UCS 16	168.4	60.9	60.9	60.9	2913	2.77	490531	1350	2 752	0° (contorted)	37	**12.7**	**[13.2]**	Unweathered dark grey, vertically contorted semi-pelitic schist.	Combined axial/shear. Refer to photo.
AP UCS 17	167.3	61.2	61.0	61.1	2932	2.74	490533	1334	2 720	70°	62	**21.1**	**[21.9]**	Unweathered dark grey, pelite schist; containing fine limonite laminae parallel to foliation	Shear. Formed along limonite laminae parallel to foliation
AP UCS 18	156.4	61.1	61.2	61.2	2937	2.56	459324	1232	2 681	85°	40	**13.6**	**[14.0]**	Unweathered, dark grey, pelitic schist	Shear. Failure formed along shear plane (40° from σ1, with additional fracturing of material parallel to foliation.
AP UCS 19	168.7	61.0	61.1	61.1	2927	2.76	493829	1321	2 675	80-85°	60	**20.5**	**[21.2]**	Unweathered grey, semi-pelite schist.	Axial or shear?. Single failure plane cutting through core at steep angle ≈80°
AP UCS 20	CORE BROKEN WHILE CUTTING DURING SAMPLE PREPARATION														

[1] See main text for description
[2] As proposed by Protodyakonov (1969 in; Vutukuri et.al., 1974)

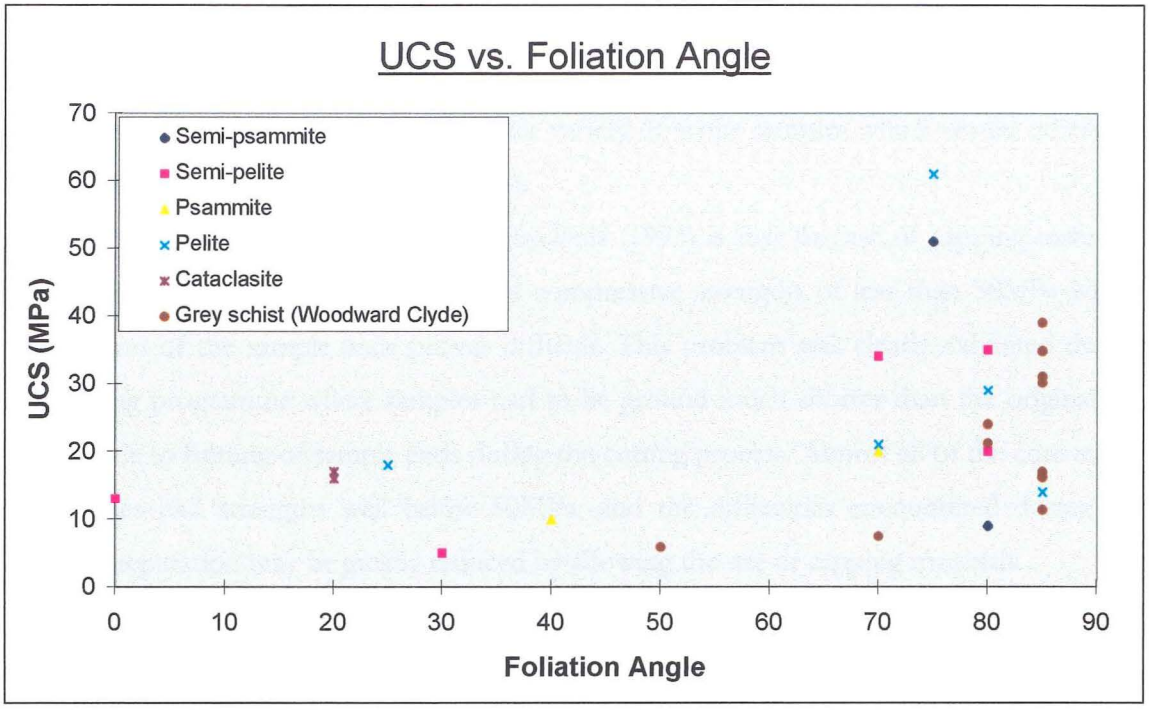

Figure 2-3: Uniaxial compressive strength versus angle of foliation in core (90° foliation angle corresponds to foliation parallel to core axis).

c) Discussion

Suitability of ISRM Guidelines for UCS Testing at Macraes

As with any core testing there is a strong sampling bias in the strength values measured due to the weaker rock in the drill core being broken into unsuitably small lengths for testing. For this reason Pells (1993) has suggested that the guidelines outlined by the ISRM are often too stringent and that weaker rock can be tested at shorter lengths standardised to a L/D ratio of 2 as proposed by Protodyakonov (1969 in; Vutukuri et. al., 1974):

$$\sigma_{c2} = \frac{8\sigma_c}{7 + 2d/h}$$

where σ_{c2} = corrected uniaxial compressive strength corresponding to standard specimen with L/D=2;

σ_c = measured uniaxial compressive strength;

d = specimen diameter and;

h = specimen height;

UCS strengths were corrected according to this formula are presented in Table 2-3. For the schist material at Macraes the application of this correction factor seems appropriate since it would allow the testing of a greater variety of schist samples which would otherwise be excluded by their geometry (Figure 2-4).

Another suggestion put forward by Pells (1993) is that the use of capping materials should be allowed on rocks with uniaxial compressive strengths of less than 50MPa where preparation of the sample ends proves difficult. This problem was clearly exhibited during this testing programme where samples had to be ground much shorter than the original cut length, due to fretting of sample ends during the cutting process. Almost all of the core tested at Macraes had strengths well below 50MPa, and the difficulties encountered during the sample preparation may be greatly reduced by allowing the use of capping materials.

Figure 2-4: Core box at Macraes showing cause of sampling bias in core selection for UCS testing. The schist in the bottom two rows of the core box is more heavily broken into shorter lengths along schistosity than the schist in the top two rows of the core box, making it unsuitable for testing according to the ISRM guidelines. Core size is HQ = 61mm diameter (Hole No. DDG31 - Box 29, 88.75m -91.75m).

Previous Work

Previous UCS testing undertaken by Woodward Clyde (1997) at Macraes on "unweathered grey schist" found strengths ranging between 5.9 MPa and 39.2MPa, with an average schist strength of 22 MPa (Figure 2-3). The strengths measured during this project as such compare very closely, although both higher (c.f. 61.2 MPa) and slightly lower (c.f. 4.8 MPa) strengths were recorded here.

A summary of the UCS test results for Macraes, and those measured at other locations in Otago, is presented in Table 2-4. From Table 2-4 it can be seen that strengths of schist at Macraes are generally much lower than those previously determined at Maniototo and Clyde. The much higher schist strengths at these other locations suggest that it is optimistic to extrapolate strength data from these projects to Macraes.

Table 2-4: Summary of UCS schist strengths at Macraes, Maniototo and Clyde.

Site	Range (UCS)	Mean (UCS)
Macraes (this project; β= 0° - 85°)	4.8 MPa - 61.2 MPa	23.7 MPa
Macraes (Woodward Clyde; β = 50-85°)	5.9 MPa - 39.2 MPa	22 MPa
Maniototo[1] (β=90°)	28 MPa - 86 MPa	53 MPa
Maniototo[1] (β=0°)	9 MPa - 46 MPa	29 MPa
Clyde[1] (β=90°)	61.4 MPa - 105.5 MPa	86 MPa
Clyde[1] (β=0°)	33.6 MPa - 72.5 MPa	46.9 MPa

[1] Sourced from Riddolls and Grocott (1997)

Lithological Strength Variations

From Figure 2-3 it appears that the pelitic schist tested is generally stronger than psammitic schist. This lithological strength variation contrasts with previous UCS testing undertaken on schist material from Otago by Moody at Maniototo (1995) and Macfarlane at Kawarau (1984; 1985). Both Moody and Macfarlane found that strengths were lower in the more micaceous material (pelitic schist) as fractures formed preferentially along these micaceous layers.

Two explanations are offered for these lithological strength variations at Macraes. Firstly, higher strengths for pelitic schist may merely reflect sampling bias and that it is only because a limited amount of samples have been tested that the pelitic schist appears stronger. More testing is required, however, to verify whether this is the case. Secondly, pelitic schist dominates within the Hyde-Macraes Shear Zone (HMSZ) while psammite schist dominates in

both the hanging wall and footwall, above and below the HMSZ. It may be that there are annealing processes associated with mineralisation of the shear zone that increase the strength of the pelitic schist and/or decrease the strength of the psammite schist. The relatively high strengths measured on the 'cataclastic' material from within the HMSZ also suggests that annealing processes may be responsible for some of the higher strengths for pelitic schist material. The effects of annealing processes on schist strengths at Macraes has not been further investigated by this project.

Strength Anisotropy

A substantial amount of work has been dedicated to determining the mechanical behaviour of anisotropic rocks and Kwasniewski (1993) provides an up to date summary of this work. In anisotropic rocks, such as schist, one would typically expect the UCS to decrease as the foliation angle (β) is increased from around 0° - 30°, be at a minimum from angles 30° - 60°, and then increase from 60° to 90° (Kwasniewski, 1993; Figure 2-5). The true nature of the trend between foliation angle and uniaxial compressive strength at Macraes is difficult to determine in this study due to a lack of core tested at foliation angles less than 70°. Figure 2-3 does seem to lend support to this relationship proposed by Kwasniewski for schist at Macraes, however much more testing is required to verify the exact relationship.

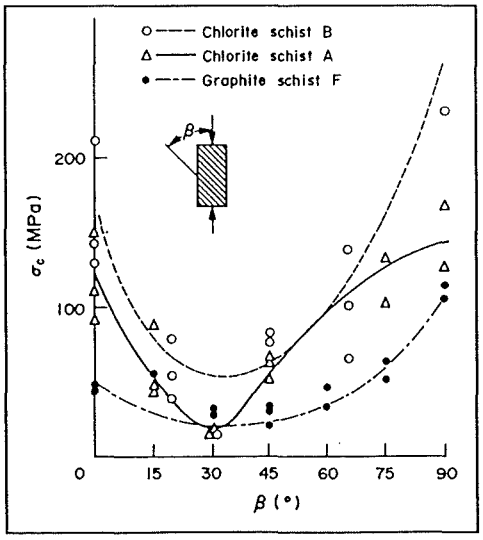

Figure 2-5: Anisotropy of uniaxial compressive strength of two chlorite and one graphite schist (after Akai et. al.,1970 and Akai, 1971; in Kwasniewski, 1993)

2.3.3 Point Load Testing

a) Introduction

Point load testing was undertaken to supplement UCS test data for the characterisation of the rock mass strength. As noted earlier intact rock strengths are of importance when considering those failures that involve breakage through intact rock. Initially developed by Broch and Franklin (1975) the point load test is a technique which allows the rapid estimation of rock strength from either irregular lumps or drill core samples in the field or laboratory. Point load testing was undertaken in accordance with the ISRM suggested methods (1985) and details of the test method and calculations are presented in Appendix C3.

The point load strength, I_s in MPa, is calculated as the ratio of the failure load to the square of the platen separation at failure. The size of the sample has an effect on the strength, and values are therefore calibrated back to a standardised platen separation of 50mm referred to as $I_{s(50)}$ (Brook, 1985). Point load testing has the distinct advantage over UCS testing in that smaller samples may be tested and there is no requirement for sample preparation. The ability to test smaller samples means that point load testing does not suffer the same test sampling bias which UCS testing does, and that quantitative strength data may be obtained for small schist samples which would otherwise be excluded from UCS testing.

Schist samples on which point load testing was performed consisted of both irregular lumps (136 samples) and drill core samples (116 samples). Because schist has anisotropic strength characteristics, testing was carried out axially (load or platens orientated $\perp$ to schistosity) and diametrally (load or platens orientated // to schistosity). The ratio of axial strength to diametral strength may be referred to as the anisotropy index. The higher the anisotropy index then the greater the strength of the schist when loading is applied perpendicular to schistosity, compared to when loading is applied parallel to schistosity.

b) Results

A summary of the point load test results is presented in Table 2-5. Average corrected ($I_{s(50)}$) point load index values for axial tests ranged from 0.20 MPa (moderately weak) to 3.14 MPa (very strong), with an average index strength of 1.44 MPa (strong). Diametral point load index values as expected were much lower, ranging from 0.03 MPa (weak) to 0.58MPa (moderately strong), with an average index value of 0.26 MPa (moderately weak). In the pelitic schist material tested axial strengths ranged from $Is_{(50)}$ = 0.65 MPa to $Is_{(50)}$ = 2.04 MPa, with an average $Is_{(50)}$ axial strength value of 1.49 MPa. In the psammitic schist material tested axial strengths ranged from $Is_{(50)}$ = 0.20 MPa to $Is_{(50)}$ = 3.14, with an average $Is_{(50)}$ axial strength value of 1.18 MPa.

The anisotropic index for the all the schist material tested at the mine site ranged between 1.3 and 23.0, with an average anisotropy index value for the schist of 7.3. For psammitic schist anisotropy indices ranged from 1.3 to 3.8 (mean = 2.6), while for pelitic schist anisotropy indices ranged from 4.3 to 23 (mean = 10.7)

Table 2-5: Summary of Point Load Testing Results.

Sample No.	Sample Location	Sample Description	Test Type	No of Samples	Average Strength (MPa)		Anisotropy Index	Strength Term[2]
					Axial $Is_{(50)}$ (UCS)[1]	Diametral $Is_{(50)}$ (UCS)[1]		
c/PLT 1	Hole DDG33	Unweathered, grey semi-pelite; with some limonite staining along broken surfaces	Core	20	2.04 (43)	0.23 (5)	9.0	Axial = strong *Diametral* = *(moderately weak)*
c/PLT 2	Hole DDG34	Unweathered, whitish grey, psammitic schist	Core	20	0.20 (4)	0.15 (3)	1.3	Axial = moderately weak *Diametral* = *(moderately weak)*
c/PLT 3	Hole DDG35	Unweathered, whitish grey, semi-pelite	Core pieces	20	1.26 (27)	0.29 (6)	4.3	Axial = strong *Diametral* = *(moderately weak)*
c/PLT 4	Hole DDG31	Unweathered, whitish grey, semi pelite; containing some cubic pyrite crystals	Core pieces	20	1.77 (37)	0.27 (6)	6.6	Axial = strong *Diametral* = *(moderately weak)*
c/PLT 5	Hole DDH127	Slightly weathered, whitish grey, psammitic schist	Core pieces	16	1.05 (22)	0.28 (6)	3.8	Axial = strong *Diametral* = *(moderately weak)*
c/PLT 6	Hole RCD2919	Unweathered, dark grey, pelitic schist	Core pieces	10	1.27 (27)	- -	-	Axial = strong
c/PLT 7	Hole RCD1682	Unweathered, dark greenish grey, semi psammitic schist	Core pieces	10	3.14 (66)	- -	-	Axial = very strong
i/PLT 8	RH pit floor (340m RL)	Unweathered, dark greyish black, cataclastic schist	Irregular lumps	28	2.16 (45)	0.58 (12)	3.7	Axial = strong *Diametral* = *(moderately strong)*
i/PLT 9	RH North wall (450m RL)	Highly weathered, dark blackish grey, limonite stained, semi psammitic schist	Irregular lumps	27	0.31 (6)	- -	-	Axial = moderately strong
i/PLT 10	RH western wall (360m RL)	Unweathered, dark grey, graphitic bearing, pelitic schist	Irregular lumps	37	1.97 (41)	- -	-	Axial = Strong
i/PLT 11	RH North wall (450m RL)	Highly weathered, limonite stained, semi-pelitic schist.	Irregular lumps	44	0.65 (14)	0.03 (0.6)	23	Axial = moderately strong *Diametral* = *(weak)*

[1] Assuming calculated correction factor of 21 (see figure 2-5)

[2] Terms after Bell and Pettinga (1983)

c) Discussion

Point load test results lend further support to UCS test results in that at Macraes pelitic schist appears to be stronger than psammitic schist. The most significant thing indicated by point load testing is the range in anisotropy index values (1.3 to 23) for schist at Macraes. It may be possible to attribute the extremely high anisotropy value (23) to the measurement accuracy of the point load equipment at low strength values. Even ignoring this miscellaneous high anisotropy index value of 23, the average anisotropy index value is still 4.8 indicating that the schist material possesses almost five times the strength perpendicular to schistosity as it does parallel to schistosity. This strength anisotropy will have considerable implications when considering the behaviour of intact rock along pit walls where schistosity dips into the pit.

Figure 2-6 shows a tentative relationship between $Is_{(50)}$ values and uniaxial compressive strength values for samples tested at Macraes by this project. While the relationship shows some scatter, the overall trend is good with the average relationship or correlation being given by:

$$UCS = 21 \times I_{s(50)}$$

This correlation factor of 21 compares closely with the generally accepted value of 22 for all rock types by Brook (1985). From Figure 2-6 it must be recognised that the maximum and minimum correlation values may fall anywhere between 16 and 45, and whichever value of correlation is taken for conversion will have a significant effect on the calculated UCS strength. Applying a correlation factor of 16 is likely to produce conservatively low values for schist strength, while an assumed conversion factor of 45 in contrast is likely to produce unrealistically high values for schist strength.

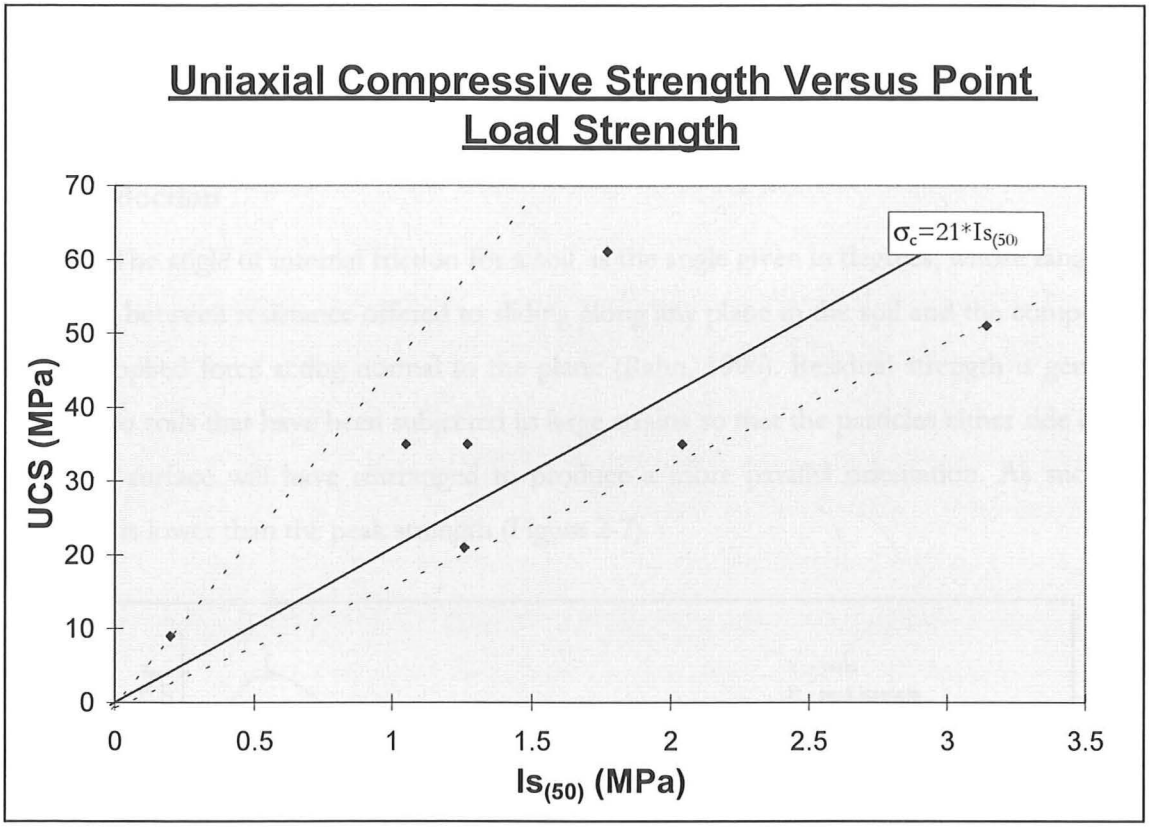

Figure 2-6: Tentative mean linear correlation between corrected axial point load index ($I_{s(50)}$) and unconfined compressive strength (UCS). Solid line represents average correlation trend (=21) while dashed lines represent maximum possible correlation (=45) and minimum possible correlation (=16).

Difficulty in deriving a good relationship between point load and uniaxial compressive strength is largely due to two factors. Firstly, the fact that the trend is derived from seven samples imposes obvious limitations due to natural statistical variance in the data. Secondly, the anisotropic nature of the schist is also likely to impose uncertainties, for example whereas all seven point load samples were orientated perpendicular to schistosity during testing, UCS samples in contrast were generally loaded at slight angles from perpendicularity to schistosity (β=70-85°). Even these slight variations in the schistosity angle between the different test methods are likely to reduce the measured strength value for UCS (as indicated by the high anisotropy index values).

Given the above problems in the conversion of point load index values to UCS it is recommended that $I_{s(50)}$ values be used as a strength measure in their own right and not directly compared with uniaxial compressive strengths. If it is necessary to gauge uniaxial compressive strength from point load index values then this need be done with caution due to the uncertainties outlined above.

2.3.4 Ring Shear Testing

a) Introduction

The angle of internal friction for a soil is the angle given in degrees, whose tangent is the ratio between resistance offered to sliding along any plane in the soil and the component of the applied force acting normal to the plane (Rahn, 1996). Residual strength is generally applied to soils that have been subjected to large strains so that the particles either side of the shearing surface will have rearranged to produce a more parallel orientation. As such the strength is lower than the peak strength (Figure 2-7).

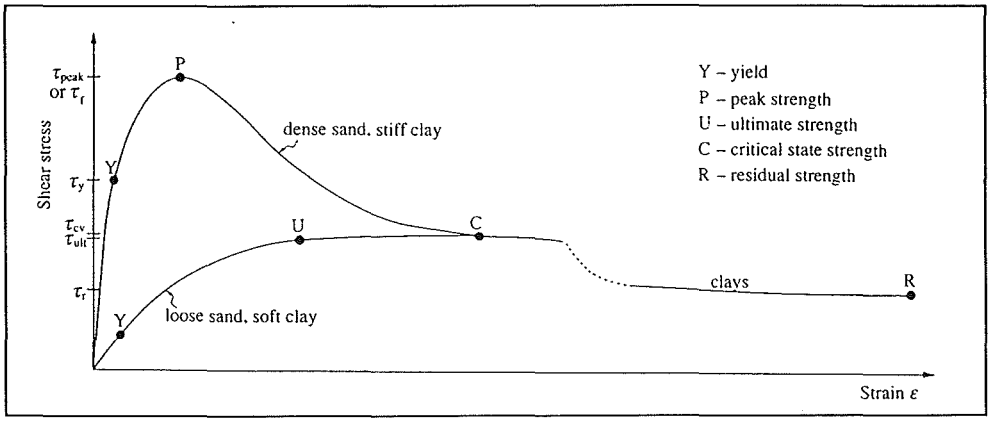

Figure 2-7: Definition of shear failure types in soils (Barnes, 1995).

Samples tested for residual strength were all fault gouge samples collected in the field during the field investigation phase of this thesis. All the samples tested were taken from Round Hill Pit, with four of the samples being taken from failures in the pit (FG1-FG4) while the other two samples were taken from faults not involved in failures at the time for comparison (FG5 & FG6). Sample descriptions and collection locations are given in Appendix C1.

Residual shear strength was measured using a Bromhead ring shear apparatus according to the British standards BS1377:Part 7:1990. Testing was carried out on the material passing a 1.18mm sieve (-0.25ϕ) at normal loads ranging between approximately 50kPa and 500kPa (the approximate limits of the test equipment), with material tested at a moisture content just wet of the plastic limit. The ring shear test methodology is outlined in Appendix C4.

Ring shear testing was chosen over direct shear testing for two principal reasons:

1. The samples are of tectonic origin and in the case of samples FG1-FG4 have been subjected to landslide activity, and therefore essentially represent zones along which high displacements (large strains) have already taken place. Since the material has already been subjected to large strains, one would not expect any real difference in the results measured by peak strength test methods and those measured by residual strength test methods (Wyllie and Norrish, 1996).
2. The fault gouge material contains significant gravel size and larger fault breccia material, which due to limitations in the direct shear equipment needs to be removed prior to testing. Shearing on undisturbed samples therefore is not possible and the ring shear test provides a much better alternative to the shear box (which requires undisturbed samples).

b) Results

The results plots for each of the six samples tested are presented in Figure 2-7 to Figure 2-11. Residual friction angles (ϕ_r) measured during this study were extremely low and ranged between $\phi_r = 3.1°$ and $\phi_r = 6.4°$, with an average $\phi_r = 5.0°$.

During the initial stages of testing some problems were encountered with getting material to reach a residual strength reading. This was attributed to computer software problems as well as the shearing of materials at too rapid a rate. The effect of testing the sample at too rapid a rate caused material to be exuded from out between the rings into the water bath. Consequently the sample became too thin and the upper and lower rings rested on each other before a residual reading could be reached. By slowing the rate of shearing to 0.12°/min (0.08904mm/min) this problem was avoided.

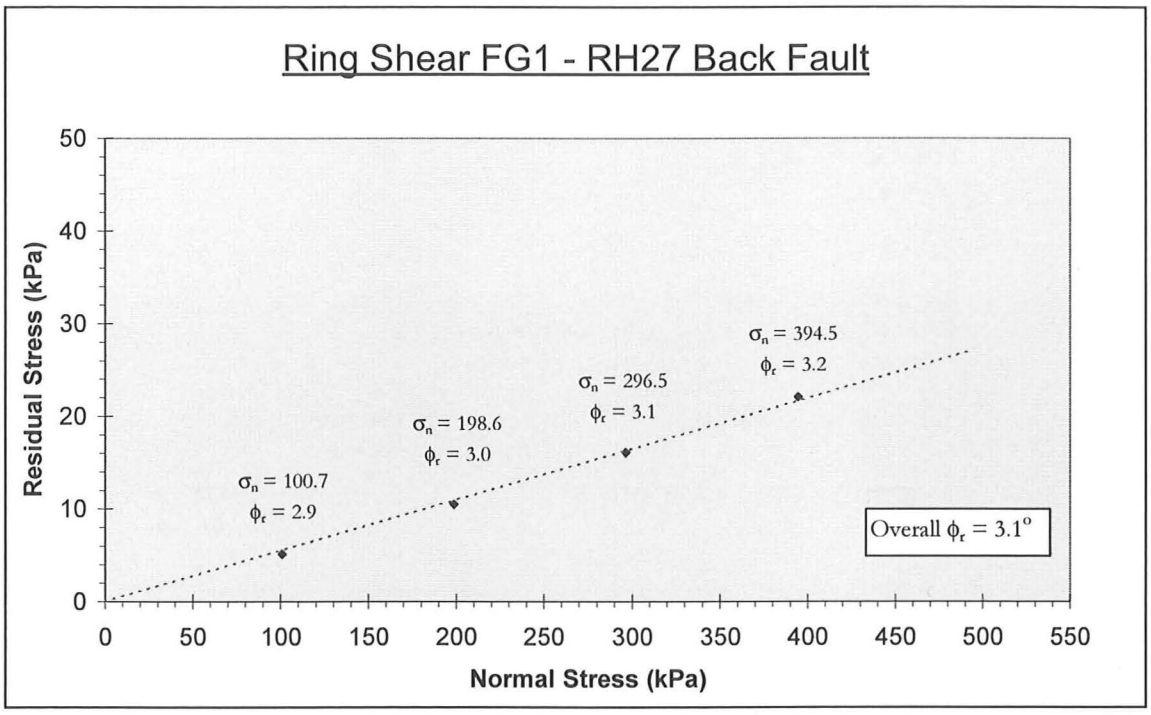

Figure 2-8: A plot of normal stress (σ_n) versus residual shear stress (τ_r) for sample FG1

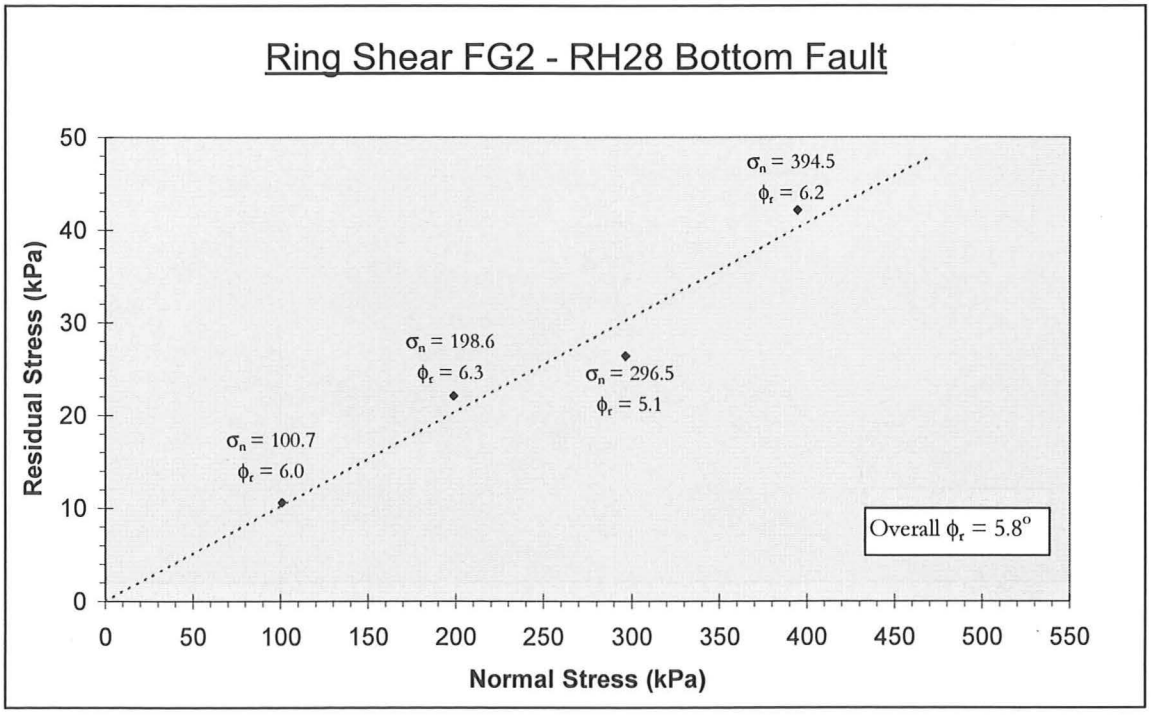

Figure 2-9: A plot of normal stress (σ_n) versus residual shear stress (τ_r) for sample FG2

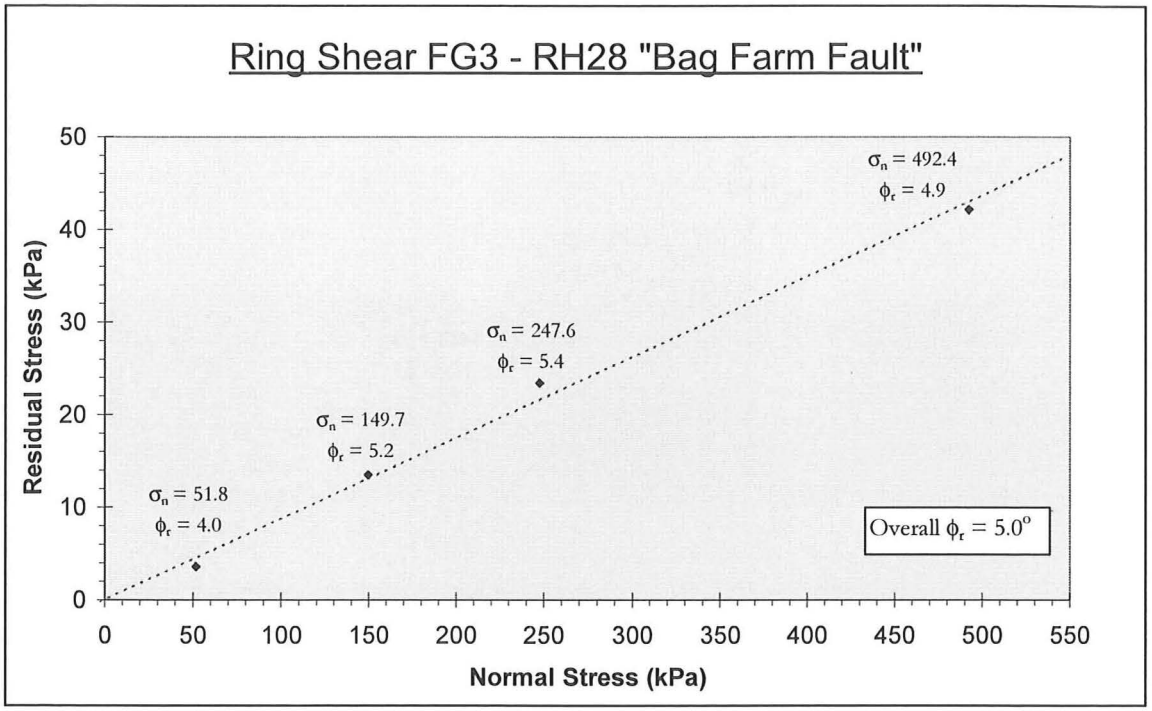

Figure 2-10: A plot of normal stress (σ_n) versus residual shear stress (τ_r) for sample FG3

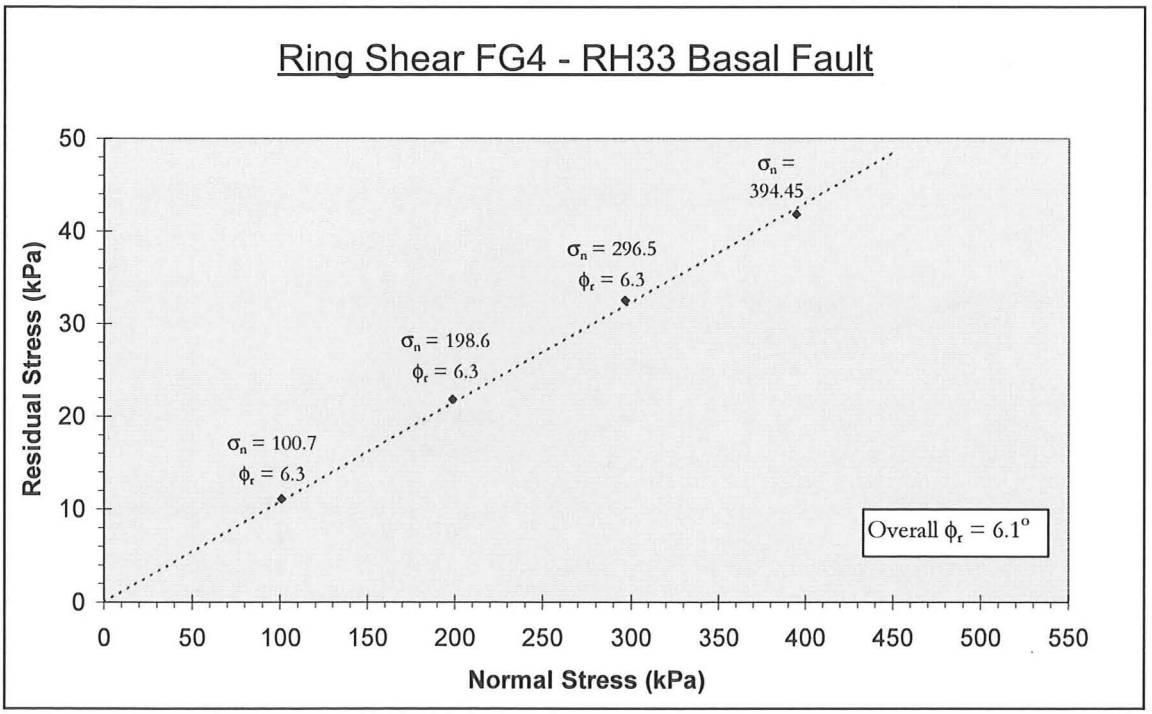

Figure 2-11: A plot of normal stress (σ_n) versus residual shear stress (τ_r) for sample FG4

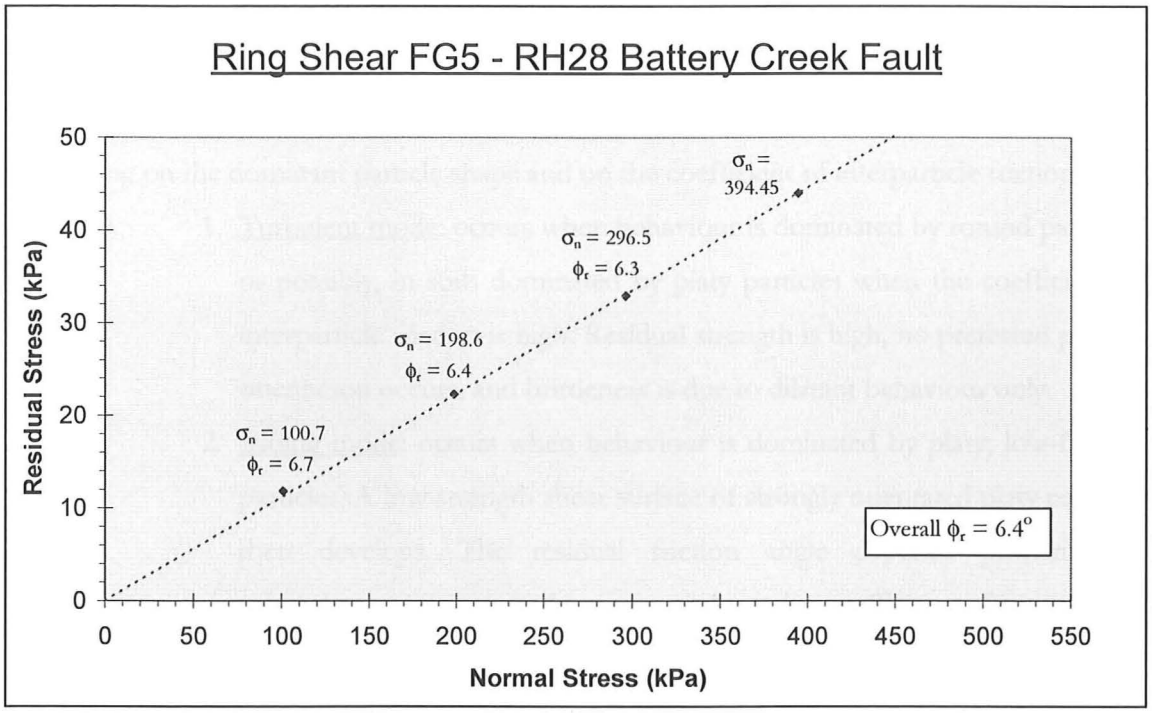

Figure 2-12: A plot of normal stress (σ_n) versus residual shear stress (τ_r) for sample FG5

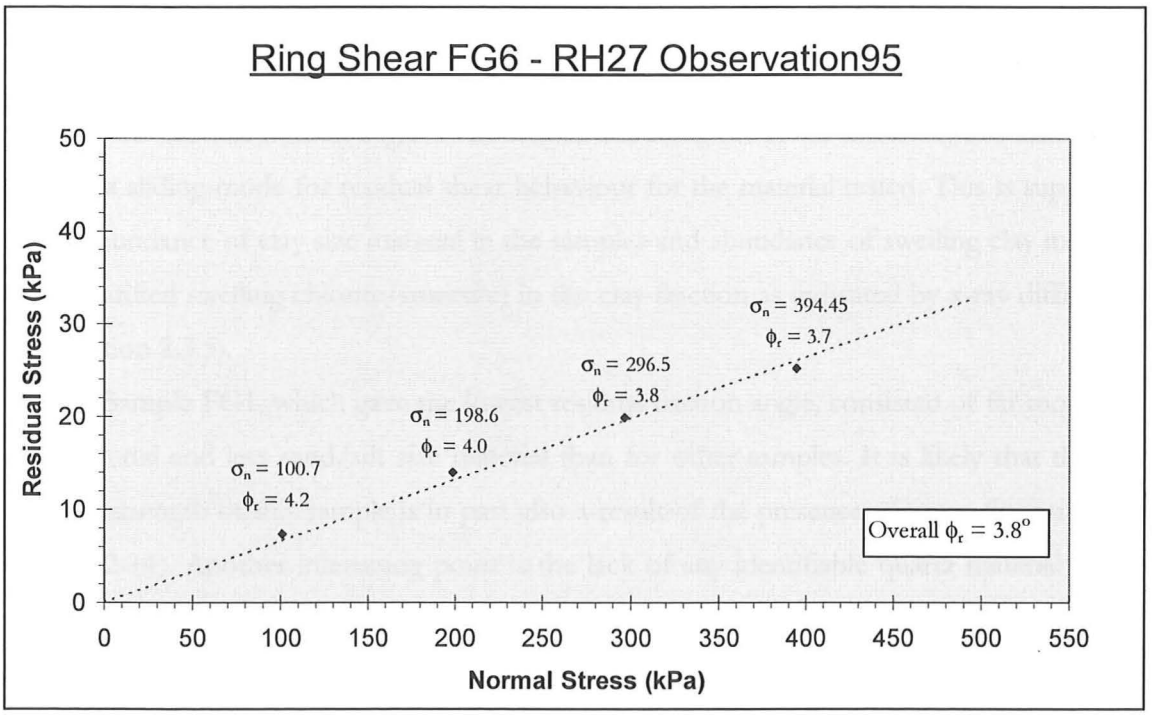

Figure 2-13: A plot of normal stress (σ_n) versus residual shear stress (τ_r) for sample FG6

c) Discussion

Lupini et. al. (1981) recognised three modes of residual shear behaviour in soils depending on the dominant particle shape and on the coefficient of interparticle friction:

1. Turbulent mode: occurs when behaviour is dominated by rotund particles, or possibly, in soils dominated by platy particles when the coefficient of interparticle friction is high. Residual strength is high, no preferred particle orientation occurs, and brittleness is due to dilatant behaviour only.
2. Sliding mode: occurs when behaviour is dominated by platy, low-friction particles. A low strength shear surface of strongly orientated platy particles then develops. The residual friction angle depends primarily on mineralogy, pore water chemistry, and on the coefficient of interparticle friction.
3. Transitional mode: occurs when there is no dominant particle shape, and involves turbulent and sliding behaviour in different parts of the shear zone. In this mode the residual friction angle is sensitive to small changes in grading of the soil, and the changes in grading to cross this range entirely are, typically, small.

The residual friction angles measured in this study are at the extremely low and would suggest a sliding mode for residual shear behaviour for the material tested. This is supported by an abundance of clay size material in the samples and abundance of swelling clay minerals (interstratified swelling chlorite/smectite) in the clay fraction as indicated by x-ray diffraction (see Section 2.3.5).

Sample FG1, which gave the lowest residual friction angle, consisted of far more clay size material and less sand/silt size material than for other samples. It is likely that the low residual strength of this sample is in part also a result of the presence of more finer material (Figure 2-14). Another interesting point is the lack of any identifiable quartz material in the clay fraction of FG1, and this combined with an abundance of swelling clay material may also play a part in the low residual angle measured (see discussion in Section 2.3.5).

Previous testing of fault gouge material (sieved to 600μm) at Macraes by Works Consultancy (1996) measured a residual friction angle of 8.8°, while testing undertaken by Auckland UniServices Ltd. (1996) measured residual friction angles ranging between 10.0° and 26.5°. While the residual strengths measured here differ from those measured by Works

Consultancy and Auckland UniServices it is possible to reconcile the variations in results. Differences in measured residual friction angles may be influenced by sampling technique and sample preparation, or be due to the variations in grain sizes of the material tested by different groups. Variations in ϕ_r may also be attributable to differences in moisture contents and clay mineralogy between samples.

The effects of grain size on residual friction angles in crushed material from the Maniototo power scheme was noted by Moody (1985). Moody noted residual friction angles on crushed material (with a similar clay mineralogy to those tested here) were as low as 6.6° on samples containing 60% clay and only 10% sand, which contrasted with more typical ϕ_r = 14° on more representative crushed zone material containing 29% sand and 10% gravel size material (clay content not given). The effects of increasing clay content on residual friction angle on have also been noted by other workers (Figure 2-14).

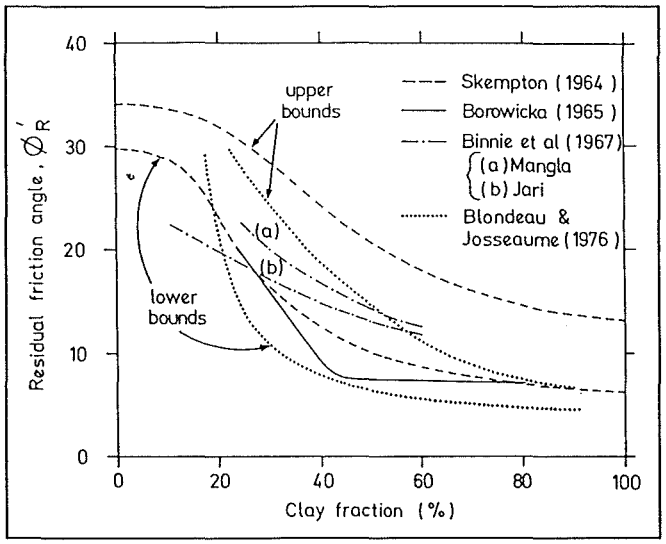

Figure 2-14: Residual strength: correlation's with clay fraction (Lupini et. al., 1981.)

The effects of moisture content and clay mineralogy on residual shear strength were demonstrated by Lupini et. al. (1981), who showed that as the ratio of volume of clay + water to the volume of soil increases then the relative residual shear strength decreases (Figure 2-15). It may be that the samples tested here were at higher moisture contents than those tested by Works Consultancy Ltd. and Auckland UniServices Ltd.

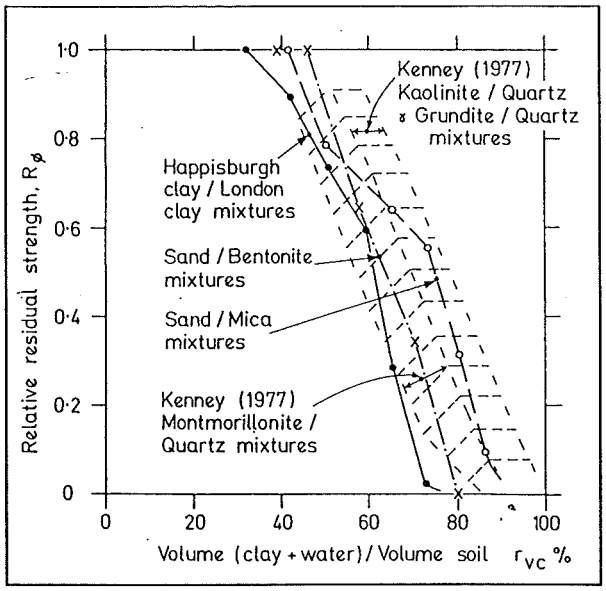

Figure 2-15: Relative residual strength against volume ratio (Lupini et. al., 1981)

2.3.5 X-ray Diffraction (XRD) Analysis

a) Introduction

X-ray diffraction (XRD) analysis is a widely used technique for the identification of clay minerals which cannot be easily identified through more conventional methods such as petrography. In this study the 9ϕ (clay) fraction, taken from six samples of fault gouge material collected from around Round Hill Pit during field investigations, was analysed for clay mineralogy. Five of the six samples (FG1 - FG5) for XRD analysis were taken from the same samples used in ring shear investigations in order to correlate residual strengths with clay mineralogy. Percentages of each mineral present were visually estimated as the proportion of the areas corresponding under each peak for each mineral to the total area encompassed under all peaks for all minerals. The XRD test technique used in this study is presented in Appendix C5.

b) Results

The diffractograms for each of the six fault gouge samples tested are presented in Appendix C5, while Table 2-6 presents a summary of the constituent clay minerals identified in each of the samples tested. Clay minerals identified in all samples were: kaolinite, muscovite, and interstratified swelling chlorite/smectite. The presence of interstratified clays makes identification difficult, however discussions (S. Brown pers. comm., 1996) suggest that the smectite is of the Na variety as opposed to the Mg/Ca variety since in some mounts it is

possible to identify a d-spacing corresponding to 12.5Å, if the smectite were of the Mg/Ca variety then the d-spacing would be expected to lie around 15Å. Trace amounts of quartz were also identified in all mounts except FG1, and some chlorite (non-swelling) was identified in most of the mounts.

Table 2-6: Approximate visual percentage estimates of the mineral composition for the clay mounts analysed using X-ray diffraction.

	FG1	FG2	FG3	FG4	FG5	FG10
Chlorite (Non-swelling)	*trace*	*10%*	*trace*	-	-	*10%*
Kaolinite	*20%*	*30%*	*25%*	*25%*	*20%*	*30%*
Muscovite	*35%*	*35%*	*30%*	*40%*	*35%*	*35%*
Quartz	-	*trace*	*trace*	*trace*	*trace*	*trace*
Swelling Chlorite/Smectite	*45%*	*25%*	*45%*	*35%*	*45%*	*25%*
TOTAL	100%	100%	100%	100%	100%	100%

c) Discussion

XRD testing previously carried out on clay material from gouge material from the Maniototo power scheme by Moody (1985) identified the following mineralogy: smectites, muscovite, kaolinite, chlorite, illite and quartz. Clay minerals identified during this study compare closely with those identified by Moody at Maniototo although no illite was identified at Macraes. A comparison of diffractograms from Maniototo and Macraes, shows there is a far greater percentage of swelling clay material at Macraes than there is at Maniototo.

From an engineering geological viewpoint in terms of pit slope stability the presence of swelling clays, namely the interstratified swelling chlorite/smectite, is extremely significant. In the presence of water these swelling clay minerals will have a similar effect to high pore water pressures by volume expansion and heaving. However the amount of increased instability is difficult to estimate quantitatively.

While quartz was present as breccia in the coarser material, its absence in the finer clay fraction may also be a factor in explaining the low strength values obtained during ring shear testing. Lambe and Whitman (1979) have pointed out that for quartz, the residual friction angle may fall somewhere between 26° and 30°, but for parallel clay particles whose faces are "super smooth", then the friction angle may be below 8° as for those at Macraes. The effects of clay mineralogy on shear strength is also supported by other authors (Horne and Deere, 1961), where for montmorillonitic minerals such as those identified at Macraes residual friction angles may be as low as 4° -10°. The clay mineralogy identified by XRD

clearly explains the low residual friction angles measured during the ring shear testing part of this thesis.

2.4 DISCUSSION AND SYNTHESIS

The principal aim of the engineering geological investigations undertaken during this thesis has been to provide geotechnical input data to assist in the long term performance of the Macraes Gold Mine. Investigations fall into the categories of field investigations, laboratory investigations and desktop investigations (Chapters 3 & 5).

Hydrologic data available for the mine site includes rainfall data, permeability data and piezometric data. Hydrologic data shows that annual rainfall for the mine is 650mm/yr, the permeability of the rock mass ranges between 10^{-7}m/sec and 10^{-8}m/sec, while piezometric data is somewhat difficult to interpret due to variabilities in the recording of information. It would appear that while surficial pit slope failures (<5m deep) generally occur within 24 hours of rainfall, piezometers in contrast indicate that lag times from peak rainfall to reach groundwater deeper and further back into the pit slope, is in the order of one to two weeks, which has significant implications when considering those much deeper seated failures (depth >50m).

Laboratory testing was undertaken in this thesis to determine strength parameters for intact rock and fault gouge. These strength parameters may be used for both the strength characterisation of these features at the mine (and comparison with other locations), as well as assisting in the interpretation and analysis of pit slope stability at the mine.

UCS testing of schist core encountered a number of problems during the sample preparation and this is attributed to the weak fissile nature of the rock parallel to schistosity. It is suggested that because of these sample preparation problems for the schist at Macraes that it may prove of use to ignore some of the guidelines outlined by Brown (1981) and allow both the use of end-capping materials and testing of shorter core lengths. Strengths indicated by UCS testing in this thesis ranged between 5MPa and 61MPa, with a average calculated strength of 24MPa. These strengths are much lower than previously calculated for schist in the Otago region at projects such as Maniototo and Clyde. Analysis of the available UCS test data at the mine site suggests that as previously interpreted the UCS strength varies depending on the angle between the applied load and schistosity (β), with strength decreasing as β is increased from around 0°-30°, be at a minimum from β angles 30°-60°, and then

increase from β angles 60-90°. Much more testing is required to establish the exact nature of this relationship at Macraes.

Point load testing was also undertaken to determine strengths for intact rock at Macraes gold mine for strength characterisation, and to evaluate the strength anisotropy for schist at Macraes when loads are applied perpendicular and parallel to schistosity. While there is more uncertainty with strengths calculated by point load testing, there is a distinct advantage over UCS testing in that no sample preparation is required, and because smaller samples can be tested the method is not as susceptible to sampling bias (although more samples need to be tested for statistical certainty).

Point load testing showed that schist at Macraes is on average around five times weaker when a load is applied parallel to schistosity than when a load is applied perpendicular to schistosity, and this will have considerable implications when considering those pit walls where the schistosity dips into the pit. A tentative site specific correlation factor of 21 for conversion of point load strengths to UCS was calculated for the mine site. Converted point load to UCS strengths may be of use for stability assessment in areas where UCS data is unavailable. It is recommended that the conversion of point load strengths to UCS is applied with a great degree of caution due to the current statistical uncertainty associated with calculation of this correlation factor. Point load strengths are best referred to as a measure of strength of material at the mine in their own right.

Ring shear testing of fault gouge material at the mine site passing a 1.18mm sieve produced very low frictional strengths ranging between 3.1° and 6.4°, which suggests a sliding mode for residual shear behaviour. These residual strength values are very low and lower than those measured by other authors for similar material taken from faults in and around the mine. Differences in values may be attributed to variations in the grain size distribution of material tested, variations in moisture contents, or mineralogical variations.

X-ray diffraction analysis shows that there is a high proportion of swelling clay minerals (smectite/swelling chlorite) in the fault gouge material at Macraes, and this may also explain the low residual shear strengths measured at Macraes. The presence of a high proportion of swelling clay minerals is of significance with regards to pit slope stability at Macraes since any introduction of water into the clay will cause them to swell, in turn increasing the effects that pore water pressures would normally have, by heaving the mass above the clays and reducing the effective normal stress. The amount of instability caused as a result of heaving is difficult to estimate quantitatively.

There are significant variations in both the strength properties for schist, and the strength and mineralogical properties of fault gouge at Macraes, and with data previously determined at other civil engineering projects in Otago. These differences are most likely due to the different geological conditions at each site, and in particular the fact that Macraes occupies a large mineralised shear zone within the schist, which other sites like Clyde and Maniototo do not. Variations observed between testing carried out during this thesis and those conducted at other project locations inevitably means that in most circumstances it is probably not appropriate to extrapolate strength data from these locations, and emphasises the need for site specific engineering geological investigations at Macraes Gold Mine.

CHAPTER 3 : STRUCTURAL DOMAIN ANALYSIS

3.1 INTRODUCTION

Structural domain analysis in this thesis can be regarded as the investigation and delineation of structural characteristics within the rock mass at the Macraes Gold Mine (Hume, 1983), and besides orientation data includes other important parameters such as defect length, defect spacing and defect aperture characteristics (Piteau and Associates, 1977). In this thesis the aim of structural domain analysis has been to divide the rock mass at the Macraes mine into a series of zones/domains having approximately homogeneous geometric fracture characteristics.

Structural domain analysis serves two principal purposes in this thesis. Firstly, analysis was undertaken to check the structural domains previously interpreted by Coffey Partners International Pty Ltd (1992) to see if their earlier structural model still applied at the mine, or if this earlier model could be refined from the data collected during the face mapping of berms at the mine over the past 5 years. Secondly, domain analysis was aimed at assessing the influence of the rock mass structure on pit slope failures at the mine site (see Chapter 5).

3.2 PREVIOUS INTERPRETATION

Consultancy work carried out by Coffey Partners International Ltd. (May, 1992) for MMCL identified two structural domains present within the rock mass at Macraes mine. The boundary to these two structural domains is delineated by the Hanging Wall Shear (HWS) for the Hyde-Macraes Shear Zone (HMSZ), with the Hanging Wall Zone Domain comprising of the rock mass above the HWS and the Ore Zone Domain comprising structures below the HWS.

3.2.1 Hanging Wall Zone Domain (HWZD)

The HWZD comprises the schist above the HMSZ (hanging wall schist), and the main structural features identified in the HWZD by Coffey Partners International Pty. Ltd. (May 1992), in terms of Macraes Mine Grid (MMG), are:

1. Two moderate to steeply dipping fault sets. One dips east while the other dips west, both with an average dip of approximately 60°. Two minor, moderate to steeply dipping fault sets orthogonal to the major sets are also present, with an average dip of 65°. In general both these sets consist of smooth, undulating to curved continuous defects .
2. Shallow dipping shears. The major shear set dips at an average 25° towards the west; an intermediate set at 20° towards the east; and a minor set, which may be a subset of the first at 30° towards the west-north-west. Most are infilled with clay up to 20mm thick, and 60% of those recorded are longer than six metres.
3. A prominent foliation shear set dipping at an average of 25° towards the east following the schistosity. This set is typically smooth, curved and longer than six metres.
4. Three steeply dipping to subvertical joint sets. The major joint set is subvertical with a east-west strike. The two minor joint sets dip at 60° to the east and 70° to the west. Joints are generally less than two metres in length, and rarely greater than six metres. Joint surfaces are generally smooth-stepped to rough-stepped surfaces.
5. A schistosity fabric that predates the HMSZ and parallels the rarely observed bedding, generally dipping at an average of 20° towards the east.

3.2.2 Ore Zone Domain (OZD)

The ore zone domain comprises of schist within the HMSZ (ore schist) and the same discontinuity sets identified in the HWZD are also present in the ore zone, indicating that the structures identified may post date the HMSZ. The main structural difference identified between the HWZD and OZD is that in the ore zone the schistosity principally dips at an average of 15° towards the west (MMG).

3.3 MACRAES GEOTECHNICAL DATABASE

Structural information for discontinuities at Macraes mine has been collected since the onset of present mining activities. Face mapping of newly excavated berms created by mining operations is carried out on a sporadic basis at the mine by both staff and contract geologists. Face mapping involves the selective logging of discontinuity information in much the same manner as normal geologic mapping, with information recorded on a standard recording sheet developed by the mine (Figure 3-1). Defect characteristics recorded include: defect type, dip direction and dip, length, spacing, roughness, Inter-Limb Angle (ILA), infilling, water, and weathering. It must be noted that a substantial amount of the recording terminology used on the sheet is ambiguous (and consequently of limited use), which may better replaced with more accepted standard terminology (refer defect sheet - Appendix F4). For example, water and infilling characteristics are poorly described, while termination of the defect ends is ambiguous since Macraes do not record the termination type at each end of the defect, which standard sheets such as Priest (1993) do.

Faces that have been mapped are then surveyed for the accurate determination of the berm orientation for the face log. By fixing the location of the face log, the discontinuity information recorded may be digitised into the Techbase database programme so that each structural observation has a spatial information locating that discontinuity. Face mapping at Macraes to date has recorded information on 6186 discontinuities and this data is stored in a computer database that will be referred to here as the Macraes Geotechnical Database. This thesis appears to represent the first serious attempt at analysing the information available within the Macraes Geotechnical Database (L. Williams pers. comm., 1996). Information in this database has not been well maintained and as a consequence a number of inconsistencies and errors are present in the database, many of which had to be corrected before my analysis of the data. It was not possible to correct errors in 153 of the records, and the initial 6186 structural records in the database were reduced to 6033 for analysis.

Prima facie the amount of discontinuity information recorded at the mine appears to be substantial, however by the time the information is separated into data above and below the HWS and broken down into its constituent components (schistosity, joints and faults), the available data for analysis for different features is substantially reduced (Figure 3-2). Data coverage across the mine site is also highly variable and while Round Hill pit has the greatest data coverage, the available data for discontinuities in both Innes Mills and Southern pits is sparse (refer to Map sheets 1 - 6b in Map Volume).

DEFECT MAPPING SHEET

Project: Macraes Date: 17/5/95

Location: Round Hill Logged by: SJF

MACRAES

Identification	Traverse		Datum.	Datum. Grid Reference		
	Trend	Plunge		Northing	Easting	RL

Discontinuity				Continuity		Spacing (m)	Roughness		Waves	Filling			Water	Weathering	Identifier
Obs No	Type	Dip Direction	Dip	Length (m)	End		Scale Large	Scale Small	RA	Open	Filling	Thickness (mm)			
5582	rsh	125	10	42	Y	1	und	sm	178	n	br	500	1	2	
5583	slt	253	58	12	n	1	und	sm	175	n	cly	10		2	
5584	nslt	270	57	5	Y	1	und	sm	178	n	cly	5			
5585	nsh	270	36	6	Y	1	und	sm	178	n	cly	5			
5586	slt	078	56	9	n	1	und	sm	178	n	cly	10		2	
5587	slt	086	54	9	n	1	und	sm	178	n	cly	5			
5588	sh	260	30	8	Y	1	und	sm	178	n	cly	15			
5589	slt	110	44	7	Y	1	und	sm	178	n	cly	20		2	
5590	nsh	100	40	12	n	1	und	sm	178	n	br	30		2	
5591	jt	248	48	3	n	3	und	sm	175	Y				2	
5592	nslt	260	47	11	n	1	und	sm	175	n	cly	5		2	
5593	slt	262	45	12	n	1	und	sm	170	n	cly	5		2	
5594	jt	163	62	5	Y	1	und	r	178	Y				2	
5595	jt	190	82	6	Y	3	und	r	175	Y				2	
5596	slt	198	58	10	n	1	und	sm	178	n	br	30		2	
5597	slt	213	47	6	Y	1	und	sm	175	n	br	20		2	
5598	jt	260	42	7	Y	1	und	r	175	Y				2	
5599	slt	087	67	10	n	1	und	sm	178	n	br	1000		2	
5600	slt	087	67	10	n	1	und	sm	178	n	br	400		2	
5601	Rsh	095	12	65	n	1	und	sm	178	n	br	200		2	HW
5602	nsh	095	12	65	n	1	und	sm	178	n	br	300		2	HW
5603	dv	175	80	4	Y	1	und	sm	170	n	qtz	180		2	
5604	jt	230	40	3	Y	2	und	sm	178	Y				2	
5605	slt	105	45	37	n	1	und	sm	175	n	cly	5	1	2	
5606	jt	305	70	6	Y	2	und	r	175	Y				2	
5607	jt	243	36	3	Y	1	und	r	175	Y				2	
5608	jt	214	36	3	Y	3	und	r	175	Y				2	
5609	jt	218	30	3	Y	3	und	r	175	Y				2	
5610	jt	278	57	2	Y	1	und	r	175	Y				2	
5611	jt	290	42	2	Y	1	und	r	178	Y			2	2	

Discontinuities

fol foliation
flt fault
nflt normal fault
rflt reverse fault
sh shear
nsh normal shear
rsh reverse shear
fsh foliation shear
nfsh normal foliation shear
jt joint
dv discordant vein

Roughness

Large	Small
pl planar	r rough
und undulating	sm smooth
st stepped	pol polished

Water	Weathering
1 damp	1 oxidised
2 wet	2 oxide staining

Filling

OPEN
y yes
n no

FILLING
cly clay
br breccia
gu gouge
qtz quartz
cc calcite

Figure 3-1: Standard defect recording sheet used during structural mapping at Macraes

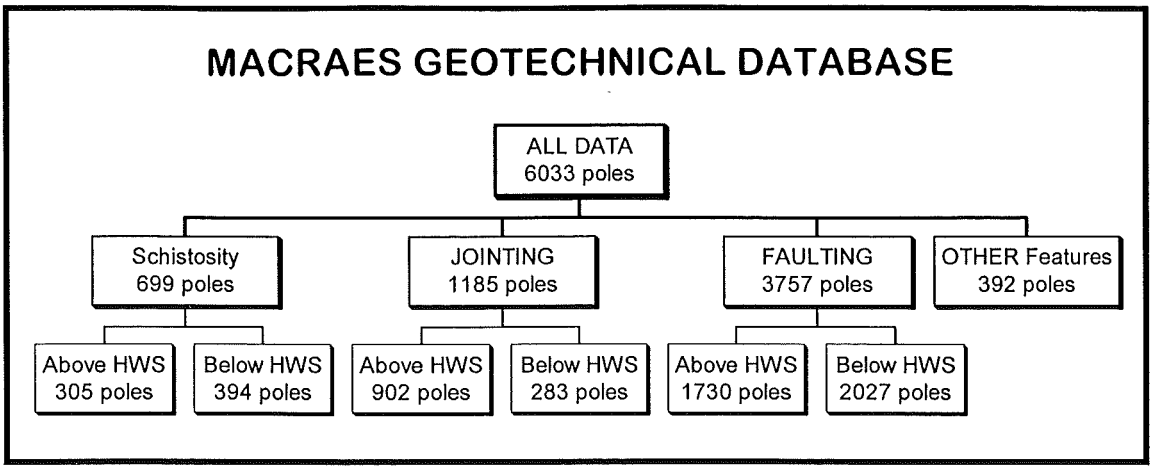

Figure 3-2: Flow chart illustrating break down of geotechnical database into its constituent components and consequent data reduction.

3.4 METHODOLOGY

3.4.1 Introduction

From the beginning of structural domain analysis it was decided that the most important factors that would influence structural domain interpretation were five fold:

1. Insufficient data collection.
2. Lack of good spatial coverage for data that was available.
3. Bias introduced by the method of data collection.
4. Division of the data into above and below the HWS for separate interpretation. The HWS is the largest structure in the area likely to control domain boundaries and it is therefore desirable to select and plot data either side of the HWS for independent interpretation.
5. Lack of information in the database on locations and orientations of major geological structures (other than the HWS) that could be responsible for controlling other structural domain boundaries.

3.4.2 Sampling Bias

Two principal sources of sampling bias arise from the method of structural data collection at the Macraes mine. Firstly, as Priest (1993) points out, in the collection of structural data, a bias is likely to arise due to the selective mapping of features, and here this will be referred to as 'operator bias'. Operator bias may generally be attributed to subjectivities of the data collector. For example, it may be that those features with a greater length, aperture width, etc., are recorded more often as they are more easily observed during data collection. The second source of bias is here called a 'geometric bias' and has been recognised in the field of rock mechanics for some time. Geometric bias arises at the mine site because the number of features mapped on a particular berm will be dependent on the orientation of the features relative to the berm. For example, two discontinuity sets with different orientations but the same spacing will be sampled differently since the apparent spacing, and consequently sampling distance at which observations are measured will be different (Figure 3-3).

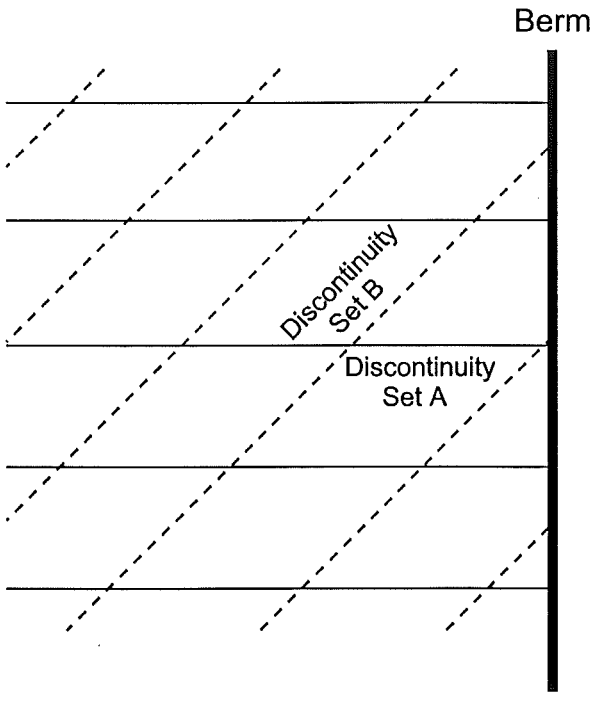

Figure 3-3: Plan view through berm illustrating effect of sampling orientation on observed discontinuity frequency of two discontinuity sets with the same true spacing. Measurements taken along the berm will record more discontinuities in set A (solid line) than set B (dashed line) even if both sets have the same spacing because the apparent spacing of Discontinuity Set A is greater than Discontinuity Set B.

No simple quantitative method exists for correcting the effects of operator bias (Priest, 1993). However it is reasonable to assume that this bias may be dramatically reduced at the mine by making personnel who collect the data aware of the potential for bias. The adoption of one of the more rigorous sampling techniques as outlined by Priest (1993), such as the scanline method or window mapping, will also serve to dramatically reduce operator bias.

A method for correcting the effects of geometrical bias was first put forward by Terzaghi (1965), and this is the method of correction followed here (see Appendix D3 for calculations). To correct for geometric bias each structural observation needs to be tagged with a traverse value. The traverse value is an orientation which corresponds to the orientation of the berm from where the structural observation was measured.

At the time of analysis, structural data collected at the mine came from 340 berms with different orientations. To correct for geometric bias at Macraes it was first necessary to reduce the number of berm orientations to a more manageable number. By stereoplotting the poles to berm orientations and contouring these poles, groupings of berms become apparent which may be grouped by a window which defines both a range in dip and dip/direction (Figure 3-4). Each window grouping of berms may be also characterised by a mean berm orientation (Figure 3-5). This process enabled the initial 340 berm orientations to be grouped into a more manageable number of 24 berm groupings characterised by 24 mean berm orientations. The low variation for the calculated mean berm orientations (Figure 3-5) would suggest that the window groupings chosen for berms at the mine, whilst subjective, were reasonable for the available data.

Structural data was then filtered in Techbase according to the limits of the window groups defined by stereoplotting (Figure 3-4), with each structural observation being assigned the mean berm orientation corresponding to the original berm orientation from where the structural data was initially mapped. Finally, there was some miscellaneous structural data in the database from foundation mapping carried out around the mine plant site. This structural data from foundation mapping had no berm orientations associated with it and was tagged with a traverse orientation of 000/00 (corresponding to horizontal ground).

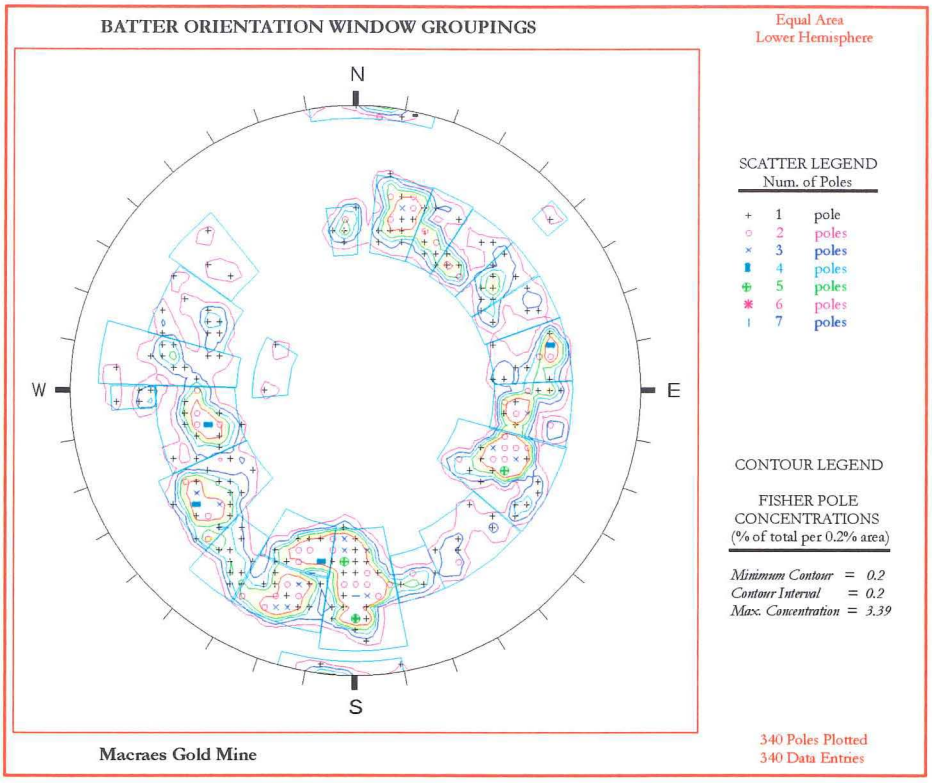

Figure 3-4: Contour plot of poles to berm orientations from Macraes Geotechnical Database and showing window groupings of poles.

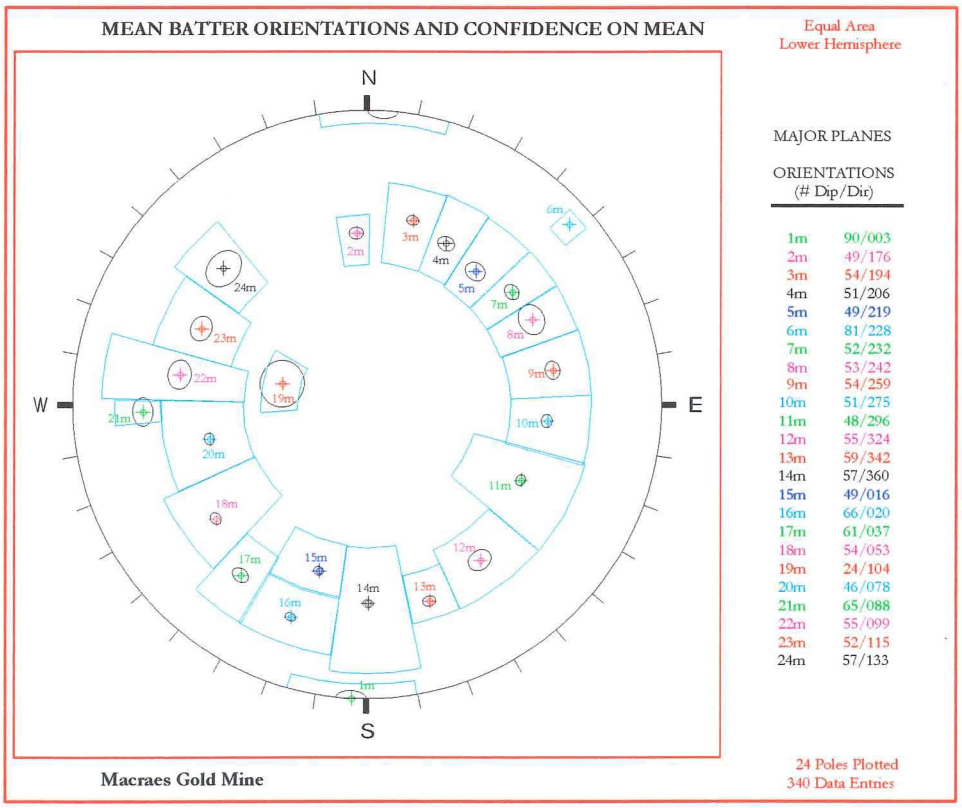

Figure 3-5: Mean batter orientations for window groupings chosen. Circles around poles represent 68% confidence interval that mean pole orientation falls within that circle

The calculation of these mean berm orientations enabled the Terzaghi correction factor for geometric bias (see Appendix D3) to be applied during the generation of stereoplots for structural domain analysis. While assigning structural data values a mean berm orientation rather than their true berm orientation is likely to introduce uncertainties in the calculation of the Terzaghi weighting factor, it was decided that these uncertainties were outweighed by the advantage of being able to correct for the geometric bias, associated with the method of structural data collection at the mine. Without correcting for geometric bias during structural interpretation it was inferred that it could be possible to interpret different structural domains from contour plots purely as a result of geometric bias. As such the errors associated with calculations correcting for geometric bias (because of the use of mean berm orientations rather than real berm orientations) outweighed the disadvantage of not correcting for geometric bias.

3.4.3 Surface Model for Hanging Wall Shear (HWS)

The HWS for the HMSZ is the largest structural feature recognised at the mine and as such is also the most likely feature to control structural domain boundaries. Structural domains previously identified by Coffey Partners International Ltd. (1992) also showed the Hanging Wall Shear as the main feature controlling structural domain boundaries. In order to separate structural records in the Macraes geotechnical database into those above and below the Hanging Wall Shear for separate generation of plots (and the structural domains previously identified), it was necessary to generate a surface model for the Hanging Wall Shear.

Modelling of the Hanging Wall Shear was based on the assumption that the shear approximates a uniform plane along strike and dip in the mine area where structural data has been collected from, and as such can be modelled as a planar surface. This assumption is supported by Figure 1-7 which shows that from the data collected to date the Hanging Wall Shear has a reasonably uniform planar orientation. Assuming the Hanging Wall Shear approximates a uniform plane a first order trend surface of the Hanging Wall Shear data was generated.

The results of modelling of the HWS were excellent and a 98.8% fit to real data was obtained for the trend surface generated. Variance of real data values away from the modelled trend surface ranged between 0.05m and 14.73m. This variance corresponds to the distance between the modelled surface and the height of the actual HWS in reality. The variance equates to less than the height of one berm at the mine, meaning that at most only one berm

height of structural data will be modelled incorrectly; i.e. that data may be modelled above HWS when it is below or vice versa.

Inverse distance modelling as described by Swan and Sandilands (1995) was then used to calculate the height of the generated trend surface at each structural data point location. Each data point was then tagged with an identifier according to whether its height location fell above or below the modelled Hanging Wall Shear surface. The tagging of structural data with an identifier then allows structural data from above and below the Hanging Wall Shear to be selected for separate analysis.

3.4.4 Interpretation Technique

A number of theories have been proposed in the literature for the quantitative determination of structural domain boundaries (Hume, 1983; Piteau and Russell, 1981; Pointe and Hudson, 1985; Wise and McCrory, 1982). Given the problems associated with structural domain analysis at Macraes as outlined in Section 3.4.1, a visual assessment of stereoplots and histograms was chosen as the basis for analysis. As Hume (1983) points out visual methods are probably the most widely used technique for domain delineation because of their simplicity.

A number of advantages were recognised in using a visual method for structural domain analysis at Macraes Gold mine. Visual models are simple to interpret and require little knowledge of complex geostatistics which many of the other methods of analysis rely upon. Geostatistical methods also generally require good data coverage and a large number of points to produce reasonable results (Swan and Sandilands, 1995). As noted above the data coverage of features in the Macraes Geotechnical Database is highly variable and not many points are available for analysis by the time the data has been broken down into its constituent components (Figure 3-2).

The visual method of interpretation used here involves a combination of stereographic plotting of orientation data, and histogram plotting of the distributions of selected discontinuity features. The use of stereoplots for interpretation also allowed for the correction of geometric sampling bias as outlined previously in Section 3.4.2.

There are significant variations in the amount of data coverage between different localities around the mine, meaning the densities of poles on a stereoplot will vary at different localities around the mine. For a fixed counting circle size of 1.0% the significance of any generated contours will depend on the pole densities on a stereoplot. By varying the size of the counting circle the significance of points falling within an area on the stereonet can be

varied and the contours smoothed (Kamb, 1959). Figure 3-6 illustrates the effects of adjusting the size of the counting circle for a plot of 283 poles. As the counting circle is progressively increased the contours are progressively smoothed and noise is removed.

The maximum counting circle that could be used during this project was a 5% counting circle, which meant that approximately 170 poles needed to be present for the generation of statistically significant contour plots. During analysis where plots had less than 170 poles, uncontoured scatter plots were produced instead which, although not contoured, may still be visually compared to contour plots from adjacent areas for similarities and differences.

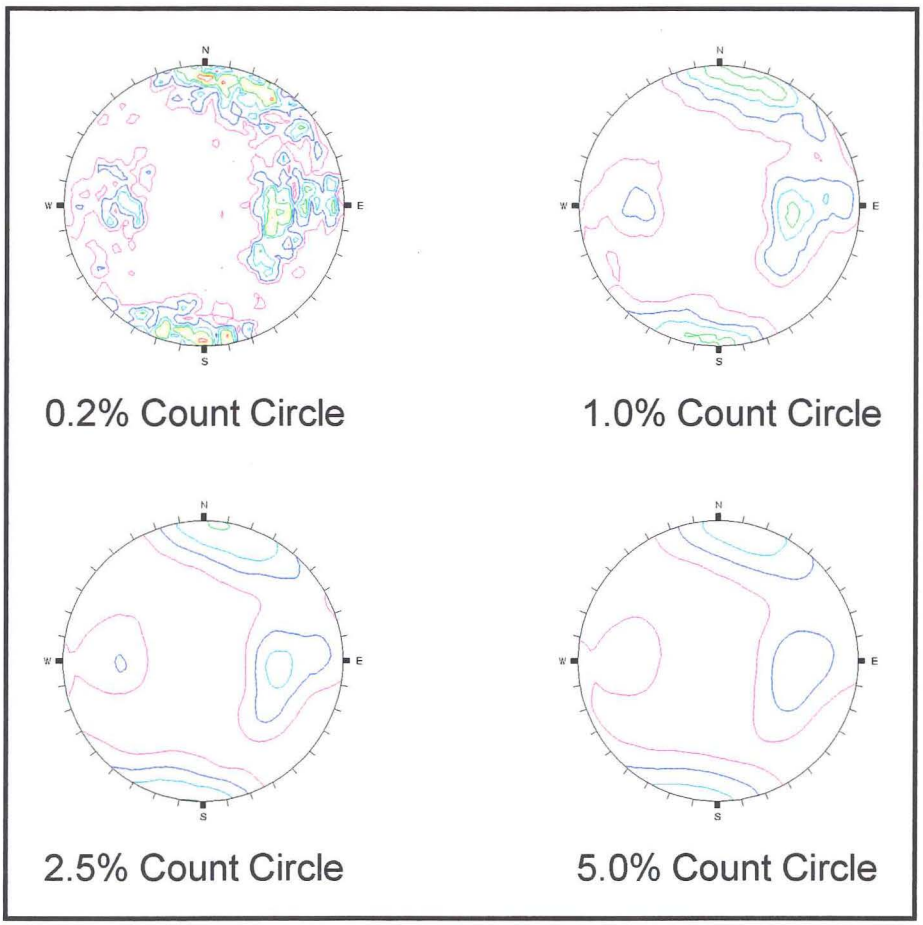

Figure 3-6: Effects of counting circle size on generated contour plot for the same data set. As size of counting circle is increased noise is removed and contours are smoothed. Plots are equal area and generated from 283 poles.

Without information in the database on the locations of the major structural features that may delineate structural domain boundaries, areas were selected subjectively for plotting in a grid-like fashion. Beyond the plotting of basic orientation data, histograms of selected discontinuity properties related to the structures were also plotted. Histograms were used because it was inferred that even if the orientations of structures did not appear to change

between different areas, a change in the histogram distribution for a given discontinuity property between areas may indicate a change in structural domains.

The discontinuity properties that could be chosen for distribution plotting were effectively limited by the amount of available information in the database. For faults the properties plotted between areas were fault length and roughness, while for joints length and spacing properties were selected for histogram plotting and analysis.

Apart from the use of these discontinuity properties in delineating structural domains, discontinuity properties are also of importance with regards to pit slope stability. Length (or continuity) of faults and joints is probably one of the most important features controlling the potential size of failures and potential failure volumes, while roughness may alter the frictional strength of discontinuities, and joint spacing will control the size of failed blocks and the dilatancy of the rock mass during shear displacement (Norrish and Wyllie, 1996). While interpretation of joint roughness would have been desirable for the interpretation of shear strength, not enough roughness data for joints was available within the database to make interpretations for different areas.

3.5 STRUCTURAL INTERPRETATIONS

3.5.1 Schistosity

a) Above Hanging Wall Shear

Interpretation of schistosity above the HWS is presented on Map Sheet 1 (Map Volume) and was taken from 305 observations. Most of observations of schistosity above the Hanging Wall Shear were from Round Hill Pit although 20 observations were available for interpretation outside of Round Hill Pit.

Above the HWS schistosity is more consistent than it is below the HWS, and generally dips at low angles to the east (max. concentration ≈ 15/105; Figure 3-7). Where schistosity does dip to the west, field observations would suggest that this is generally localised and predominantly a result of folding and fault drag on the larger faults in the area.

A comparison between scatter plots outside of Round Hill pit and the contour plot for Round Hill Pit suggests there is little deviation from the general trend described above, and that schistosity continues to dip at low angles to the east in the southern parts of the mining area (refer Map Sheet 1).

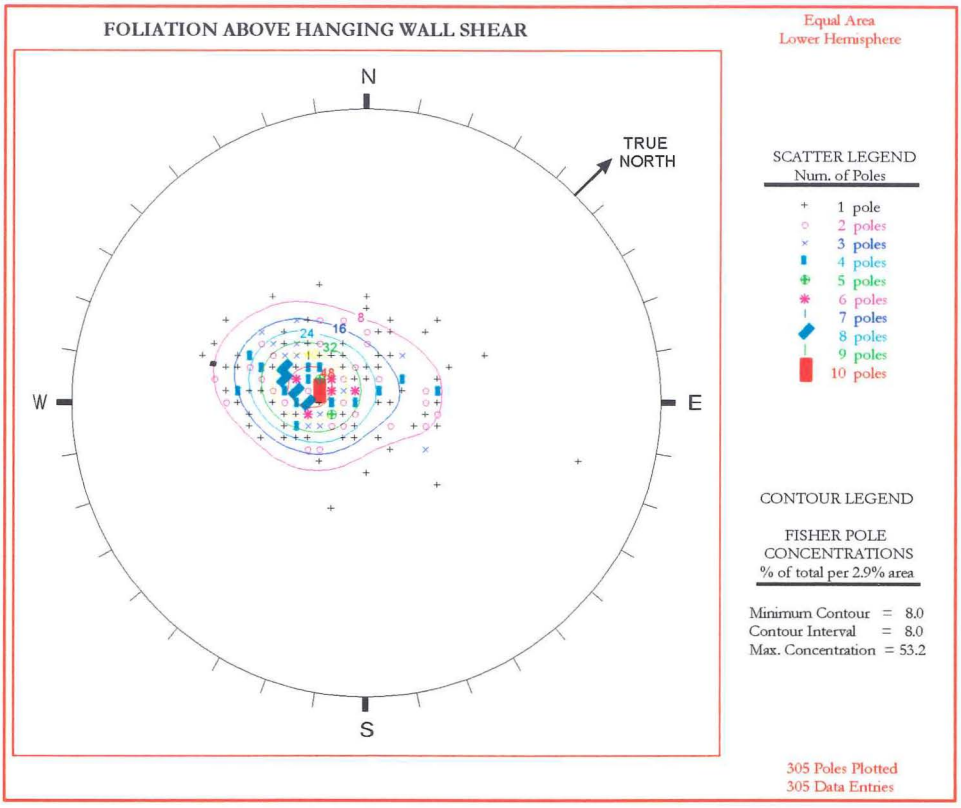

Figure 3-7: Orientation (MMG) of schistosity above the Hanging Wall Shear (all data).

b) Below Hanging Wall Shear

Interpretation of schistosity below the Hanging Wall Shear is presented on Map Sheet 2 (Map Volume) and based on 394 poles. As for above the Hanging Wall Shear, most of the observations of schistosity below the HWS are sourced from Round Hill Pit and interpretation of the structure of schistosity outside of Round Hill pit is not really possible.

Schistosity below the Hanging Wall Shear shows a much greater variation in orientation. Below the Hanging Wall Shear schistosity predominantly dips at low angles to the west (max. concentration ≈ 20/295; Figure 3-8), although there is still a high concentration of easterly dipping schistosity. This greater variation in the orientation of schistosity below the Hanging Wall Shear is interpreted as a product of the higher amount of strain and associated deformation that the schist within the shear zone has undergone.

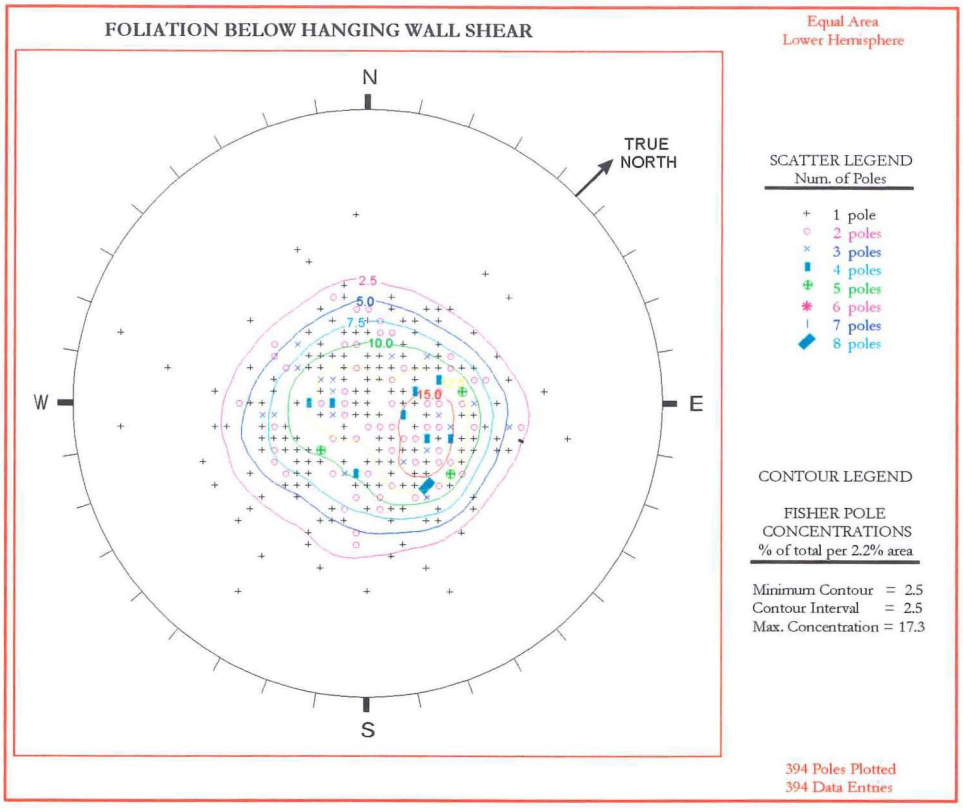

Figure 3-8: Orientation (MMG) of schistosity below Hanging Wall Shear (all data).

Map Sheet 2 suggests that westerly dipping schistosity increases in concentration as one transverses from west to east across Round Hill Pit and towards the main Hanging Wall Shear. It may be that the main cause of westerly dipping schistosity is purely a result of fault drag along the main Hanging Wall Shear, and that schistosity may return to an easterly dip as one gets deeper beneath the HWS. Further field investigations need to be undertaken to check this possibility.

3.5.2 Jointing

a) Above Hanging Wall Shear

Structural domain analysis for joints above the Hanging Wall Shear is presented on Map Sheets 3a & 3b, based on 902 observations. Interpretation shows two dominant joint sets (JA1 & JA2) and one minor joint set (JA3) are evident above the HWS (Figure 3-9; Map Sheet 3a). The mean orientations of each of these joint sets is: JA1 = 45/270; JA2 = 80/190; and JA3 = 50/090. The orthogonal dip orientation between joint sets JA1 and JA3 suggests that these sets may have formed as a conjugate pair of joints.

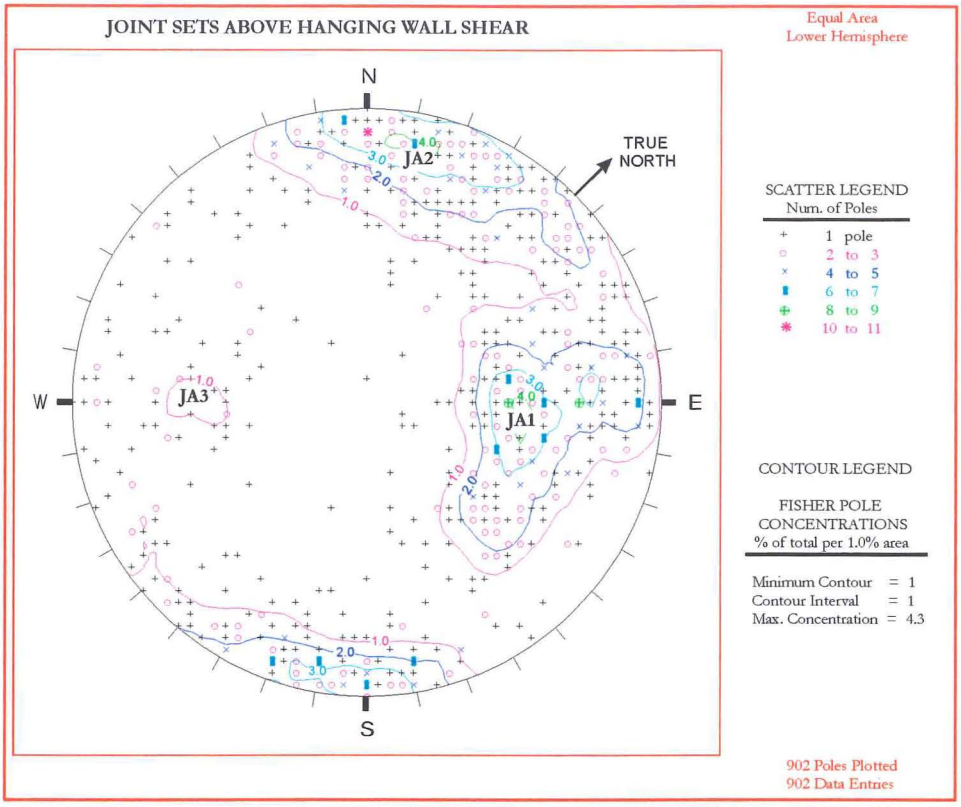

Figure 3-9: Orientation of joint sets above Hanging Wall Shear (all data).

Above the Hanging Wall Shear joint lengths are moderate to high (average 5m; Map Sheet 3b), whilst joint spacing is typically very wide (average 1.7m; Map Sheet 3b). Interpretation of Map Sheet 3b suggests that joint spacing may increase slightly moving south from Round Hill Pit to Innes Mills Pit. This apparent increase in joint spacing to the south may merely reflect operator bias introduced by the time interval between the different areas being mapped. Once again field checking should establish whether the apparent length of joints is real or merely a result of operator bias.

b) Below Hanging Wall Shear

Structural domain analysis for joints below the Hanging Wall Shear is presented on Map Sheets 4a & 4b and is based on 283 observations. As for joints above the Hanging Wall Shear, two dominant joint sets (JB1 & JB2) and one minor joint set (JB3) are evident (Figure 3-10; Map Sheet 4a). The mean orientations for each of these sets are: JB1 = 50/090; JB2 = 75/010; and JB3 = 45/270.

A comparison with jointing above the Hanging Wall Shear shows that while set JB1 has the same orientation as JA3, and set JB3 has the same orientation as JA1, the dominance of the sets is reversed. Once again sets JB1 and JB3 are orthogonal in dip to each other,

suggesting they formed as a conjugate pair. Joint set JB2 also appears to be the same set as JA2, although the dip appears to be more towards the north below the Hanging Wall Shear.

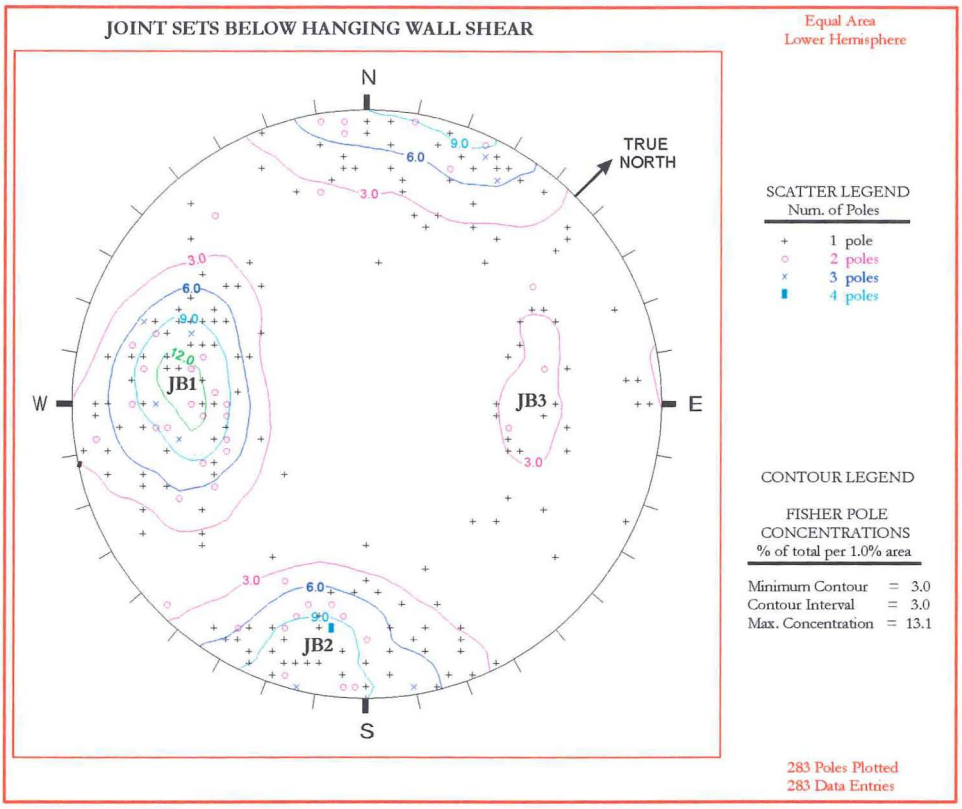

Figure 3-10: Orientation of joint sets below Hanging Wall Shear (all data).

Interpretation of joint length and spacing is presented on Map Sheet 4b. Joint lengths below the HWS across the mine site are generally moderate (average length 4m; Map Sheet 4b), whilst joint spacing is generally very wide (average spacing 1.6m; Map Sheet 4b). Spacing of joints below the HWS shows the same general trend as joints above the HWS, and spacing increases as one moves south from Round Hill Pit to Innes Mills Pit.

3.5.3 Faulting

a) Above Hanging Wall Shear

Structural domain analysis for faulting above the HWS across the mine site is depicted on Map Sheets 5a & 5b (Map Volume), and is based on 1730 observations. Four major fault sets (FA1-FA4) and one minor fault set (FA5) are identified here (Figure 3-11). The orientations of these sets are: FA1 = 60/090; FA2 = 18/090; FA3 = 30/270; FA4 = 45/205; and FA5 = 75/020. Like jointing the orthogonal orientation of sets FA1 and FA3 to each other would suggest that these faults may have formed as a conjugate set. Fault set FA2

has the same orientation as the HWS (Figure 1-7), suggesting that this set of faults has developed as a synthetic set to the main HWS.

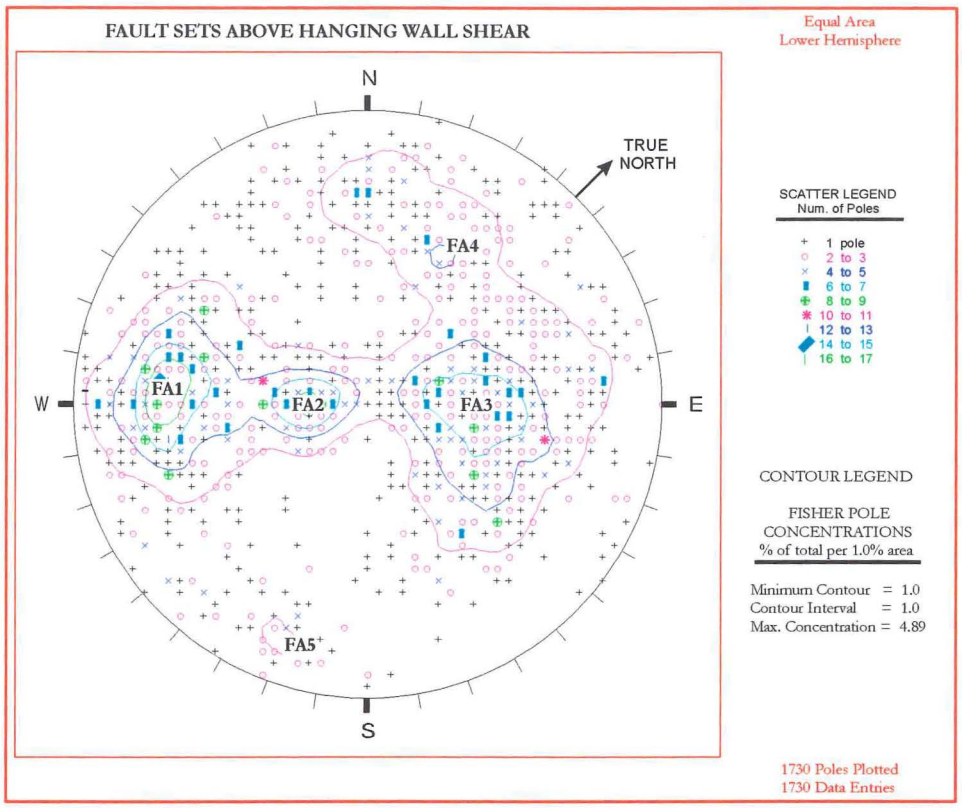

Figure 3-11: Orientation of major fault sets above Hanging Wall Shear.

Map sheet 5a depicts fault orientations above the HWS and shows that fault structure appears to be generally consistent above the Hanging Wall Shear throughout the currently mapped areas of the pits. While fault sets FA4 & FA5 appear absent in some areas, a closer assessment of these areas suggests that the absence of these sets may be attributable to geometric sampling bias. For example, on the plot for the area 69800E to 70000E/14800N to 15100N the absence of sets FA4 & FA5 can be attributed to the wall orientation being nearly parallel to fault sets FA4 & FA5. Even though these fault sets are present in this area as indicated by the presence of poles on the stereoplot, the geometric bias is sufficiently strong that even the application of the Terzaghi correction factor fails to correct for this.

Fault length and roughness profiles above the HWS are presented on Map Sheet 5b. Above the HWS faults typically show a 'very high' continuity with an average length of 13.8 metres. Fault lengths also show a logarithmic distribution, with a few faults being recorded having a length of greater than 100 metres (Map Sheet 5b). Map Sheet 5b also shows that almost all faults throughout the mine site exhibit a roughness profile of 5 (undulating

smooth). The length and roughness profiles of faults appears to be generally consistent across the mine site with little deviation from the trend outlined above.

Movement senses on faults above the HWS shows that of those recorded, fault sets FA1, FA4, and FA5 are almost entirely normal faults, while set FA2 consists almost entirely of reverse faults. Fault set FA3 consists of both normal and reverse faults (see plots in Appendix E).

b) Below Hanging Wall Shear

Structural domain analysis for faults below the HWS across the mine site is depicted on Map Sheets 6a & 6b, and is based on 2027 observations. Three major fault sets (FB1-FB3) and one minor fault set are interpreted below the Hanging Wall Shear (Figure 3-12). The respective orientations of these fault sets are: FB1 ≈ 60/100; FB2 ≈ 18/090; FB3 ≈ 40/275; and FB4 ≈ 65/200.

The structure of faulting below the HWS is almost identical to that above the HWS with corresponding fault sets being: FB1 & FA1; FB2 & FA2; FB3 & FA3; FB4 & FA4. While fault set FB4 corresponds with FA4, below the Hanging Wall Shear FB4 appears to steepen and decrease in concentration.

A review of Map Sheet 6a suggests that the orientations of fault sets below the Hanging Wall Shear is generally consistent across the currently mine area. The only area appearing to deviate significantly from the model outlined above is the area 69300E to 69500E/15200N to 15450N, where detailed foundation mapping was carried out. This disparity can probably be attributed to operator bias during foundation mapping.

Fault length and roughness profiles below the HWS are presented on Map Sheet 6b. Below the HWS fault lengths also show a logarithmic distribution (average length = 12.67 metres) and are typically classed as 'very high' continuity. Map Sheet 6b also shows that fault lengths and roughness profiles are consistent across the mine site with little deviation from the trend outlined above. Movement sense for faults below the Hanging Wall Shear shows the same trend as for faults above the HWS; with FB1 and FB4 consisting of almost entirely normal faulting, FB2 almost entirely reverse faults, and FB3 consisting of both normal and reverse faults (see plots in Appendix E).

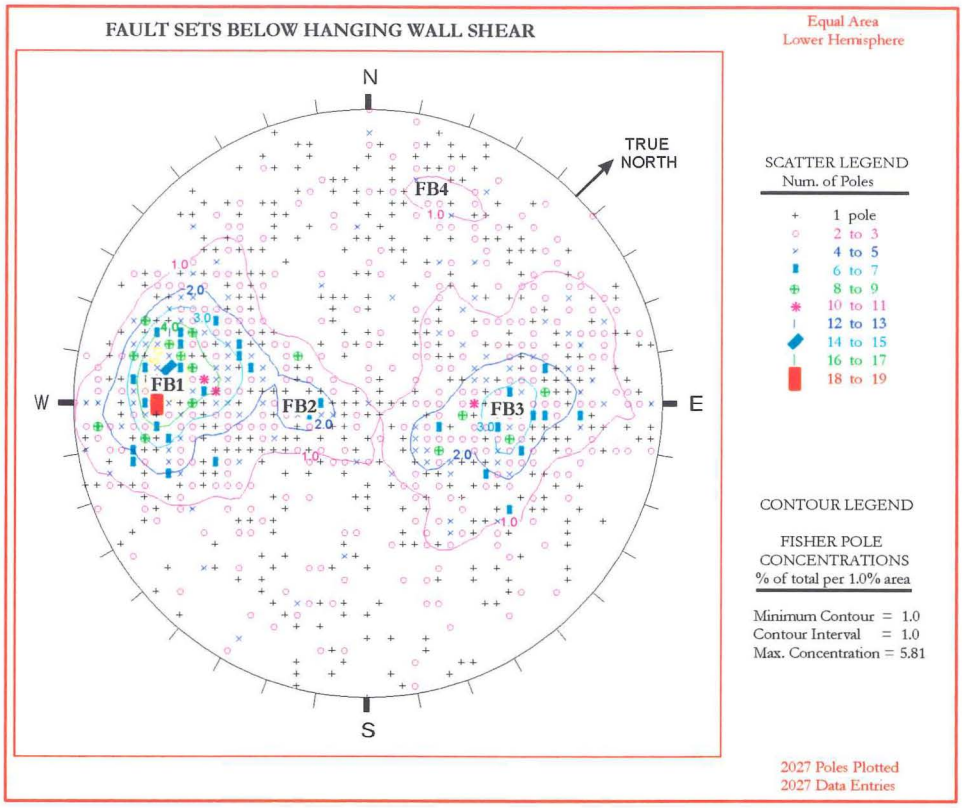

Figure 3-12: Orientation of major fault sets below Hanging Wall Shear

3.5.4 Other Structural Features

The most notable recorded structural features measured during the collection of geotechnical data apart from schistosity, jointing and faulting, are foliation shears (which are very important in terms of pit slope stability). While features such as discordant quartz veins are recorded, these do not represent a break in the rock and because no pit slope failures have been recorded forming along them, they have not been assessed here.

The orientation of foliation shears both above and below the HWS is illustrated in Figure 3-13, and as expected they have a similar orientation to schistosity. Foliation shears above the HWS dip at low angles to the east, whilst below the HWS they generally dip at low angles to the west and east (Figure 3-13). High angle foliation shears below the HWS once again are probably due to high strain within the shear zone, and contortion of foliation shears against the much larger fault structures present in the shear zone. A review of foliation shear properties at the mine recorded in the Macraes Geotechnical Database shows that mean

foliation shear length is 20 metres (although some exceed 100m), most are undulating smooth and have a gouge infilling.

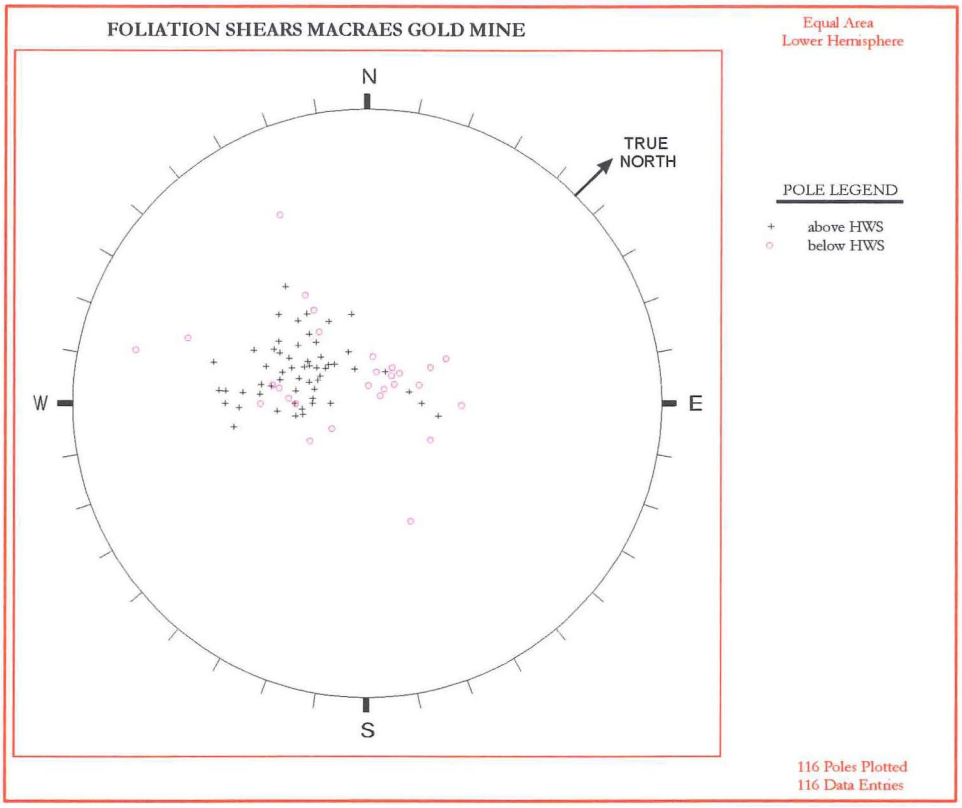

Figure 3-13: Orientation of foliation shears both above and below Hanging Wall Shear.

3.6 INTERPRETATIONS OF STRUCTURAL DOMAINS

No new structural domains are interpreted in this study beyond those previously interpreted by Coffey Partners International Pty. Ltd (1992) as controlled by the Hanging Wall Shear of the Hyde Macraes Shear Zone. Information collected through face mapping of pit slope berms has enabled this earlier model to be refined particularly with regards to the orientations and properties of the discontinuities as follows:

Hanging Wall Zone Domain

1. A regional schistosity that generally dips to the east (15/015) above the Hanging Wall Shear.
2. A set of foliation shears that parallel the schistosity and dips at low angles to the east.

3. Three joint sets are identified above the Hanging Wall Shear. These sets consist of what appears to be a conjugate joint set dipping at moderate angles (≈45°) to the east and west. A further subvertical joint set is also apparent which dips to the south. Joint lengths above the Hanging Wall Shear are moderate to high (avg. = 5m), with a very wide spacing (avg.=1.7m).
4. Four major (FA1 - FA4) and one minor (FA5) fault sets are evident above the Hanging Wall Shear. FA1 and FA3 appear to be a conjugate set of normal faults developed with FA1 dipping at 60° to the east, and FA3 at 30° to the west. FA2 appears to be a synthetic set of reverse faults developed parallel to the main Hanging Wall Shear. FA4 dips at around 45° to the south-west and it appears that the minor fault set FA5 which dips at 75° to the north-east may be a conjugate set to FA4. Average fault length above the Hanging Wall Shear is approximately 14 metres and fault roughness profiles generally fall into the undulating smooth category (class 5).

Ore Zone Domain

1. Regional schistosity is more variable below the Hanging Wall Shear. Schistosity dips at low angles to both the east (as above) and the west (20/295). This greater variability is interpreted as a result of greater deformation and the higher strain within the shear zone.
2. A set of foliation shears developed along the same orientation as the schistosity and predominately dips at low angles to the east and west
3. The same three joint sets as for the Hanging Wall Zone are identified in the Ore Zone. Below the Hanging Wall Shear easterly dipping joints appear to be far more dominant than the westerly dipping joint set. The steeply dipping joint set appears to dip more to the north than the south below the Hanging Wall Shear. Joints lengths are moderate (avg. = 4m), with a very wide spacing (avg.=1.6m).
4. Four of the five major fault sets identified above the Hanging Wall Shear are also present below the HWS. The south-westerly dipping set appears to be far less predominant below the Hanging Wall Shear than above while the minor north-easterly dipping fault set is pretty much absent below the Hanging Wall Shear. Average fault length above the Hanging Wall Shear is approximately 13 metres and fault roughness profiles also generally fall into the undulating smooth category.

3.7 DISCUSSION AND SYNTHESIS

Structural domain analysis involves the delineation of zones of a rock mass into areas of approximately homogenous geometric fracture characteristics. Structural domain analysis was undertaken in this thesis to check and refine the earlier structural domain model interpreted by Coffey Partners International Pty Ltd where two structural domains were recognised at the mine. These earlier interpreted domains are controlled by the main Hanging Wall Shear contact, and are referred to as the Hanging Wall Zone Domain (HWZD) and Ore Zone Domain (OZD). Face mapping of berms exposed in the Macraes pits by mining activities is carried out on a sporadic basis and stored in the Macraes Geotechnical Database at the mine.

Five important factors that influence structural domain interpretation at the mine are: insufficient data; spatial coverage of data; sampling bias; separation of collected data into above and below Hanging Wall Shear; and lack of information on locations of major structures.

Two forms of sampling bias arise as a result of the method of data collection at the mine, and these may be referred to as operator bias and geometric bias. Operator bias is a result of the subjectivity of the person mapping the berm, while geometric bias is a result of the orientations of different structural sets to the berm being mapped. It was not possible to correct for operator bias during this project. It is recommended in the future that personnel mapping pit faces be made aware of the potential for operator bias so that its impact is minimised during the actual face mapping process. The correction of geometric bias involved characterising the 340 berm orientations from which structural data was collected with 25 mean berm orientations. Each structural data value was assigned the corresponding mean berm orientation so that a Terzaghi correction weighting factor could be applied.

The creation of a trend surface for the Hanging Wall Shear and inverse distance modelling of this surface enabled structural data to be separated into above and below the HWS for separate interpretation. A 98.8% fit was calculated for the modelled trend surface of the Hanging Wall Shear to real data. It is recommended in future data collection that all data be tagged with an identifier according to the position of the observed structural feature relative to the main Hanging Wall Shear so that there no error associated with the position of structural features in relation to the Hanging Wall Shear.

A number of techniques have been proposed in the literature for the determination of structural domain boundaries. Interpretation techniques often involve complex geostatistics,

but the lack of data and spatial distribution for data that is available at Macraes, means a visual method of interpretation, while subjective, is still the most appropriate for the mine site at present.

The lack of information on the locations of the major structures in relation to mapped structural information in the Macraes Geotechnical Database means that it was not possible to construct stereoplots either side of major structural features at the mine. Consequently, areas for stereoplotting were selected subjectively for plotting in a grid like pattern based on both the pit slope orientation and data coverage. It is recommended that in the future two schemes of mapping be undertaken at the mine. These mapping programmes are the present detailed face mapping, and secondly a new large scale mapping programme that identifies the major fault (>100m) and fold? (hinge areas etc.) structures in the area that may be controlling structural domain boundaries. The recognition of these potential structural domain boundaries will allow separate plotting of structural data so that checks can be made to establish if and which of these features are responsible for controlling sub-domain boundaries.

The structural domain analysis here has involved a significant amount of extrapolation due to poor data coverage. As Hume (1983) points out, while it is possible that widely separated areas of rock mass may be structurally similar this should be demonstrated and not just assumed. It is recommended on a routine basis at the mine site that the structural models constructed here are taken into the field and visually checked for consistency. Any variations between the stereoplots and field observations indicate that more data collection is required in these areas so that new structural models may be developed.

The method of data collection at Macraes also appears to involve a significant amount of operator bias from data being collected in an arbitrary, subjective manner, since not all structures on a given berm are mapped. The use of more rigorous sampling techniques such as scanline and window sampling as outlined by Priest (1993) may be more appropriate for Macraes. The implementation of techniques such as these would allow for better interpretation of structural domain boundaries where the structures controlling boundaries are unknown. Combining these sampling techniques with techniques such as those outlined by Wise and McCrory (1982), where subsequent cutbacks of the pit walls are compared may prove of use for future structural domain interpretations.

CHAPTER 4 : PIT SLOPE FAILURE DATABASE AND MODELS

4.1 INTRODUCTION

As outlined in Chapter 1, one of the principal objectives of this thesis was the collation of pit slope failures at Macraes Gold Mine into a consistent format. The collation of failures into a database has a number of functions during mining operations which include:

- to assess any continuing development (progressive/retrogressive) or enlargement of failures with time, which is of particular importance when considering large developing pit slope failures such as RH27 and RH28.
- to develop failure models for the mine site.
- to assess the effectiveness of any remedial measures undertaken.
- to calibrate and adjust predictive rock mass failure models for pit slope failures that are developed for the mine.
- to assess defect strength characteristics by means of back analysis.
- to provide records for the ongoing assessment of pit slope design.

This chapter develops a standard recording sheet for pit slope failures at the Macraes Gold mine, and collates existing failure records into a database for pit slope failures at the mine. A classification system for pit slope failures is then developed for Macraes based on the records in this database, and observations of failures during the field investigation phase of this thesis. The last part of this chapter involves a case study of two of the largest failures at the mine, and assesses these in terms of failure mechanisms, stability, and future implications to current mining operations.

4.2 PIT SLOPE FAILURE DATABASE

4.2.1 Previous Work

A review of records held in the office at Macraes Gold Mine shows that 29 failures had been recorded at the mine site prior to the commencement of this thesis, and these failures had been numbered sequentially (failures 1-29). No formal pit slope failure database

was in operation at the mine, and failure records were located in a number of places around the mine office. Information recorded on these 29 failures also varied significantly, and while descriptive failure reports are available for failures 2, 3, 5, 6, 8 and 10, the information available on other failures is often extremely limited (for example with some failures the only available information is movement monitoring records). It appears that while much more pit slope failure data may have initially been collected, this data has since been archived to whereabouts unknown, or lost (G. Ryan pers. comm., 1996).

Earlier failure reports where available are often subjective, with wide variations in the amount, type, and quality of information recorded by different personnel. Early failure reports also suffer from serious deficiencies in a number of respects. For example, there is a poor use of geotechnical terminology, with terms like "sticky clay" being somewhat ambiguous in its interpretation. While it may be assumed that "sticky clay" is an indicator of plasticity this is not obvious. Further, seemingly vital information such as the failure location is often not recorded. Simple kinematic checks for stability as outlined by Richards and Atherton (1987) have not generally been undertaken, and even worse when they have been, plots are often misinterpreted (Figure 4-1).

Plots of earlier failures show that a number of the previously interpreted failure mechanisms are not kinematically possible because the interpreted failure surface dips steeper than the slope in which the failure occurs (Figure 4-1). Two large slope failures that have occurred in Round Hill Pit (failures RH27 and RH28) have been studied in some depth prior to this project by the Australian geotechnical consulting firm Pells Sullivan Meynink Pty Ltd. Information on these two failures was available in the form of correspondence and reports to Macraes Gold Mine from Pells Sullivan Meynink Pty Ltd.

4.2.2 Work This Project

New failures observed during the course of this project were failures RH30 -RH36 (Round Hill Pit) and failures IM2 - IM3 (Innes Mills Pit). Locations and kinematic interpretations of these new failures are presented on Map Sheet 7, while a summary of the failure database is presented in Appendix F5. As well as these new failures, a large amount of field work was dedicated to the existing failures RH27 and RH28 in Round Hill Pit which are still active as of December 1997.

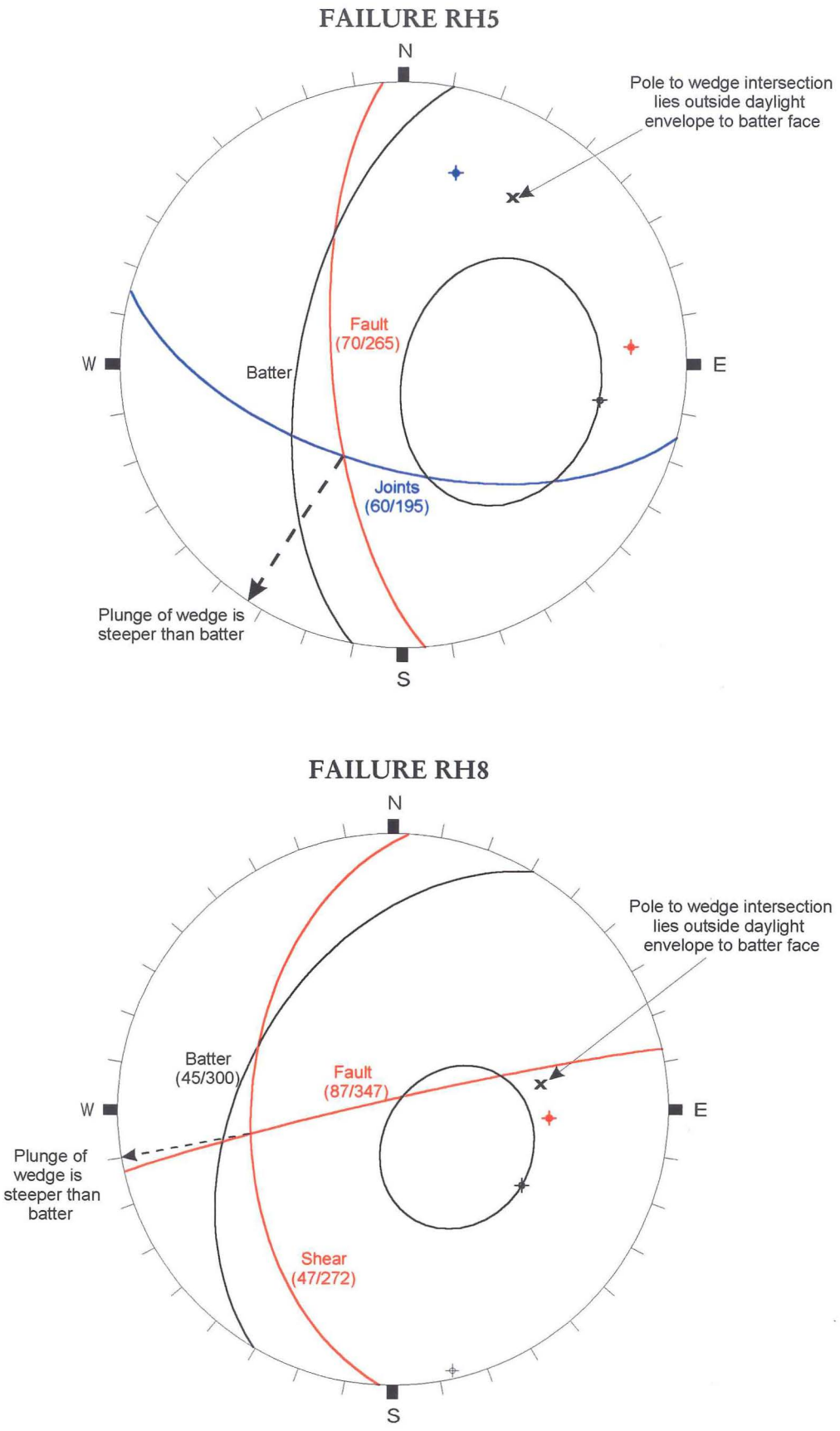

Figure 4-1: Previously interpreted failure mechanisms for failures RH5 and RH8. A check for stability following the method outlined by Richards and Atherton (1987) quickly establishe that the above failure mechanisms are not kinematically possible, since the wedge intersection plunges at an angle steeper than the berm and pole to wedge

4.2.2 Standard Recording Sheet

During the early stages of this project a standard recording sheet for pit slope failures at Macraes Gold Mine was developed. The purpose of such a recording sheet is to assist in engineering geological investigations of pit slope failures by documenting the relevant information in a consistent format. As with the collection of any engineering geological data the information must be relevant and accurate, with a clear distinction drawn between fact and inference (Bell and Pettinga, 1983).

A standard recording sheet increases consistency both of records over time and those collected by different workers. A standard recording sheet also increases the speed with which data can be collected, and allows for fast and accurate comparison between different failures. The information recorded is used for failure interpretation, and may assist in the implementation of remedial works where required. Reports also provide records to the open-pit designer for the ongoing assessment of the pit slope design as mining operations proceed.

The standard recording sheet developed during this thesis is presented in Appendix F4, and records the following information:

- failure name (abbreviated pit name and sequential number, e.g. 1st failure in Round Hill pit would be RH1, while 3rd failure in Innes Mills Pit would be IM3, etc.).
- timing details.
- location and pit slope geometry (pit slope angle and orientation, berm width, bench height and angles etc.).
- antecedent conditions contributing to failure (rainfall, removal of toe support, blasting etc.).
- failure type (plane, wedge, toppling, complex).
- failure dimensions (crest length, toe length, height, depth and volume).
- failure material (description of rock mass encompassed by failure).
- maps (maps and cross sections of failures).
- stereoplots (kinematic analysis of failure to check interpreted failure mechanism for validity, orientations of structures in the area).
- photographs (photographs detailing failure).
- other relevant records where available (rainfall records, movement records, testing records, excavation records etc.)

The standard recording sheet has been integrated into Microsoft's Access for Windows 95 database package. The added advantage of integrating the standard recording sheet into a computer database is that it allows for the rapid searching and retrieval of specific pit slope failure information. A summary report generated from this computer database is presented in Appendix F5.

4.3 FAILURE MODELS

4.3.1 Classification

Pit slope Failures observed at Macraes Gold Mine can be classified according to Hoek and Bray (1981; Appendix F1) as:

i) Planar Failures, where sliding occurs along a single discontinuity which strikes within approximately ± 20° of the slope face. Release surfaces must also be present in the rock mass to provide lateral boundaries to the slide.

ii) Wedge Failures, where sliding takes place along the line of intersection of two discontinuities and may or may not involve additional release surfaces.

iii) Toppling Failures, where failure occurs along steeply inclined discontinuities and involves the forward rotation of blocks of rock about some fixed point out of the rock mass. The discontinuity must strike within ± 10° of the slope face and release surfaces must also be present to provide lateral detachments to the block.

A fourth failure model after Varnes (1978), and Cruden and Varnes (1996) is also evident at the mine site:

iv) Complex Failures, where failure involves either a combination of the above failure types, or the change and progression from one failure type to another with continuing failure development.

Circular/rotational failure types were not observed during the course of this study as a primary failure mechanism for pit slopes at the mine. However, rotational mechanisms were

apparent as localised auxiliary features in the larger, more complex failure systems such as RH28. Rotation occurs here as a result of the rock mass dilating and breaking up along jointing during failure development (see Section 4.4.2).

4.3.2 Planar Failures

A review of planar failures occurring both during this study and those recorded previously at the mine suggests that planar failures at Macraes can generally be grouped into one of two categories:

a) High angle planar failures, where the basal failure plane occurs along a discontinuity dipping at greater than 30° (typically 40° - 50°).

b) Low angle block failures, where the basal failure plane is along a discontinuity dipping at less than 30°.

a) High Angle Planar Failures

Three high angle planar failures (Table 4-1; Map Sheet 7) were observed during the field work phase of this thesis, them being RH30 (Figure 4-2), RH34 (Figure 4-3) and RH35. Available records at the mine site suggest that these type of failures have also been relatively common at the mine in the past.

The relatively high angle of the failure surface in this type of failure has three main implications. Firstly, the failure surface may form along either joints or faults, since the dip of the failure surface will be close to or higher than the frictional strength of the discontinuity. Secondly, once movement is initiated failure movement speeds lie at the faster end of the scale (>5m/sec) and consequently movement is generally impossible to stop once initiated. Thirdly, the relatively small angle between the pit slope and the failure surface has the implication that the failure will not generally extend very far back into the slope, and as such failure is generally limited to bench scale and relatively small volumes (50-100m^3).

The predominant cause of high angle planar failures as evidenced by failures RH34 and RH35 is undercutting of the failure toe by mining activities thereby allowing the failure surface to daylight in the berm. Where failure is not immediate, increased groundwater pressures following rainfall may act as a catalyst to failure. RH30 (Figure 4-2) is an example of this where failure occurred along an open joint in the berm, following a period of rainfall.

Table 4-1: Summary of failures RH30, RH34 and RH35.

Failure RH30 (16/02/96) - Round Hill Pit (Grid Reference: 69785mE, 15145mN, 375mRL)
Occurred along a east dipping joint (45/100) on the west wall of Round Hill Pit adjacent to the main haul road following 5 days rainfall (total = 25.1mm). Failure was below the HWS and had an approximate volume of 100m^3. Failed material was blasted and then removed the following day. There has been no further development of the failure.
Failure RH34 (15/05/96) - Round Hill Pit (Grid Reference: 70165mE, 15180mN, 355mRL).
Occurred along a westerly dipping joint set (40/300) on the east wall of Round Hill pit following excavation of the 340mRL - 355mRL berm. Failure was within the HWS and a result of about 2 metre thick zone of highly sheared weak material (and blast damaged?) material. The failed material was removed and there has been no further development of the failure. Total failure volume was approximately 100m^3
Failure RH35 (15/05/96) - Round Hill Pit (Grid Reference: 70170mE, 15255mN, 355mRL).
As for RH34 failure occurred along a westerly dipping joint set (48/240) on the east wall of Round Hill pit following excavation of the 340mRL - 355mRL berm. Failure was within the HWS and a result of about 2 metre thick zone highly sheared weak material (and blast damaged?) material. The failed material was removed and there has been no further development of the failure. Total failure volume was approximately 50m^3

Back analyses (Appendix F6) of failures RH30 and RH34 show that for joints in schist at the mine with no cohesion (c') acting along the failure surface, the friction angle (ϕ') is about 50° to 55°. If the failure surface does break through intact rock then there will be a cohesive component that needs to be exceeded in order for failure to occur. In the literature friction angles for schist are typically quoted between 25 and 35° (Hoek and Bray, 1981), and the variance (15°-30°) between these values may be attributed to an apparent friction due to joint roughness/waviness at low normal stresses (Pender, 1994; Figure 4-4).

While high angle planar failures generally have small volumes (50-100m^3) for pit slope failures at the mine, these failures are still of importance. High angle planar failures are most likely to occur soon after the excavation of a bench and removal of toe support, and as such are a significant hazard to mine personnel and equipment in the area at the time of failure. In addition, even where failure is not immediate after excavation of a bench (e.g. RH34 & RH35), later failure following precipitation, blasting etc., adjacent to a haul road may represent a significant hazard to equipment and personnel in the vicinity at the time of failure (Figure 4-2).

Figure 4-2: Failure RH30 adjacent to main haul road. Failures such as this represent a significant hazard to equipment in the area at the time of failure. Grid reference: 69785mE, 15145mN.

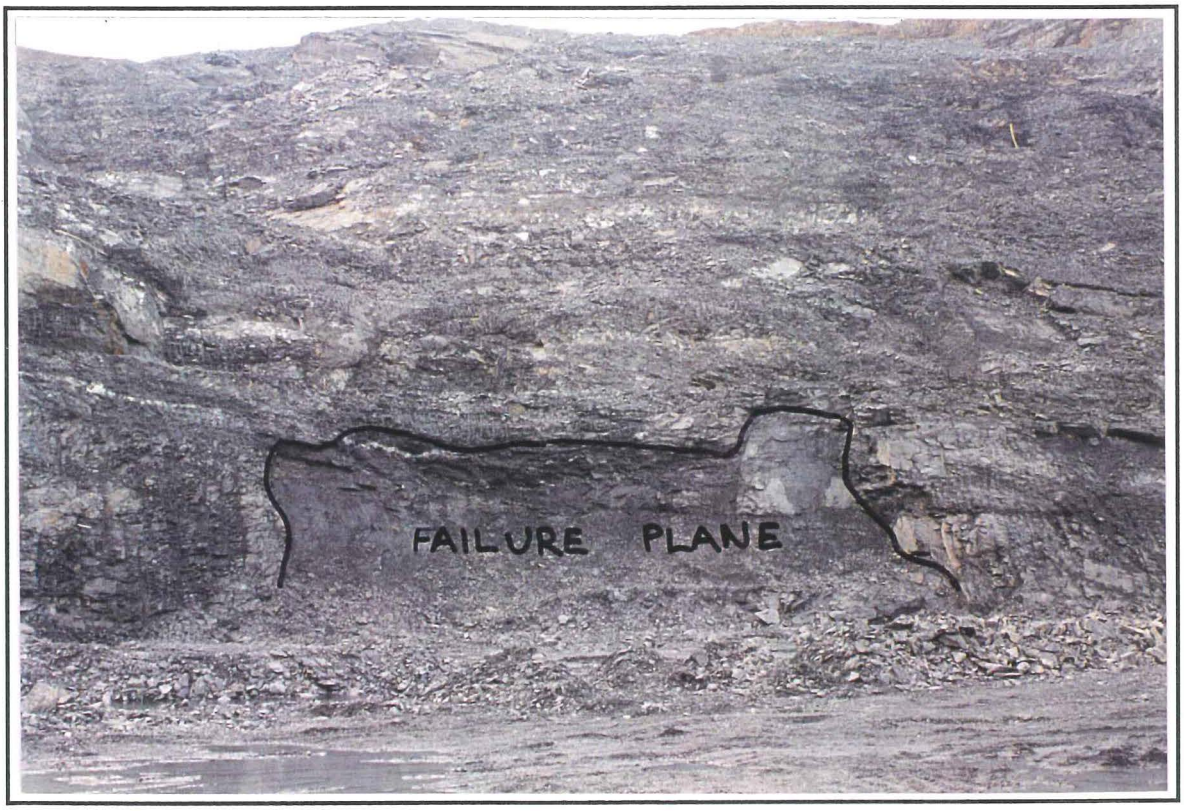

Figure 4-3: Failure RH34. Grid reference: 70165mE, 15180mN

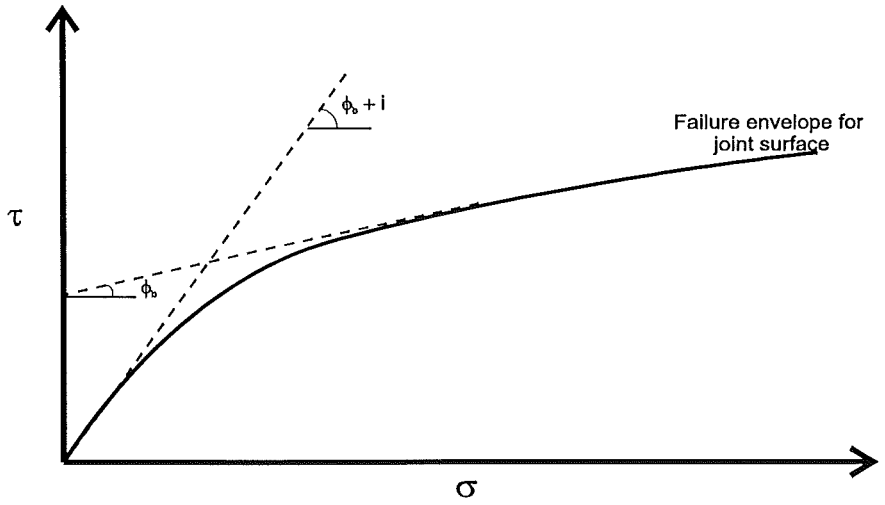

Figure 4-4: Effect of joint roughness on joint shear strength. At low stresses the shear strength for a joint (ϕ_b) is increased by roughness (i) and dilation during shearing. At high stresses the friction angle is controlled by a smooth joint surface with no dilation (ϕ_b) (*redrafted after* Pender, 1994).

b) Low Angle Block Planar Failures

Two low angle block failures (Table 4-2) were observed at Macraes Gold Mine during field work for this thesis, these being RH33 (Figure 4-5) and IM3 (Figure 4-6).

Table 4-2: Summary of failures RH33 and IM3.

Failure RH33 (3/05/96) - Round Hill Pit (Grid Reference: 70075mE, 15070mN, 360mRL).
Occurred on east wall of Round Hill Pit along a shallow westerly dipping foliation shear (13/300) following rainfall (0.5mm) and production blast. Initial failure movement rates were slow but have since stopped. High groundwater pressures were inferred to be the main factor driving the initial failure. A small catch bench (see Map Sheet 7) has been created beneath the failure to catch the material should it fail completely. Total failure volume is approximately 375m^3.
Failure IM3 (29/05/96) - Round Hill Pit (Grid Reference: 69960mE, 14000mN, 360mRL).
Occurred on north-eastern wall of Innes Mills Pit along gentle south dipping foliation shear (20/211) following rainfall (1.3mm). Initial movement rates were slow to moderate, and material was removed by bulldozer. The total failure volume was approximately 500m^3.

The relatively low angle of the failure surface in low angle block failures has a number of implications that contrast with high angle planar failures. A low angle for the failure surface means that there must be a low shear strength along the failure surface in order for sliding to be occurring (since the resisting forces to sliding, must be less than the forces driving failure), and as such failures of this type are only observed on gouge filled fault planes. Bounding discontinuities that release the failure block will typically dip at high angles (>40°) and may form along either joints or faults. Movement rates associated with these failures, in contrast to high angle planar failures, are generally moderate or slower (<1.8m/hour). The fact that the failure surface dips at a low angle and is formed along a fault also has the implication that the potential failure volume can be quite large, since faults are the most continuous structures at the mine (Chapter 3) and the failure surface will generally extend well back into the slope (>10m). The volume encompassed by low angle planar failures will generally be more a result of the orientation, location and continuity of the lateral and/or rear bounding discontinuities that release the failure block from the pit slope.

In low angle block failures where the failure surface dips at less than 15° such as RH33, it seems reasonable to infer one of the following:

1. high groundwater pressures along the failure surface, and/or bounding release surfaces are driving the failure;
2. shear strength properties along the failure surface are very low;
3. a combination of 1 & 2.

As noted in Chapter 2 ring shear testing of the <1.18mm fraction of fault gouge for RH33 showed a residual shear strength of 6.1°, although as also noted previously the true friction angle of the material will be higher in the field due to the effects of larger grain size crushed material within the fault and surface roughness along the fault.

Back analyses of failures IM3 and RH33 were performed and are presented in Appendix F6. Resulting back analysis curves showed that, assuming there was no cohesion acting along the failure surface, the effective ϕ angles are IM3 = 14° and RH33 = 9°. For both analyses an increase in cohesion to 1kPa shows a rapid drop in ϕ to 10° (IM3) and 6° (RH33). The low calculated shear strength for RH33 compares favourably with that measured through ring shear testing (6.1°). As noted in Chapter 2, because faults at Macraes are structures which have been subjected to large strains in the past, cohesion would be expected to lie close to zero.

Figure 4-5: Failure RH33. Grid reference: 70070mE, 15070mN

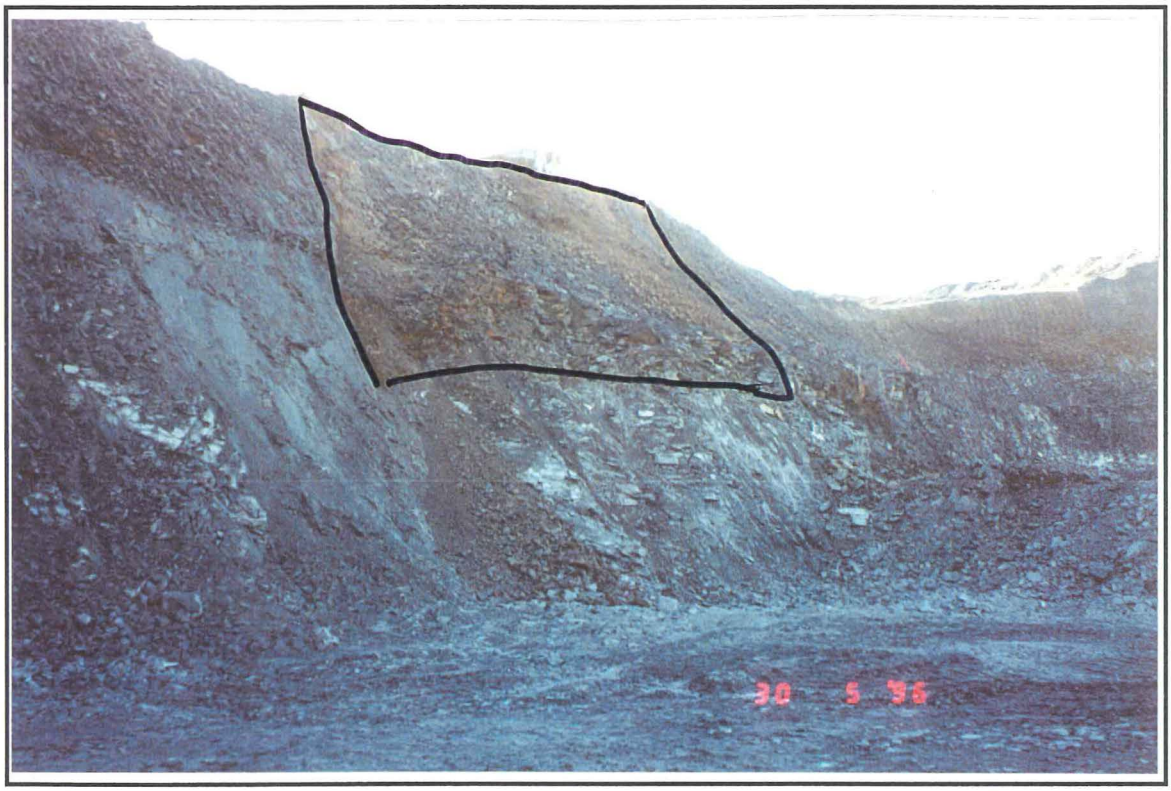

Figure 4-6: Failure IM3. Note blade of Caterpillar D10 bulldozer pushing failure material down for removal. Grid reference: 69970mE, 14000mN

Field observations and factor of safety analyses for both RH33 and IM3 support the hypothesis that groundwater pressures formed along the bounding surfaces to the failure block are an important geotechnical factor in driving failure. Groundwater pressures along these releasing defects that bound the failure will create a hydrostatic force that effectively pushes the block from behind. The slow movement of these failures and consequent dilation of the failure block may be enough to stop its movement, as groundwater pressures are alleviated through the creation of new secondary permeability by the opening up of the failure block along discontinuities (Figure 4-7).

Figure 4-7: Cracking along jointing trending to 017° in 360mRL bench of failure RH33. Dilation of rock mass along joints such as these may be enough to provide natural drainage paths to relieve groundwater pressures driving failure and thus stop further failure movement. Note hammer for scale. Grid reference: 70080mE, 15065mN, 360mRL.

Low angle planar failures are of importance at the mine since they are generally a good indicator of high groundwater pressures in the area where failure is occurring. As such the best method for dealing with failures of this type is preventative, by ensuring that there is adequate slope depressurisation so that failure is not initiated in the first place. This slope depressurisation is best achieved through the installation of horizontal drains in the pit slope as development of the mine proceeds, and this will be discussed in more detail in Chapter 5.

RH33 had a small catch bench created on the pit floor beneath the failure to catch the failure mass should it fail at a later date. In contrast IM2 could be accessed at the crest of the failure and was dealt with by bulldozing the failure mass down from the crest to the pit floor, where it was removed. While both these solutions appear acceptable, had these failures occurred higher up the pit slope then neither of these remedies would have been possible, and a significant hazard would have been posed to personnel and equipment on the pit floor beneath the failure.

4.3.3 Toppling Failures

RH31 (Figure 4-8; Table 4-3) was the only toppling failure observed at the mine during field investigations, although toppling mechanisms were observed as secondary features in the larger complex failures like RH27 and RH28 (see Section 4.4). Available records at the mine show that only one other possible toppling failure has been recorded previously (RH24), but the only information available for this failure is the orientation of the failure surface (see Appendix F5).

Table 4-3: Summary of failure RH31.

Failure RH31 (16/02/96) - Round Hill Pit (Grid Reference: 70025mE, 15325mN, 400mRL).
Occurred on the northern wall of Round Hill Pit along a vertical north/south dipping joint. Failure was inferred to be a result of 5 days of rain prior to failure, and movement and dilation of the north wall associated with failure RH28. A wide catch bench was created at 365mRL to catch any further toppling failures along the 400mRL bench and this appears to have been sufficient.

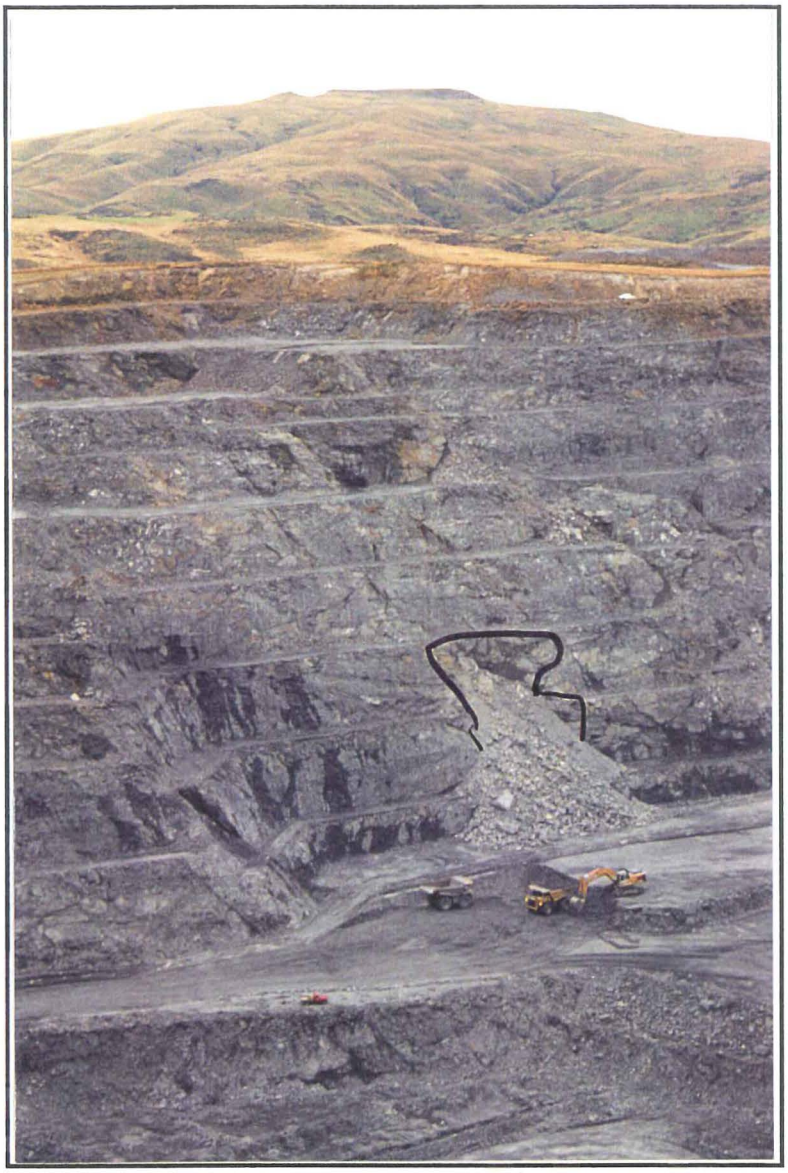

Figure 4-8: Failure RH31. Grid reference: 70025mE, 15325mN.

While toppling failures are relatively rare at Macraes, Figure 4-8 shows that when failures of this type occur they can involve a large volume of material. RH31 failed along a subvertical joint which was released laterally by steeply inclined faults. Once again failure appears to be related to increased groundwater pressures following rainfall, although movement and dilation of the northern wall associated with RH28 may also contribute to failure. Continued cracking along the 460mRL bench (Figure 4-9) suggests that this failure will continue. Further failure development is to be expected since, once a void is created in the pit slope by failure, lateral support to one side of the potential toppling blocks is also effectively removed and it is much easier for failure to extend along the slope. A large catch bench has been created at 365mRL and this should minimise any future hazard associated with this failure.

Figure 4-9: Cracking along 460mRL bench illustrating continued development of RH31 can be expected. Grid reference: 70050mE, 15325mN

4.3.4 Wedge Failures

Wedge failures at the mine can be classified into three groups depending on the type of discontinuities defining the main wedge failure block as follows:

1. Joint - Joint Wedges, where both the failure surfaces forming the wedge are joints.
2. Joint - Fault Wedges, where one failure surface is formed along a joint plane, and the other is along a fault plane.
3. Fault - Fault Wedges, where both the failure surfaces defining the wedge geometry are faults

In all of the above wedge failure types, joints or faults may also serve as auxiliary release surfaces in tension surrounding the wedge.

a) Joint - Joint Wedges

Two joint-joint wedges (Figure 4-10; Table 4-4) were recognised during the field investigation phase of this thesis, and these were RH32 and RH36. Both RH32 and RH36 are located at the northern end of the western wall of Round Hill Pit. Rainfall once again appears to be the main contributing factor to failure initiation. In the case of RH36 it also seems reasonable to assume that prior loading of failure material from RH32 would have also contributed to instability.

Table 4-4: Summary of failures RH32 and RH36.

Failure RH32 (29/04/96) - Round Hill Pit (Grid Reference: 69825mE, 15310mN, 400mRL).
Occurred on the north-western wall of Round Hill Pit below the HWS along south (58/182) and east (53/094) dipping joints, forming a wedge intersection (132/46). Failure followed one day of rainfall (20.2mm), and increased groundwater pressures are inferred to be the catalyst to failure. The failure was contained by the 380mRL bench. Total failure volume is approximately 100m^3.
Failure RH36 (18/06/96) - Round Hill Pit (Grid Reference: 69840mE, 15295mN, 380mRL).
Occurred on the north-western wall of Round Hill below the HWS along south-east (51/150) and east (48/103) dipping joints forming a wedge intersection (123/47). Failure in part is attributed to increased head loading following failure RH32. The failure was contained by the 360mRL bench. Failure may lead to further failure of the 345-360mRL bench below, due to crest loading. Total failure volume is approximately 100m^3.

As noted in Chapter 3 joints at the mine site have a smaller continuity (≈4-5m) than faults (≈13m), and as such wedges formed along joints are typically the smallest of the wedge failures observed. The higher frictional strengths of joints compared to faults also means that the wedge intersection formed between the two joints must plunge at a high angle (generally >40°) in order for sliding to occur. This high wedge intersection means that movement rates for joint-joint failures will generally be similar to high angle planar failures (>5m/sec). Further, like high angle planar failures, a much steeper failure intersection will inevitably mean that not as much of the pit slope is encompassed by the failure, and volumes of joint-joint wedges will generally be smaller than wedges with wedge intersections dipping at shallower angles.

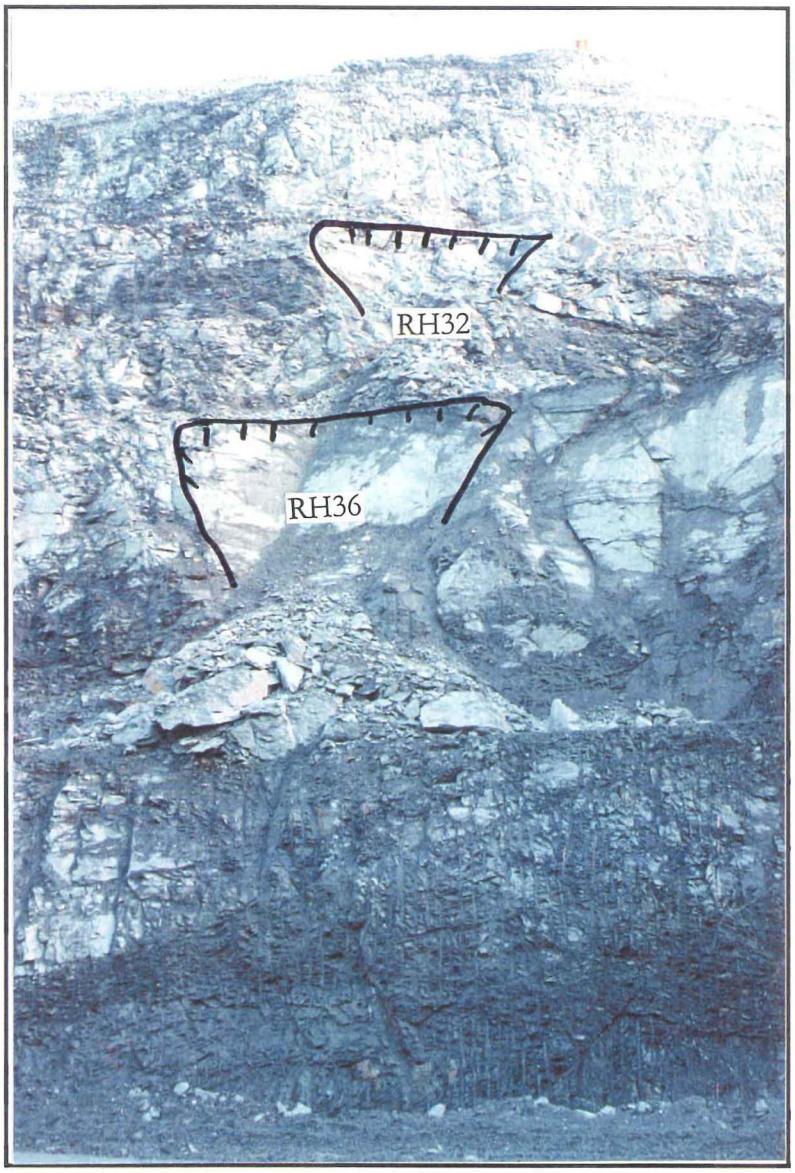

Figure 4-10: View of failures RH32 and RH36.

Back analyses of joint-joint wedge failures (RH32 and RH36) suggest ϕ angles of around 45° assuming no cohesion along the failure surface (see Appendix F6). As for high angle planar failures the frictional strengths are much higher than typically quoted in the literature (c.f. 30°), and once again suggest apparent friction due to surface roughness/waviness along the joints of approximately 15° (Figure 4-4).

RH32 and RH36 show that, unlike high angle planar failures, undercutting of the failure surface may not be enough to initiate failure. Increased groundwater pressures following rainfall/snowmelt generally appear necessary to initiate failures of this type, although if the wedge intersections were even more steeply dipping (>50°) then toe undercutting may be enough to initiate failure. This suggests that there is a cohesive

component to be overcome for failure to occur, involving breakage through intact rock, which is supported by back analysis curves (see Appendix F6) that show for the same assumed value of friction much higher values of cohesion exist for wedge failures than for high angle planar failures.

The main implication posed by joint-joint wedge failures is the hazard associated with rapid failure adjacent to personnel or equipment, such as failure of a berm adjacent to a haul road, or a berm at the pit floor. Observations of RH32 and RH36 suggest that typical 5-10m bench widths are large enough to catch the material from a failure of this type formed in a 15m high berm. Cracking was also evident in the benches at the top before failure occurred, although the time period between cracks appearing and failure is unknown (at least 3 months in the case of RH36). Regular berm inspections should be undertaken to identify potential wedges by identifying bench cracking before failure occurs, so that access of personnel and equipment can be minimised beneath problem areas or other remedial measures can be implemented (e.g. toe buttressing, removal of failure material etc.).

b) Joint - Fault Wedges

Joint-fault wedges are those wedges formed where one of the margins to the wedge is a joint (or joint set) and the other is a fault, and as such represent an intermediate type of wedge failure between the two end-members, joint-joint wedges and fault-fault wedges. Joint-fault wedges may range from bench scale (e.g.IM2; Table 4-5) to the multiple bench scale such as the large RH27 wedge failure complex (see Section 4.4.1).

Table 4-5: Summary of failure IM2.

Failure IM2 (9/03/96) - Innes Mills Pit (Grid Reference: 69800mE, 14020mN, 560mRL).
Occurred on the northern wall of Innes Mills Pit above the HWS along east dipping joint (60/110) and west dipping fault (70/240), forming a wedge intersection (169/41). Failure followed a days rainfall (12.3mm) and increased groundwater pressures are inferred to be the catalyst to failure. The failed material was removed. Total failure volume is approximately 100m^3.

Joint-fault wedge failures are the most difficult of the wedge failures to analyse since the two bounding surfaces to the wedge possess significantly different strength properties. While high frictional strengths are characteristic of joints (45-55°, c=0), faults in contrast are characterised by much lower frictional strengths (6-14°, c=0). Back analyses of joint-fault wedges by conventional two dimensional methods is restrictive, since any assessment of

values of c and ϕ is effectively a measure of a combination of joint and fault properties acting along the wedge intersection. The values for these properties will depend on the proportion of the total failure surface that the discontinuities encompass, and could effectively lie anywhere in the range of values indicated between joint-joint wedges and fault-fault wedges. For example, if the joint plane encompasses a much greater area to the wedge than the fault plane, then the ϕ and c values for the overall wedge would lie much closer to those calculated for joint-joint wedges, and vice versa. Back analysis of failures (see Appendix F6) IM2 and RH27 show values of cohesion and frictional strength ranging from: c=0 - 0.6kPa, ϕ = 41°-30° (IM2); and c=0 - 13kPa, ϕ=39°-30° (RH27). These calculated values as expected fall within the range indicated by back analyses for joint-joint wedges and fault-fault wedges.

c) Fault - Fault Wedges

The pre-existing failure RH28 (see Section 4.4.2) on the north wall of Round Hill pit was the only fault-fault wedge observed during the field investigation phase of this thesis. The lower shear strength of faults compared to joints, and the greater continuity of faults at the mine, means wedges of this type are the probably the most significant (purely from a volumetric point of view). As for low angle block failures the lower shear strength of faults and greater continuity means that sliding may occur on much lower wedge intersections, and form larger volumes than compared to joint-joint and joint-fault wedges.

The consistent nature of the fault structure at the mine (Chapter 3) would suggest that any wedge failure formed along faults, no matter how small in volume, has the potential to increase in scale with time as the pit increases in depth and much deeper fault-fault wedge intersections are undercut. Failure RH28 is testament to this scaling up of an initially small fault-fault wedge (see Section 4.4.2).

4.3.5 Complex Failures

Complex failures are typically an end-product of larger pit slope failures at the mine. Failures typically begin as one of the failure types outlined above, but because of the substantial volume of material involved the failure will inevitably develop and involve other failure mechanisms. A principal reason for this is the more a failure block moves the more dilation of the block along joints and faults will occur, leading to localised toppling, circular failures, etc. The two best examples of complex failures at the mine are failures RH27 and RH28, and these are discussed some detail in the following Section 4.4.

4.4 CASE STUDIES OF SELECTED FAILURES

As part of this thesis two large existing failures RH27 and RH28 in Round Hill pit (Figure 4-11) were studied in some detail. The main purpose was to construct failure models through detailed engineering geological mapping and interpretation for assisting in the design of any remedial measures. This section discusses these investigations and their results.

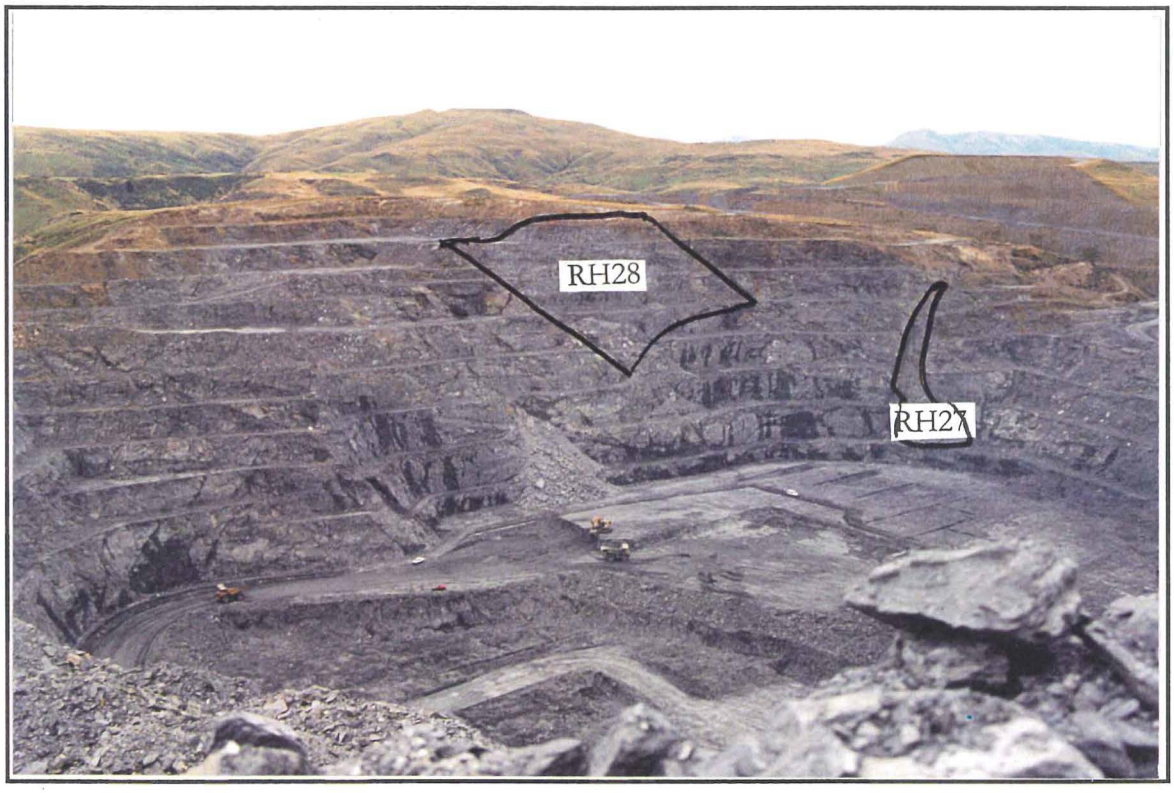

Figure 4-11: View looking towards the northern wall of Round Hill pit showing the locations of the large pit slope failures RH27 and RH28.

4.4.1 Failure RH27

a) Introduction and Previous Work

RH27 currently forms a large pronounced scree slope from 370mRL to 460mRL (Figure 4-13) and is located on the north-eastern wall of Round Hill Pit, above the Hanging Wall Shear (HWS) (Map Sheets 7 & 8). The exact timing of the failure is unknown, although an unpublished MMCL geotechnical report covering the period 16th October 1994 to 4th January 1995 describes failure as occurring a few days before the 7th of December 1994. This initial failure is described as occurring between 430mRL and 460mRL due to undercutting of the failure plane with mining of the 430mRL bench. The presence of the scree slope currently

extending another 60 metres down into the pit (to 370mRL) is evidence of further failure development between the earlier report and the commencement of this project.

RH27 has previously been interpreted (Bertuzzi, 1995) as an oblique planar failure driven by water pressures along a large exposed fault plane referred to as the 'Slip 27 fault' belonging to what is commonly referred to as the 'Back Fault Set' (= Fault Set FA4). Kinematic assessment of this proposed failure mechanism would suggest, that oblique planar failure formed along the Slip 27 fault is unlikely, since the fault plane dips steeper than the pit slope and lies more than 20° in strike away from the face (Figure 4-12).

Detailed engineering geological mapping of RH27 was undertaken in March 1996 to identify the main features associated with this failure, as well as for the construction of a failure model for RH27. Data is presented on Map Sheet 8.

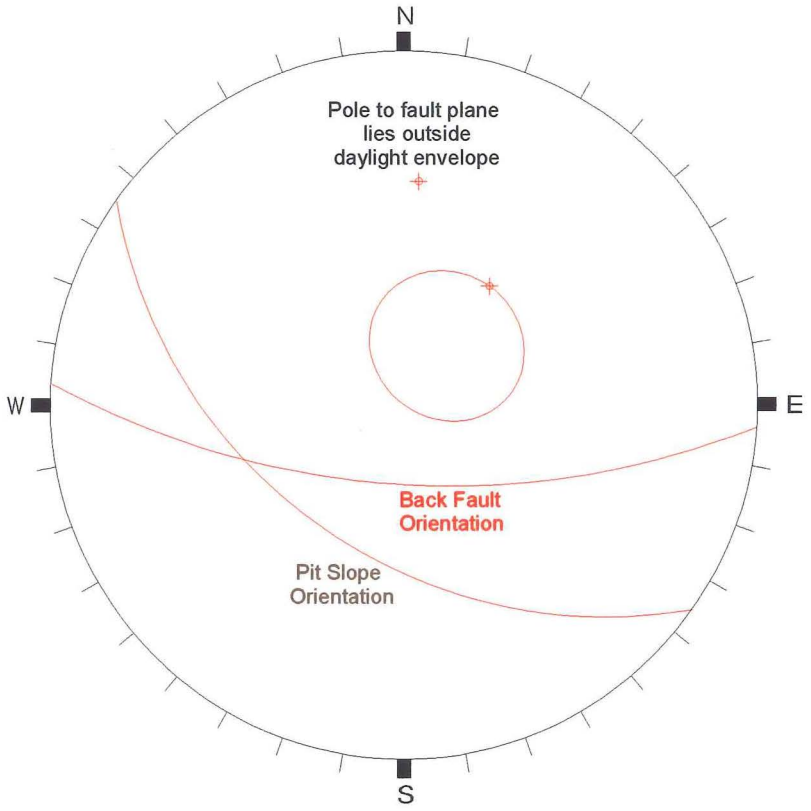

Figure 4-12: Previously interpreted failure mechanism for failure RH27 by Bertuzzi (1995). This failure mechanism appears to not be kinematically possible since the Slip 27 fault plane dips at a much steeper angle than the pit slope, and the dip direction for the Slip 27 fault lies more than 20° away from the dip direction of the pit slope face.

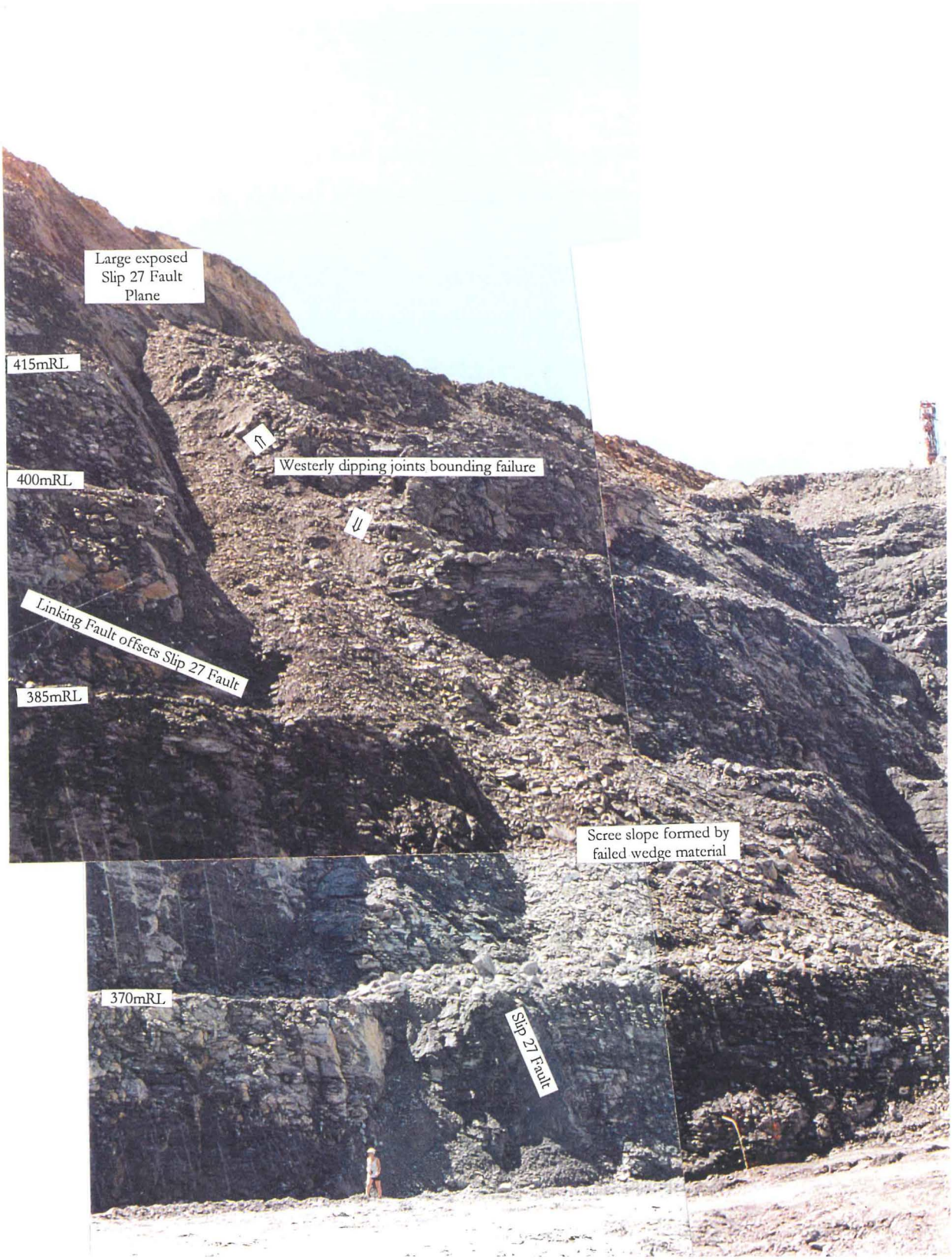

Figure 4-13: View of failure RH27 from Round Hill Pit Floor

b) Field and Laboratory Investigations

The main features identified associated with RH27 during the course of field investigations are as follows:

1. A large exposed fault plane (Slip 27 fault) with an orientation of approximately 70/200 (dip/dir) at 450mRL, which swings around to 65/170 at 410mRL. The Slip 27 fault is offset by the 'Linking Fault' at 390mRL (Map Sheet 8; Figure 4-13), and the observed change in orientation of the Slip 27 fault with depth is inferred to be a result of fault drag associated with displacement of the Slip 27 fault along the Linking Fault.
2. A series of large exposed joint faces with an approximate orientation of 50/290 were observed forming much of the south-eastern margin to the scree slope (Figure 4-13). These joints are interpreted to form the detachment surface to a large wedge failure formed between westerly dipping joints and the Slip 27 Fault (Figure 4-13; Figure 4-16).
3. A series of scarps and large cavernous openings formed along both easterly and westerly dipping joint sets in the more weathered schist material between 430mRL and 440mRL (Figure 4-14). These are inferred to represent toppling and dilation of the schist into the void created in the pit slope by failure of the wedge.

Laboratory testing (Chapter 2) of fault gouge material passing a 1.18mm sieve collected from the Slip 27 fault during field investigations produced the lowest residual friction angle of 3.1° measured during the whole of this study, while x-ray diffraction analysis for clay mineralogy showed a high proportion (45%) of mixed swelling chlorite/smectite was present in the fault gouge. The true friction angle of the material in the field (as discussed in Chapter 2) will be higher than that determined by ring shear testing due to the presence of coarser material in the fault gouge which is removed for testing. Back analyses of fault controlled failures previously, suggests that the shear strength for fault gouge at Macraes is anywhere between 9° (RH33) and 14° (IM3) for c=0. It seems reasonable to assume that the shear strength of the RH27 fault gouge is similar to these in reality (say ≈ 10°), meaning the presence of coarse material in the fault gouge is responsible for an increase in shear strength of about 7° from that determined by ring shear testing.

Figure 4-14: Cavernous opening along north-south striking joints formed as weathered schist material slowly dilates and topples into void formed by failure of wedge. View is to the south and note hammer for scale on eastern margin of opening. Grid reference: 70275E, 15275N.

c) Failure Mechanism

The wedge failure mechanism for RH27 interpreted during field investigations is further supported by kinematic analysis, which shows a wedge formed between westerly dipping joints (50/290) and the Slip 27 fault forms a line of intersection between the two structures plunging out of the pit slope at 240/37 (Trend/Plunge) (Figure 4-15). The proposed wedge failure mechanism also explains the observed increase in the size of RH27 as mining operations have proceeded (Figure 4-16). With progression of mining of Round Hill pit deeper wedge intersections formed between the Slip 27 Fault and the westerly dipping joint set have been intersected, resulting in an increase in the volume of the wedge . The present toe of the wedge is inferred to lie around 390mRL (70125E, 15270N), which corresponds with the approximate height at which the Slip 27 fault is offset. The offset of the Slip 27 fault by the Linking Fault appears to have controlled and prevented further development of the wedge deeper than the 390mRL level (Phase 3 of Figure 4-16).

The volume of the current wedge failure from 460mRL to 390mRL is calculated according to Hoek and Bray (1981) at approximately 900m³ (≈2 430 tonnes). In comparison, the volume of the initial wedge from 430mRL - 460mRL is calculated at approximately 200m³ (≈540 tonnes). This emphasises the substantial increase in failure volume as the wedge has stepped out and down the pit wall.

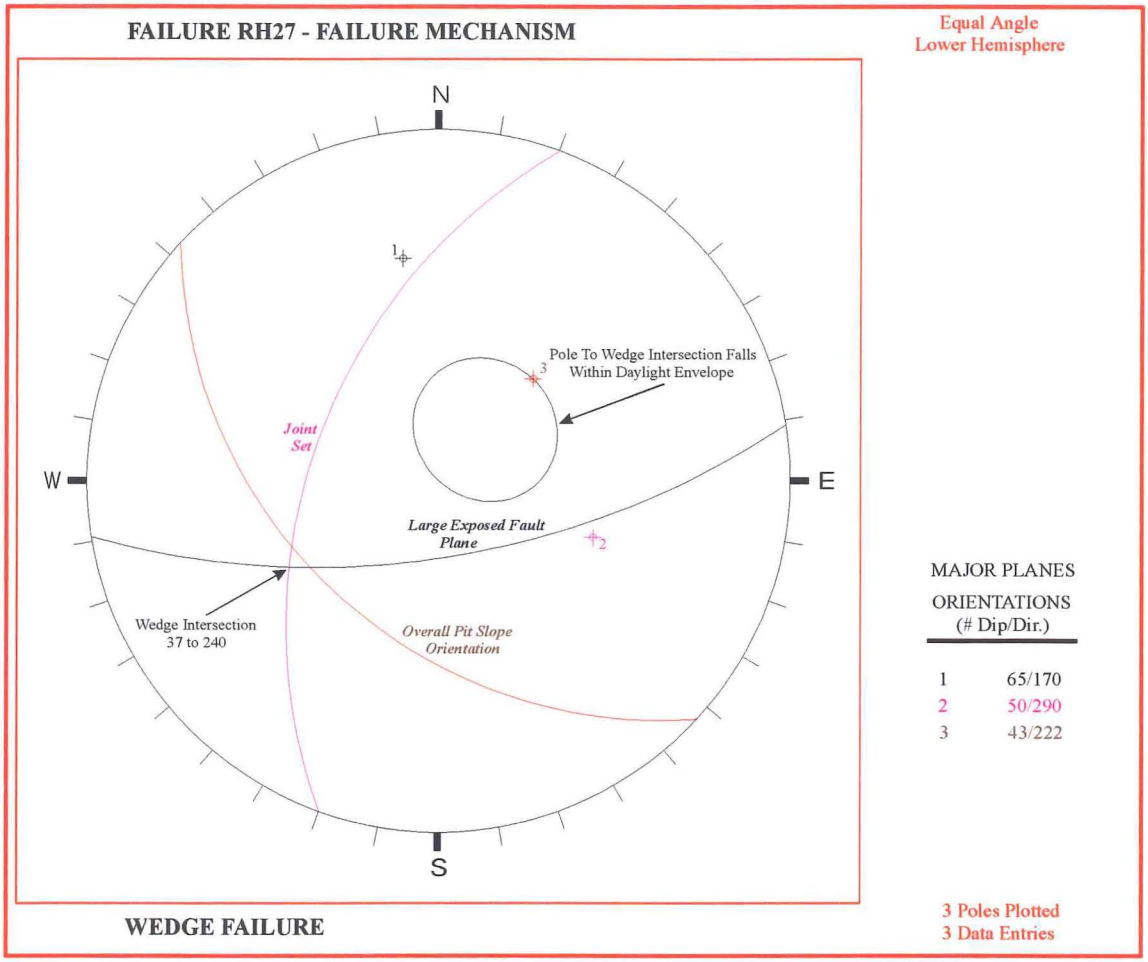

Figure 4-15: Kinematic failure mechanism of RH27

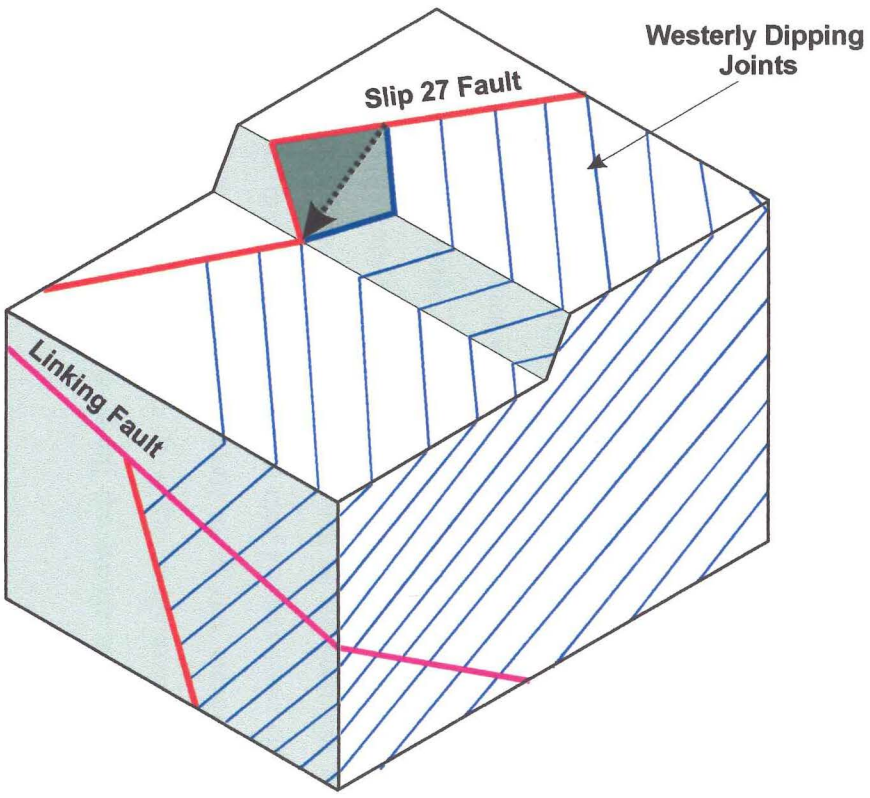

Phase 1: Initial wedge failure as intersection of westerly dipping joint set and 'Slip 27 Fault' is undercut by mining of berm.

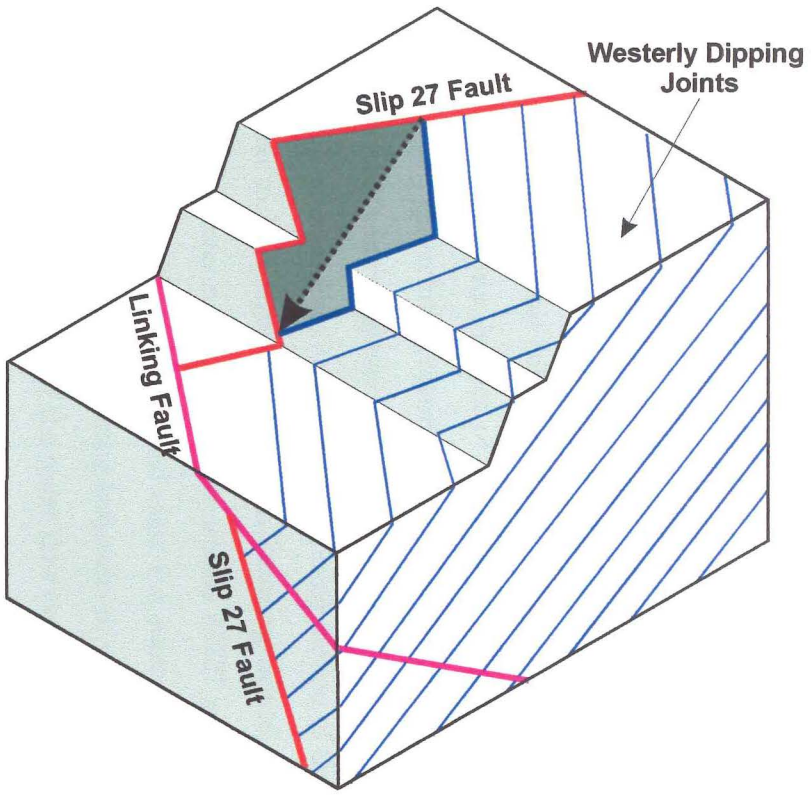

Phase 2: Enlargement of wedge failure. As mining proceeds deeper intersections between the westerly dipping joint set and the 'Slip 27 Fault' are undercut, increasing failure size.

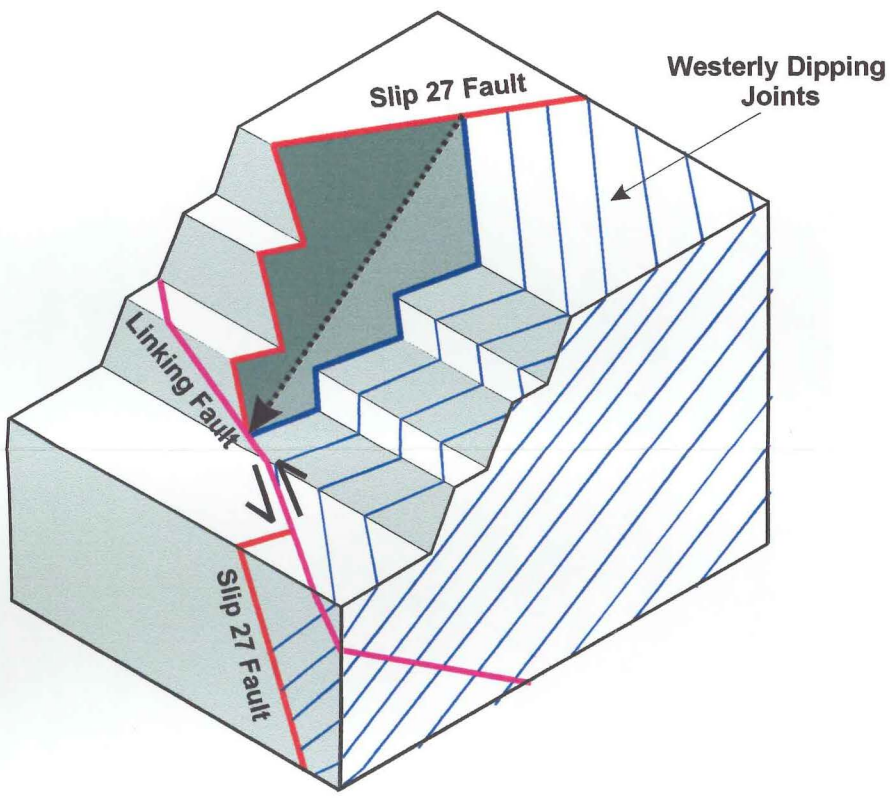

Phase 3: Wedge size increases as in Phase 2 however, maximum wedge development controlled by the reverse displacement of the "Slip 27 Fault' along the Linking Fault as indicated by arrows.

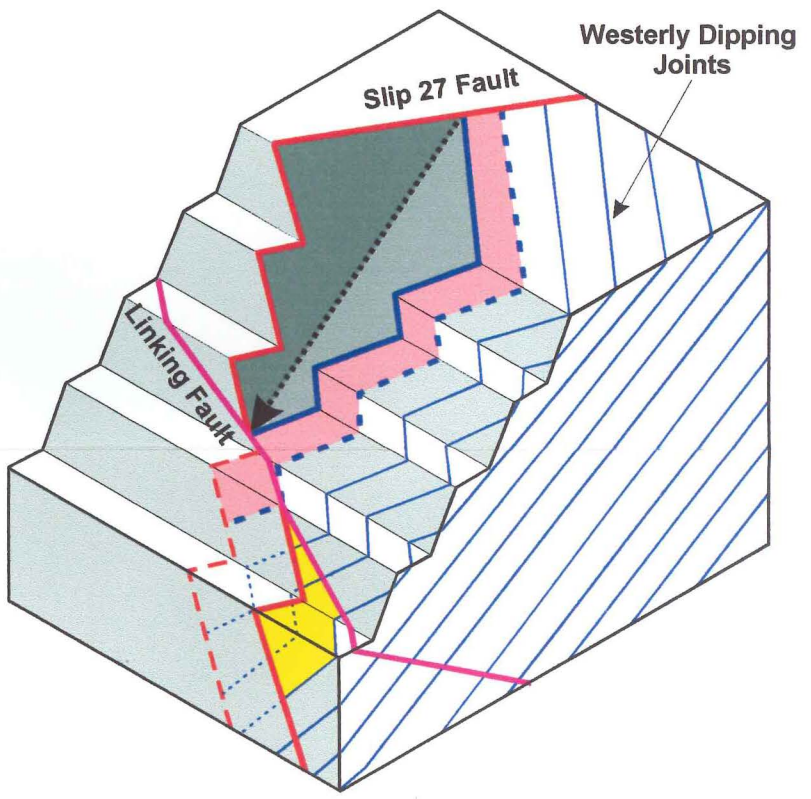

Phase 4: Possible future scenario with continued mining. Pink area indicates the expected increase in wedge size if the 'Slip 27 Fault' were not offset (dashed redl line) by the 'Linking Fault'. Yellow area indicates likely area of new wedge development between 'Slip 27 Fault' and westerly dipping joints as for phases 1& 2.

Figure 4-16: Schematic block diagram illustrating RH27 failure development. Westerly dipping joints are only shown for the hanging wall side of the 'Slip 27 Fault' for clarity. In reality westerly dipping joints are present on either side of the 'Slip 27 Fault'.

d) Stability Analysis

The steep inclination of the wedge intersection and the shallow depth of the failure surface beneath the pit slope (Figure 4-17) would suggest that water pressures are not a major contributing factor to this failure. Low rainfall records for the months and days leading up to failure further supports the lack of groundwater pressures in driving failure (see Appendix B1). The early geotechnical report that described failure occurring as a result of mining of the 430mRL bench adds weight to the hypothesis that water pressures are not a significant factor, and that failure is merely a result of undercutting the toe of the wedge. While groundwater is not inferred to be a significant factor in initiating failure, there is a poor management of surficial groundwater runoff in the area around RH27 (as shown on Map Sheet 8) and this will decrease the stability of the failed mass and surrounding slope. Deep channelling in the berms and patches of mud are strong indicators of water ponding following rainfall and then being released rapidly. Some of the water flow paths pass directly into tension cracks around the failure formed (see Map Sheet 8), and groundwater entering these areas will naturally only add to instability of the rock mass through an increase in groundwater pressures and reducing the frictional strength along potential failure surfaces.

Back analysis of RH27 was based on the failure geometry as depicted in Figure 4-17, a schist density (ρ) of 2.7t/m^3 (from UCS test data), and assumed that water pressures are not a major factor contributing to failure. Analysis was undertaken following the Sarma method of slices as outlined by Hoek (1987), and for no cohesion (c'=0) suggests a friction angle (ϕ') of around 39° for the wedge intersection (Figure 4-18). If water pressures are a significant factor contributing to failure, then the back analysis curve depicted in Figure 4-17 is conservative and the ϕ angles will be higher than indicated.

From back analyses of failures previously (Section 4.3), it was established for the Macraes mine that ϕ' angles for joint surfaces with c'=0 ranged from 41°-55°, while for failures along fault planes with c'=0 then ϕ' ranged from 9°-14°. The back analysis results for RH27 seem reasonable given that the calculated ϕ' of 39° (for the wedge intersection) falls within the upper and lower limits defined by joint and fault shear strength properties. It may be unreasonable to assume that there will be no cohesion acting along the surface of the wedge, since the fault gouge material may possess some cohesion while the joints from the joint set controlling failure are unlikely to all join, meaning some failure will occur through intact rock. Assuming a ϕ angle along the wedge intersection ranging from 25° to 35° then the apparent cohesion acting along the wedge intersection ranges from 20kPa to 6kPa respectively (Figure 4-17).

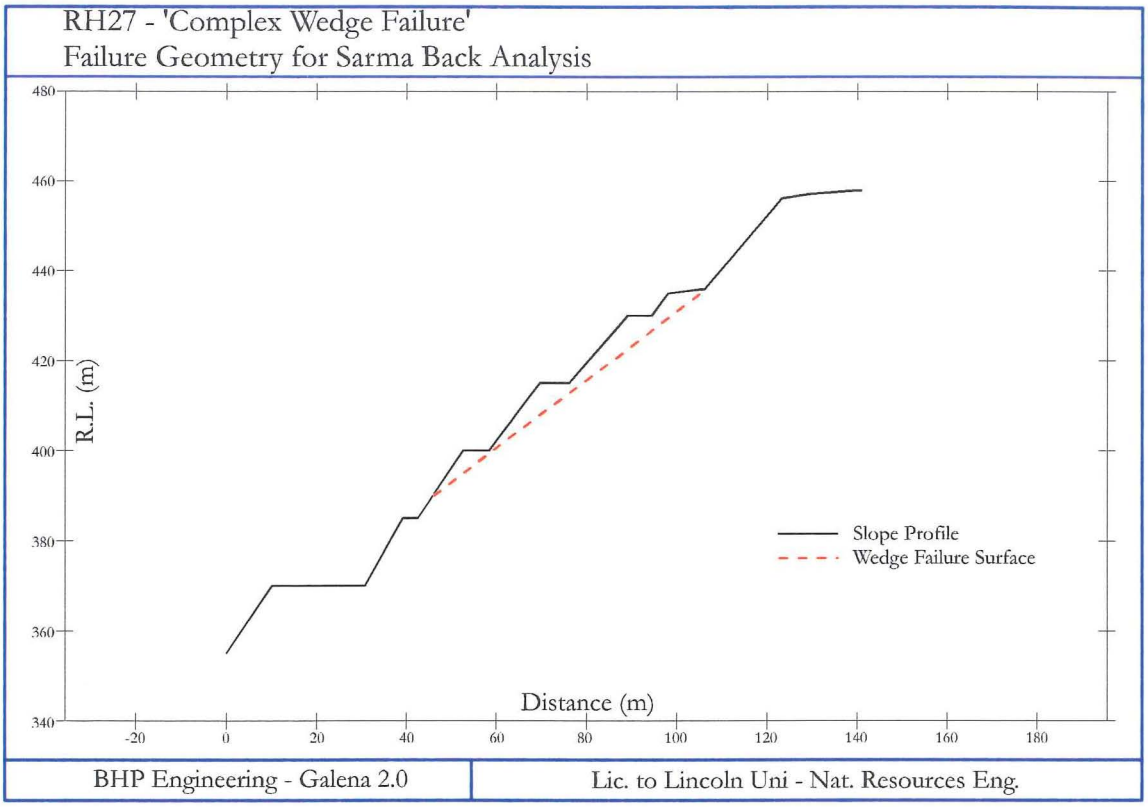

Figure 4-17: RH27 failure geometry for Sarma Back Analysis

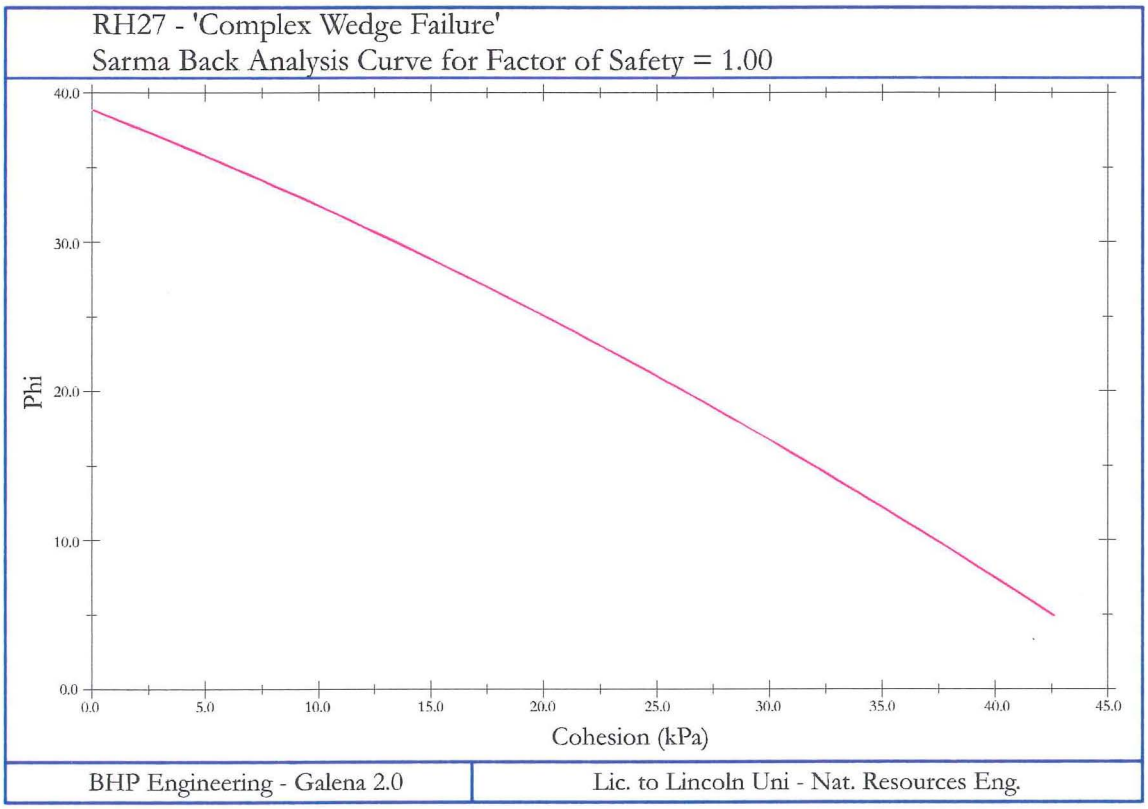

Figure 4-18: Calculated Sarma back analysis curve for failure RH27 illustrating possible combinations of friction (ϕ) and cohesion for the wedge line of intersection as depicted in Figure 4-17.

e) Future Development and Implications

Implications posed by RH27 to future mining operations can be divided into two categories:

1. Rock fall hazard from either the material forming the scree slope, or material derived from failure of the large toppling blocks in the 430 - 435mRL benches to the east of the main wedge (refer Map Sheet 8).
2. Increase in the development of the main failure wedge by stepping out and down along westerly dipping joint set controlling failure with increased depth of excavation of Round Hill pit.

The hazard posed by rockfalls has been virtually eliminated with the creation of a large triangular shaped catch bench (≈20m wide) at 370mRL and a 2 metre high windrow built around the outside of this bench. Field observations suggest that the low strength psammitic schist (dominant above the HWS) breaks up rapidly along schistosity on movement, a fact which is further supported by laboratory testing which showed that psammitic schist has low intact rock strength (see Sections 2.3.2 - 2.3.3). The breaking up of the schist parallel to schistosity tends to produce disc shaped blocks that tend to slide rather than roll. Benches alone should halt the movement of any such rockfalls. Surface runoff following rainfall may contribute to this rockfall instability, and it is recommended that cut-off drains are created at the top of the pit to control surface water runoff.

Figure 4-16 shows that an increase in the development of the current RH27 wedge is unlikely given the reverse offset of the Slip 27 Fault along the Linking Fault. A wedge formed between the westerly dipping joints and Slip 27 fault is inferred to probably daylight somewhere around 390mRL. If this is the case then future development of the wedge is unlikely since the lowest possible wedge intersection between this segment of the Slip 27 Fault and westerly dipping joints has already been reached (Phase 3 of Figure 4-16). A new wedge may develop between westerly dipping joints and the Slip 27 fault below the Linking Fault as illustrated in Figure 4-16 (phase 4). Any new wedge development below the Linking Fault is unlikely to be significant due to the proximity of the Slip 27 Fault below the Linking Fault to the HWS (355mRL in this area). Structural domain analysis (Chapter 3) shows that the joint set (JA1) controlling the south eastern margin to the failure is far less persistent below the Hanging wall shear (Section 3.5.2), and consequently there may be no westerly dipping joints for a new wedge to develop along below 355mRL. Field observations also suggest that the Slip 27 fault plane controlling failure is truncated against other fault structures

in the 340mRL - 355mRL berm. This observation is also supported by structural domain analysis carried out in Chapter 3, which shows that south dipping faults (FA4 c.f. FB4) are far less persistent below the HWS (Section 3.5.3).

4.4.2 Failure RH28

a) Introduction And Previous Work

RH28 is located on the north wall of Round Hill Pit above the Hanging Wall Shear (HWS) (Figure 4-19). RH28 is the second largest pit slope failure currently at the mine and the largest studied during this project, with the only larger pit slope failure being that associated with the current tailing dams movement. Records at the mine show RH28 was first recognised by a contractor as a 'massive slip' on the 14th February 1995. Since this date work associated with RH28 has predominantly been undertaken by Bertuzzi, Eggers and Sullivan from the Australian consulting firm Pells Sullivan Meynink Pty Ltd. Consulting work initially focused on stabilising the failure, however with continuing movement and development the emphasis of present work has begun to focus on failure management, and minimising the impact of the failure on current mining operations.

Bertuzzi (1995) described RH28 as a complex failure consisting of both block sliding to the south along a flat basal surface and a 'quasi-circular failure mechanism', involving westward rotation of a number of fault bounded blocks. The main block (wedge) sliding movement is controlled by the intersection of Bag Farm/Linking fault set and Top/Bottom fault set (Figure 4-19) which plunge to the south out of the face at less than 5° (Eggers and Sullivan, 1995; Bertuzzi, 1995). This wedge failure is released at the rear by a steeply inclined southerly dipping fault plane (Back Fault set). Monitoring prisms located on RH28 show a south-westerly movement out of the face. Bertuzzi (1995) described that while southward movement of the prisms was a result of the main wedge block movement, the westerly component of movement is controlled by quasi-circular movement along the Top/Bottom Fault set (Figure 4-20) with rotational movement to the west. High groundwater pressures along faults in the north wall have been identified as the main feature contributing to failure, with the main wedge failure block being pushed by groundwater pressures formed along the Back Fault Set (Eggers and Sullivan; 1995, Bertuzzi, 1995).

Figure 4-19: Photograph of failure RH28. Photo taken from grid reference: 70159E, 14856N, 497mRL.

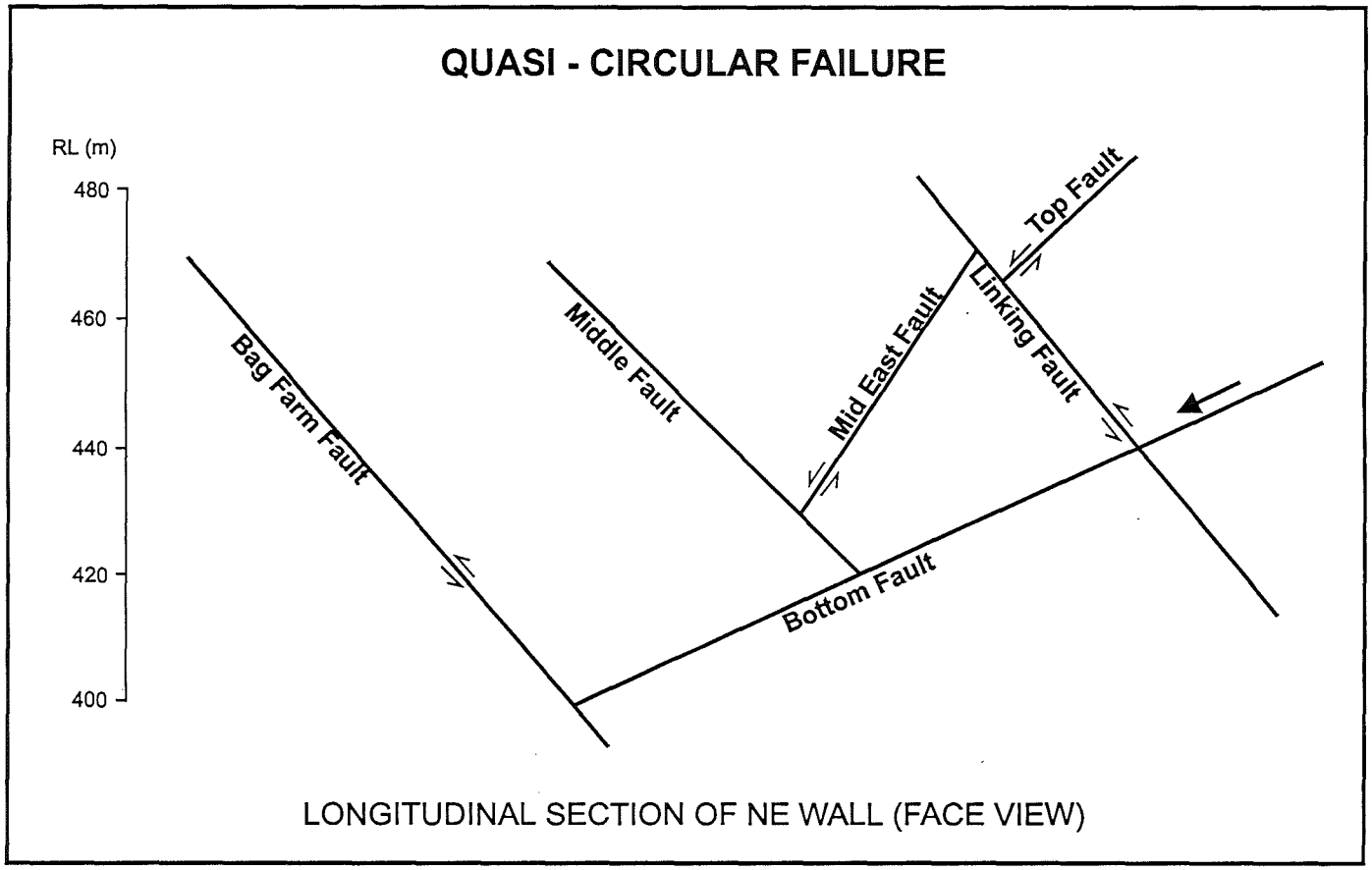

Figure 4-20: Quasi-circular failure movement proposed by Bertuzzi (1995). This movement seems unlikely however with westward movement being more easily explained as complex sliding along westerly dipping structures (see text).

b) Field and Laboratory Investigations

Prior to this project no detailed engineering geological map of failure RH28 was available and most of the north wall appears not to have been mapped as part of the routine face mapping programme at Macraes. Accordingly, engineering geological mapping of RH28 was undertaken during the period April and May 1996, and is presented on Map Sheet 9. The primary objectives of RH28 mapping were: recording of the main features associated with RH28, collection of discontinuity data for the determination of the rock mass structure on the northern wall of Round Hill Pit, and the collection of both fault gouge and schist samples for later strength testing in the laboratory.

The three types of geologic structures observed during field mapping are: schistosity, joints and faults. In addition to the orientation of these structures, other features describing the structures were also recorded such as continuity (length), spacing, roughness, groundwater flow aperture width, and a description of infill material. The recording of this additional discontinuity information serves to aid in the delineation of different structural domains (Priest, 1993), as well as assisting in failure interpretation (both past, present and future). The continuity of defects will control the potential failure volume, while spacing will influence the dilatancy of the rock mass during displacement (Norrish and Wyllie, 1996). The structural information recorded during field mapping of RH28 is presented in Appendix B4.

The main discontinuity sets delineated from field mapping of discontinuities are consistent with those delineated in Chapter 3 and are as follows (Figure 4-21; Map Sheet 9):

1. Schistosity that generally dips at around 20° to the east. Adjacent to faults, the schist may dip at angles up to as much as 45° as a result of fault drag.
2. Three joint sets. An easterly dipping joint set (65/107); a westerly dipping joint set (45/270); and a south- westerly dipping joint set (85/200).
3. Three fault sets. An easterly dipping fault set (50/085); a westerly dipping fault set (35/295); and a southerly dipping fault set (63/192).

Ring shear testing was undertaken on the fraction of fault gouge material passing a 1.18mm sieve for both the 'Bottom Fault' and the 'Bag Farm Fault' (see Section 2.3.4). As for RH27 the ϕ_r angle measured on the material passing a 1.18mm sieve for these faults was very low, with the Bottom Fault giving a $\phi_r = 5.8°$ and the Bag Farm Fault giving a $\phi_r = 5.0°$. As for RH27, because only the fine fraction of the gouge material was tested, the true ϕ_r for the fault gouge material in the field is likely to be considerably higher ($\approx 8°$) than that indicated by ring shear testing (see Stability Analysis).

c) Failure Mechanism Interpretation

Field mapping of RH28 (Map Sheet 9) identified as previously interpreted, that the main failure block for RH28 is controlled by four large faults (Bottom Fault, Bag Farm Fault, Back Fault and Linking Fault) which belong to the three dominant fault sets (FA1, FA3, and FA4) in the area. The main failure block is simply a wedge formed between the Bottom and Bag Farm Faults. The Bottom Fault is truncated along its eastern margin against the Linking Fault, and the failure block is released from the rear by the Back Fault (Figure 4-19; Map Sheet 9). The volume of this main failure block is calculated according to Hoek and Bray (1981) as encompassing approximately 450 000m^3 (≈1.22Mt).

The wedge intersection formed between the Bag Farm Fault and Bottom Fault is interpreted to plunge out of the pit slope at about 182/03 (Figure 4-22). The faults defining the wedge are almost parallel in strike, and because there will be some inherent error associated with measurement of the true orientation, then the true trend and plunge could vary from that calculated (Figure 4-23).

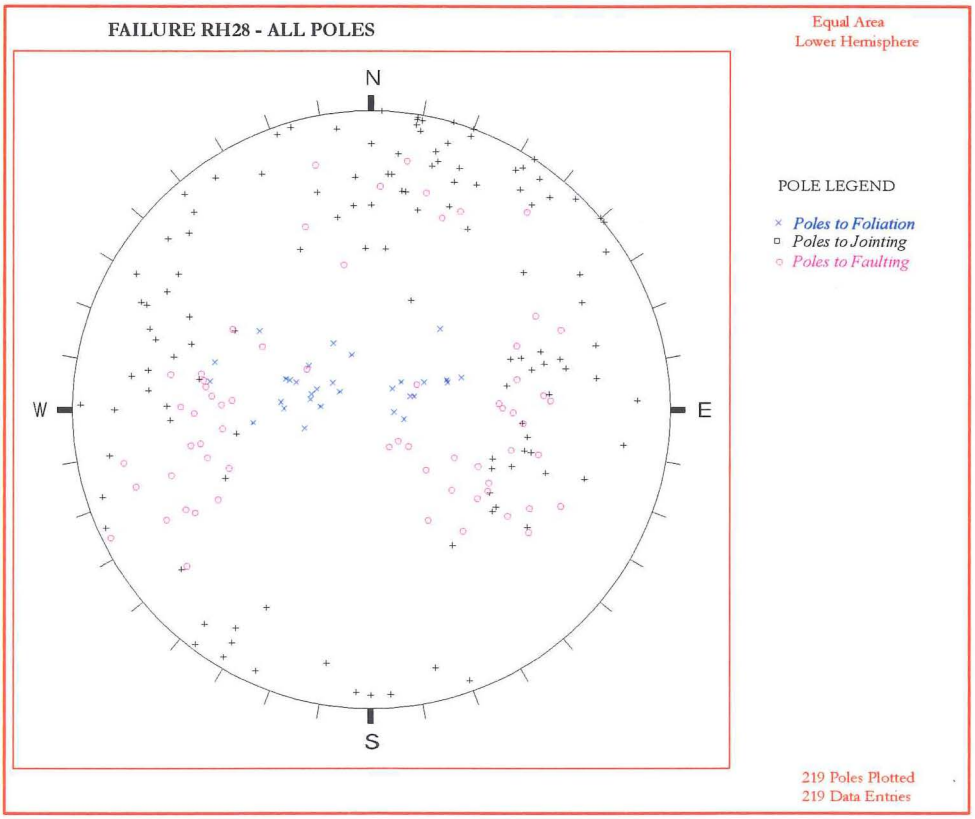

Figure 4-21: Orientation (MMG) of structural features from field mapping of failure RH28

The low angle for the wedge intersection (3°) is of significance in assessing the stability of the failure block. Given that the direction of movement for the failure along the wedge intersection plunges at a very low angle (≈3°) out of the slope, it is clear that there must be a very high shear stress and/or low shear strength material (supported by laboratory testing) along the failure surface in order for movement to be occurring. A program of head unloading was undertaken on RH28 between 470mRL and 460mRL prior to commencement of this project (as indicated on Map Sheet 9). This program of head unloading appears to have had a very limited effect on alleviating movement rates. The lack of success of the head unloading program may be clearly explained as a result of the low plunge for the wedge intersection. The shear force component of a gravitational force (from a weight) acting along the wedge intersection (and sliding direction) is likely to be very small because of the almost orthogonal angle between the weight and the direction of sliding (meaning most of the force from the weight will act as a force, normal to the failure surface).

The 415mRL and 430mRL benches have collapsed above the intersection of the Bottom and Bag Farm Faults in the central area of the main failure block (Figure 4-28) . This collapse appears to be controlled by the release of large schist blocks within the main failure along joints (Set=JA2) striking sub parallel to the berm, intersecting the Bag Farm Fault and daylighting in the pit slope face to the east.

Benches tilt back into the scarp formed along the Back Fault between 460mRL to 470mRL. The tilting of benches is interpreted as localised rotation associated with the breaking up of the main failure mass predominantly along the south dipping joint set. The breaking up of the failure mass and associated rotation of benches back into the main scarp at the rear of the failure block seems possible by either one or both of the two mechanisms listed below:

1. Rotation may be a result of toppling of the benches back into the void created at the back of the wedge as the main failure block moves out of the wall; and/or
2. Rotation may be a result of breaking up of the failure along jointing at the back of the failure, and development of circular failure planes through the broken rock mass.

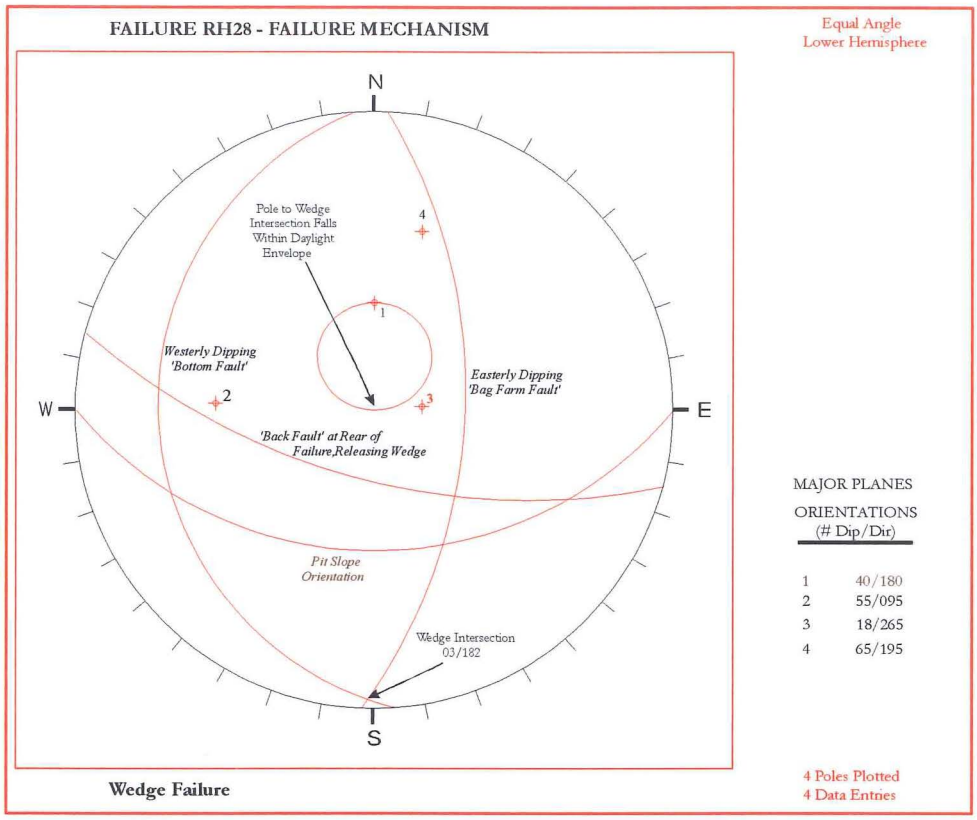

Figure 4-22: Kinematic wedge failure mechanism for failure RH28

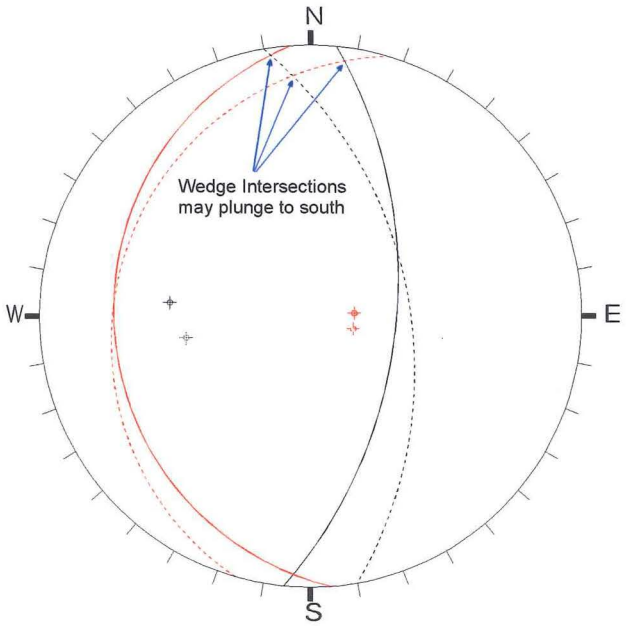

Figure 4-23: Possible error associated with calculation of wedge intersection for RH28 due to measurement error in recording of orientation. Solid lines represent measured fault orientations while dashed lines illustrate possible variances in the measured orientation. It is clear that with even a variation in dip direction of as little as 10° in one or the other of the faults may produce a wedge intersection that plunges to the north.

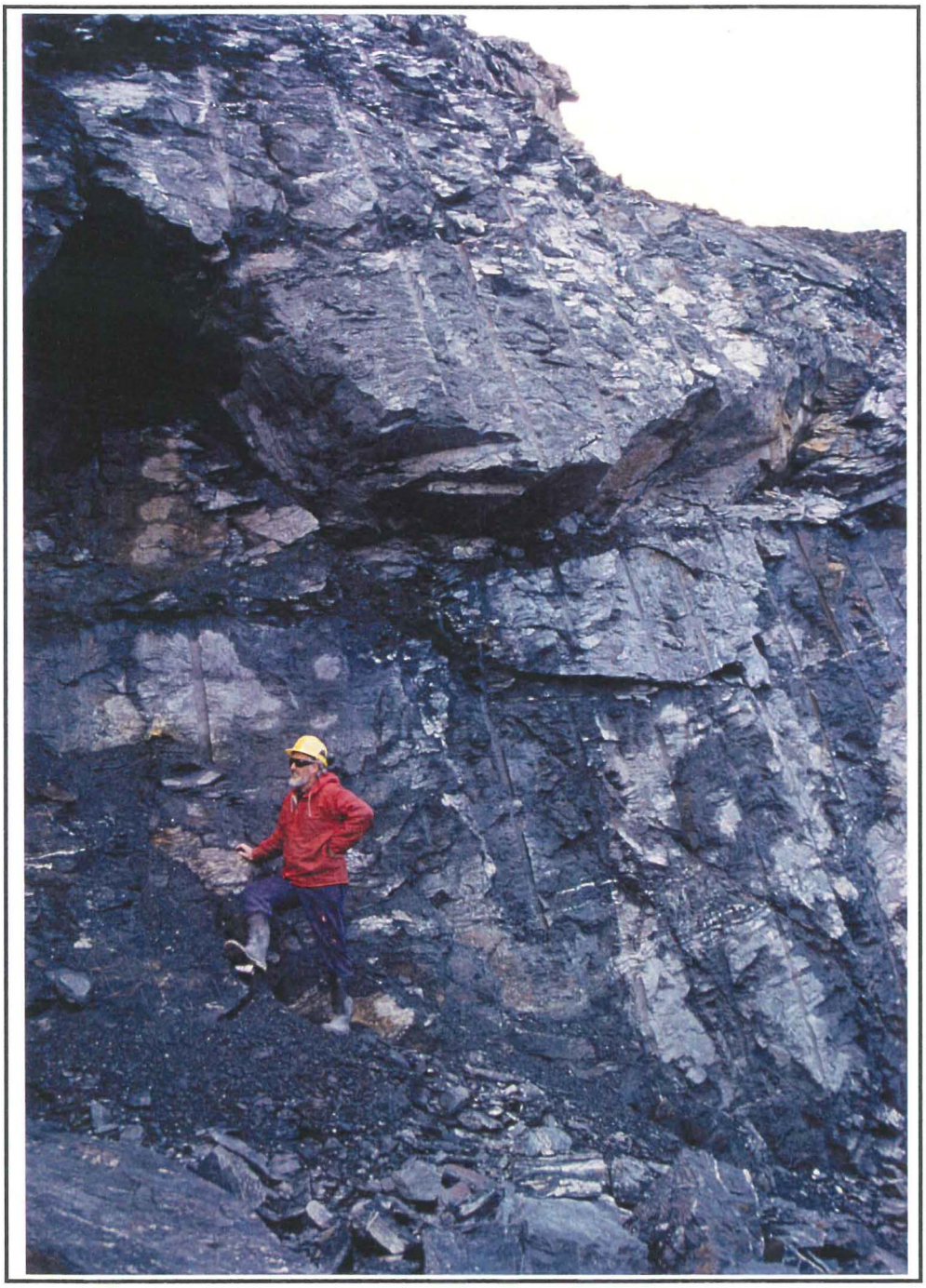

Figure 4-24: Overhang formed along Bottom fault as main wedge failure block is pushed out of pit slope. Offset of smooth wall blast holes indicates that total movement to date along the Bottom Fault is approximately 1.5 metres. Grid reference: 70165mE, 15350mN.

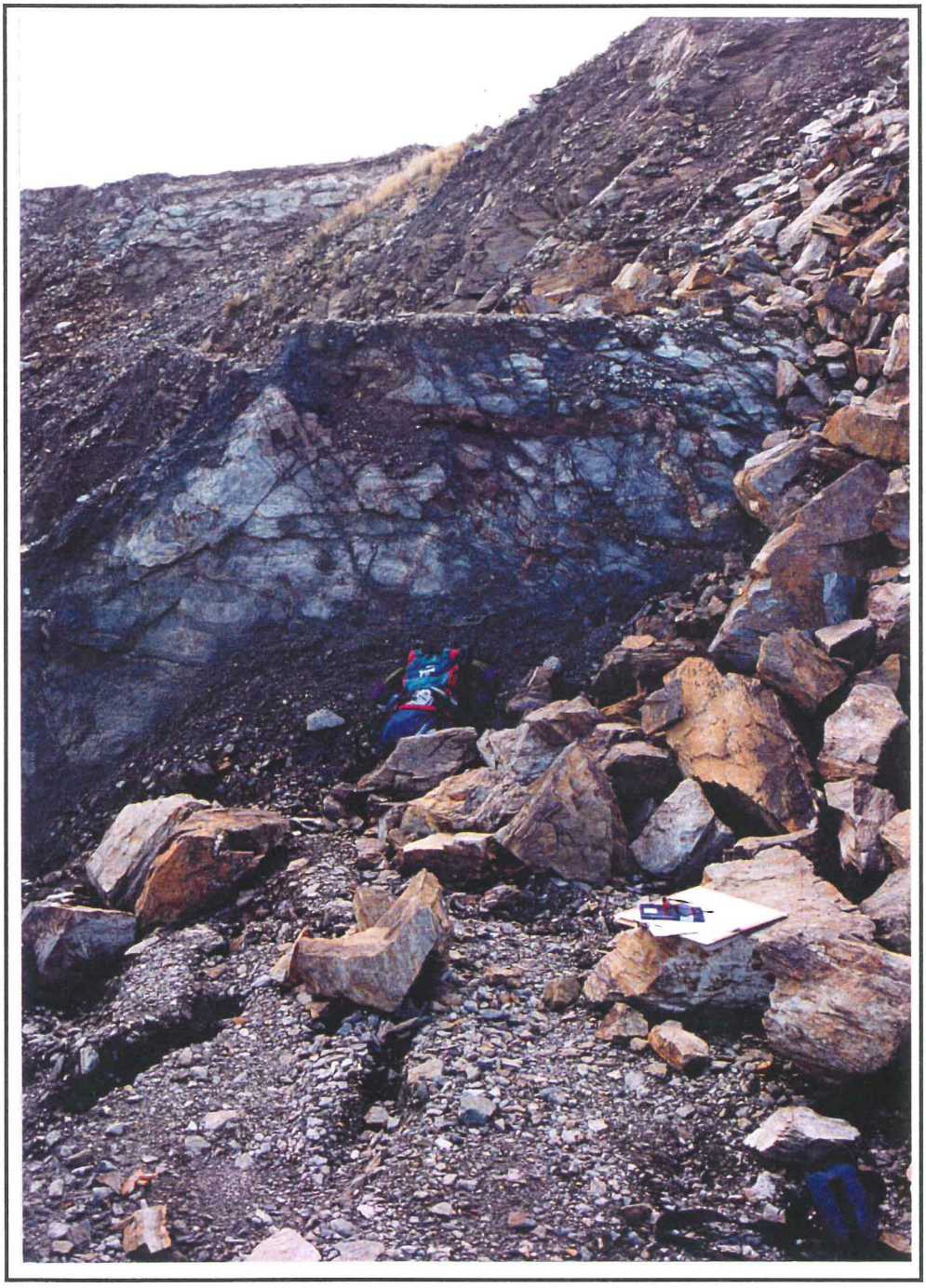

Figure 4-25: Two metre high scarp formed along the Back Fault in the 460mRL - 470mRL berm. Grid reference: 70100E, 15430N.

Figure 4-26: Scarp formed along back fault in 460mRL bench. Note tension cracks along joints in front of scarp formed from dilation of the rock mass. Grid reference: 70075mE, 15425mN.

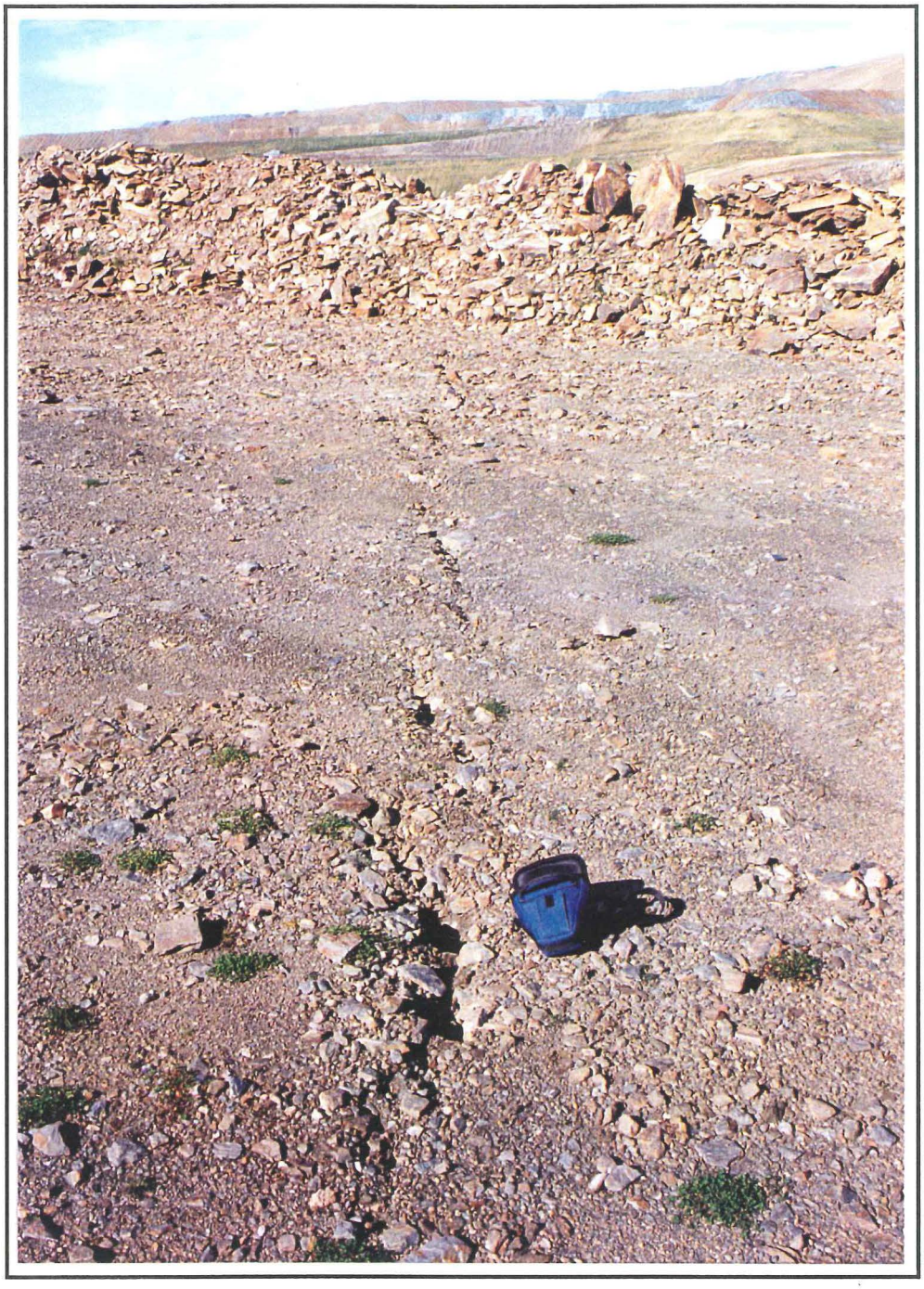

Figure 4-27: Cracking through 470mRL bench interpreted to be indicative of movement on Linking Fault. Note camera bag for scale. Grid reference: 70170mE, 15405mN, 470mRL.

Figure 4-28: Collapse of 430mRL bench in central area of RH28. Bench is released by vertical joint trending sub-parallel to pit slope. Grid reference: 70080mE, 15360mN.

Apart from the large obvious features associated with the main RH28 block movement and described above, a number of other smaller features have also developed around the northern wall of Round Hill pit outside of the main failure block. Smaller features related to movement include cracking, small scarps, and deep tension cracks (up to 5m) formed by dilation along joints. These features are all interpreted to be indicative of movement and dilation of the whole northern wall into the void created in the pit slope by the outward movement of the main failure block.

Small overhangs up to 5cm are also evident along westerly dipping faults below the Bottom Fault as shown on Map Sheet 9. These overhangs are interpreted here to be a result of continuing volumetric growth of the failure and stepping out of the main wedge onto more distal faults from those currently defining the main wedge failure block between the Bottom and Bag Farm Faults. These increases in the size of the wedge merely reflect the structure of the north wall (and above the HWS) where steep easterly dipping (fault set FA1) and shallow westerly dipping (fault set FA3) faults intersect to form gently dipping (<10°) north-south trending wedge intersections, which are released by the south westerly dipping fault set (fault set FA4). For example the increase in failure volume represented by the wedge formed between the overhangs present in the 370mRL - 385mRL and the Bag Farm fault is approximately 800 000m^3 (≈2.16Mt), representing an increase in failure volume in the order of 350 000m^3. Recent communications with the Macraes Engineering Geologist (D. Stewart pers. comm., June 1997) suggest that failure may have even increased beyond this size, and that the present wedge intersection may now daylight as low as 360mRL in the pit wall If this is the case then the total volume encompassed by wedge failure movement is now in the order of $1.6\times10^{-6}m^3$ (≈4.32Mt).

Movement records are available for a number of prisms around the north wall and these are presented in Appendix B5. Monitoring from these prisms shows that movement is generally in a south westerly direction (Bertuzzi, 1995). Unlike Bertuzzi (1995) this south-westerly movement is not interpreted as a result of quasi-circular failure within the major fault bounded blocks. Field mapping showed no evidence for westerly rotation of blocks within the main wedge failure complex. Indeed a more simplistic solution to the westerly component of movement is that it is a result of dilation and complex sliding along major westerly dipping fault and joint sets (FA3 & JA1), and/or movement along south westerly trending wedge intersections formed between some of the westerly (FA3) and easterly (FA1 & FA2) dipping faults. Given that the majority of failure movement appears to be occurring in the central area

of the block, the natural tendency of the outer margins of the block will be to move towards the main wedge intersection, and down the dip of the structures forming the wedge.

In addition to the prisms already installed around the north wall, simple crack pins were also installed on some of the cracks around the north wall during field studies. Crack pins have the advantage over prisms that they are of negligible cost, easily installed, allow for quicker and more regular data collection than prism data, and can be combined with routine visual inspections of the failure. The disadvantage of using crack pins, however, is limitations in the accuracy of the data collected. Pins were constructed from cut pieces of stainless steel pipe into lengths of about 30cm and forced into the ground either side of cracks (Figure 4-29). A steel tape is then used to measure the distance between the pins (outer edge of pin to outer edge). Locations of crack pins are shown on Map sheet 9 while the measurement records are given in Appendix B6.

Crack pin data failed to show any definite trends of movement over the two month period for which monitoring data was collected. Although pins generally failed to show any detectable movement, the appearance of new cracks in areas where pins were installed is clear evidence that movement in areas of installation was occurring. As previously pointed out for RH33, it may be that if water pressures were driving movement, then the opening up of cracks may be enough to alleviate the groundwater pressures on that particular structure and halt movement. Subsequently groundwater pressures may then build up on an adjacent structure and cause movement on that structure, and the creation of new cracks.

Figure 4-29: Typical set up of steel crack pins across a crack on failure RH28. Crack pin Q, grid reference: 70200mE, 15430mN

d) Stability Analysis

Back analysis of RH28 was based on the model depicted in Figure 4-30 and an assumed pit slope profile, prior to failure and the program of head unloading. Only two piezometers (SP10 & SP13) are available in the area around RH28 from which groundwater data could be interpreted. Accordingly there is some uncertainty for this part of the failure model. Back analysis is based on an assumed schist density of 2 700 kg/m^3 and fault gouge density of 2 000 kg/m^3. The calculated back analysis curve for this model of failure RH28 is depicted in Figure 4-31.

Given that the faults controlling failure RH28 are structures which have been subjected to a considerable amount of shear strain in the past, then as discussed previously in Chapter 2 it would seem reasonable to assume a value of cohesion equal or close to zero, giving a friction strength for the fault gouge controlling RH28 of around 13° (Figure 4-31). If the fault gouge does possess some cohesion then from Figure 4-31 it can be seen that the ϕ_r angle will be even lower than 13°. The calculated friction angles for RH28 are much lower in this study than those previously assumed for the mine site of c' = 10 to 14kPa and ϕ' = 15° to 17° (Bertuzzi, 1992).

Once again there is a discrepancy between the residual friction angles measured during ring shear testing (Bottom Fault = 5.0° and Bag Farm Fault =5.8°) and those calculated by back analysis (ϕ_r = 13°). This discrepancy can be explained by the fact that the coarser material present in the fault gouge in the field which is not tested in the laboratory will increase the ϕ_r of the material, while surface irregularities (roughness/waviness) along the fault walls will also increase the frictional strength if the fault aperture width is small enough to allow contact. Hence a correction value between the laboratory ϕ_r for material passing a 1.18mm sieve (≈5-6°) and the in-situ ϕ_r calculated by back analysis (13°), appears to be equivalent to about 8°.

Factor of safety (FS) analysis of RH28 was undertaken to assess the influence of the different geotechnical components influencing instability. FS calculations were based on the slope geometry depicted in Figure 4-30 and on assumed schist properties of c'=15kPa, ϕ=35° and ρ = 27kN/m^2, and on assumed fault gouge properties of c'=0kPa, ϕ=13° and ρ = 20kN/m^2. Calculations show that for a piezometric surface as depicted in Figure 4-30, the FS is slightly below one (0.950) indicating the slope will be unstable. If the piezometric surface were drained to beneath the failure surface then the factor of safety may increase to slightly above one (1.029). This analysis indicates that, while reducing the water pressures in the slope would increase the overall stability, RH28 would still only be marginally safe and susceptible to movement following the introduction of significant groundwater by either rainfall and/or snowmelt.

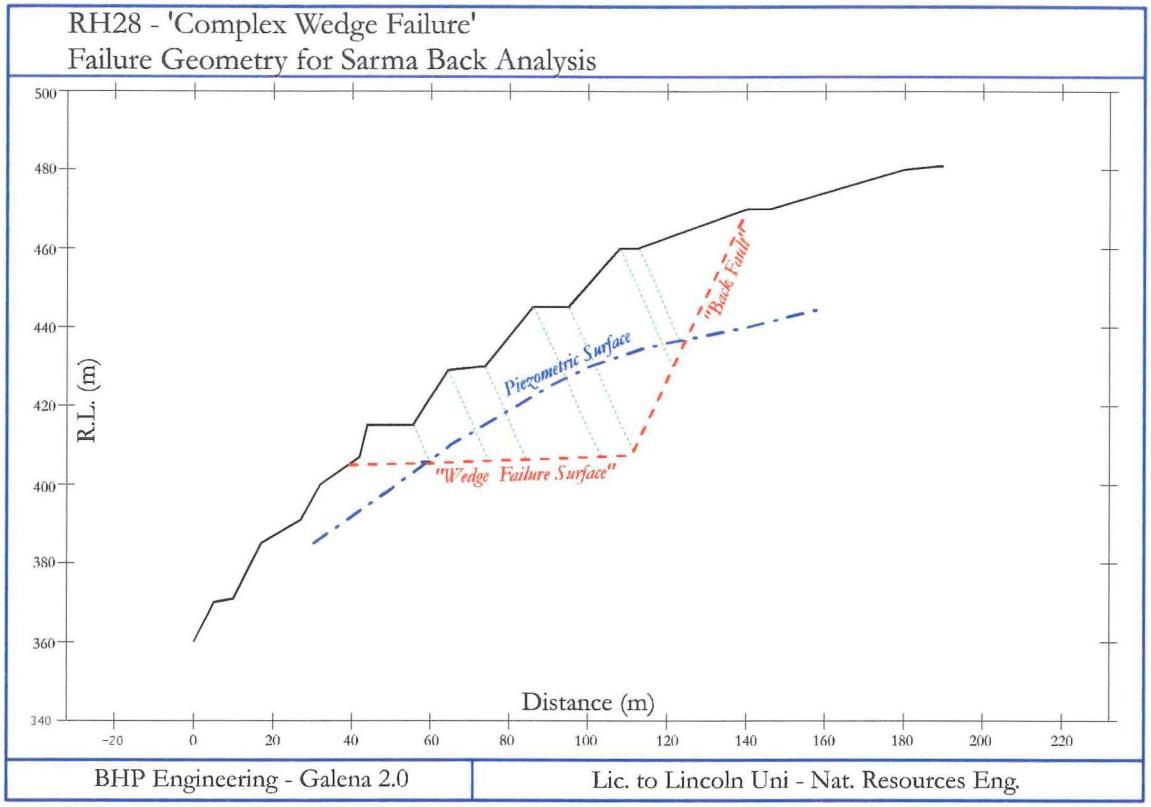

Figure 4-30: RH28 model for back analysis.

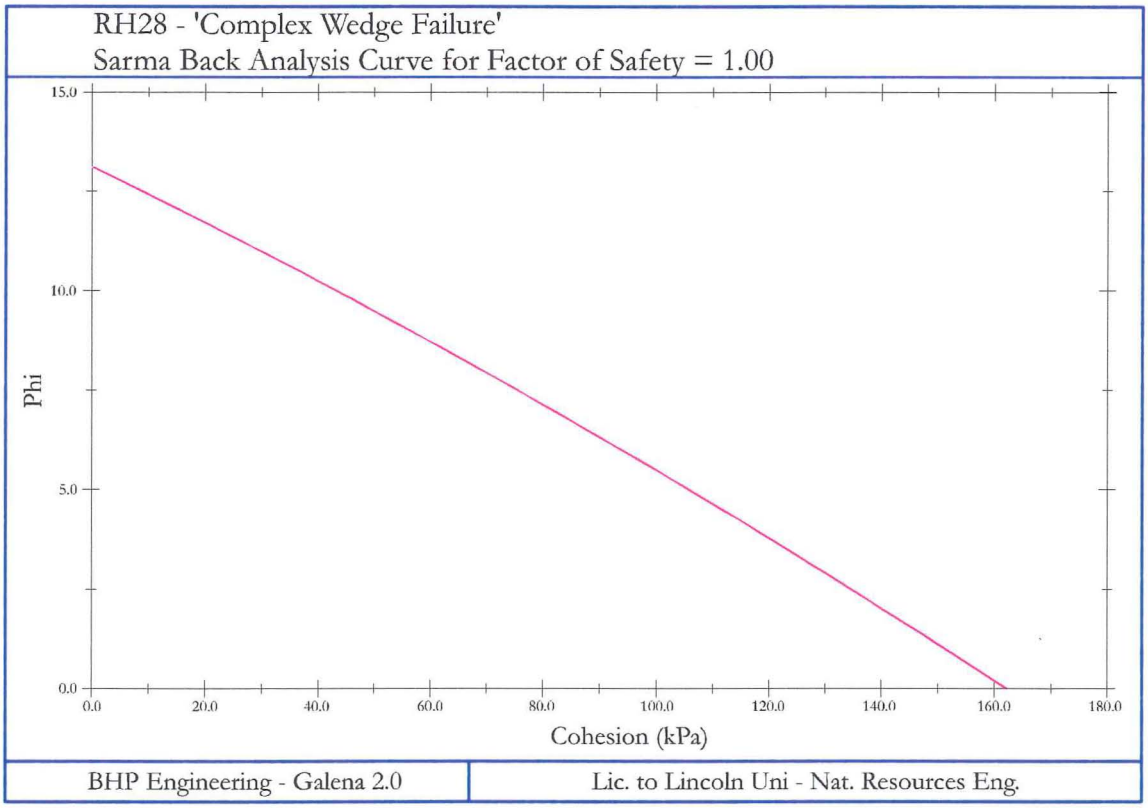

Figure 4-31: Sarma back analysis curve result for failure RH28 illustrating possible combinations of friction (ϕ) and cohesion (c) for the wedge line of intersection as depicted in Figure 4-30.

e) Future Development and Implications

The effects of groundwater pressures driving failure RH28 have been recognised and emphasised for some time now (Sullivan, 1995; Eggers and Sullivan, 1995), and the assessment undertaken here only reiterates this point. However, while groundwater and slope depressurisation have previously been interpreted as the most significant geotechnical factor (Sullivan, 1995), laboratory testing and back analysis undertaken during this project shows that the presence of swelling clay minerals of lower than previously calculated shear strength is also of geotechnical significance.

The fact that the FS is so close to equilibrium, combined with the extremely low ring shear readings recorded, suggests that even reducing water pressures may not be sufficient to stabilise movement of this failure. Further, the construction of a toe buttress to the failure is not a viable option due to the height of the wedge intersection above the pit floor and access problems (Figure 4-19). Accordingly current work needs to be based around failure management and evaluating suitable alarm criteria for the slide to minimise risk to personnel in the pit should rapid failure occur.

Five hazard scenarios can be recognised as being associated with failure RH28:

1. Release of the more rapid moving block in the central area of the slide (Map Sheet 9)
2. Toppling of blocks at the 465mRL (Grid reference: 70110E, 15390N)
3. Failure of one of the smaller wedge blocks underneath the Bottom fault in turn releasing the main failure block (Ryan pers. comm., 1996).
4. Complete failure of the main wedge block.
5. Continuing and increasing expansion of movement on the north wall of Round Hill pit.

Release of the more rapidly moving block in the central area of the failure represents a hazard from two aspects. Firstly, there is the immediate hazard to personnel on the pit floor associated with failure of that block. Secondly, there is the hazard associated with failure of the main wedge failure, as a result of a sudden loss of toe support following failure of one of these smaller more rapidly moving blocks at the toe of the main wedge.

A number of deep (≈5m) tension cracks along joints are present within the main wedge failure block associated with movement of the block. Most of these cracks are formed along vertical-subvertical east-west striking joints. The potential exists for toppling failures along these tension cracks out of the pit slope. Lateral detachments to toppling are abundant

in the form of easterly and westerly dipping discontinuities (both joints and faults). RH31 is a prime example of this type of toppling failure. Presently the main area at risk to toppling appears to be the large toppling crack passing from 445mRL to 470mRL (70110E, 15390N). This crack can be traced for tens of metres and no wide catch benches are present beneath it (unlike further to the west where a large catch bench is present at 365mRL). Installation of a prism at the top of this block where the greatest amount of rotation, and hence most movement would be occurring was recommended (Chapple, 1996).

On the more rapidly moving areas of the slide like those described above it is recommended that simple wire extensometer alarm systems be installed as an added precaution (Figure 4-32). In this system a threshold for acceptable movement for a given time period should be determined. Once movement exceeds this threshold an alarm would be triggered, and the pit should be evacuated beneath the failure until the failure is visually inspected and checked for stability. This warning system has the advantage that it is cost effective, with the only disadvantage being determining an appropriate threshold at which the alarm should be triggered. A threshold is probably best determined by the review of prism monitoring records (by experienced personnel) and some trial and error, with initial judgements for acceptable daily movement lying on the conservative side.

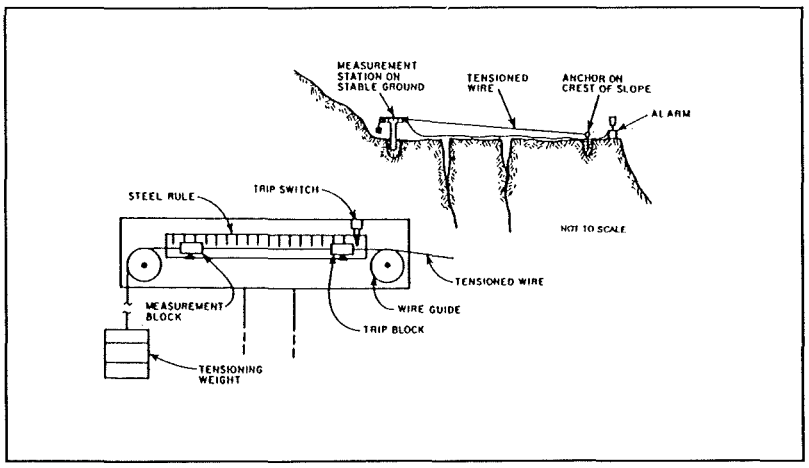

Figure 4-32: Simple wire extensometer alarm system that may be used across tension cracks to warn of failure. Once tensioned wire tightens a given amount due to slope movement a trip switch is triggered activating alarm (Johnson, 1982).

As can be seen from Map Sheet 9 the presence of a number of large faults passing through the wall means that the wall as a whole consists of a number of fault bounded blocks. If one of the blocks in the lower part of the wall were to fail then toe support of the main failure block would be removed. The weight of the failure mass above these blocks would suggest that failure of these lower blocks is probably unlikely. However, a significant

build up of groundwater water pressures behind a block may cause a blow-out effect and failure of the block. For this reason installation of prisms on some of the lower fault bounded blocks was also recommended (Chapple, 1996; see Map Sheet 9). Prisms would be monitored for accelerations in these areas and provide early warning of possible failures, as well as minimise any risk associated with visual inspections of these areas to mine personnel. Accessibility problems with equipment has meant that as yet these prisms are yet to be installed (Stewart pers. comm., June 1997).

With continuing movement of RH28 complete failure of the slope becomes a significant risk due to breaking up and weakening of the rock. Countering this is the fact that if the failure is being driven by groundwater pressures then breaking up of the failure will create new secondary permeability that will drain groundwater from the failure increasing stability. Probably one of the more important facts relating to RH28 that does not appear to have been recognised by previous workers relates to the geometry of the faults controlling failure. As discussed earlier the parallel strike of the two defects controlling the main wedge, means that a slight variation in the orientation of either fault (due to undulations along the fault) could produce a wedge intersection that plunges to the south (see Figure 4-23). If the same fault structures are present in the south walls of pits, which they appear to be from both field and structural domain analysis (Chapter 3), then the same major failure complex may develop in a north facing wall. Therefore it is recommended that the south walls of the major pits be mapped and checked for this type of failure mechanism. Movement monitoring prisms should also be installed on potential failure areas as an early warning system of movement and possible failure.

It is not practical to alter the strength properties of the fault gouge on which failure is occurring, and as described above, head unloading of the failure is likely to have limited success (unless very large volumes of material are removed) due to the low angle of the wedge intersection. The installation of horizontal drains (Figure 4-33) as previously recommended (Bertuzzi, 1995; Eggers, 1995; Eggers and Sullivan, 1995; Sullivan, 1995) is further emphasised here as the only practical means of stabilising this failure through the alleviation of the groundwater pressures that are driving the failure.

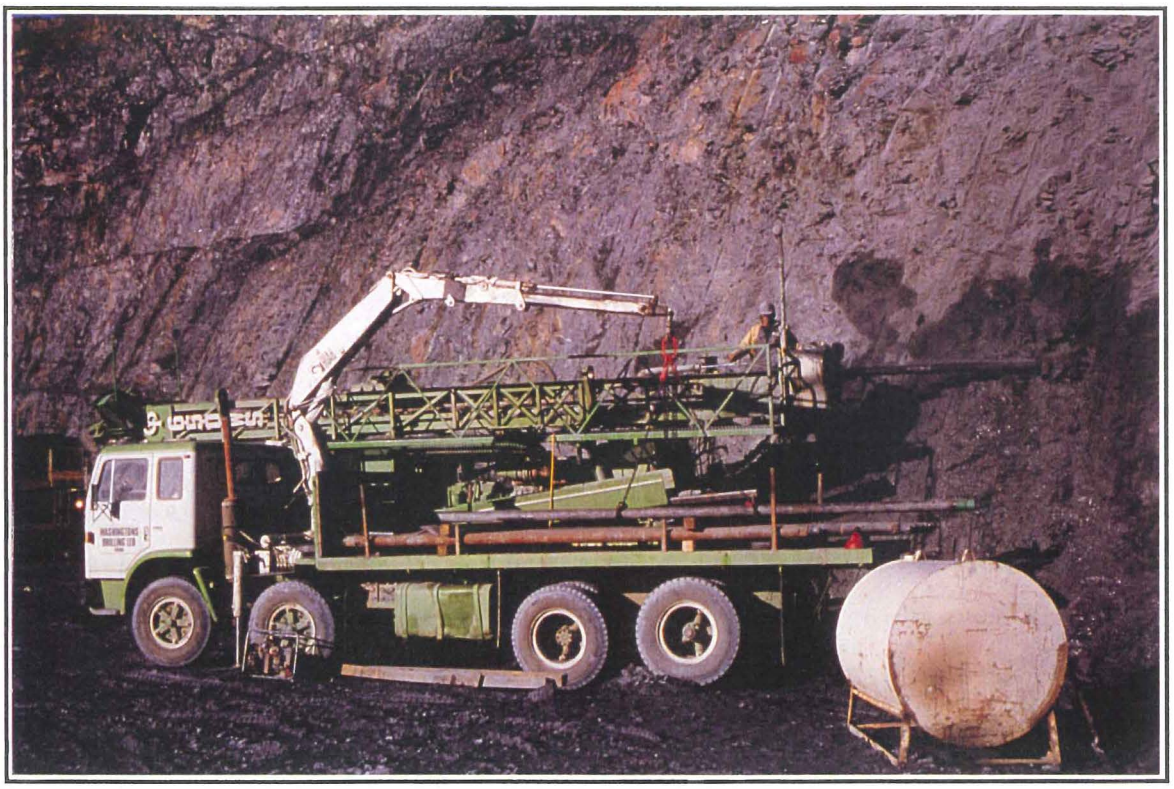

Figure 4-33: Installation of horizontal drains like these form the most practical solution to stabilising failure RH28.

4.5 DISCUSSION AND SYNTHESIS

A pit slope failure database serves a number of functions during mining operations including: assessing failure development, assessing the effectiveness of remedial measures, developing failure models, calibrating predictive rock mass models for pit slope failures, providing data for determination of shear strengths by back analysis, and providing construction records for the ongoing assessment of pit slope design. Prior to this project there was no formal pit slope failure database at the mine, and as such a substantial amount of information that would normally be expected to be available is not. A number of failures previously recorded also appear not to be kinematically possible with failure surfaces dipping at angles steeper than the slope.

A standard recording sheet for pit slope failures at the mine was developed with the primary purpose of the sheet being to assist in engineering geological site investigations by documenting failures. Such a recording sheet increases consistency between different personnel and ensures that key information is recorded. Reports collected over time will form a pit slope failure database which may have a number of uses at the mine as discussed above.

The recording sheet has also been incorporated into Microsoft's Access for Windows95, which increases the ability to search for and report specified failure information.

During field investigations 9 new failures were observed (RH30-RH36, IM2 and IM3). These new failures combined with previously recorded failures show that pit slope failures at the mine can be classified into the groups recognised by Hoek and Bray (1981) as: planar, toppling, and wedge failures. A fourth failure type as described by Varnes (1978) and Cruden and Varnes (1996) is also evident at the mine, and these are referred to as complex failures involving a combination of the Hoek and Bray (1981) failure types.

Planar failures at the mine can be further classified according to the angle of the failure plane as low angle block planar failures, and high angle planar failures. Wedge failures can also be further characterised depending on the discontinuities controlling the wedge in increasing order of significance as joint-joint wedges, joint-fault wedges and fault-fault wedges. Back analysis of failures observed during field investigations suggests high frictional strengths ranging from approximately 45° to 55° (cohesion = 0) for joint surfaces, with high friction being attributed to surface roughness/waviness. The shear strength of joints at Macraes is discussed in more detail in Chapter 5 (Section 5.3.2).

Back analysis of failures occurring along faults supports low frictional strengths as previously measured by ring shear testing. Frictional strengths calculated by back analysis for faults ranged from 9° - 14° (cohesion =0). The discrepancy between laboratory tests and back analysis calculations is largely inferred to be a result of the coarse material present in the gouge material in the field, which has to be removed for laboratory testing (but surface irregularities along the fault walls may also be responsible for some of the increase in friction). It would appear that the need to remove the coarse material from the sample for laboratory testing inevitably produces much lower frictional strengths than those existing in reality in the field. It is recommended that ring shear test results are unsuitable to apply directly to the fault gouge material in the field, and that ring shear results need to be corrected for this discrepancy. The use of a larger ring shear apparatus which can test larger grain size material may solve this problem in the future. Testing in this thesis would suggest that the sieving out of the material greater than 1.18mm has the effect of lowering the frictional strength by approximately 3 - 8°. Once again the shear strength of faults is discussed in more detail in Chapter 5 (Section 5.3.2(b)).

RH27 and RH28 are two large failures present in Round Hill pit that occurred prior to this project and these were studied in some detail. Mapping of RH27 suggests that the previously interpreted oblique planar failure mechanism by Bertuzzi (1995) is unlikely, and it

is suggested here that RH27 is actually a wedge failure formed between a large fault and a westerly dipping joint set which has a current failure volume of approximately 900m^3 (or 2 430 tonnes). The failure of RH27 seems to be a result of low shear strength material and undercutting of the wedge line of intersection. The Slip 27 fault defines the north-western margin to the wedge, and this is offset by the Linking fault. The offset of the Slip 27 fault appears to have prevented wedge development beyond 390mRL. Future development of the wedge appears to be possible below the Linking fault although structural domain analysis would suggest that this is unlikely due to a change in the rock mass structure below the Hanging Wall Shear.

RH28 is a complex wedge failure in the north wall of Round Hill pit. Failure is formed between easterly and westerly dipping faults which form a wedge failure block that plunges gently to the south. A relatively steeply dipping fault releases the wedge failure block from the back. Bertuzzi (1995) described a quasi-circular failure mechanism to account for the westward movement of survey monitoring prisms. Structural interpretation of the north wall during this project suggests westward movement of survey prisms may be more simply explained by dilation and complex sliding along westerly and south westerly dipping structures. At the time of mapping a total of about 1.5 metres movement on the main faults controlling failure appears to have occurred, and the volume calculated being encompassed by the Bag Farm, Bottom, Linking and Back Faults is approximately 450 000m^3. RH28 also appears to have stepped out on to more outlying faults involving a substantial increase in failure volume, which may be as high as 1.6×10^6m^3 (if the wedge intersection now extends to 360mRL). RH28 as previously described appears to be driven by high water pressures, however back analysis suggests fault gouge material is of much lower shear strength than previously assumed ($c' = 0$, $\phi'=13°$ c.f. c'=14-10kPa, ϕ'=15-17°), and low shear strength material is consistent with laboratory data. Prior to this project a programme of head unloading of the failure was undertaken, although this appears to have had limited success. The lack of success can largely be explained by the lack of gravitational force that is transferred as a shear stress due to the low angle of the wedge intersection.

Five hazard scenarios are evident with RH28 and these range from localised failure to total collapse of the northern wall. It is recommended here that simple trip wire alarms be installed on the more rapidly moving areas of the failure. An appropriate movement threshold needs to be determined, where movement beyond this threshold triggers an alarm, and personnel and equipment are restricted access to beneath the failure until the failure has

been visually inspected for stability. The management and monitoring of failures is discussed in more detail in Chapter 5 (Section 5.6).

The fact that the faults controlling the main wedge intersection are almost parallel in strike to each other means the wedge intersection tends to form a low angle. This also has important implications for the southern walls of the pits at Macraes which does not seem to have been recognised by previous workers. Even a small variation in orientation of either the westerly or easterly dipping faults may result in a wedge intersection that plunges to the north. If the same type of fault structure controlling RH28 occurs in a southern wall, and if the material properties and groundwater pressures are similar to the northern wall then the same large complex wedge failure may develop in a south wall. It is recommended that the south walls of the main pits are mapped and inspected for this type of failure. If a potential failure(s) of this type is recognised, then more monitoring prisms will need to be installed to provide early warning of failure. Adequate slope depressurisation through the installation of horizontal drains should prevent this type of failure in the future.

CHAPTER 5 : INTEGRATED PREDICTIVE ROCK MASS MODEL FOR PIT SLOPE FAILURES

5.1 INTRODUCTION

As outlined in Chapter 1, one of the principal objectives of this thesis was the construction of an integrated predictive rock mass model for pit slope failures at the Macraes Gold Mine. Like all engineering geological investigations undertaken in this thesis the construction of a predictive rock mass model for pit slope failure aids the long term performance of the mine through the reduction of any adverse effects associated with pit slope failures through prediction and associated intervention where possible. This chapter integrates the information from Chapters 2-4 for the future prediction of pit slope failures at the mine. As such this chapter looks at the influences of the following factors on pit slope failures at the mine:

- hydrological influences (Section 5.2);
- intact rock strength and shear strength properties on pit slope failures (Section 5.3);
- structural controls on pit slope failures (Section 5.4);

Predicted models for slope failures at Macraes are developed based on the above factors and comparison with those failures recorded to date at the mine site (Section 5.5). Finally, the importance of monitoring and management of pit slope failures is discussed (Section 5.6).

5.2 HYDROLOGICAL INFLUENCES ON PIT SLOPE FAILURES

As noted previously in Chapter 4 groundwater pressures are a major factor in contributing to the instability of the pit slopes at Macraes Gold Mine, particularly with regards to failures with low angle shear surfaces or wedges with low wedge intersection angles (i.e. less than 20°).

Groundwater pressures in the pit slope contribute to instability by two separate mechanisms (Figure 5-1). Firstly, groundwater pressures along discontinuities within the slope

will reduce the effective stress in the slope material, thereby reducing the frictional resistance to sliding. Secondly, groundwater pressures at the back of the slope may generate a significant force towards the open pit. It is important to understand that both of these mechanisms are a result of groundwater pressure rather than groundwater quantity (Hoek and Bray, 1981; Cook, 1982; Brown, 1982).

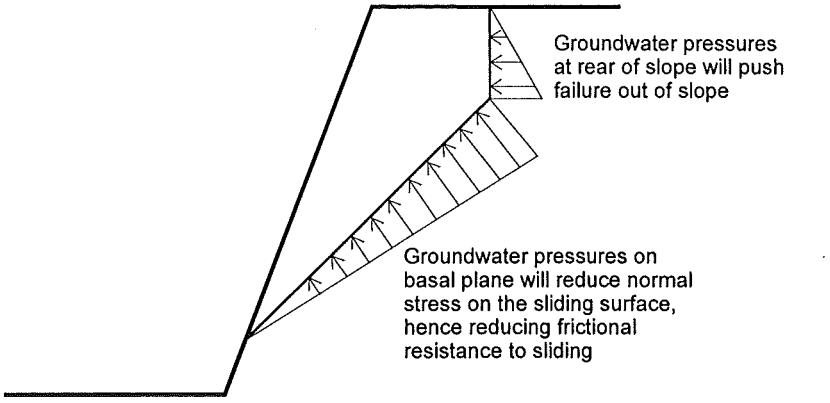

Figure 5-1: Effects of groundwater on rock slope stability.

Although significant water flows into the pits at Macraes were not generally observed during field investigations it has been suggested that groundwater pressures are probably still very high at Macraes as evidenced by seepage from faults (Figure 5-2; Sullivan, 1995). Apart from these field observations, the effects of high groundwater pressures contributing to pit slope failures is also supported by the pit slope failure database. As noted in Chapter 2 comparison of failures with rainfall records shows that surficial pit slope failures (where the failure surface is less than 5 metres deep) typically occur within 24 hours. Further, it was noted that for piezometers the lag time between rainfall and piezometric response was in the order of one to two weeks, and this greater lag time is interpreted as the greater distance over which water needs to permeate to affect piezometers (since piezometers are located further back into the pit slope).

The importance of adequate slope depressurisation for the prevention of failures at Macraes as previously recommended and discussed by workers Bertuzzi, Eggers and Sullivan, is once again emphasised here. Slope depressurisation may be best achieved at the mine through the installation of horizontal drains as new berms are excavated. The low interpreted permeability for intact schist (Chapter 2) means that slope depressurisation will only be effective through drainage of the rock mass structures in the pit slope. Currently most of the horizontal drains at the mine are orientated perpendicular to the pit slopes. It is suggested here that horizontal drainage will be most effective when drains are installed such that they

intersect as many of the main fault and joint sets per length of drill hole as possible (Figure 5-3). For example, above the Hanging Wall Shear (HWS) (and within the Hanging Wall Zone Domain (HWZD)) the major fault structures to drain are FA1, FA2, FA3, FA4 and FA5. Consequently for south facing pit slopes fault sets FA1-FA3 will be perpendicular to the slope and should drain relatively freely in the face, and holes should therefore be targeted at draining fault sets FA4 (45/205) and FA5 (75/020), trending into the wall perpendicular to the strike of these structures (towards 020 to 025; Figure 5-3 ($90-\alpha=70°$)). The successful orientation of drainage holes emphasises the importance of good structural information so the relevant α angle (see Figure 5-1) is known with some certainty. It should be noted that all of the holes will also need to be angled up into the wall so that water can drain out of the holes under the influence of gravity.

Figure 5-2: Photo of the eastern wall of Round Hill pit following a day of rainfall. Wet patches indicate groundwater seepage from a number of faults present in the pit slope.

Installation and daily monitoring of piezometers around the pit slopes is also recommended so that the effectiveness of installed horizontal drainage may be assessed. Monitoring of piezometers should be based on developing relationships between precipitation and groundwater response, identifying areas of high groundwater pressures and monitoring the effects of horizontal drainage when it is installed. It is probably not feasible to

manually monitor every piezometer around the mine every day (although the installation of automatic monitoring would solve this problem), so it is recommended that those piezometers located above current mining activities as well as those adjacent to large active failures (such as RH28) are checked on a daily basis. All other piezometers around the area should be monitored on a weekly basis.

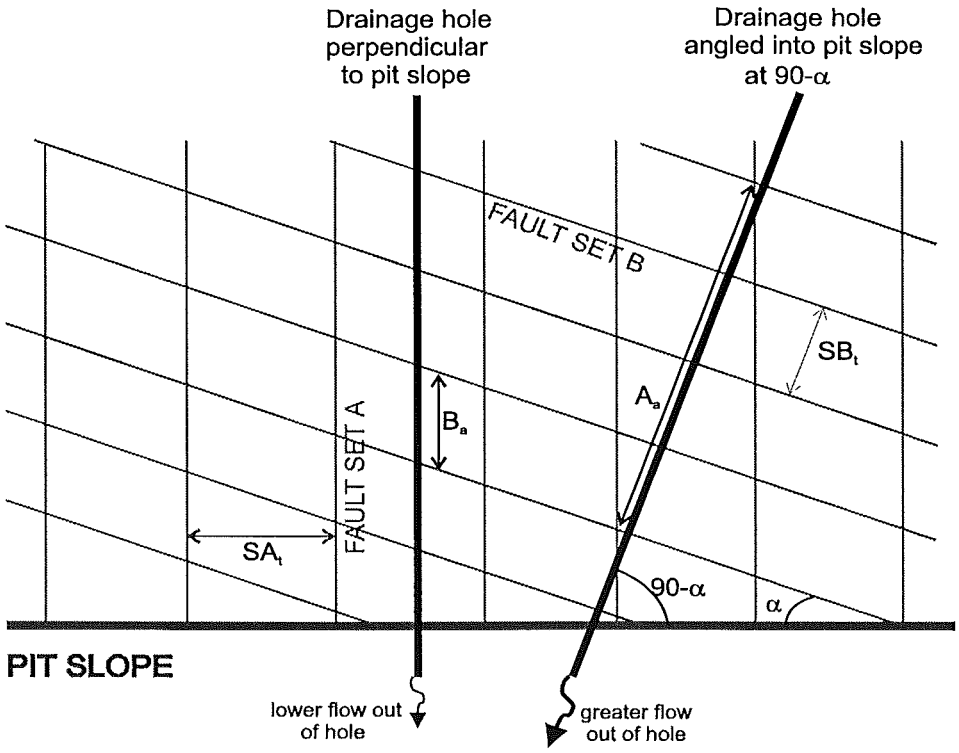

Figure 5-3: Schematic illustration of pit slope in plan view, showing the effect of drainhole orientation on intersecting permeable fault sets. For drainholes orientated perpendicular to pit slope, Fault Set A (with a true spacing of SA_t) will not be intersected by hole and Fault Set B will only be intersected at an apparent spacing (B_a). Holes orientated at an angle of 90-α will intersect Fault Set B at a true spacing of SB_t and Fault Set A at an apparent spacing A_a, effectively draining more of the rock mass per length of drill hole. (Note all holes will need to be angled up into the wall so that water can drain out under gravity)

5.3 INFLUENCE OF STRENGTH PROPERTIES ON PIT SLOPE FAILURE

Aside from the geometry of the rock mass, the shear strength of any potential failure surfaces are the next most important factor in the consideration of the stability of the rock slope (Hoek and Bray, 1981). As discussed in Chapter 4 pit slope failures at Macraes involve failure along either joints or faults, and may or may not also involve breakage through intact rock. For the prediction of pit slope failures at Macraes both the influences of intact rock and discontinuity shear strengths need to be understood.

5.3.1 Influence of Intact Rock Strength on Pit Slope Failures

A generally low stress regime is interpreted to exist in the rock mass surrounding the open pits at Macraes as a result of the surface proximity of the excavations, lack of current tectonic activity in the area, and there are no other indicators of high horizontal stresses. The strength of intact schist would therefore only appear to be of significance in terms of pit slope stability at Macraes when considering those failures that involve both shearing along discontinuities and breakage through intact rock.

Uniaxial compressive strength and point load testing of intact rock from Macraes (Chapter 2) showed that the following three factors are of importance in the consideration of pit slope stability at Macraes, these being: site specific strength properties, lithological strength variations, and schist strength anisotropy.

a) Site Specific Intact Strength Properties

Uniaxial compressive strengths of intact schist from Macraes ranges between 5MPa and 65MPa, with an average schist strength of 24MPa (Chapter 2). Average intact strengths for the schist at Macraes are much lower than those previously determined at other civil engineering projects in Otago like Maniototo (c.f. 53MPa, β=90°; 29 MPa, β=0°) and Clyde (c.f. 86 MPa, β= 90°; 46.9 MPa, β = 0°). Pit slope failures at Macraes are therefore more susceptible to development through intact rock than at these other locations. The variations in strengths means it is inappropriate to extrapolate strength data from these other civil engineering projects to Macraes.

b) Lithological Strength Variations

Strength variations in the Macraes schist apparently depend on the schist lithology. At Macraes the psammitic schist which dominates above the Hanging Wall Shear (Figure 1-4) generally appears to be weaker than pelitic schist which dominates below the Hanging Wall Shear. This lithological strength variation contrasts to normal expectations and with previous testing undertaken at other civil engineering project locations in the Otago schist, where pelitic schist was generally found to be weaker than psammitic schist. As previously suggested in Chapter 2, it may be that pelitic schist which dominates within the shear zone is stronger at Macraes due to annealing processes associated with mineralisation of the shear zone, but alternatively it may merely reflect sampling bias and/or the limited number of samples tested to date.

The implication of these lithological strength variations is that for pit slope failures involving breakage through intact rock, the stability of pit slopes will vary depending on whether the slope is above or below the Hanging Wall Shear. The easterly dip of the shear zone also means that western pit walls are generally more pelitic, while eastern walls are generally above the Hanging Wall Shear and accordingly more psammitic. It seems reasonable to assume that all other factors contributing to pit slope failures being the same, pit slopes on the western side of the mine will be more susceptible to failure development involving breakage through intact rock than pit slopes on the eastern side of the mine.

c) Schist Strength Anisotropy

Testing in Chapter 2 also showed as expected that there is a strong strength anisotropy in the schist depending on the orientation of an applied load to the schistosity. Schist at Macraes is much weaker when loads are applied parallel to schistosity than when loads are applied perpendicular to the schistosity. The implication of this strength anisotropy is that any development of failures by breakage through intact rock is likely to develop along schistosity rather than breakage across the schistosity (unless there is joint propagation into intact rock occurring, in which case the breakage may follow this path). This preferred breakage path through the schist will have a significant effect on determining the geometry of failures where the failure surface involves breakage through intact rock.

5.3.2 Influence of Shear Strength Properties on Pit Slope Failures

The shear strength of a rock along a discontinuity is affected by a number of factors including the infilling material (fault gouge etc.), asperities (roughness) and waviness (Giani, 1992). In the consideration of the shear strength of discontinuities at Macraes, and their influence on pit slope failures, it is necessary to consider joints and faults separately.

While no equipment was available for the in-situ determination of shear strengths during this project, it was possible to derive reasonable estimates of shear strength for different structural features at Macraes from the back analysis of pit slope failures (Appendix F6). Wyllie and Norrish (1996) describe back analysis of failures as probably one of the most reliable methods for the determination of the shear strength of a rock mass where failure is structurally controlled.

a)Shear Strength of Joints

Back analysis of joint-controlled pit slope failures observed during the field investigation programme as discussed previously (Chapter 4) were used to calculate possible values of cohesion (c) and frictional strengths (ϕ) for joints at Macraes. Table 5-1 presents the possible calculated values for c and ϕ for joints at Macraes (see Appendix F6).

Table 5-1: Summary of range in shear strengths for joints at Macraes.

	Cohesion (c')	Friction Angle (ϕ)
Back Analysis of joint - joint wedge failures (this project)	10.5kPa - 0kPa	30° - 45°
Back Analysis of high angle planar failures (this project)	1.5kPa - 0kPa	30° - 55°

From Table 5-1 it can be seen that for the schist material at Macraes values of c' generally lie between 0kPa and 10.5kPa, while friction angles range between 30° to 55°. Table 5-1 also shows that calculated values of cohesion for joints is typically much higher for wedge failures than it is for planar failures. The higher calculated values of cohesion for wedge failures compared to planar failures suggests that wedge failures along joints at Macraes typically involve some (or more) breakage through intact rock than do planar failures formed along joints.

Frictional angles calculated for the schist are generally much higher than that typically quoted in the literature of 23° - 29° (Hoek and Bray, 1981). As discussed in Chapter 3 joint roughness at the mine is typically undulating rough. This reasonably high roughness along the joint surface is inferred to be the principal reason for the high calculated ϕ angles, and it is reasonable to infer that for planar polished joints the friction angle is around 30° with about 25° (to give the calculated 55°) of friction added to this as a result of surface roughness/waviness along the joint surface which is not unreasonable (Figure 4-4). The collection of surface roughness/waviness information during routine berm mapping serves an integral part in the assessment of frictional strengths for joints at the mine site. In areas where joints show a greater roughness/waviness frictional strengths will be higher, whilst in areas where joints are smoother, lower frictional strengths may be assumed.

b) Shear Strength of Faults

Unlike joints where fracture surfaces involve rock-to-rock contact and no infilling, faults at Macraes contain infilling material and consequently the shear strength of faults varies markedly from that determined for joints. The shear strength properties of faults with an infilling material, will predominantly be influenced by the thickness and properties of the infilling (Wyllie and Norrish, 1996). For faults at Macraes it may be assumed that the shear strength will be more a representation of the fault gouge infilling than of the schist itself, and consequently much lower than indicated for joints.

Table 5-2: Summary of possible shear strengths for faults at Macraes.

	Cohesion (c')	Friction Angle (ϕ)
Ring Shear Testing (this project)	0kPa	3.1° - 6.4°
Strengths from Back Analysis (this project)	1.0kPa - 0kPa	6° - 14°
Woodward Clyde Ltd. (1997)	2.1kPa - 0kPa	8.3° - 13°
Bertuzzi (1992)	14kPa - 10kPa	15° - 17°

Shear strengths were calculated in this project from both ring shear testing (Section 2.2.4), and the back analysis of fault-controlled failures observed during field investigations (Appendix F6). Shear strength data for faults at Macraes is also available from ring shear and direct shear testing of fault gouge material by Woodward Clyde (1997), and from back analyses of early failures at the mine by Bertuzzi (1992). A summary of the fault shear strengths is presented in Table 5-2.

As discussed in Chapter 2 faults at Macraes represent structures along which previous tectonic shearing (and landslide movement in the case of failures) has taken place, and it therefore seems reasonable to assume c'=0. Direct shear testing and ring shear testing undertaken by Woodward Clyde (1997) also supports that c'= 0 for faults at Macraes.

Back analysis once again provides the most reliable method for the estimation of shear strength of faults at Macraes. From Table 5-2 it can be seen that while the results of back analyses undertaken during this project and those strength values measured by Woodward Clyde compare closely, ring shear results measured during this project are extremely low, while values of cohesion calculated by Bertuzzi (1992) are significantly higher. As discussed previously, estimates of the shear strengths of faults from ring shear testing are conservative due to the removal of coarser material which would otherwise increase the frictional strength. Barton (1987) points out that the shear strength of an infilled discontinuity with no clay size minerals is likely to correspond to that of massive minerals and range from 29-35°, while for discontinuities with a very high clay fraction then the strength may fall below 10°. The high calculated values for cohesion (and frictional strength) by Bertuzzi (1992) appear to be somewhat optimistic given the assumption that c'=0 at the mine site and the low frictional strengths indicated by ring shear testing.

Unlike joints, the effect of surface roughness/waviness on fault shear strength is likely to be quite variable and dependent on the aperture width of the fault. In the larger faults at Macraes where the aperture width is large (>200mm) compared to asperities/waviness along the fault walls, then there will be no wall to wall fault contact and the shear strength will be controlled by the infilling material (Figure 5-4). As aperture width decreases then the effective shear strength for faults will increase due to locking of the fault walls with movement. It has been suggested in the literature that for faults where the thickness of the infilling material is more than approximately 25% to 50% of the amplitude of the surface roughness/waviness, then there is likely to be little rock-to-rock contact and the shear strength properties of the fracture will reflect the properties of the infilling (Goodman, 1970 in: Wyllie and Norrish, 1996).

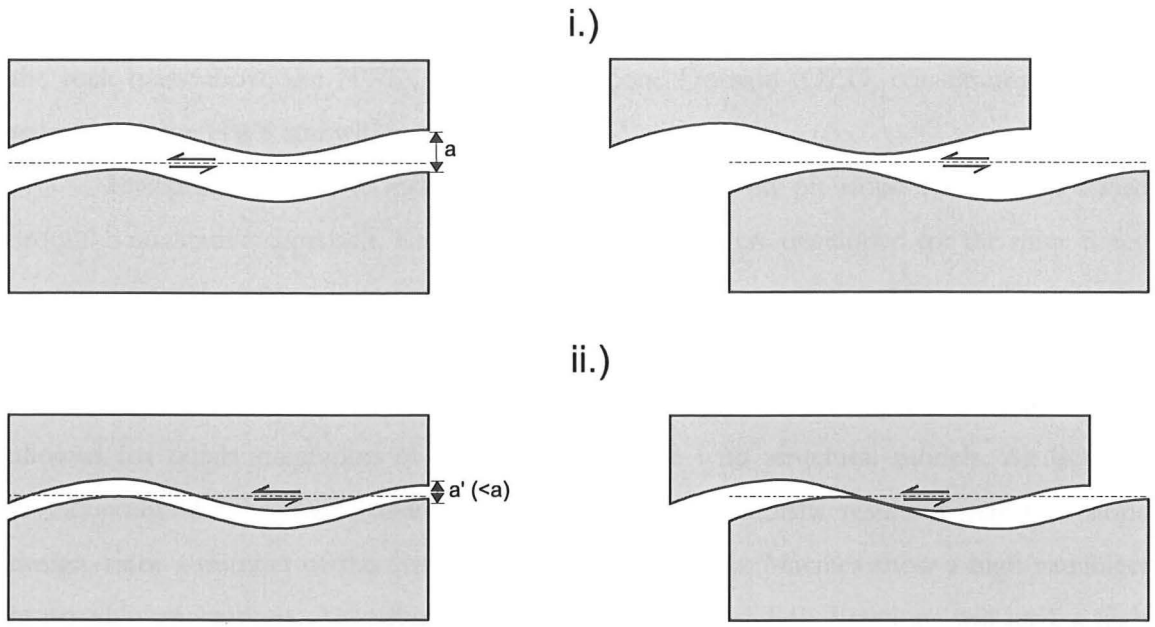

Figure 5-4: Effect of aperture width during shearing. i.) For faults with large aperture width (a) and/or low waviness, then there will be know fault wall to wall contact and shear strength will be controlled by infilling material. ii.) For faults with small aperture width (a') and/or high waviness then there will be fault wall to wall contact and shear strength will increase and controlled in part by infilling material as well as an increase due to dilation as 'waves' in fault walls pass over each other and contact.

In terms of the prediction of pit slope stability at Macraes, faults are generally much more important structures to understand than joints. Faults may be characterised by c'=0 and low frictional strengths ranging between 6° and 14°. Pit slope failures are predicted to be most likely along faults with a high continuity, low surface roughness and large aperture width. It is therefore important to identify these structures especially during routine berm mapping, and consequently to identify areas susceptible to failure development.

5.4 STRUCTURAL CONTROLS ON PIT SLOPE FAILURES

In analysing the stability of a rock slope the most important factor to be considered is the geometry of the rock mass behind the slope face (Hoek and Bray, 1981). The structure or geometry of the rock mass at Macraes was assessed in Chapter 3 and this section assesses the influence of the interpreted rock mass structure on pit slope failures at Macraes.

The Hanging Wall Shear (HWS) of the Hyde-Macraes Shear Zone (HMSZ) is the largest structure present at the mine, and the rock mass within the shear zone is likely to have been subjected to much higher strains than the rock mass above the HWS. As such, two structural domains can be recognised at Macraes mine whose boundary is delineated by the

HWS, and these may be referred to as the Hanging Wall Zone Domain (HWZD; constituting the rock mass above the HWS), and the Ore Zone Domain (OZD; constituting the rock mass below the HWS and within the HMSZ).

Interpretation of the influence of rock structure on pit slope failures was based around a qualitative approach. Kinematic failure models were developed for the mine based on the different permutations between the mean orientations of the different discontinuity sets identified in Chapter 3 for the two structural domains recognised. The use of mean defect set orientations seemed most appropriate since it kept interpretation simple, and allowed for quick integration of the failure database with structural models. As Bertuzzi (1992) points out kinematic assessments may produce optimistic results in terms of slope design, since a number of the discontinuity sets identified at Macraes show a high variability in possible orientations. Accordingly, the calculated mean sliding directions will have a high variability associated with them if all the possible permutations from all the poles in a set are assessed.

Predicted failure models for the two structural domains, based on the permutations between the means for each of the different discontinuity sets identified in Chapter 3, are presented in Table 5-3 (HWZD) and Table 5-4 (OZD). Based on the different possible permutations between the discontinuity sets, 58 structural failure models (32 models above the HWS, and 26 models below the HWS) can be recognised at Macraes. More structural models are evident above the Hanging Wall Shear due to the presence of an extra fault set (FA5) which appears to be absent below the Hanging Wall Shear.

Figure 5-5 (HWZD) and Figure 5-6 (OZD) present stereoplots of the inferred sliding direction for each of these predicted failure models. From Figure 5-5 and Figure 5-6 it can be seen that the 'sliding vectors' (which effectively represent the maximum dip of a failure surface, or the orientation of a wedge intersection) dominantly trend east and west. Given the condition that the failure surface must strike within ±20° of the slope face for sliding to occur (Richards and Atherton, 1987), then the predicted failures are most likely to affect the same slope faces as the direction of sliding (i.e. east and west facing pit slopes).

Table 5-3: Structural failure models for Hanging Wall Zone Domain or above the Hanging Wall Shear (based on mean defect orientations determined in Chapter 3).

No.	Controlling Defect Set #1 (Dip/Dir.)	Controlling Defect Set #2 (Dip/Dir.)	Predicted Failure Type	Sliding Direction (Trend/ Plunge)	Orientation of Effected Pit Slopes
1	Foliation Shear	-	Low Angle Block	105/15	East Facing
2	JA1 (45/270)	-	High Angle Planar	270/45	West Facing
3	JA2 (80/190)	-	Toppling	190/80	North Facing
4	JA3 (50/090)	-	High Angle Planar	090/50	East Facing
5	FA1 (60/090)	-	High Angle Planar	090/60	East Facing
6	FA2 (18/090)	-	Low Angle Block	090/18	East Facing
7	FA3 (30/270)	-	High Angle Planar	270/30	West Facing
8	FA4 (45/205)	-	High Angle Planar	205/45	South to South-west Facing
9	FA5 (75/020)	-	Toppling	020/75	South Facing
10	JA1 (45/270)	JA2 (80/190)	Joint - Joint Wedge	270/45	West Facing
11	JA1 (45/270)	JA3 (50/090)	Joint - Joint Wedge	000/00	North or South Facing
12	JA2 (80/190)	JA3 (50/090)	Joint - Joint Wedge	111/48	East Facing
13	FA1 (60/090)	FA3 (30/270)	Fault - Fault Wedge	000/00	North or South Facing
14	FA1 (60/090)	FA4 (45/205)	Fault - Fault Wedge	156/34	South-east Facing
15	FA1 (60/090)	FA5 (75/020)	Fault - Fault Wedge	082/59	East Facing
16	FA2 (18/090)	FA3 (30/270)	Fault - Fault Wedge	000/00	North or South Facing
17	FA2 (18/090)	FA4 (45/205)	Fault - Fault Wedge	129/14	South-east Facing
18	FA2 (18/090)	FA5 (75/020)	Fault - Fault Wedge	105/18	East Facing
19	FA3 (30/270)	FA4 (45/205)	Fault - Fault Wedge	259/30	West Facing
20	FA3 (30/270)	FA5 (75/020)	Fault - Fault Wedge	298/27	North-west Facing
21	FA4 (45/205)	FA5 (75/020)	Fault - Fault Wedge	291/04	West Facing
22	JA1 (45/270)	FA1 (60/090)	Joint - Fault Wedge	000/00	North or South Facing
23	JA1 (45/270)	FA2 (18/090)	Joint - Fault Wedge	000/00	North or South Facing
24	JA1 (45/270)	FA4 (45/205)	Joint - Fault Wedge	236/40	South-west Facing
25	JA1 (45/270)	FA5 (75/020)	Joint - Fault Wedge	303/41	North-west facing
26	JA2 (80/190)	FA1 (60/090)	Joint - Fault Wedge	117/57	South-east Facing
27	JA2 (80/190)	FA2 (18/090)	Joint - Fault Wedge	104/18	East Facing
28	JA2 (80/190)	FA3 (30/270)	Joint - Fault Wedge	274/30	West Facing
29	JA2 (80/190)	FA4 (45/205)	Joint - Fault Wedge	277/17	West Facing
30	JA3 (50/090)	FA3 (30/270)	Joint - Fault Wedge	000/00	North or South Facing
31	JA3 (50/090)	FA4 (45/205)	Joint - Fault Wedge	151/31	South-east Facing
32	JA3 (50/090)	FA5 (75/020)	Joint - Fault Wedge	279/39	West Facing

Table 5-4: Structural failure models for Ore Zone Domain or below the Hanging Wall Shear (based on mean defect orientations determined in Chapter 3).

No.	Controlling Defect Set #1 (Dip/Dir.)	Controlling Defect Set #2 (Dip/Dir.)	Predicted Failure Type	Sliding Direction (Trend/ Plunge)	Orientation of Effected Pit Slopes
1	Foliation Shear	-	Low Angle Block	105/15	East Facing
2	Foliation Shear	-	Low Angle Block	295/20	West Facing
3	JB1 (50/090)	-	High Angle Planar	090/50	East Facing
4	JB2 (75/010)	-	Toppling	010/75	South Facing
5	JB3 (45/270)	-	High Angle Planar	270/45	West Facing
6	FB1 (60/100)	-	High Angle Planar	100/60	East Facing
7	FB2 (18/090)	-	Low Angle Block	090/18	East Facing
8	FB3 (40/275)	-	High Angle Planar	275/40	West Facing
9	FB4 (65/200)	-	High Angle Planar	200/65	South Facing
10	JB1 (50/090)	JB2 (75/010)	Joint - Joint Wedge	081/50	East Facing
11	JB1 (50/090)	JB3 (45/270)	Joint - Joint Wedge	000/00	North or South Facing
12	JB2 (75/010)	JB3 (45/270)	Joint - Joint Wedge	294/42	West Facing
13	FB1 (60/100)	FB3 (40/275)	Fault - Fault Wedge	188/03	South Facing
14	FB1 (60/100)	FB4 (65/200)	Fault - Fault Wedge	145/50	South-east facing
15	FB2 (18/090)	FB3 (40/275)	Fault - Fault Wedge	003/01	North Facing
16	FB2 (18/090)	FB4 (65/200)	Fault - Fault Wedge	118/16	South-east Facing
17	FB3 (40/275)	FB4 (65/200)	Fault - Fault Wedge	40/268	West Facing
18	JB1 (50/090)	FB3 (40/275)	Joint - Fault Wedge	002/03	North Facing
19	JB1 (50/090)	FB4 (65/200)	Joint - Fault Wedge	134/41	South-east Facing
20	JB2 (75/010)	FB1 (60/100)	Joint - Fault Wedge	075/57	East Facing
21	JB2 (75/010)	FB2 (18/090)	Joint - Fault Wedge	095/18	East Facing
22	JB2 (75/010)	FB3 (40/275)	Joint - Fault Wedge	293/39	West Facing
23	JB2 (75/010)	FB4 (65/200)	Joint - Fault Wedge	284/14	West Facing
24	JB3 (45/270)	FB1 (60/100)	Joint - Fault Wedge	186/07	South Facing
25	JB3 (45/270)	FB2 (18/090)	Joint - Fault Wedge	000/00	North or South Facing
26	JB3 (45/270)	FB4 (65/200)	Joint - Fault Wedge	261/45	West Facing

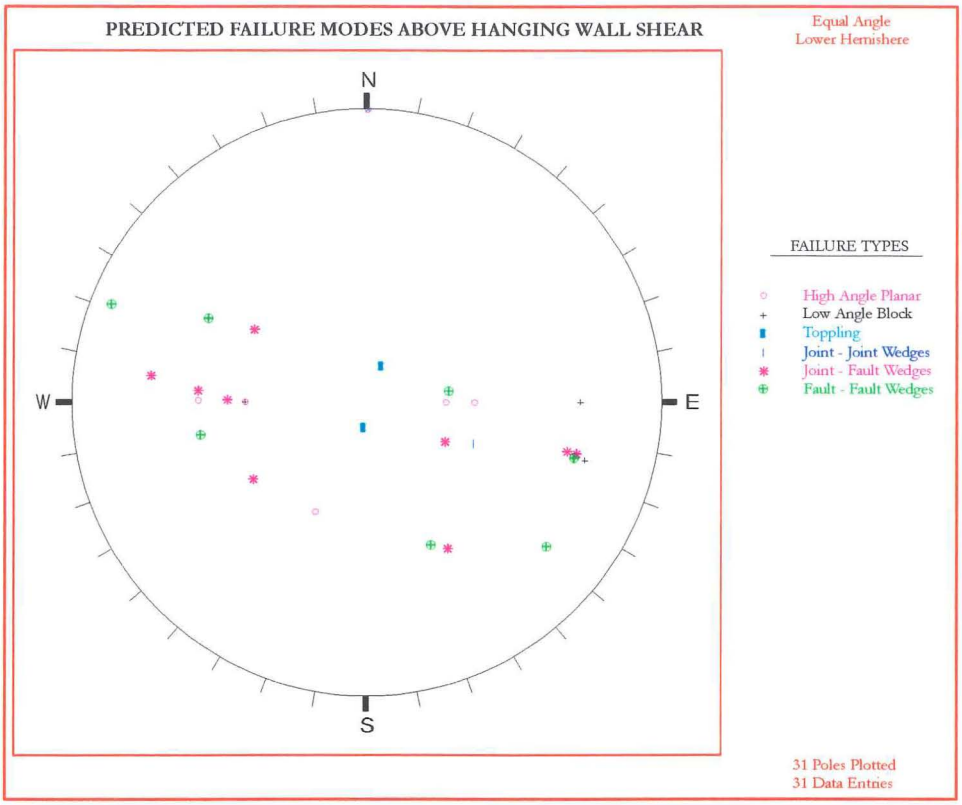

Figure 5-5: Sliding vectors for possible failure types above Hanging Wall Shear (HWZD) derived from mean structural orientations as determined in Chapter 3.

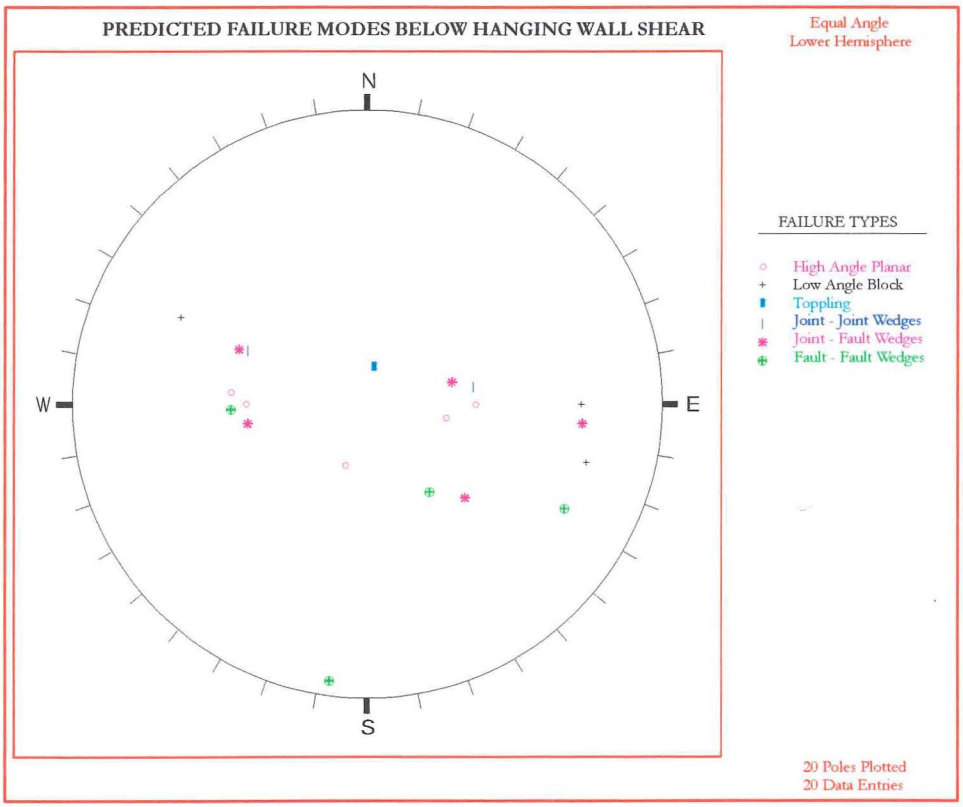

Figure 5-6: Sliding vectors for possible failure types below Hanging Wall Shear (OZD) derived from mean structural orientations as determined in Chapter 3.

5.5 INTEGRATION OF STRUCTURAL MODELS WITH PIT SLOPE FAILURE DATABASE

As discussed in Chapter 4 one of the main uses of a pit slope database is to compare those failures predicted or expected with those that have actually occurred at the mine. The compiled pit slope failure database serves as a calibration tool for any predictive rock mass models developed for the mine, and allows these models to be refined over time with the collection of an increasing amount of failure information with continuing mining operations.

As also discussed in Chapter 4 a generally poor standard of recording of pit slope failures at the mine prior to the onset of this project has meant that a significant amount of information on failures at the mine is of limited use since it has either been: not recorded, lost, or poorly interpreted. Figure 5-7 shows the interpreted direction of sliding for failures recorded at Macraes. Sections 5.5.1 - 5.5.4 compare the orientations of these recorded failures with the 58 possible failure models developed from structural assessment in Section 5.4.

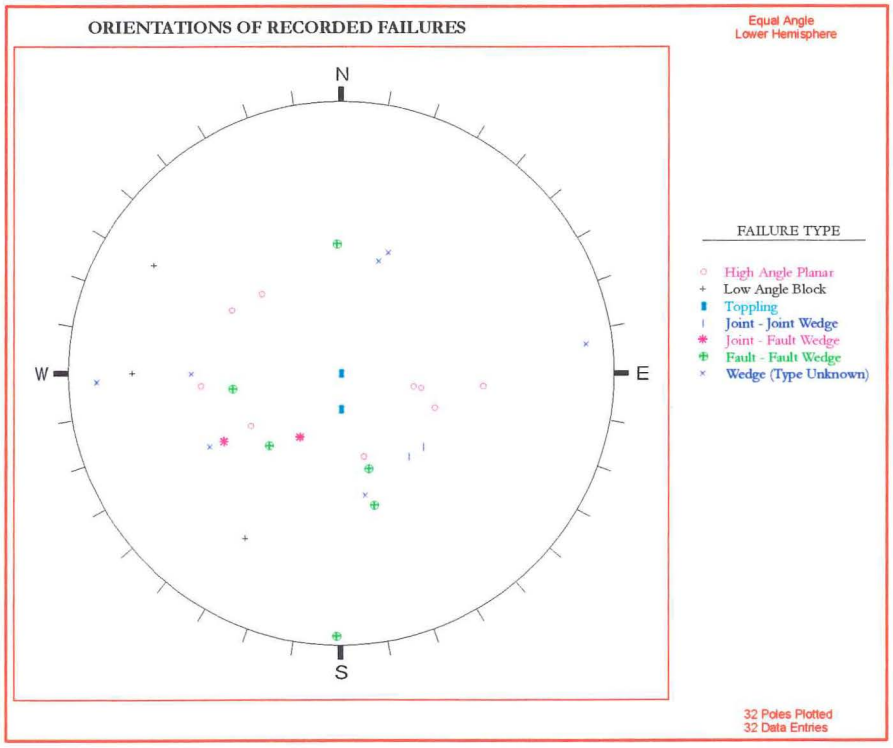

Figure 5-7: Sliding vectors for the different failure types in Pit Slope Failure Database.

Integration of the 32 failures recorded so far at the mine show that these failures can be grouped into 13 different failure models (Models I-XIII), which are presented on Table 5-5 and Map Sheet 10 (Map Box). These failure models are discussed in the following Section 5.5.1.

Table 5-5: Summary of predicted pit slope failures at Macraes Gold Mine.

Model ID.	Failure Type	Sliding Direction (Mean)	Controlling Defect Set(s)	Relation to Hanging Wall Shear	Likely Walls Effected	Approximate Failure Volume	Causes	Implications	Examples	Notes
I	High Angle Planar	270/45	JA1	Above	Westerly facing	≤ 100m³	Undercutting of failure surface and weak psammite schist above Hanging Wall Shear. Water possibly where dip of joint is <45°	Failure limited to bench scale and only poses hazard to personnel below berm at time of failure	RH34 & RH35	It is possible for a similar failure type to develop below Hanging Wall Shear along joint set JB3.
II	High Angle Planar	090/50	JB1	Below	Easterly facing	≤ 100m³	Undercutting of failure surface and weak psammite schist above Hanging Wall Shear. Water possibly where dip of joint is <50°	Failure limited to bench scale and only poses hazard to personnel below berm at time of failure	RH30	It is possible for a similar failure type to develop above Hanging Wall Shear along joint set JA3.
III	High Angle Planar	270/30 275/40	FA3 FB3	Above Below	Westerly facing	≤ 500m³	Low shear strength of fault gouge means undercutting of failure plane generally the sole cause.	This type of failure will generally occur immediately following bench excavation. Failure does not pose a hazard in the long term.	RH10, RH22,	-
IV	High Angle Planar	090/50 100/60	FA1 FB1	Above Below	Easterly facing	≤ 500m³	Low shear strength of fault gouge means undercutting of failure plane generally the sole cause.	This type of failure will generally occur immediately following bench excavation. Failure does not pose a hazard in the long term.	SP1	-
V	Low Angle Block	295/20	Foliation Shears // to Foliation	Below	Westerly facing	typically ≈ 250m³	Low angle of failure plane means generally driven by water pressures	Movement rates typically slow. Failure is likely to creep constantly once initiated (will get accelerations in movement following rainfall and alarms may need to be installed on these failures if personnel are working below the failure.	IM3, RH33 & IM7	High variance in schistosity orientation means that it is also possible for this type of failure to affect other wall orientations i.e. IM3
VI	Toppling	190/80	JA2	Above	Northerly & Southerly facing	≤500m³	High water pressures or removal of support around axis of rotation. Lateral support also needs to be low	Failure is likely to continue along berm along defect following initial failure due to lack of lateral support	RH31	Toppling failures may also develop along joint set JB2 below the Hanging Wall Shear although none have been recognised to date.
VII	Toppling	020/75	FA5	Above	Southerly facing	≤500m³	High water pressures or removal of support around axis of rotation. Lateral support also needs to be low	Failure is likely to continue along berm along defect following initial failure due to lack of lateral support	RH24	
VIII	Joint - Joint Wedge	270/45 081/50	JA1-JA2 JB1-JB2	Above Below	Westerly facing Easterly facing	≤100m³	Dependent on plunge of wedge intersection. Where plunge of wedge intersection is >50° then just undercutting, where less then groundwater pressures	Failure is likely to continue along berm along defect following initial failure due to lack of lateral support	None above RH32 & RH36	High variability in joint set distribution means that wedge intersection may vary from that shown and effect other wall orientations
IX	Joint - Fault Wedge	235/40	JA1 - FA4	Above	South-westerly facing	Variable 50m³ - 1000m³	Causes variable. High groundwater pressures will cause instability but if wedge intersection is steep enough and shear strengths low then undercutting of wedge may be sufficient to initiate failure.	Failure may continue to develop as deeper joint sets are exposed with continuing mining.	RH27 & IM2	Complex failure mechanisms are likely to be associated with the larger volume failures in this class
X	Joint - Fault Wedge	274/30	JA2 - FA3	Above	Westerly to North-westerly facing	Variable 50m³ - 1000m³	Causes variable. High groundwater pressures will cause instability but if wedge intersection is steep enough and shear strengths low then undercutting of wedge may be sufficient to initiate failure.	Failure may continue to develop as deeper joint sets are exposed with continuing mining.	RH5	-
XI	Fault - Fault Wedge (Type 1)	000/00 188/03	FA1 - FA3 FB1 - FB3	Above Below	Southerly facing	Potentially very large e.g. RH28 volume ≈450 000m³	Generally low plunge of wedge intersection means failures of this type are generally driven by water pressures formed along steeply dipping fault sets FA4, FA5 and FB4.	Like all wedge failures developed along faults there is potential for enlargement, through stepping out onto adjacent faults.	RH28 RH2	Orthogonal orientation of faults means orientation of wedge intersection is also highly variable and may effect northern or southern walls.
XII	Fault - Fault Wedge (Type 2)	156/34	FA1- FA4	Above	Southerly to South-easterly facing	≤1500m³	Causes variable. Low shear strength of faults means undercutting may be enough to release failure, although water will increase instability	Like all wedge failures developed along faults there is potential for enlargement, through stepping out onto adjacent faults.	IM11 & IM4	-
XIII	Fault - Fault Wedge (Type 3)	259/30 268/40	FA3 - FA4 FB3 - FB4	Above Below	Westerly to South-westerly facing	≤1500m³	Causes variable. Low shear strength of faults means undercutting may be enough to release failure, although water will increase instability	Like all wedge failures developed along faults there is potential for enlargement, through stepping out onto adjacent faults.	RH6 RH8	-

5.5.1 Predicted Planar Failures

a) High Angle Planar

High angle planar failures at Macraes are controlled by the moderately dipping (30-70°) structures and occur along both joints and faults. High angle planar failures appear to dominate along both east and west facing pit slopes.

Joint controlled high angle planar failures above the Hanging Wall Shear are controlled by JA1 (45/270; Failure Model I) and occur along westerly facing pit slopes. Below the Hanging Wall Shear high angle planar failures are typically controlled by JB1 (50/090; Failure Model II) which as discussed in Chapter 3 appears to form the conjugate joint set to JA1. Failures along JB1 will typically occur along easterly facing pit slopes. Volumes for these joint controlled high angle planar failures will typically be less than 100m^3.

The high effective frictional strengths (45-55°) for joints at Macraes, as previously discussed, means that high angle planar failures along JA1 and JB1 typically require groundwater pressures to initiate failure. For joints, where the dip of the joint out of the pit slope is greater than the frictional strength (i.e. >55°), undercutting of the failure surface will usually be enough to initiate failure (provided lateral release surfaces are also present).

Fault-controlled high angle planar failures above the Hanging Wall Shear are controlled by fault sets FA1 (50/090; Model III) and FA3 (30/270; Model IV) and will occur along both easterly and westerly facing pit slopes. Below the Hanging Wall Shear fault-controlled high angle planar failures are formed by fault sets FB1 (60/100; Model III) and FB3 (40/275; Model IV) and will also dominate both easterly and westerly facing pit slopes.

The interpreted low frictional strengths for faults (6°-14°) at Macraes means that high angle planar failures will usually occur as a result of the undercutting of the failure plane, provided that structures, or a change in slope orientation allow the lateral release of the failure. As discussed in Chapter 4 the high angle of the failure surface will inevitably limit the potential failure volume with failures of this size typically less than 500m^3 for single size bench failures and less than 1000m^3 for failures occurring across more than one bench.

b) Low Angle Block Failures

Two types of low angle block failures are predicted at Macraes, namely those formed along faults synthetic to the main Hanging Wall Shear affecting east facing slopes, and those that form along faults parallel to the schistosity affecting east and west facing slopes.

Integration of the failure database shows that no low angle block failures appear to have been recorded along shallow east dipping shears, and that low angle block failures at Macraes generally appear to be restricted to shallow westerly dipping foliation shears (20/295; Model V). West dipping schistosity is most dominant below the Hanging Wall Shear, and low angle block failures are predicted to dominate west facing pit slopes below the Hanging Wall Shear. Local variations in the orientation of schistosity mean that this type of failure may also develop above the Hanging Wall Shear (IM33), or along south-west (i.e. IM3) and north-west facing pit slopes.

The low angle of the failure surface also means that low angle block failures are not generally predicted to occur as a result of simple undercutting of the failure surface, except in areas where groundwater pressures are present along favourable release structures to the failure as discussed in Chapter 4.

5.5.2 Predicted Toppling Failures

Toppling failures are only likely to occur along steeply inclined discontinuities (>75°) at Macraes. Comparison of recorded toppling failures with those predicted suggests that toppling is restricted to the HWZD (above the HWS) along the steep dipping discontinuity sets JA2 (80/190; Model VI) and FA5 (75/020; Model VII).

Within the OZD (below the HWS), while toppling is kinematically possible along joint set JB2 (75/010) on south facing slopes, none of this type of failure appears to have been recorded. The absence of toppling failures below the Hanging Wall Shear further lends support to the fact that pelitic schist at Macraes, which dominates below the Hanging Wall Shear is stronger than the psammitic schist which dominates above the Hanging Wall Shear (see Section 5.3.1(b)).

The high frictional strengths for joints at Macraes once again suggests that high groundwater pressures are generally required to initiate toppling failures, which is supported by failure RH31. While the actual toppling failure may occur rapidly, regular berm inspections of north and south facing pit slopes should identify development of these failures as the rock mass dilates and creates cracks parallel to the berm prior to the actual failure event, and thereby minimise the impact of unexpected failure on mining operations (see Section 5.6).

5.5.3 Predicted Wedge Failures

a) Joint-Joint Wedges

Three joint sets are recognised above (JA1, JA2, and JA3) and below (JB1, JB2, and JB3) the Hanging Wall Shear at Macraes, and two of these joint sets are inferred to have formed as a conjugate set (Chapter 3). The orthogonal orientation of joints of these conjugate sets to each other means that wedge intersections formed between these sets will generally plunge at low angles (<10°). Since joints at Macraes are characterised by high frictional strengths (45°-55°), it would seem joint-joint wedge failures formed between conjugate joint sets are highly unlikely, since wedges formed between conjugate sets will typically produce very low angle wedge intersections. The pit slope failure database supports this idea and shows no joint-joint failures between the conjugate joint sets have recorded to date.

Above the Hanging Wall Shear joint-joint wedge failures may form between JA1 (45/270) and JA2 (80/190), and will generally plunge out of the face at 270/45 and affect west facing pit slopes. The high variation in the orientation of joint orientations for each of these joint sets, means that a variety of wedge intersections are possible which could effect other wall orientations. While no joint-joint wedge failures have been recorded above the Hanging Wall Shear there seems no reason why they may not develop in the future.

Below the Hanging Wall Shear joint-joint wedge failures may form between JB1 (50/090) and JB2 (75/010), will plunge out of the face at 081/50 and generally affect east facing pit slopes (e.g. RH32 & RH36; Model VIII). Average joint length both above and below the Hanging Wall Shear is approximately 5m, and joint-joint wedge failures formed along such joints are only likely to form small failure volumes (less than $100m^3$).

b) Joint-Fault Wedges

Three joint sets above (JA1, JA2, and JA3) and below (JB1, JB2, and JB3) the Hanging Wall Shear, and five fault sets above the Hanging Wall Shear (FA1 - FA5) and four fault sets below the Hanging Wall Shear (FB1 - FB4), are evident at Macraes. Integration of the failure database with the structural failure models shows that joint-fault wedges seem to be surprisingly rare at the mine and generally restricted to above the Hanging Wall Shear. As for joint-joint wedges, a number of the joint and fault set orientations at Macraes are

orthogonal to each other, and consequently form wedge intersections which plunge at low angles (<10°), and are therefore unlikely to fail.

Integration of structural models with the failure database also shows that joint-fault wedges are predicted to occur above the Hanging Wall Shear either between JA1 and FA4 (Model IX) or between JA2 and FA3 (Model X). Both of these joint-fault wedges are predicted to affect south-westerly to north-westerly facing pit slopes. Failure RH27 suggests failure volumes for this type of failure will be restricted to less than 1000m^3 at most.

c) Fault-Fault Wedges

Fault-fault wedges represent the most significant of the failure types at the mine for two reasons. Firstly, as discussed above in Section 5.3.2(b), faults at Macraes appear to be characterised by relatively low shear strengths and also form the most persistent of the structures with an average length of approximately 15 metres (although a number of faults at the mine easily exceed 100's of metres). Secondly, the orientation of fault sets is generally consistent across the mine site. As discussed in Chapter 4 the consistent nature of faulting means that any fault-fault wedges that develop have the potential to increase in size by stepping out onto adjacent synthetic faults.

Integration of the failure database with structural models for the mine shows that three types of fault-fault wedges are predicted to occur at Macraes, and here these will be referred to as Types 1-3:

Type 1 (Model XI)

Fault-fault wedges above the Hanging Wall Shear formed between fault sets FA1 and FA3, and below the Hanging Wall Shear between fault sets FB1 and FB3. Mean orientations of these sets suggest that these fault-fault wedges will generally affect south facing pit slopes plunging out at of the slope at very low angles (above=000/00 and below=188/03). The orthogonal orientation of the fault sets means that with slight variations in the orientation of the controlling faults shallow dipping wedges which plunge out of north facing walls may also be formed.

The low angle of the wedge intersection means that high groundwater pressures formed along fault sets parallel to the north and south walls will typically be the main factor driving these failures. Above the Hanging Wall Shear these structures are FA4 (45/205) and FA5 (75/020) while below the Hanging Wall Shear the relevant fault set is FB4 (65/200).

Failures of this type (as for low angle block failures) are only predicted to occur when groundwater pressures in the pit slope are high, and therefore slope depressurisation should

prevent failure. Movement rates are generally predicted to be very slow to extremely slow (<1.6m year) as a result of the low plunge for the wedge intersection, however, as long as there are high water pressures along the releasing structures, movement is likely to continue. The slow movement rate of this type of failure means that these failures are predicted to be of most significance in the long term as the cumulative movement increases.

The predicted volume of these Type 1 failures will be controlled by the size of the controlling faults and the area of the pit slope, which is affected by high groundwater pressures and may be extremely high as in the case of RH28 (≈450 000m^3). Failure size is predicted to be a product of the continuity of the wedge controlling defects (although this may be extended by breakage through intact rock), and the area along the fault set parallel to the pit slope upon which high groundwater pressures are acting. As determined in Chapter 4 reducing groundwater pressures to below the rear releasing surfaces which are driving failure may be enough to stabilise movement.

Type 2

Type 2 fault-fault wedges formed between fault sets FA1 and FA4 plunge at moderate angles out of south to south east facing pit slopes (156/34; Model XII). The moderate angle of the wedge intersection compared to the low frictional shear strength means that for this type of failure groundwater pressures are not necessary to cause failure. As for all fault-fault wedges the consistent structure of faulting at Macraes means that these types of failure have the potential to enlarge, by stepping out onto more distal faults with increasing excavation of the pits and the undercutting of deeper wedge intersections on these more distal faults.

Type 3

Fault-fault wedges between fault sets FA3 and FA4 above the Hanging Wall Shear, and FB3 and FB4 below the Hanging Wall Shear, plunge out of west facing pit slope at moderate angles (above ≈ 259/30; below 268/40; Model XIII). Failures of this type recorded in the pit slope failure database are RH6 and RH8, which both occurred prior to this project. Failures of this type were not observed during study, however records at the mine show both these earlier failures occurred as a result of undercutting the toe of the slope.

5.5.4 Predicted Complex Failures

Complex failures are the most difficult of the failure types to predict. As mentioned previously two complex failures, RH27 and RH28, were recognised at Macraes as during the field investigations of this thesis (see Section 4.4). The complex nature of these failures is generally a result of the large failure volumes, and it is sufficient to predict that any large volume failure at the mine will typically develop into a complex failure.

The type of complex failure that develops will generally be a reflection of the failure volume, wall orientation and the structure in the area, whilst the orientation of artificial voids created in the slope by movement of the main failure mass may also determine what type of secondary failure models are kinematically possible. As such, each large volume failure (>1000m^3) should be investigated for complex failure development following initial failure. Structural interpretations of the initial failure geometry and structure in the area should allow future failure development to be predicted on a case by case basis.

5.6 FAILURE MANAGEMENT AND MONITORING

Good failure management and monitoring is an essential part of both the prediction of new, and management of existing, pit slope failures at Macraes. Unexpected pit slope failures not only represent a significant hazard to personnel and equipment, particularly when they are located adjacent to current mining activities or main access ways like haul roads, but may also have significant economic consequences (e.g. failed material may need to be removed, mining activities may be disrupted etc.).

Monitoring should be based around identifying potential problem areas for failure prior to the event, as well as managing active failures so that hazards associated with unexpected movements are minimised. Table 5-6 gives a summary of monitoring techniques that should be used on a routine basis for the monitoring and management of pit slope failures.

Table 5-6: Recommended monitoring techniques to be used at Macraes for pit slope failure management.

	General Monitoring
Routine Berm Walk Over and Visual Inspections of Active Failures	Berms above actively mined areas should be inspected on a weekly basis for signs of movement. When mining activities are situated immediately below a pit slope then these slopes should be inspected on a daily basis. Where movement is identified then features should be mapped photographed and have the appropriate movement monitoring installed. Predicted models should be taken into the field to assist in visual inspections.
Photographic Records	Final berms should be photographed, and this can be undertaken at the same time as berms are logged for structure. Failures and features associated with movement (cracks, scarps, etc.) should be photographed for future reference and comparison. Photos should be catalogued according to location and date of photo, for easy retrieval and future reference.
	Movement Monitoring
Crack Pins	Crack pins provide a relatively crude method for monitoring failure movements, but are cheap and information can be collected rapidly. Pins and crack should be photographed at time of installation for future reference.
Survey Prisms	Survey prisms are much more accurate than crack pins and while more expensive have a number of advantages. Prisms will detect movement that may not be detectable by visual observation or crack pins. **Prisms should be installed on failures and areas of the pit slope which are difficult/and or hazardous to access, to monitor movements.**
Inclinometers	Inclinometers should be installed on large deep seated pit slope failures (failure surface >50m deep) at an early stage to supplement other data and identify how and which areas of the main failure block are moving. Data from inclinometers will supplement other movement monitoring data so that the most appropriate remedial measures may be undertaken (toe buttressing, dewatering, head unloading etc.)
	Hydrologic Monitoring
Rainfall Records	Precipitation records should be kept to correlate with both piezometric records and movement records so relationships between rain and groundwater response, and precipitation and movement rates of failures may be established.
Piezometric Records	Piezometers should be monitored to assess groundwater levels in the slope and effectiveness of horizontal drainage as it is installed, as well as to correlate with both movement and rainfall records
Horizontal Drain Records	Horizontal drains should be monitored for flow rates and correlated with piezometric records to assess the effectiveness of slope depressurisation.
	Warning Monitoring
Alarms	Trip wire alarms (**Figure 4-32**) should be installed on active failures which are located above mining activities, which are triggered after a predetermined movement threshold is exceeeded, so that access is restricted beneath failures until visual inspections can verify the safety of the failure.
	Operational Monitoring
Blast Records	Ground vibrations associated with blasting at the mine may affect failure movements. Records and locations of major blasts should kept to correlate with movement rates of failures (particularly those situated immediately adjacent to blasts).
Excavation Records	Excavation records should be kept to correlate between excavation and development of failure

5.7 DISCUSSION AND SYNTHESIS

Groundwater pressures are a major factor in contributing to pit slope failures at Macraes. High groundwater pressures will reduce the effective stress acting along the failure surface, thereby reducing the frictional resistance to sliding, whilst high groundwater pressures at the back of the slope may generate a significant force toward the open pit. Surficial pit slope failures, where the failure surface is <5m deep, driven by high groundwater pressures are predicted to occur within 24 hours following rainfall, while deeper seated failures (5-50m deep) may not be affected for up to one to two weeks later because of the greater distance that water needs to permeate to reach the failure plane.

Intact rock strengths at Macraes will only influence failures where failure development involves some breakage through intact rock. Strengths of schist at Macraes are generally lower than for other civil engineering projects in the Otago schist such as Maniototo and Clyde. Intact strengths indicate that pelitic schist, which dominates below the Hanging Wall Shear, is generally much stronger than the overlying psammitic schist which dominates above the Hanging Wall Shear. Schist also shows a high strength anisotropy, meaning that development of failures through intact schist is more likely to occur along the foliation than cutting across it (unless there is joint propagation into intact rock).

Shear strengths at Macraes differ depending on whether faults or joints are being considered. Faults represent the most significant features in terms of pit slope stability and are characterised by low frictional strengths (6° - 14°) and probably no cohesion, with increases in shear strength possible depending on the roughness/waviness of the fault walls compared to the aperture width for the fault. Joints in contrast, from back analysis, generally appear to be characterised by high frictional strengths (45° - 55°) as a result of surface asperities/waviness along the joint.

By evaluating all the permutations possible for the mean discontinuity set orientations 58 structural models of failure (both above and below the Hanging Wall Shear) can be recognised. Integration of these structural failure models with those recorded at the mine however shows that of the failures recorded to date these 58 structural models can be grouped into 13 predicted failure models (Table 5-5; Map Sheet 10). The predicted pit slope failure models here are by no means an exhaustive list of failures predicted to occur at Macraes. It is likely that over time even more failure types may be recorded at the mine. However, the predicted failure models developed here are to serve as a tool aiding site

investigations of pit slope failures at the mine. Predicted failure models will aid in both the interpretation of failures as well as identifying future failures.

Unexpected pit slope failures represent a significant hazard to personnel and equipment, particularly when they are located adjacent to current mining activities or main access ways like haul roads, and will also have significant economic consequences if mining operations are disrupted by slope failure. Monitoring and management of failures at Macraes should be based around identifying potential problem areas to prior failure as well as managing active failures so that adverse effects associated with unexpected failure movements are minimised. This is best achieved through a variety of monitoring methods which can be classified as general monitoring (berm inspections and photography), movement monitoring (crack pins, survey prisms, and inclinometers), hydrologic monitoring (rainfall records, piezometric records and horizontal drain records), warning monitoring (alarms), and operational monitoring (blasting and excavation records).

CHAPTER 6 : SUMMARY AND CONCLUSIONS

6.1 PROJECT OBJECTIVES

The five principal objectives of this thesis were:

1. To carry out geotechnical testing on intact rock and fault gouge material for the determination of relevant strength parameters for geotechnical data evaluation at Macraes Gold Mine, Macraes Flat, Otago.
2. To assess structural domains for the rock mass at Macraes.
3. To construct a standard recording sheet for pit slope failures at Macraes and to collate pit slope failures at the mine into a consistent format for the development of failure models.
4. To analyse failures RH27 and RH28 and to provide geotechnical input data to assist in the design of possible remedial measures.
5. To construct integrated predictive rock mass model(s) for pit slope failures at the Macraes Gold Mine.

6.2 PROJECT RESULTS

6.2.1 Geotechnical Testing

a) Intact Rock

i.) Preparation of schist core samples from Macraes is difficult because of the weak fissile nature of the rock material parallel to schistosity.

ii.) Uniaxial compressive strength (UCS) for schist at Macraes ranges between 4.8 MPa and 61.2 MPa, with an average value of 24 MPa. These strength results compare closely with those previously measured by Woodward Clyde (5.9 MPa - 39.2 MPa, average = 22MPa), but are much lower than previously determined at Clyde (average = 86MPa) and Maniototo (average = 53MPa) by other workers.

iii.) UCS testing to date supports the observation that schist strength varies depending on the angle (β) between the foliation and the applied force, with schist strength decreasing between β = 0-30°, being at a minimum from β = 30-60° and increasing from β = 60-90°.

iv.) Diametrical $Is_{(50)}$ point load strengths values at Macraes ranged from 0.65 MPa to 2.04 MPa (average = 1.49 MPa) for pelitic schist; and 0.20 MPa to 3.14 MPa (average = 1.18 MPa) for psammitic schist.

v.) Anisotropy index values for schist at Macraes range from 1.3 to 3.8 (mean = 2.6) for psammitic schist and 4.3 to 23 (mean = 10.7) for pelitic schist.

vi.) A tentative correlation factor of 21 for the conversion of point load strength to UCS was calculated during this project, which compares closely with the generally accepted value of 22 in the literature.

vii.) Both point load test and UCS test results suggest that pelitic schist at Macraes is stronger than psammitic schist, and this contrasts with testing undertaken at both Clyde, Maniototo, and elsewhere in Otago where psammitic schist has generally found to be stronger than pelitic schist.

b) Fault Gouge

i.) Residual friction angles measured on sieved fault gouge material from Macraes were very low, ranging between 3.1° and 6.4°, and these residual friction angles are much lower than previously determined by other workers at Macraes.

ii.) X-ray diffraction analysis of the 9ϕ fraction taken from six fault gouge samples identified interlayered swelling chlorite/smectite (25-45%), muscovite (30-40%), kaolinite (20-30%), quartz (trace) and chlorite (<10%) as being present at Macraes.

6.2.2 Assessment of Structural Domains at Macraes

Structural domains at Macraes were assessed by the author as part of this project from structural data collected by Macraes staff at the mine to date. Two sources of sampling bias were identified from the method of data collection, and these are referred to as operator bias and geometric bias. While it is not possible to correct for operator bias, geometric bias may be reduced. By stereoplotting poles to berm orientations it is possible to distinguish different berm groupings, with average berm orientations which allow the Terzaghi correction weighting factor to be applied.

A visual approach to structural domain interpretation was used in this thesis based upon both the interpretations of stereoplots and histograms. Plots were interpreted both above and below the Hyde-Macraes Shear Zone Hanging Wall Shear in a grid like fashion, but no new structural domains were identified beyond those previously described by Coffey Partners International Pty. Ltd (1992).

6.2.3 Pit Slope Failure Database and Models

The quality of recording of failures at the mine prior to this project was of a poor standard, and no formal pit slope failure database was in operation at the mine. A standard recording sheet for pit slope failures at the Macraes open-pit mine site was developed at an early stage of this project, and new failures were recorded on this sheet. This standard recording sheet has been integrated into a computer database that allows simplified searching and retrieval of pit slope failure information. The purpose of such a recording sheet is to assist in engineering geological investigations of pit slope failures by documenting the relevant information in a consistent format. The use of a standard recording sheet increases the speed of data collection, aids consistency over time, and allows fast and accurate comparison between different workers.

Pit slope failure models at Macraes can be classified both according to the geometry of the failure and the types of discontinuities controlling failures as:

a) Planar Failures
   - *High angle planar failures*
   - *Low angle block failures*

b) Wedge Failures
   - *Joint-joint wedges*
   - *Joint-fault wedges*
   - *Fault-fault wedges*

c) Toppling Failures

d) Complex Failures

Back analyses of failures observed at Macraes during the field investigation programme shows that for joints shear strengths range from ϕ = 30°-55° (c' = 10.5kPa - 0kPa), while for faults shear strengths range from ϕ' = 6° -14° (c' = 1.0kPa - 0kPa).

6.2.4 Failures RH27 and RH28

a) Failure RH27

Previous work on RH27 by Bertuzzi (1995) interpreted this failure as an oblique planar failure along the Slip 27 fault driven by water pressures. While failure RH27 occurred prior to this project, investigations undertaken during the project suggest that the failure

developed as a result of undercutting of subsequent wedge intersections that plunge out of the slope at approximately 240/70 and are formed between the southerly dipping Slip 27 Fault and a westerly dipping set of joints. The creation of a void in the pit slope by the failed wedge material has allowed dilation and toppling of the rock mass along easterly and westerly dipping joints into this void. The present volume of the wedge is calculated as encompassing approximately 900m^3.

b) Failure RH28

Detailed engineering geological mapping identified RH28 (as previously interpreted by Bertuzzi (1995)) as a large complex wedge failure formed between the low west dipping Bottom Fault (18/265) and the steep east dipping Bag Farm Fault (55/095), and driven by high groundwater pressures formed along the steep south dipping Back Fault set (65/195). This wedge plunges out of the face at low angles (182/03) and has a total failure volume of 450 000m^3.

Ring shear testing of material taken from the Bottom and Bag Farm faults measured residual friction angles (ϕr) of 6° and 5° respectively (c' = 0). Back analysis in contrast determined a frictional strength for the faults of 13° for the faults. Ring shear and back analysis results may be reconciled by taking into consideration the increase in friction strength due to the coarser material present in the field which is removed for ring shear testing, as well as the effects of roughness/waviness along the fault walls.

Future implications posed by failure RH28 include:

1. Release of the more rapid moving blocks in the central area of the slide
2. Toppling of blocks at the top of the failure (460mRL)
3. Failure of a smaller wedge block, underneath the main failure block, which in turn releases the main failure block above.
4. Complete failure of the wedge block
5. Continuing and increasing expansion the wedge movement on the north wall of Round Hill Pit by stepping out onto more distal faults from the main failure block.

6.2.5 Integrated Predictive Rock Mass Models For Pit Slope Failures

The development of integrated rock mass models for pit slope failures at Macraes serves to aid in the long term performance of the mine site by minimising any adverse effects associated with an unexpected slope failure. High groundwater pressures are concluded to be

a major contributing factor in driving a number of pit slope failures at the mine through both a reduction in friction along the failure surface, as well as pressures at the rear of failures pushing the material out of the slope. The movement of failures and associated dilation of the rock mass may be enough to stabilise failure movement as groundwater pressures are alleviated. Assessment of piezometers and rainfall suggests surficial failures (<5m deep) driven by groundwater pressures occur within 24 hours of rainfall while deeper seated failures (>50m deep) driven by groundwater may take up to two weeks to be affected by groundwater (as a result of the greater distance over which water has to permeate).

From the mean structural orientations recognised in the two structural domains at the mine site, 58 kinematic models of failure have been identified. Integration of these 58 failure models with 32 failures recorded in the pit slope failure database shows that 13 main kinematic failure models have occurred at Macraes so far. These 13 kinematic failure models form predictive models which allow prediction of future slope failures, as well as the main factors that are likely to contribute to failure (i.e. toe undercutting, precipitation etc.).

These 13 identified kinematic failure models will assist berm inspections by identifying the types of likely failure models in a particular part of the pit which may be looked-out for.

The documentation of failures through use of the standard recording sheet developed here, photographic records, movement and groundwater monitoring are all essential for effective failure management. Regular inspections of berms particularly above currently mined areas is required to identify new areas of movement and any development of existing failures. Berm inspections should also be undertaken throughout the whole mine on a regular basis to supplement monitoring data.

6.3 PROJECT CONCLUSIONS

6.3.1 Geotechnical Testing

a) Intact Rock

- The low strength of schist at Macraes (particularly // to schistosity) means that the preparation of core samples for UCS testing according to the ISRM guidelines is difficult. For testing of this material it may be appropriate to allow the testing of shorter lengths and allow the use of end capping materials.

- Schist at Macraes is significantly weaker in terms of UCS than values measured for schist at other project locations in the Otago Schist. Consequently it is concluded that the application of strength data from these other project locations is likely to produce overly optimistic results if applied at Macraes.
- Strength testing undertaken on schist at Macraes suggests that the pelitic schist is stronger than psammitic schist. Since pelitic schist dominates within the Hyde Macraes Shear Zone it may be that annealing processes are responsible for the relatively high shear strengths of pelitic schist since this behaviour was not expected.
- The uncertainty with calculation of the correction factor (due to limited testing) for point load strength to UCS data means that this should be applied with a great deal of caution, and that point load strength data is best used as a rock mass strength characterisation index in itself until the correlation factor ascertained in this project is verified with more certainty (if it ever can be).

b) Fault gouge

- The high proportion of coarse material present in fault gouge which needs to be removed for ring shear testing means that the ring shear results are not appropriate to apply directly to field data.
- Low residual strengths measured during ring shear testing suggest a sliding mode of residual shear behaviour for fault gouge at Macraes.
- There is a high proportion of swelling clay minerals present within the fault gouge at Macraes, and this will increase the instability of the rock mass above fault zones by heaving and reducing the effective stress acting along the fault (potential failure surface(s)).

6.3.2 Structural Domain Analysis

- There is a lack of good spatial data collected at the mine during face mapping to conduct quantitative analyses of structural domains. Much more structural mapping needs to be undertaken of newly exposed berms on a regular basis. It should be easily possible for Macraes to collect between 100 and 200 good structural observations per week (25-50 per day). Within one year this would approximately double the amount of structural information available and represent a substantial improvement on the currently limited structural database.

- There is no integration of maps of the major faults in the area with collected structural data. Major faults are likely to control structural domain boundaries and it is important to delineate these more important features during the collection of structural data so that data may be selected from different regions for separate interpretation.
- The use of standard geological mapping techniques for structural data collection at the mine site at present is likely to introduce both an 'operator bias' and a geometric bias. Standard scanline or window mapping techniques should be used to minimise the effects of operator bias during the structural mapping process. Geometric bias will arise because the number of structures sampled from different discontinuity sets along a berm, will depend on the orientation of the discontinuity set relative to the berm, and can be reduced by applying the Terzaghi weighting function.

6.3.3 Pit Slope Failure Database and Models

- A standard recording sheet for pit slope failures aids engineering geological investigations. The recording of failures on this sheet should be continued in the future as it will provide records of any failure development with time, assess effectiveness of remedial measures undertaken, be used for further determination of strength parameters by back analysis and provide records for the ongoing assessment of pit slope design.

6.3.4 Failures RH27 and RH28

a) Failure RH27

- The previous interpretation of RH27 as an oblique planar failure seems unlikely from a kinematic assessment. Engineering geological mapping of RH27 identified that the main failure is controlled by the structure of the rock mass in the area, and is a wedge formed between a fault and a westerly dipping joint set, emphasising the importance of mapping of the rock mass structure for failure interpretation.
- Continuing development of failure RH27 would appear unlikely due to proximity of the present wedge intersection to the Hanging Wall Shear. Both structural domain interpretation and field observations suggest that the Slip 27 Fault is terminated or truncated against the Hanging Wall Shear, while the westerly dipping joint set is far less significant below the Hanging Wall Shear which effectively limits future development of RH27.

b) Failure RH28

- Failure RH28 is essentially controlled by the structure of faulting in the area where a wedge is formed between fault sets FA1 and FA3 and driven by high groundwater pressures formed along fault set FA4. This being the case, failure development is merely a reflection of stepping out onto more distal faults as deeper wedge intersections are undercut by mining activities.
- The westward component of movement of monitoring prisms can be more easily explained by dilation and complex sliding along westerly dipping structures than by a quasi-circular failure mechanism.
- The low angle of the wedge intersection (and direction of sliding) means head unloading is unlikely to have a significant effect on stabilising the failure. Shear stresses must be high for sliding to occur along such a low angle, and the component of shear stress derived from the gravitational force (of a weight) is likely to be low, since most of the force will act normal to the failure surface.
- Alleviation of high groundwater pressures formed along the south dipping fault set parallel to the pit slope is likely to be the most effective mechanism at preventing further movement.
- Installation of alarms and installation of prisms is required to minimise the potential impact of a rapid failure on mining operations.
- The orthogonal orientation of the two fault sets controlling failure means that any slight change in dip direction of the controlling faults from one side of the pit to the other could create a similar type of wedge that plunges to the north out of north dipping pit slopes.

6.3.5 Predictive Rock Mass Models

- Surficial slope failures (<5m deep) are likely to occur within 24 hours of rainfall, while deeper failures (5-50m deep) are predicted to be most effected by rainfall one to two weeks after precipitation. For this reason access to berms needs to restricted where possible in the first 24 hour period following rainfall.
- Failures at Macraes are controlled by the structure of the rock mass and failure types may therefore be predicted kinematically based on mean orientations for the different discontinuity sets identified.
- Thirteen kinematic failure modes are predicted at Macraes based on those failures recorded to date and an assessment of strength characteristics of the rock mass. Kinematic

models are given which should assist in routine berm inspections identifying potential failures on pit slopes with different orientations.

- Recording of pit slope failures on a standard recording sheet into the pit slope failure database is essential for effective management of failures, and for improving the predictive rock mass models developed here by calibrating those observed with those predicted.
- Monitoring and management of pit slope failures, consisting of survey data, photographic and movement records, piezometric and rainfall data, combined with visual inspections and walkovers, is an essential part of predicting pit slope failure behaviour.

6.3 FURTHER WORK

It is recommended that the following further work be carried out at the Macraes mine site. While it is understood that some of these recommendations have already been implemented they are nevertheless reiterated here as:

1. **Intact rock strength testing:**
    i.) Future intact rock testing should be aimed at determining whether the conclusion that pelitic schist is stronger than psammitic schist is correct for the mine site, or whether this lithologic strength difference merely reflects the limited sampling and testing.
    ii.) Future intact rock strength testing should also be used to determine the exact nature of the strength anisotropy for schist at Macraes when forces are applied at various angles to the foliation (schistosity).
    iii.) Combined point load testing and UCS testing should be undertaken to assess the accuracy of the tentative correlation factor of 21 calculated in this project, and to modify it as required.

2. **Fault gouge shear strength:**
    i.) While the effects of clay mineralogy on shear strength are understood qualitatively, much more work needs to be dedicated to determining more quantitative relationships between clay mineralogy and residual shear strength of the different clay minerals at Macraes.

ii.) The effects of swelling clays on reducing the effective stress acting along discontinuities needs to be assessed and quantified for improved pit slope stability analyses.

iii.) Quantification of the effects of grain size distribution on residual strength needs to be undertaken. Ideally it would be useful to have some form of chart(s) that allow residual shear strengths measured in the laboratory to be calibrated back to realistic values for field material, which contains a high proportion of coarse material (which is sieved out for laboratory testing), and/or high waviness/roughness along the fault walls.

3. Improved structural data collection and interpretation:

i.) The present structural database at Macraes is limited and a lot more structural data needs to be collected in order to get more accurate structural interpretations. Improved data collection and data coverage will allow improved quantitative geostatistical interpretations to be undertaken.

ii.) The standard recording sheet used during berm mapping needs to be significantly improved and replaced with a sheet that uses standard engineering geology/rock mechanics terminology.

iii.) Structural interpretations developed here should be subject to further field checking and assessed for consistency.

iv.) The adoption of more rigorous sampling techniques during berm mapping, such as the standard scanline technique, will help in reducing the effects of operator bias during structural data collection.

v.) Structural data collected during face mapping also should be assigned with a tag according to whether it lies above or below the Hanging Wall Shear (the feature controlling the two structural domains identified here). Tagging of collected structural data in this manner will assist future interpretations of structural domains since data may be more easily assessed separately according to the two main structural domains identified for separate plots.

4. Structural mapping programmes:

A new geotechnical mapping programme needs to be undertaken which identifies any major faults (>100m in length) in the area, in relation to mapped structural data from the face mapping programme. The identification of major faults will assist future attempts at structural domain interpretation by giving possible domain boundaries. Data may then be selected separately either side of these major structures for structural homogeneity.

5. Groundwater and drainage:

i.) While groundwater pressures appear to be a major contributing factor to pit slope failures at Macraes, the groundwater regime appears to not be well understood. Areas of high groundwater need to be identified and targeted for drainage.

ii.) Regular monitoring of piezometers needs to be undertaken on a daily basis so that a better understanding of the lag time between precipitation events and groundwater response may be developed.

iii.) Horizontal drainage needs to be installed to alleviate areas of high groundwater pressures identified by piezometric data. Drains should be orientated when they are installed so that they intersect as many of the permeable discontinuities as possible (good structural interpretations are emphasised here). Once again newly installed drains should be monitored for flows and correlated with piezometers to determine trends and effectiveness, and to aid in future slope depressurisation programmes.

6. Alarms and alarm criteria:

Simple trip wire alarms need to be installed on active failures, particularly on those failures which are situated above current mining activities. In order for these alarms to be effective appropriate movement alarm criteria need to be developed based on determining an unacceptable amount of movement for active failures before the alarm is activated. The appropriate alarm criteria needs to be a balance between minimising the disruption to mining activities from false alarms, yet maximising the safety of personnel and equipment from unpredicted pit slope failure.

7. Predictive rock mass models for pit slope failures:

New failures should continue to be recorded on the standard recording sheet and added to the failure database. The continuing recording of pit slope failures should allow better calibration and refinement of the predictive rock mass models for pit slope failure models developed during this thesis. Failures should be checked for consistency with the failure models developed here and where inconsistencies are found, new failure models should be developed.

ACKNOWLEDGMENTS

I would like to gratefully acknowledge the assistance of the following organisations and people, given to me during this thesis:

My family for their support, loans, encouragement and gentle nagging on when I was going to finish university. Your contribution has been awesome.

My supervisor Dave Bell for helping initially organise the project and reading of draft chapters and useful comments.

Macraes Mining Company Ltd for funding this project. A special thanks is extended to Laura Williams and Bernie O'Leary for approving funding for this project and the provision of accommodation in Palmerston during field work.

Greg Ryan of Waikouaiti for his help on slope failures both in and out of the field. Your sarcasm and wit was also much appreciated.

David Stewart the Macraes Engineering Geologist, for the provision of 3 weeks core logging during August 1996, and continued correspondence throughout most of the project.

Derek Wood for the provision of base maps of the mine site and Phil Lundy for his advice, discussions and many lifts into and out of the pits.

The staff at Macraes who have always been helpful, supportive and friendly.

Greg Slaughter and Brett Hewett who put up with me as a flatmate at Palmerston, and who provided many hours of entertainment both at the pub, and playing Risk on those bloody cold winter nights (even when the games got a bit heated).

Simon Ward for all his chats and especially all his help on and Techbase and with other computing problems (the bottle of scotch is on its way !).

The technicians of the Geology Department. Especially Cathy Knight, Arthur Nicholas, Rob Spiers for all their assistance in the Engineering Geology Laboratory. Cathy I extend extra thanks to you for your efforts in helping solve the problems encountered during ring shear testing. Steven Brown is also extended thanks for his assistance with XRD testing. Thanks to John Southward for always being prepared to help and the organising of both paper and printing facilities.

George Clarke and John from the Civil Engineering Department for allowing me to use their concrete crushing equipment during UCS testing.

My dear friend Emily Doornenbal for her friendship, support and reading of draft chapters it was very much appreciated.

I would like to extend thanks to my roommates, Edgardo (you're a machine), Kane, and Rob who have all provided great support and advice during my career as a professional university student. You're all very great friends, but Ed you work too bloody hard (see you in Peru 2000?). Kane thanks for the help with sorting of the thesis and numerous drinking sessions especially after handing in), and Rob even though you were there to the end your spading techniques like Ed's have provided interesting entertainment (I'm not sure who's better?) .

I would also like to thank my classmates Hamish and Matt, you are also good friends and have provided much support and advice during our many discussions on all sorts of issues. Thanks Hamish for the help with UCS testing, and discussions, best of luck with the cheese muffins (hope you mange to get some). Matt thanks for the enlightenment on GPR and spit development, even if half the time I had no idea what you were talking about.

So long and thanks for all the fish. Time now, to go and join the real world .

REFERENCES

Angus, P. V. M., (1992), *The structural evolution of the Hyde-Macraes Shear Zone at Round Hill, Otago, New Zealand*, **in:**, Proceedings of the 26th Annual Conference 1992, New Zealand Branch of the Australasian Institute of Mining and Metallurgy, p.1-6.

Anon., (1994), *Pit slope stability*, **in:**, Slope Stability Course for Coalcorp NZ Ltd., Tuesday 25 - Thursday 27 October 1994.

Auckland UniServices Ltd., (1996), Ring Shear Tests (Macraes Mines Samples), Unpublished consultants report prepared for Woodward Clyde, Ref: 6801.00, 10 September 1996

Barnes, G.E., (1995), Soil Mechanics - Principles and Practice, Macmillan Press Ltd., London, 365pp.

Barton, N., and Choubey, V., (1977), *The shear strength of rock joints in theory and practice*, **in:**, Rock Mechanics, Vol. 10, p.1-54.

Bell, D.H., and Pettinga, J.R., (1983), *Presentation of geologic data*, **in:**, Proceedings of the Symposium Engineering for Dams and Canals, IPENZ, Volume 9, Issue 4(G), p.4.1-4.35.

Bell, F.G., (1987), *Geological Considerations*, **in:**, Ground Engineers Reference Book, Bell (ed.), Butterworths, London, p.1/1 - 1/29.

Bell, F.G., (1987), *Open excavation*, **in:**, Ground Engineers Reference Book, Bell (ed.), Butterworths, London, p.39/1 - 39/18.

Bertuzzi, R., (1995), Review of NE Wall Stability - Round Hill Pit, Letter to Mr Bernie O'Leary (Mine Superintendent), 10 November 1995, PSM71.L3, 5pp. + photos and maps.

Bertuzzi, R., (1992), *Philosophy of Slope Design: A Case Study of Geotechnical Investigations at Macraes Flat Gold Mine*, **in:**, Proceedings of the 26th Annual Conference, New Zealand Branch of the Australasian Institute of Mining and Metallurgy, p.1-8.

Bishop, D.G., (1972), *Progressive metamorphism from prehnite-pumpellyite to greenschist facies in the Dansey Pass area, Otago, New Zealand*, **in:**, Geological Society of America Bulletin, Vol.83, p.3177-3198.

Braithwaite, R..L., (1989), *Geological setting of mineralisation in New Zealand*, **in:**, D. Kear (ed.), Monograph 13 - Mineral Deposits of New Zealand, Australasian Institute of Mining and Metallurgy, p.1-8.

Broch, E., and Franklin, J., (1972), *The point load strength test*, **in:**, International Journal of Rock Mechanics and Mining Sciences, Vol.9, p.669-697

Brook, N., (1985), *The equivalent core diameter method of size and shape correction, in point load testing*, **in:**, International Journal of Rock Mechanics and Mining Sciences & Geomechanics Abstracts, Pergamon Press Ltd., p.61-70

Brown, A., (1982), *The influence and control of groundwater in large slopes*, **in:**, Third International Conference on Stability in Surface Mining, C.O. Brawner (ed.), American Institute of Mining and Metallurgy and Petroleum Engineering, New York, p.19-41.

Brown, E.T., (1981), Rock Characterisation Testing and Monitoring, ISRM Suggested Methods, Pergamon Press.

Cheeney, R.F., (1982), Statistical Methods in Geology, George Allen & Unwin Ltd, London, 169pp.

Coffey Partners International Pty. Ltd., (20th May 1992), Assessment of Pit Slope Design, Unpublished Consultancy report prepared for Macraes Mining Company Ltd., Report Z160/1-AA, May 1992.

Coffey Partners International Pty. Ltd., (December 1992), Slope Monitoring Programme, Unpublished Consultancy report prepared for Macraes Mining Company Ltd., Report Z160/3-AB. 23pp. + attachments

Coffey Partners International Pty. Ltd., (20th October 1993), Site Visit and Geotechnical Review, Unpublished Consultancy report prepared for Macraes Mining Company Ltd., Report Z160/4-AC, 13pp. + figures

Cook, N.G.W., (1982), *Groundwater problems in open-pit and underground mines*, **in:**, Geological Society of America - Special Paper 189, p.397-405.

Coombs, D.S.C., Landis, C.A., Norris, R.J., Sinton, J.M., Borns, D.J., and Craw, D., (1966), *The Dun Mountain Ophiolite Belt, New Zealand, its tectonic setting, constitution and origin with special reference to the southern portion*, **in:**, American Journal of Science, Vol.276, p.561-603.

Cruden, D.M., and Varnes, D.J., (1996), *Landslides types and processes*, **in:**, Landslides Investigation and Mitigation - Special Report 247, Turner and Schuster (eds.), Transportation Research Board, National Research Council, National Academy Press, Washington D.C., p.36-75.

Domenico, P.A., and Schwartz, F.W., (1990), Physical and Chemical Hydrogeology, John Wiley and Sons, New York, 824pp.

Eggers, M., and Sullivan, T., (1995), Round Hill Pit - NE Wall Failure, Memorandum to Brent Ashton (Macraes Mining Engineer), 27 February 1995, 2pp.

Eggers, M., (1995), re: NE Cutback - Failures 27 and 28, Facsimile to Brent Ashton (Macraes Mining Engineer), 9 June 1995, 7pp.

Giani, G.P., (1992), Rock Slope Stability Analysis, A.A. Balkema, Rotterdam, 361pp.

Hawkes, I., and Mellor, M., (1970), *Uniaxial testing in rock mechanics*, Engineering Geology, Vol.4, p.177-285.

Hoek, E., (1987), *General two-dimensional slope stability analysis*, **in:**, Analytical and Computational Methods in Engineering Rock Mechanics, Brown (ed.), Allen & Unwin, London, p.95-128.

Hoek and Bray, (1981), Rock Slope Engineering - Revised third edition, Institution of Mining and Metallurgy, London, 358pp.

Hoek, E., and Diederichs, M., (1989), DIPS - A program for plotting, analysis and presentation of structural geology data using spherical projection techniques, Rock Engineering Group, University of Toronto, 138pp.

Horn, H.M., and Deere, D.U., (1962), *Frictional characteristics of minerals*, **in:**, Geotechnique, Vol.12, p.319-335.

Hume, H.R., (1983), Geotechnical Slope Stability Analysis, B & G Sector, Bingham Canyon Open Pit, Utah, with a Consequent Investigation of Methods for Delineating Rock Mass Fracture Domains, PhD thesis, University Microfilms International, 391pp.

International Union of Geological Sciences Working Group on Landslides, (1995), *A suggested method for describing the rate of movement of a landslide*, **in:**, Bulletin of the International Association of Engineering Geology, No.52, October 1995, p.75-78.

Johnson, R.S., (1982), *Slope Stability Monitoring*, **in:**, Proceedings of the Fourth Canadian Symposium on Mining Surveying and Deformation Measurements, Alberta, June 7th - 9th, p.364-379.

Kamb, W.B., (1959), *Ice Petrographic Observations*, **in:**, Journal of Geophysical Research, Vol.64, No.11, p.1891-1909.

Kwasniewski, M.A., (1993), *Mechanical Behaviour of Anisotropic Rocks*, **in:**, Comprehensive Rock Engineering - Volume 1 - Fundamentals, Hudson (ed.), Pergamon Press, Oxford, p.285-312.

Lambe, T.W., and Whitman, R.V., (1979), Soil Mechanics - SI Version, John Wiley & Sons, New York, 553pp.

Lee, M.C., (1987), *The Round Hill gold-scheelite deposit, Macraes Flat, Otago, New Zealand*, Proceedings of the 21st Annual Conference NZ Branch, Australasian Institute of Mining and Metallurgy, p.71-80.

Lee, M.C., Batt, W.D., and Robinson, P.C., (1989), *The Round Hill Gold-Scheelite Deposit, Macraes Flat, Otago, New Zealand*, **in:**, D. Kear (ed.), Monograph 13 - Mineral Deposits of New Zealand, Australasian Institute of Mining and Metallurgy, p.173-179.

Lupini, J.F., Skinner, A.E., and Vaughan, P.R., (1981), *Drained Residual Strength of Cohesive Soils*, **in:**, Geotechnique, Vol.31, No.1, p.181-213.

Macfarlane, (1984), Kawarau River Power Investigations - Engineering Geological Feasibility Investigations at the KW35 Damsite, DSIR, New Zealand Geological Survey Report EG387, October 1984, 40pp.

Macfarlane, (1985), Kawarau River Power Investigations - Engineering Geological Feasibility Study of the Proposed KW35 to KW28/29 Canal, DSIR, New Zealand Geological Survey Report EG390, June 1985, 41pp.

Macraes Mining Company Limited, (1996), 1996 Annual Report, 64pp.

Macraes Mining Company Limited, (Nov.1995), Macraes Gold Project - Macraes Line of Strike Tour Supplement, 9pp.

McKeag, S.A., Craw, D., and Norris R.J., (1989), *Origin and deposition of a graphitic schist-hosted metamorphogenic Au-W deposit, Macraes, east Otago, New Zealand*, **in:**, Mineralium Deposita, Vol.24, p.124-131.

Moody, K., (1985), Engineering Geology Assessment of Batter Stability Paerau Diversion Works, Maniototo, Central Otago, Unpublished M.Sc. Thesis, University of Canterbury, Christchurch, New Zealand, 199pp.

Mortimer, N., (1993), *Geology of the Otago Schist and adjacent rocks*, Scale 1:500 000, Institute of Geological and Nuclear Sciences geological map 7, 1 sheet, Institute of Geological and Nuclear Sciences Ltd., Lower Hutt, New Zealand.

Mutch, A.R., (1963), Sheet 23 Oamaru - Geological Map of New Zealand 1:250 000 (1st ed.), Department of Scientific and Industrial Research, Wellington, New Zealand.

Norrish, N.I., and Wyllie, D.C., (1996), *Rock slope stability analysis*, **in:**, Landslides - Investigation and Mitigation, Transportation Research Board Special Report 247, National Academy Press, Washington, p.391-425.

Pells, P.J.N., (1993), *Uniaxial strength testing*, **in:**, Comprehensive Rock Engineering - Volume 3 - Rock Testing and Site Characterization, Hudson (ed.), Pergamon Press, Oxford, p.67-85.

Pender, M.J., (1984), "Stability of slopes", **in:**, Slope Stability Course for Coalcorp NZ Ltd., Tuesday 25 - Thursday 27 October 1994.

Piteau, D.R., and Associates Ltd., (1977), Workshop on Rock Slope Engineering - Part C: Approach and Techniques in Geologic Structural Analysis, Piteau and Associates, West Vancouver B.C..

Piteau, D.R., and Russell, L., (1971), *Cumulative sums technique: A new approach to analysing joints in rock*, **in:**, Stability of Rock Slopes, 13th Symposium on Rock Mechanics, August 30th - September 1st 1971.

Pointe, P.R., and Hudson, J.A., (1985), Characterisation and Interpretation of Rock Mass Joint Patterns, Geological Society of America, Special Paper 199, 39pp.

Priest, S.D., (1993), Discontinuity Analysis for Rock Engineering, Chapman & Hall, London, 473pp.

Richards, L.R., and Atherton, D., (1987), *Stability of slopes in rock*, **in:**, Ground Engineers Reference Book, Bell (ed.), Butterworths, London, p.12/1 - 12/16.

Standards Association of New Zealand, (1986), NZS 4402:1986 Methods of Testing Soils for Civil Engineering Purposes.

Sullivan, T.D., (1995), Letter to Bernie O'Leary (Macraes Mine Superintendent), PSM71.L3, 13 November 1995, 3pp.

Swan, A.R.H., and Sandilands, M., (1995), Introduction to Geological Data Analysis, Blackwell Science, Oxford, 446pp.

Teagle, D.A.H., Norris, R.J. and Craw, D., (1990), *Structural controls on gold-bearing quartz mineralisation in a duplex thrust system, Hyde-Macraes Shear Zone, Otago schist, New Zealand*, **in:**, Economic Geology, Vol.85, 1990, p.1711-1719.

Terzaghi, R., (1965), *Sources of errors in joint surveys*, **in:**, Geotechnique, Vol.15, p.287-304.

Varnes, D.J., (1978), *Slope movement types and processes*, **in:**, Landslides: Analysis and Control, Schuster, R.L., and Krizek, R.J., (eds.), Transportation Research Board, Special Report 176, National Academy of Sciences, Washington, p.11-33.

Vutukuri, V.S., Lama, R.D., and Saluja, S.S., (1974), Handbook on Mechanical Properties of Rock, Vol.1, Trans Tech Publications, Switzerland, 280pp.

Williamson, J.H., 1939, *The geology of the Naseby subdivision, Central Otago*, New Zealand Geological Survey Bulletin, 141pp.

Windsor, C.N., (1991a), *The relationship between the Hyde-Macraes Shear Zone, deformation episodes, and gold mineralisation potential in eastern Otago, New Zealand*, **in:**, New Zealand Journal of Geology and Geophysics, Vol.34, p.237-245.

Windsor, C.N., (1991b), *Low-angle shear zones in Central Otago, New Zealand - their regional extent and economic significance*, **in:**, New Zealand Journal of Geology and Geophysics, Vol.34, p.501-516.

Wise, D. U., and McCrory, T.A., (1982), *A new method of fracture analysis: Azimuth versus traverse distance plots*, **in:**, Geological Society of America Bulletin, Vol. 93, p.889-897

Wood, J.A., (1970), Gold Trails of Otago, A.H. & A.W. Reed Ltd., Wellington, 88pp.

Woodward-Clyde (NZ) Ltd, (1997), Round Hill Pit Stability Studies, Consulting Report prepared for Macraes Mining Company Ltd., Unpublished.

Works Consultancy Services Ltd., (1996), Shear testing results for Toe Fault, Battery Creek -Sample UTϕ1, Unpublished consultants report prepared for Woodward Clyde, Report No.522416.00, 6 August 1996

Wyllie, D.C., and Norrish, N.I., (1996), *Rock strength properties and their measurement*, **in:**, Landslides - Investigation and Mitigation, Transpotation Research Board Special Report 247, National Academy Press, Washington, p.372-390.

APPENDICES

APPENDIX A: ROCK AND SOIL CLASSIFICATION

A1 Terminology

Intact Rock	*a continuum or polycrystalline solid consisting of an aggregate of minerals or grains (Bell, 1987)*
Discontinuity	*any significant mechanical break or fracture of negligible tensile strength in a rock (Priest, 1993)*
Rock Structure	*The complex three-dimensional structure of discontinuities in a rock*
Rock Mass	*Intact rock + rock structure*
Schistosity	*A fabric of intact rock created by the planar alignment of platy minerals, such as micas.*
Joint	*a break of geological origin along which there has been no visible displacement (Bell, 1987)*
Fault	*A fracture in rock along which displacement has taken place (Bell, 1987)*
Joint set	*a group of parallel joints*
Fault set	*a group of parallel faults*

ENGINEERING GEOLOGICAL FIELD DESCRIPTION FOR ROCK MATERIAL

WEATHERING

	TERM	GRADE	ROCK DESCRIPTION
6.	* residual soil (RW)	VI	discolouration and complete transformation to soil; original fabric destroyed
5.	completely weathered (CW)	V	discolouration and transformation to soil; original fabric largely preserved
4.	highly weathered (HW)	IV	material pervasively altered with discolouration and loss of strength; fabric preserved; lithorelicts
3.	moderately weathered (MW)	III	penetrative discolouration and alteration of rock material, with some loss of strength
2.	slightly weathered (SW)	II	slight discolouration of rock fabric; no loss of material strength
1.	unweathered (UW)	I	no discolouration or loss of strength, or any other effects due to weathering

STRENGTH

	TERM	POINT LOAD STRENGTH INDEX Is(50)	FIELD ESTIMATION OF STRENGTH
1.	extremely strong (ES)	more than 10	can only be chipped with geological hammer
2.	very strong (VS)	3 to 10	several hard blows required to break hand specimen
3.	strong (S)	1 to 3	few firm blows of hammer required to break specimen
4.	moderately strong (MS)	0·3 to 1	breaks readily with one blow of hammer
5.	moderately weak (MWk)	0·1 to 0·3	broken by hand only with difficulty; small thin pieces broken by finger pressure
6.	weak (Wk)	0·03 to 0·1	broken by hand; pieces 25 mm or more broken by finger pressure
7.	*very weak (VWk)	less than 0·03	crushed or remoulded by hand (grades into soil materials)

* may require description as soil material

GEOLOGICAL CLASSIFICATION

CRYSTAL OR GRAIN SIZE	SEDIMENTARY (†) CLASTIC	SEDIMENTARY (†) CHEM/ORGANIC	IGNEOUS (†) Mode of Occurrence	IGNEOUS (†) Silicic	IGNEOUS (†) Intermed.	IGNEOUS (†) Mafic	IGNEOUS (†) Ultramaf.	METAMORPHIC (†) FOLIATED	METAMORPHIC (†) MASSIVE
very coarse 64	CONGLOMERATE (1)							GNEISS (34)	HORNFELS (39)
coarse 2	AGGLOMERATE (2)								
	BRECCIA (3)		INTRUSIVE	GRANITE (27)	SYENITE (29)	GABBRO (31)	PERIDOTITE (32)	SCHIST (35)	MARBLE (40)
medium	SANDSTONE (4)	Calcareous LIMESTONE (9)		GRANODIORITE (28)	DIORITE (30)		DUNITE (33)	PHYLLITE (36)	QUARTZITE (41)
0·06		Siliceous CHERT (10) OTHER (11)							
fine	SILTSTONE (5)	Carbonaceous COAL (12) OTHER (13)		RHYOLITE (19) OBSIDIAN. (20) DACITE (21)	TRACHYTE (22) ANDESITE (23)	DOLERITE (24) BASALT (25)	SERPENTINITE (26)	SLATE (37)	AMPHIBOLITE (42)
TUFFS (7)	MUDSTONE (6)	Ferruginous LATERITE (14) OTHER (15)						MYLONITE (38)	(†) OTHERS: Specify (43)
very fine 0·002 (mm)	CLAYSTONE (8)	Saline ROCK SALT (16) GYPSITE (17) OTHER (18)	EXTRUSIVE						

WEATHERING TERM | STRENGTH TERM | COLOUR | FABRIC | ROCK NAME

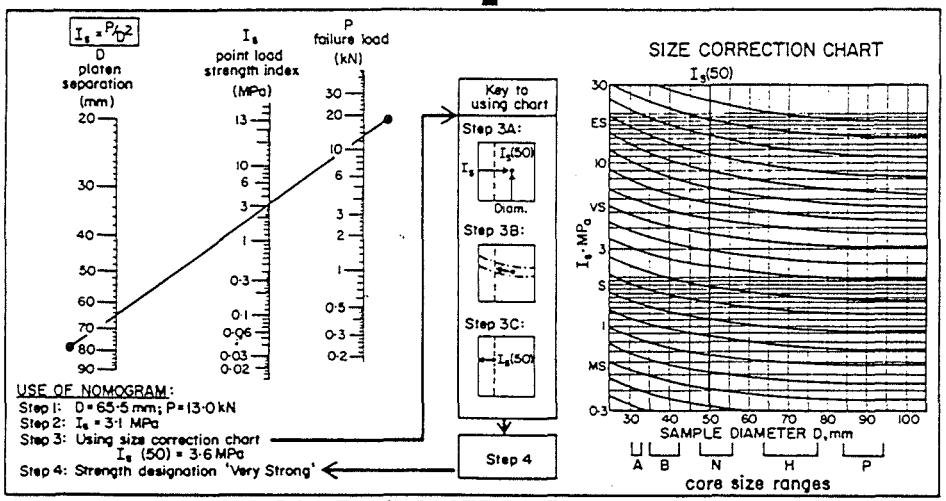

POINT LOAD STRENGTH INDEX

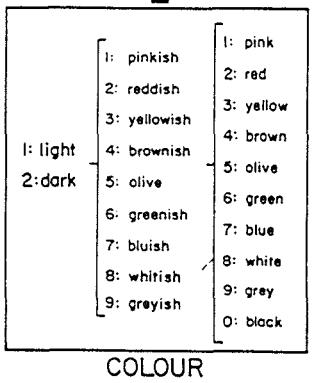

COLOUR

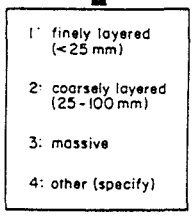

FABRIC

ENGINEERING GEOLOGICAL FIELD DESCRIPTION FOR SOIL MATERIAL

WEATHERING

	TERM	GRADE	SOIL DESCRIPTION
5	Completely Weathered (CW)	V	completely discoloured and altered, no trace of original fabric
4	Highly Weathered (HW)	IV	mostly altered and weakened, little trace of original fabric
3	Moderately Weathered (MW)	III	large discoloured portions of original soil separated by more altered material; significantly weakened
2	Slightly Weathered (SW)	II	minor discolouration of some parts of the original soil, no loss of strength
1	Unweathered (UW)	I	original soil with NO discolouration, loss of strength or other effects due to weathering
0	NOTE ✱ in coarse-grained soils record weathering grade of DOMINANT fraction here and qualify weathering grade of subordinate and/or minor fractions if appropriate		

STRENGTH

	TERM	FIELD CRITERIA
1	loose	can be removed from exposure in disaggregated form by hand
2	compact	only removed from exposure by implement; material readily disaggregated by physical means
3	+cemented	only removed from exposure by implement; material does not disaggregate
4	hard	may be removed from exposure with difficulty by implement or hand, softened on immersion in water and may be remoulded
5	stiff	indented by thumb pressure, but not moulded by fingers; softened on immersion in water, and may be remoulded
6	firm	moulded or indented only by strong finger pressure; easily moulded after immersion in water
7	soft	easily indented or moulded by finger pressure
8	very soft	exudes between fingers when squeezed
9	spongy	readily compressed by finger pressure, but cannot be remoulded

+ may require description as rock material

UNIFIED SOIL CLASSIFICATION SYSTEM

			FIELD IDENTIFICATION	GROUP SYMBOL	TYPICAL NAMES
COARSE-GRAINED SOILS	GRAVELS (<50% larger than 2mm)	clean gravels	wide range in grain size and substantial amounts of all interm. sizes	GW	well graded GRAVELS
			predom. one size or a range of sizes with some interm. sizes missing	GP	poorly graded GRAVELS
		gravels with fines	non-plastic fines (see ML below)	GM	poorly graded SILTY-GRAVELS
			plastic fines (see CL below)	GC	poorly graded CLAYEY-GRAVELS
	SANDS (<50% smaller than 2mm)	clean sands	wide range in grain sizes and substantial amounts of all interm. sizes	SW	well graded SANDS
			predom. one size or a range of sizes with some interm. sizes missing	SP	poorly graded SANDS
		sands with fines	non-plastic fines (see ML below)	SM	poorly graded SILTY-SANDS
			plastic fines (see CL below)	SC	poorly graded CLAYEY-SANDS

		LIQUID LIMIT	SHINE	DILATANCY (1)	TOUGHNESS (1)		
FINE-GRAINED SOIL SILTS AND CLAYS		<50	none to very dull	quick to slow	none	ML	INORGANIC SILTS with slight plasticity
			moderate	none to very slow	medium	CL	INORGANIC CLAYS of low to medium plasticity
			none to very dull	slow	slight	OL	ORGANIC SILTS & CLAYS of low plasticity
		>50	dull	slow to none	slight to medium	MH	INORGANIC SILTS of high plasticity
			very glossy	none	high	CH	INORGANIC CLAYS of high plasticity
			moderate to v. glossy	none to very slow	slight to medium	OH	ORGANIC CLAYS of medium to high plasticity
HIGHLY ORGANIC SOILS			identified by colour, odour, spongy feel and fibrous texture			Pt	PEAT and other highly organic soils

PROCEDURES FOR FINE-GRAINED SOILS OR FRACTIONS (1)

DILATANCY (reaction to shaking) -

1) Prepare pat of moist soil, adding water to make soft - but not sticky.

2) Place pat in palm of hand, shake horizontally by striking vigorously against other hand.

Positive Reaction: appearance of water on surface of pat, which becomes glossy. When squeezed between fingers, water and gloss disappear, pat stiffens and may crumble.

TOUGHNESS: (consistency near plastic limit) -

1) Mould sample to consistency of putty, adding water or air drying as required

2) Roll to thin (3mm) thread, fold and reroll repeatedly until thread crumbles at plastic limit

3) Knead together and continue until lump crumbles.

Diagnosis: a tough thread and stiff lump indicate high plasticity; a weak thread and lump low plasticity clays.

GROUP SYMBOL CODINGS FOR USCS

COLUMN 1		COLUMN 2	
G:1	C:4	W:1	C:4
S:2	O:5	P:2	L:5
M:3	Pt:6	M:3	H:6

BOUNDARY CLASSIFICATIONS specify, enter 0,0

WEATHERING TERM | WATER CONTENT TERM | STRENGTH TERM | COLOUR | FABRIC | SOIL NAME | USCS SYMBOL

	TERM	FIELD CRITERIA
1	Dry	looks and feels dry; fine-grained soils usually hard, powdery or friable; coarse-grained soils may run freely through hands
2	Moist	soil feels cool and may be darkened in colour; particles tend to adhere in coarse-grained materials; fine-grained soils may be softened
3	Wet	soils feel cold and are darkened in colour; free water forms on hands when sample is disturbed
4	Saturated	restricted to wet soils below the water table or the static water level in excavations or drill holes

WATER CONTENT

COLOUR

1: light	1 pinkish	1 pink
	2 reddish	2 red
	3 yellowish	3 yellow
	4 brownish	4 brown
	5 olive	5 olive
	6 greenish	6 green
	7 bluish	7 blue
	8 whitish	8 white
	9 greyish	9 grey
2: dark		0 black

FABRIC

1: finely layered (<25 mm)
2: coarsely layered (25-100 mm)
3: massive
4: other (specify)

✱SUBORDINATE FRACTION
20-50% volume visual estimate

DOMINANT FRACTION
>50% volume visual estimate

✱ MINOR FRACTION
<20% volume visual estimate

1	coarse	gravelly
2	medium	gravelly
3	fine	gravelly
4	coarse	sandy
5	medium	sandy
6	fine	sandy
7	silty	
8	clayey	
9	peaty	

PARTICLE SIZE

	SOIL TYPE TERM		PARTICLE SIZE (mm)	GRAPHIC LOG
1	coarse	gravel	> 60	
2	medium	gravel	20-60	
3	fine	gravel	2-20	
4	coarse	sand	0·6-2·0	
5	medium	sand	0·2-0·6	
6	fine	sand	0·06-0·2	
7	silt		0·002-0·06	
8	clay		< 0·002	
9	peat		NA	

WITH SOME

1	coarse gravel
2	medium gravel
3	fine gravel
4	coarse sand
5	medium sand
6	fine sand
7	silt
8	clay
9	peat

APPENDIX B: FIELD DATA

1991 PRECIPITATION RECORDS AND FAILURE DATES

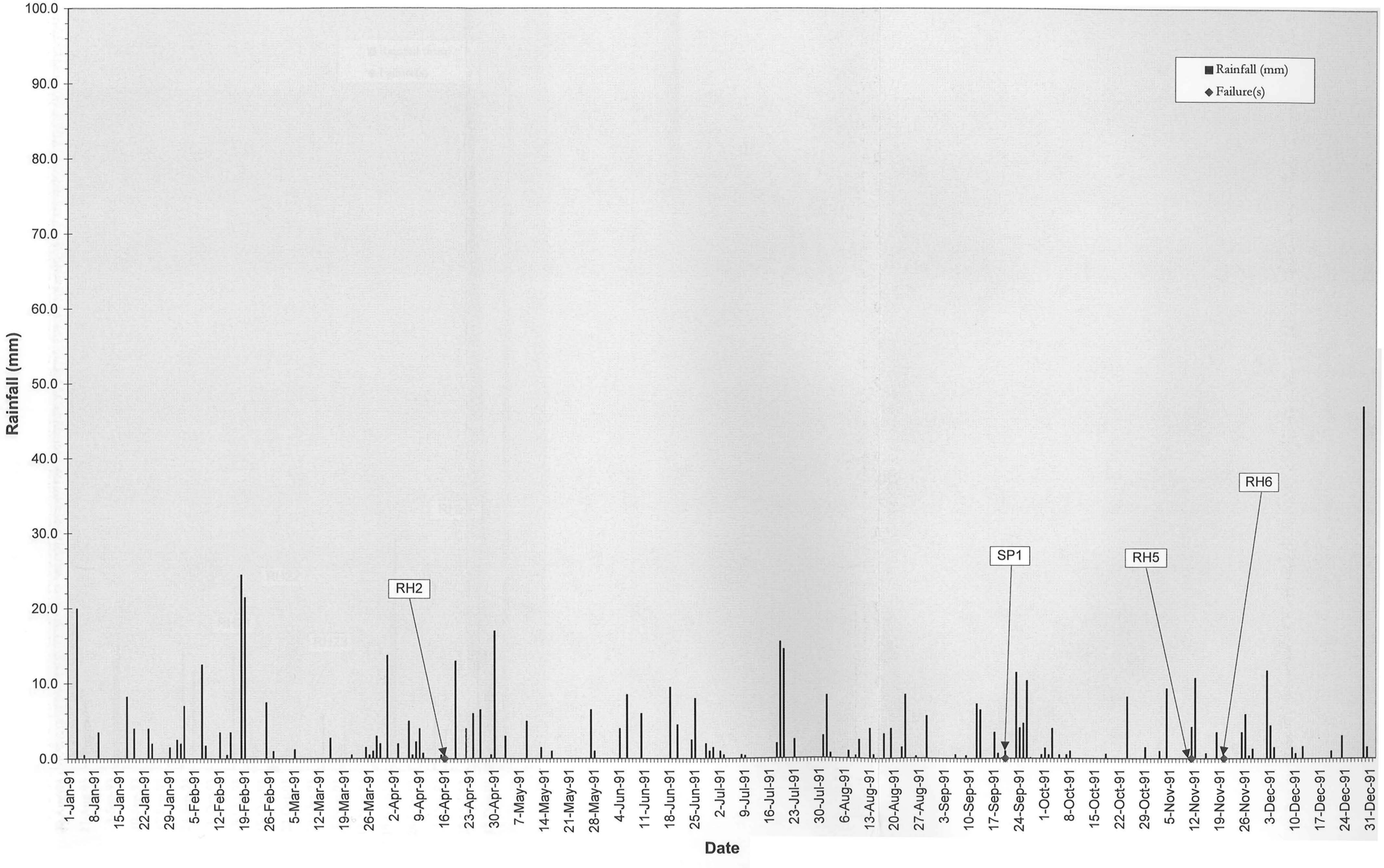

Figure B1-1: 1991 Precipitation Records

1993 PRECIPITATION RECORDS AND FAILURE DATES

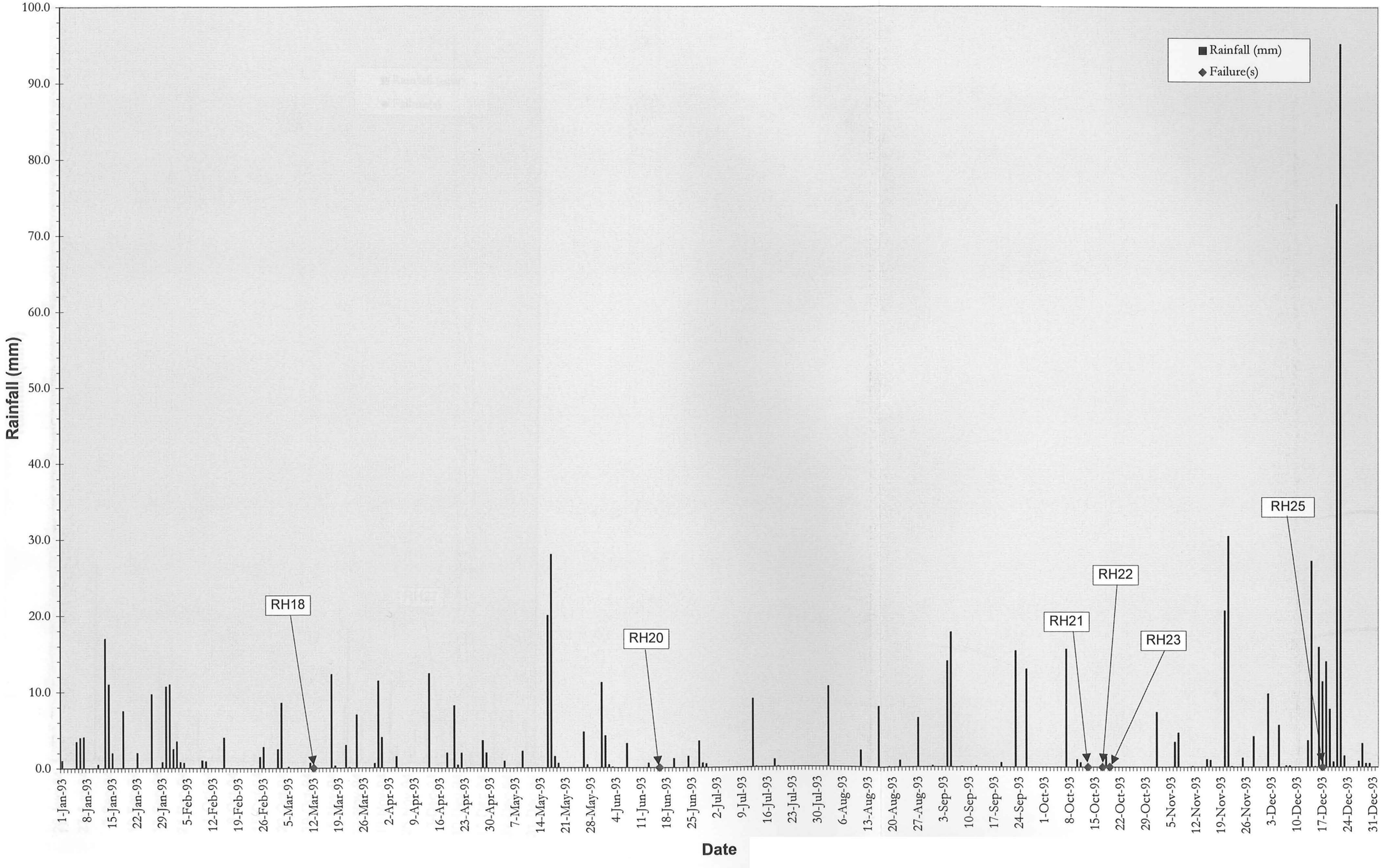

Figure B1-2: 1993 Precipitation Records

1994 PRECIPITATION RECORDS AND FAILURE DATES

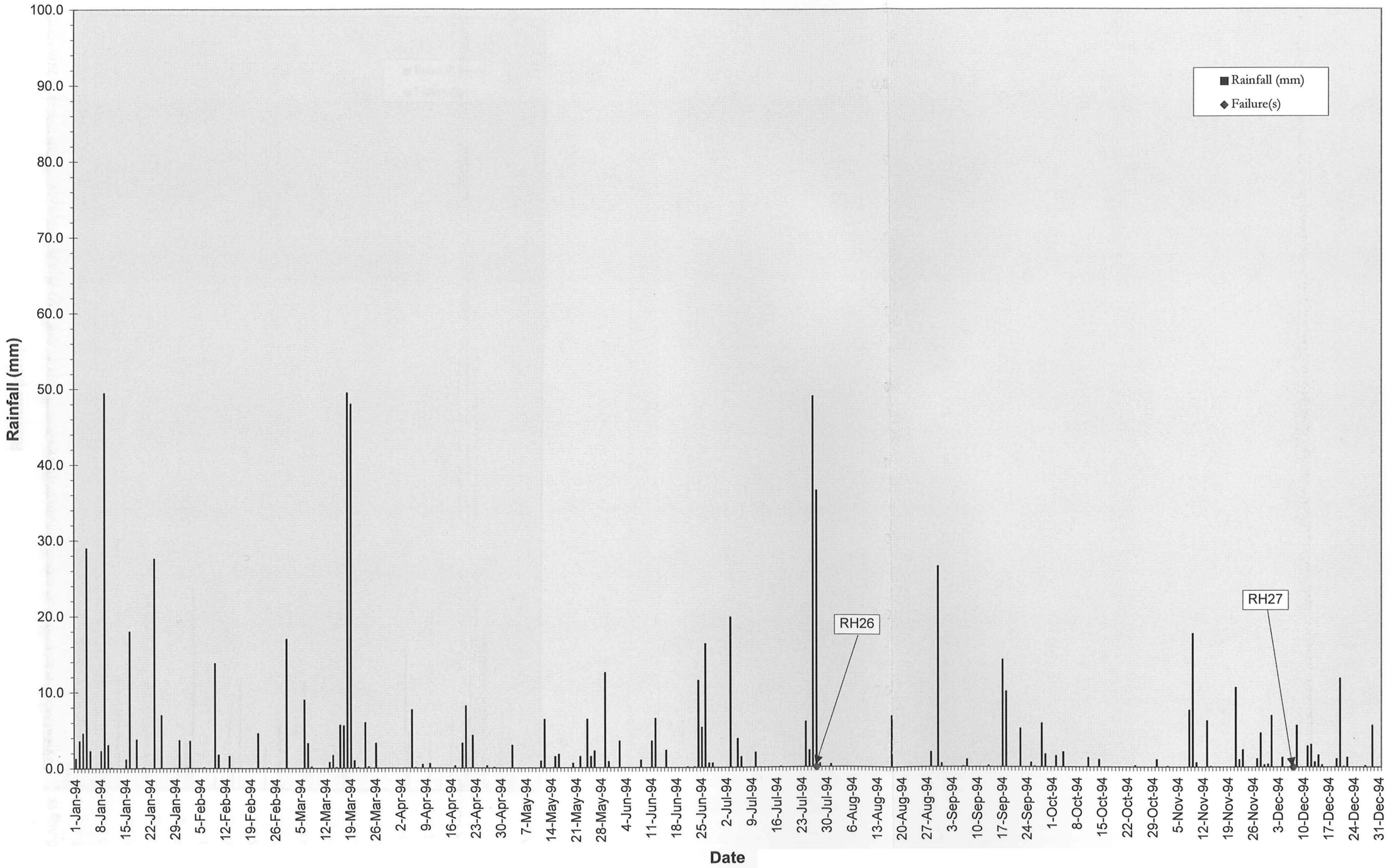

Figure B1-3: 1994 Precipitation Records

1995 PRECIPITATION RECORDS AND FAILURE DATES

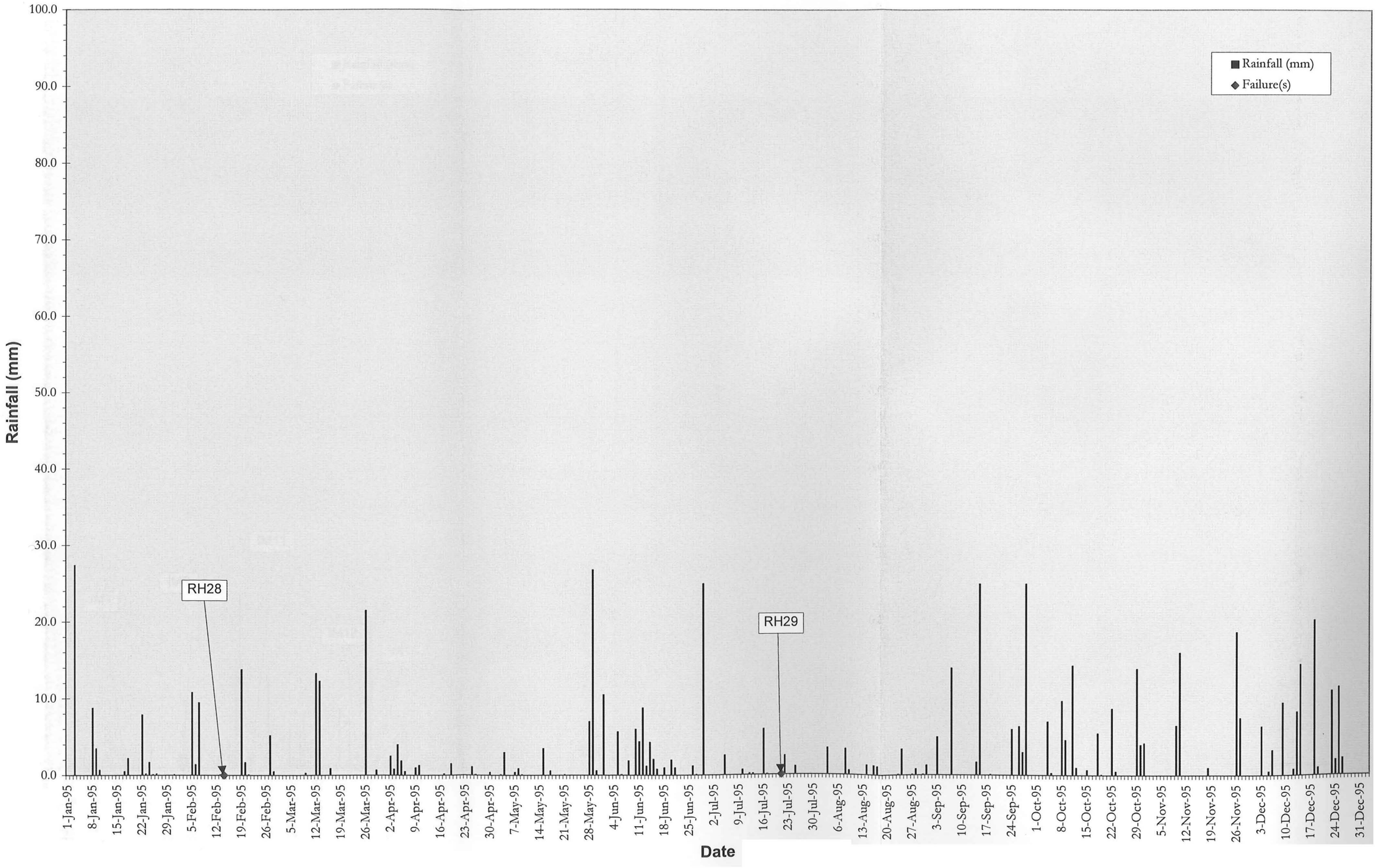

Figure B1-4: 1995 Precipitation Records

1996 PRECIPITATION RECORDS AND FAILURE DATES

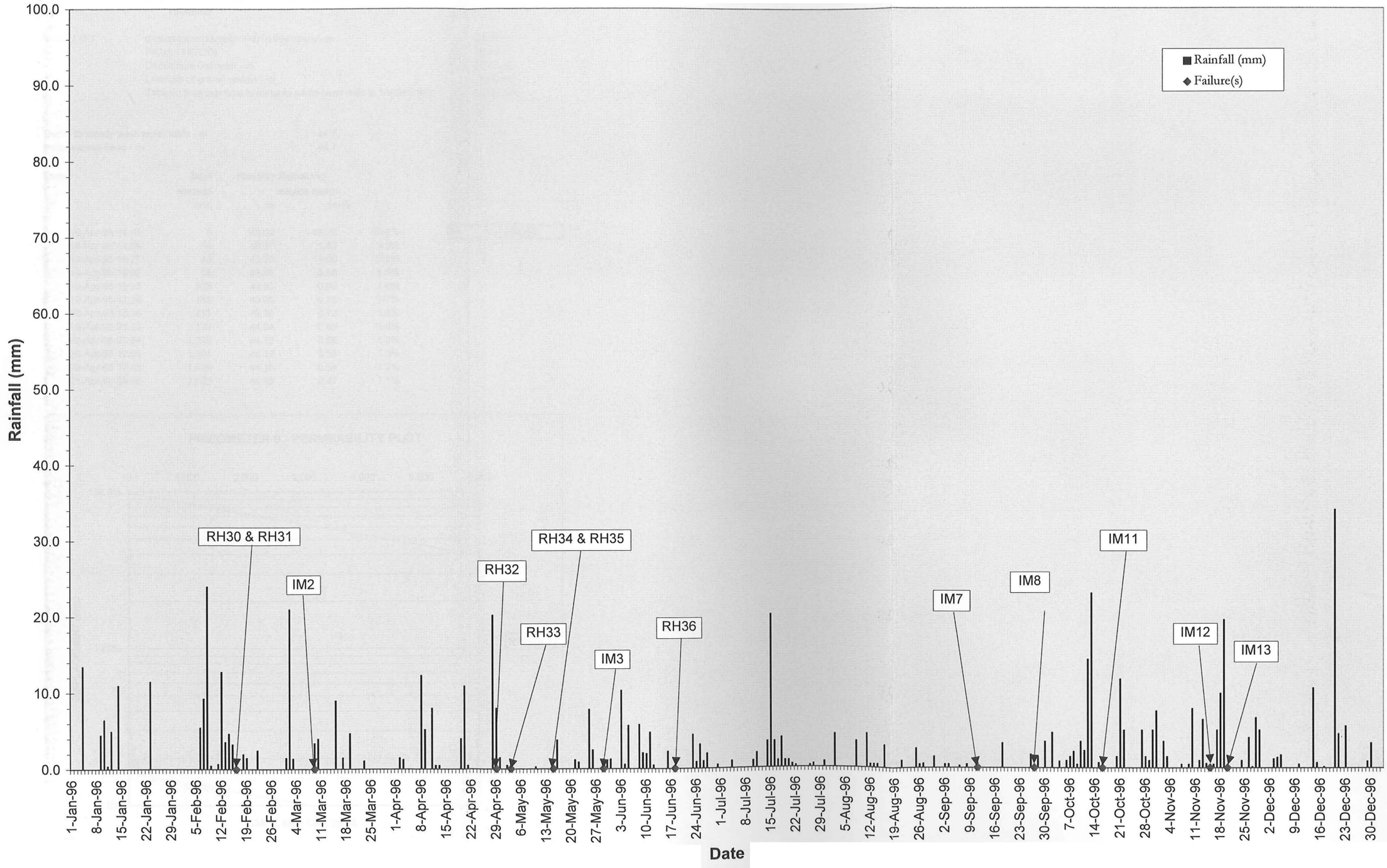

Figure B1-5: 1996 Precipitation Records

B2 Falling Head Permeability Test

SP9 - FALLING HEAD PERMEABILITY TEST

Piezometer SP9 15,322N 70,273E 456.9mRL
Date 19-Apr-95

$k=\pi d^2 / 4FT$

d=standpipe diameter (=D in this case) - m	0.127	m
F=2πL / ln(2L/D)	72.68	
D=drill hole diameter - m	0.127	m
L=length of gravel screen - m	83.0	m
T=basic time lag=time in minutes when head ratio is 1/e (ie 0.37)	6,200	min

Depth to steady state water table - m 44.7
Initial excess head - m 44.7

Date	Time elapsed min	Reading m	Remaining excess head m	%	
19-Apr-95 14:44	0	28.00	16.70	37.4%	k= 2.8E-08
19-Apr-95 14:58	14	43.37	1.33	3.0%	
19-Apr-95 15:27	43	43.70	1.00	2.2%	
19-Apr-95 16:02	78	43.85	0.85	1.9%	
19-Apr-95 16:33	109	43.90	0.80	1.8%	
19-Apr-95 17:29	165	43.95	0.75	1.7%	
19-Apr-95 18:15	211	43.98	0.72	1.6%	
19-Apr-95 21:50	426	44.04	0.66	1.5%	
20-Apr-95 07:34	1,010	44.12	0.58	1.3%	
20-Apr-95 12:25	1,301	44.12	0.58	1.3%	
20-Apr-95 17:43	1,619	44.16	0.54	1.2%	
21-Apr-95 09:00	2,536	44.23	0.47	1.1%	

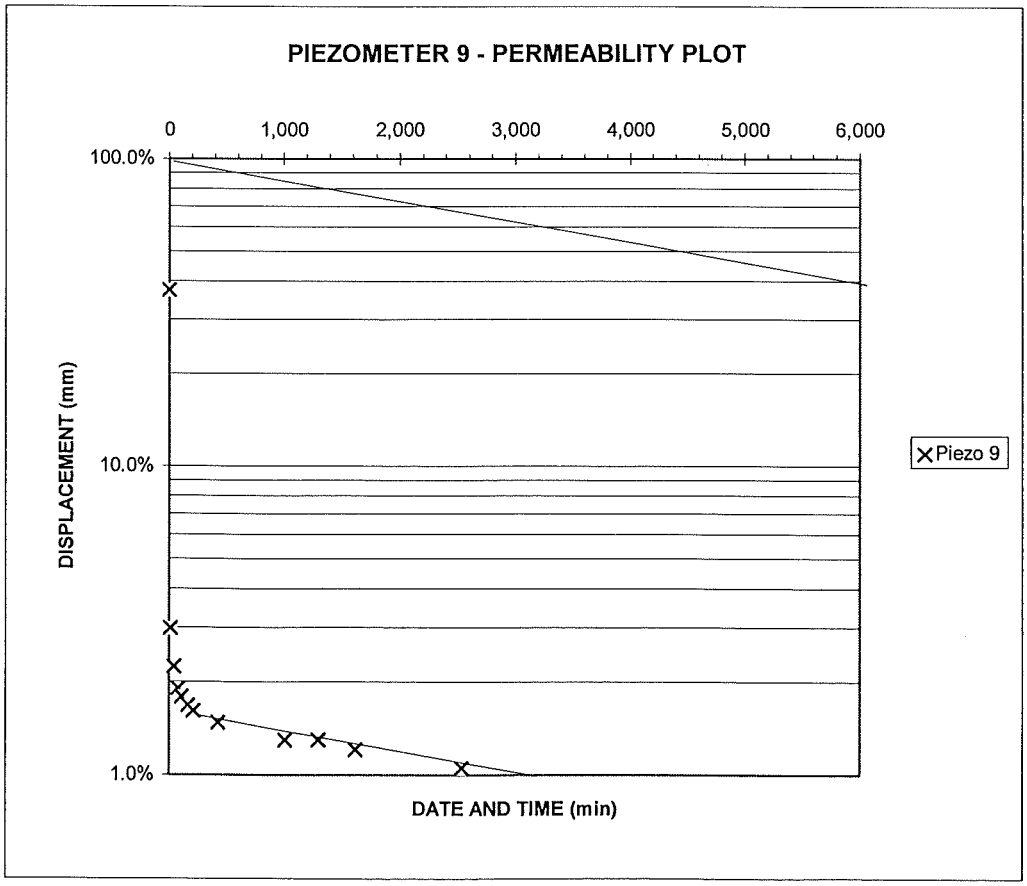

SP10 - FALLING HEAD PERMEABILITY TEST

Piezometer SP10 15,429N 70,184E 475.1mRL
Date 19-Apr-95

$k=\pi d^2 / 4FT$	d=standpipe diameter (=D in this case) - m	0.127 m
	F=2πL / ln(2L/D)	71.40
	D=drill hole diameter - m	0.127 m
	L=length of gravel screen - m	81.3 m
	T=basic time lag=time in minutes when head ratio is 1/e (ie 0.37)	2,100 min

Depth to steady state water table - m 33.25
Initial excess head - m 33.25

Date	Time elapsed min	Reading m	Remaining excess head m	%	
19-Apr-95 14:49	0	0.00	33.25	100.0%	k= 8.4E-08
19-Apr-95 14:52	3	17.00	16.25	48.9%	
19-Apr-95 14:55	6	18.65	14.60	43.9%	
19-Apr-95 15:24	35	19.42	13.83	41.6%	
19-Apr-95 16:00	71	20.01	13.24	39.8%	
19-Apr-95 16:30	101	20.43	12.82	38.6%	
19-Apr-95 17:32	163	21.12	12.13	36.5%	
19-Apr-95 18:12	203	21.60	11.65	35.0%	
19-Apr-95 21:46	417	23.48	9.77	29.4%	
20-Apr-95 07:31	1,002	26.45	6.80	20.5%	
20-Apr-95 12:20	1,291	27.19	6.06	18.2%	
20-Apr-95 17:40	1,611	27.77	5.48	16.5%	
21-Apr-95 09:00	2,531	28.51	4.74	14.3%	

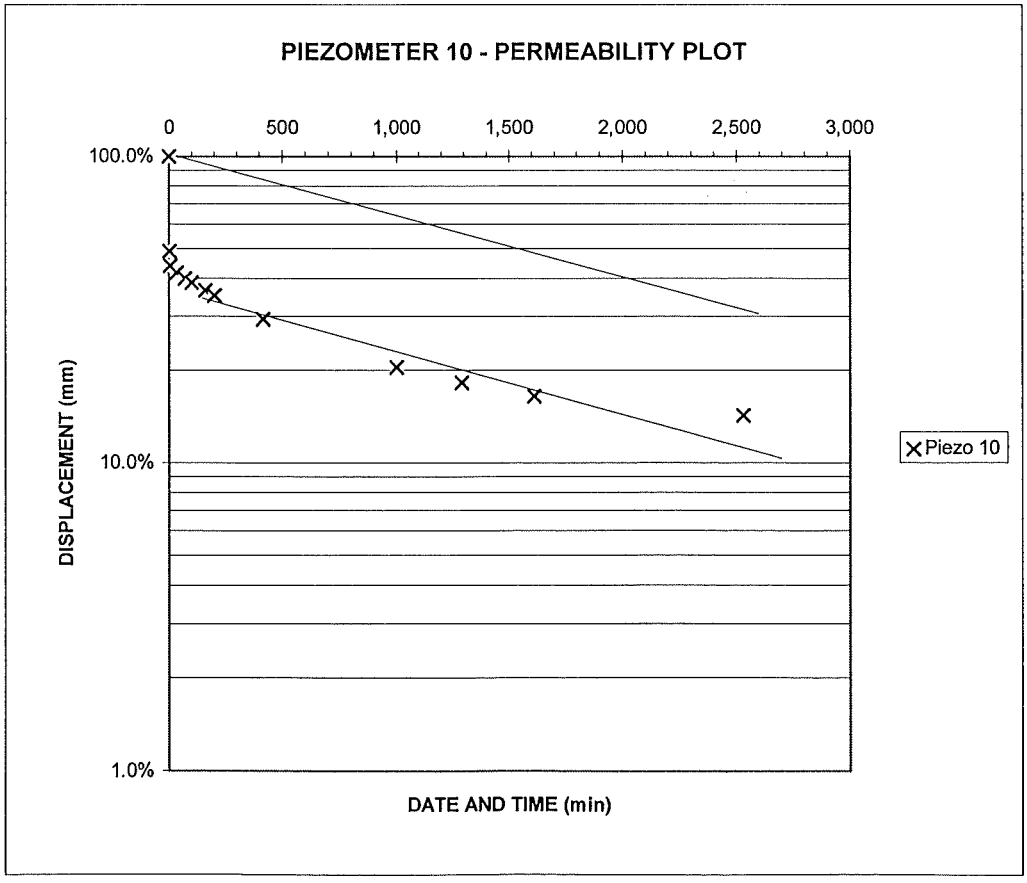

SP11 - FALLING HEAD PERMEABILITY TEST

Piezometer SP11 15,145N 69,689E 435.2mRL
Date 19-Apr-95

$k=\pi d^2 / 4FT$

d=standpipe diameter (=D in this case) - m	0.127	m
$F=2\pi L / \ln(2L/D)$	56.59	
D=drill hole diameter - m	0.127	m
L=length of gravel screen - m	62.0	m
T=basic time lag=time in minutes when head ratio is 1/e (ie 0.37)	400	min

Depth to steady state water table - m 16.34
Initial excess head - m 16.34

Date	Time elapsed min	Reading m	m	Remaining excess head %	
19-Apr-95 12:09	0	0.00	16.34	100.0%	k= 5.6E-07
19-Apr-95 12:14	5	3.12	13.22	80.9%	
19-Apr-95 12:19	10	3.51	12.83	78.5%	
19-Apr-95 12:24	15	3.81	12.53	76.7%	
19-Apr-95 12:44	35	4.93	11.41	69.8%	
19-Apr-95 12:59	50	5.68	10.66	65.2%	
19-Apr-95 13:24	75	6.73	9.61	58.8%	
19-Apr-95 13:55	106	7.88	8.46	51.8%	
19-Apr-95 14:12	123	8.45	7.89	48.3%	
19-Apr-95 16:25	256	11.57	4.77	29.2%	
19-Apr-95 17:36	327	12.63	3.71	22.7%	
19-Apr-95 18:43	394	13.37	2.97	18.2%	
19-Apr-95 21:39	570	14.68	1.66	10.2%	
20-Apr-95 07:25	1,156	15.92	0.42	2.6%	
20-Apr-95 12:13	1,444	16.02	0.32	2.0%	
20-Apr-95 17:55	1,786	16.29	0.05	0.3%	
21-Apr-95 08:50	2,681	16.33	0.01	0.1%	

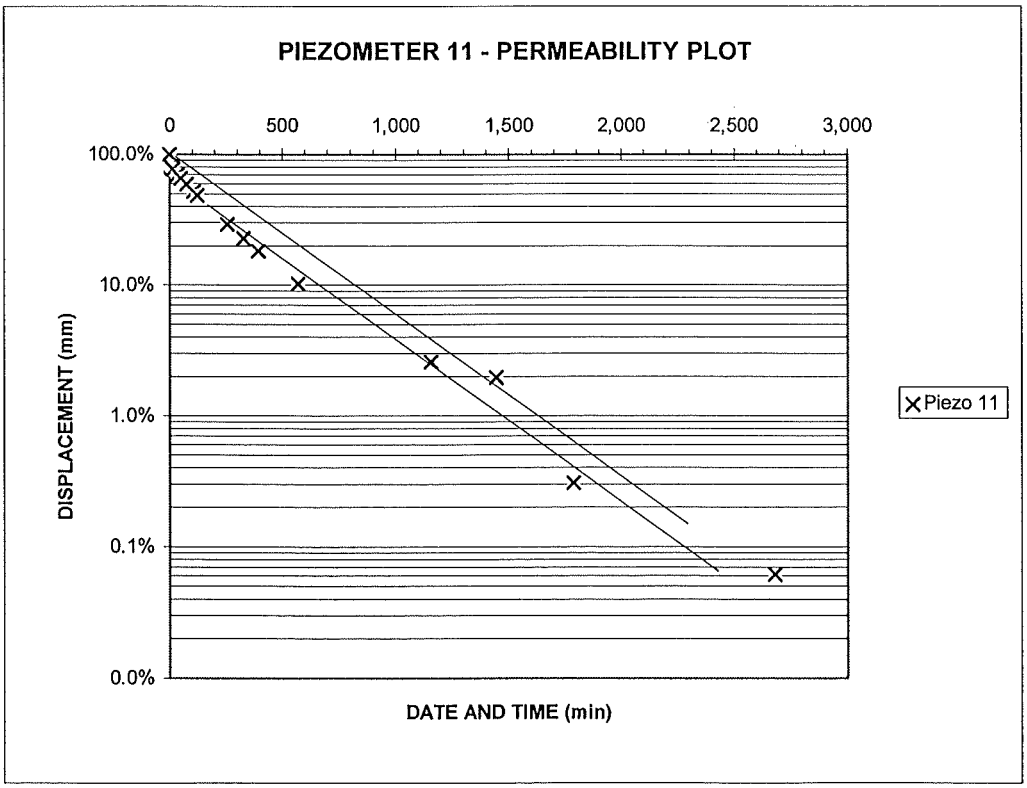

SP12 - FALLING HEAD PERMEABILITY TEST

Piezometer SP12 15,027N 70,185E 440.5mRL
Date 19-Apr-95

$k=\pi d^2 / 4FT$

d=standpipe diameter (=D in this case) - m	0.127	m
F=2πL / ln(2L/D)	72.68	
D=drill hole diameter - m	0.127	m
L=length of gravel screen - m	83.0	m
T=basic time lag=time in minutes when head ratio is 1/e (ie 0.37)	1,700	min

Depth to steady state water table - m 14.17
Initial excess head - m 14.17

Date	Time elapsed min	Reading m	m	Remaining excess head %	
19-Apr-95 15:34	0	0.00	14.17	100.0%	k= 1.0E-07
19-Apr-95 15:39	5	10.07	4.10	28.9%	
19-Apr-95 15:44	10	11.03	3.14	22.2%	
19-Apr-95 15:49	15	11.61	2.56	18.1%	
19-Apr-95 15:54	20	11.96	2.21	15.6%	
19-Apr-95 16:08	34	12.50	1.67	11.8%	
19-Apr-95 16:15	41	12.65	1.52	10.7%	
19-Apr-95 16:37	63	12.88	1.29	9.1%	
19-Apr-95 17:24	110	13.02	1.15	8.1%	
19-Apr-95 18:20	166	13.12	1.05	7.4%	
19-Apr-95 21:56	382	13.31	0.86	6.1%	
20-Apr-95 07:38	964	13.53	0.64	4.5%	
20-Apr-95 12:32	1,258	13.6	0.57	4.0%	
20-Apr-95 17:48	1,574	13.72	0.45	3.2%	
21-Apr-95 09:06	2,492	13.99	0.18	1.3%	

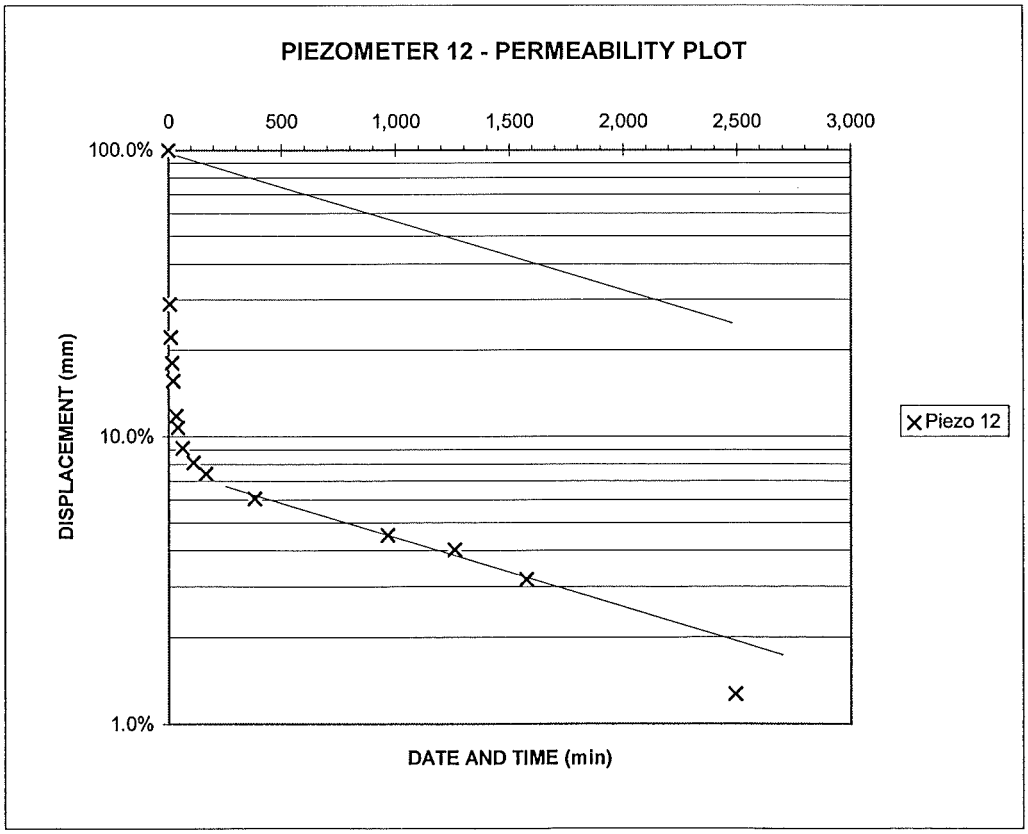

B3 Piezometric Records

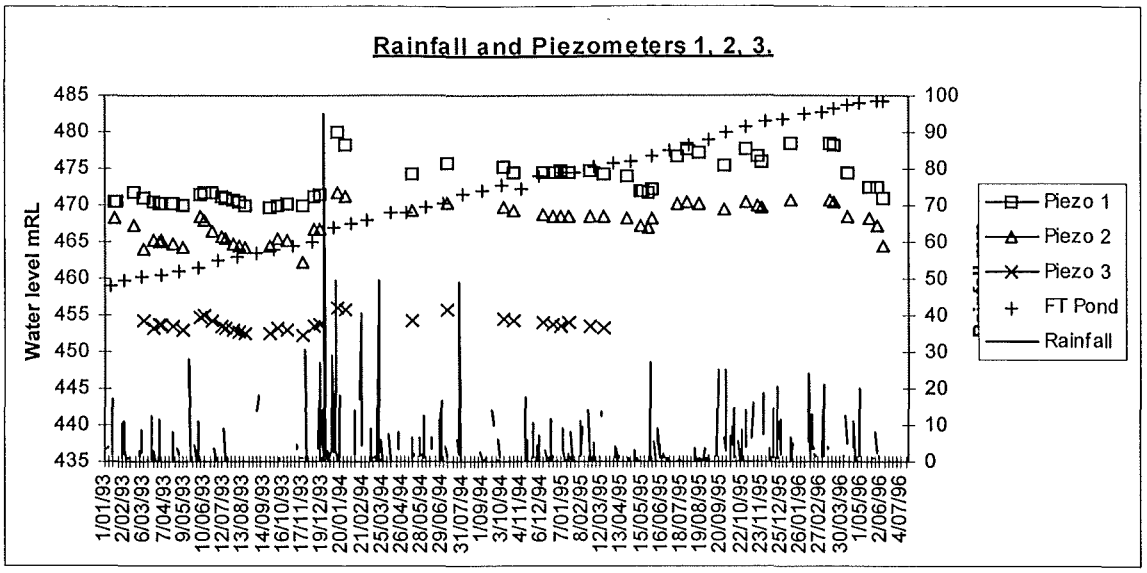

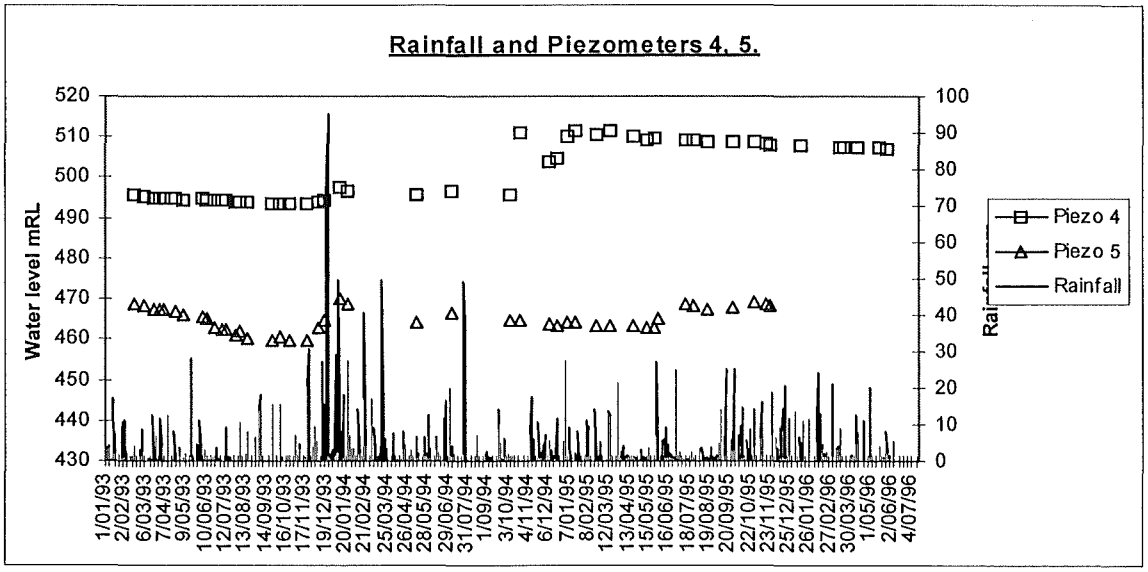

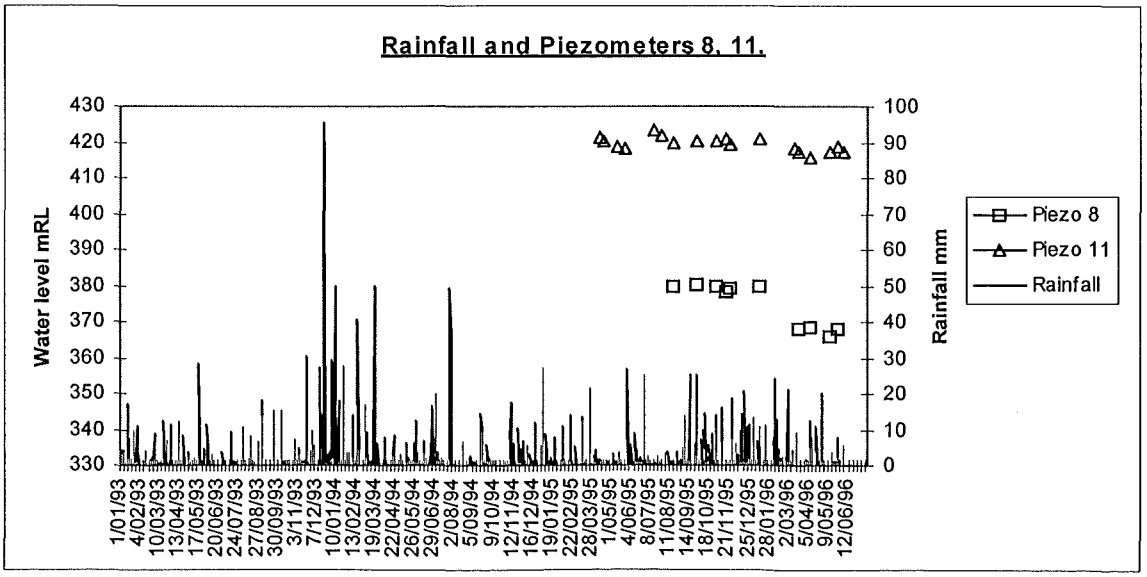

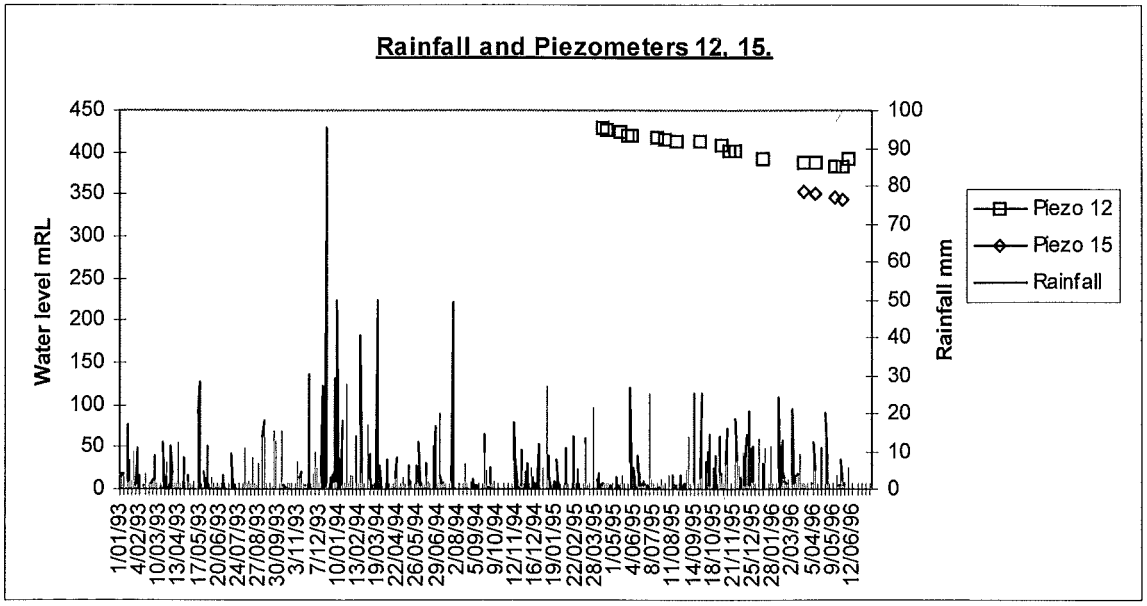
Rainfall and Piezometers 12, 15.
Water level mRL
Rainfall mm
Piezo 12
Piezo 15
Rainfall

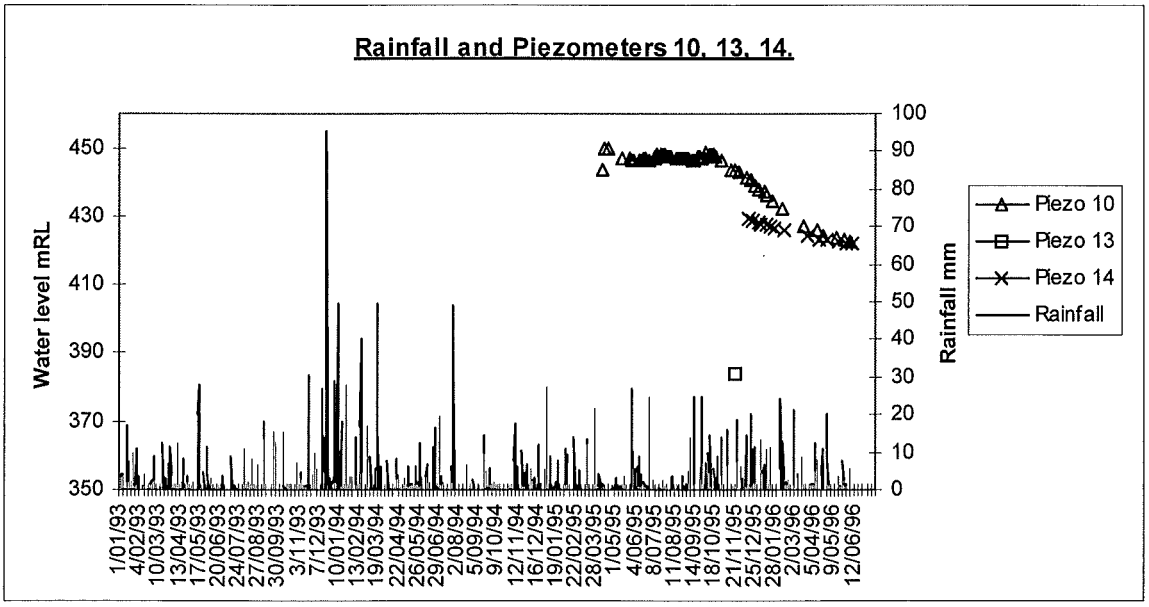
Rainfall and Piezometers 10, 13, 14.
Water level mRL
Rainfall mm
Piezo 10
Piezo 13
Piezo 14
Rainfall

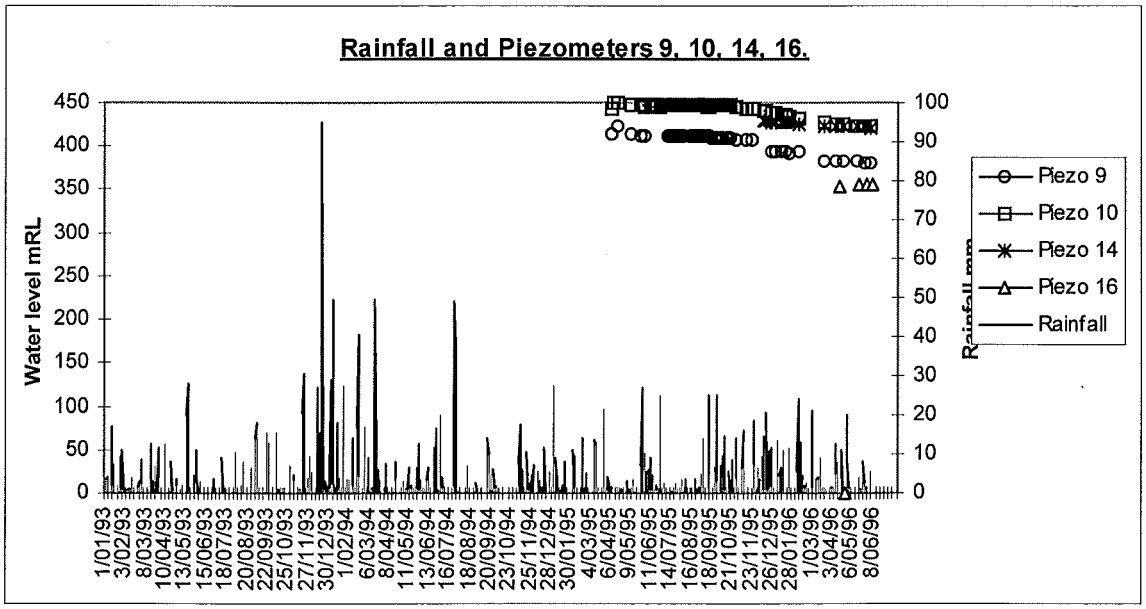
Rainfall and Piezometers 9, 10, 14, 16.
Water level mRL
Piezo 9
Piezo 10
Piezo 14
Piezo 16
Rainfall

B4 RH28 Structural Mapping Data

FAILURE RH28
MAPPING DATA 1996
5 Traverses
1;Planar;45;180;10m high E-W trending berms
2;Planar;45;215;10m high NW-SE trending berms
3;Planar;45;250;10m high NNW-SSE trending berms
4;Planar;70;180;15m high E-W trending berms
5;Planar;56;220;15m high NW-SE trending berms
Dip/DipDirection
0 (All readings recorded relative to Macraes Mine Grid)
No Quantity
11 Extra columns

Number	Dip	DipDirection	Traverse	Easting	Northing	R.L.	Type	Length(m)	Spacing	Left-Termn	Right-Termn	Roughness	Apeture(cm)	Groundwater	Comments
1(a)	72	205	1	_____	_____	____	Jt	0.5	0.3	I	I	VIII	0.0	0	Jointing in oxidised material
1(b)	64	095	1	_____	_____	____	Jt	0.5	1.0	I	I	VIII	0.0	0	" " " " " " "
1(c)	68	125	1	_____	_____	____	Jt	2.0	1.0	I	I	VIII	0.0	0	" " " " " " "
1(d)	72	050	1	_____	_____	____	Jt	0.5	0.5	I	I	VIII	0.0	0	" " " " " " "
2	55	160	1	_____	_____	____	Ft	5.0	-	O	O	V	-	-	Large exposed fault plane in berm (aperture covered by material from face)
4(a)	86	340	1	_____	_____	____	Jt	1.5	0.5	A	A	VIII	0.0	Dry	Jointing (Small localised toppling failure occuring where opening along this joint orien
4(b)	50	265	1	_____	_____	____	Jt	2.0	0.3	I	O	VIII	0.0	Dry	Jointing
4(c)	76	155	1	_____	_____	____	Jt	1.0	0.3	A	A	VIII	0.0	Dry	Jointing
5	74	078	2	_____	_____	____	Ft	6.0	-	O	O	II	5.0	Dry	Fault formed along jointing
6(a)	78	180	2	_____	_____	____	Jt	6.0	-	O	A	VIII	-	-	Forms north-western defect to small wedge failure
6(b)	50	255	2	_____	_____	____	Jt	6.0	-	O	O	VIII	-	-	Forms south-eastern defect to small wedge failure
7(a)	55	255	2	_____	_____	____	Jt	5.0	1	O	O	VIII	0.0	Dry	Jointing(Dominant Set at this location)
7(b)	68	185	2	_____	_____	____	Jt	1.5	1	A	A	VIII	0.0	Dry	Jointing
8	75	195	2	_____	_____	____	Jt	10.0	-	O	O	V	-	-	Bench has dropped along this joint by about 0.75m
9	85	000	2	_____	_____	____	Jt	20.0	1	O	O	II	40.0	Dry	Cavernous opening up to 2m deep (crack pins installed)
10	85	356	2	_____	_____	____	Jt	10.0	-	O	O	V	30.0	Dry	Cavernous opening along jointing
12(a)	38	260	3	_____	_____	____	Jt	3.0	0.5	O	A	VIII	-	Dry	Jointing
12(b)	68	184	3	_____	_____	____	Jt	3.0	1.0	O	O	VIII	-	Dry	Jointing
13	06	275	3	_____	_____	____	Fo	-	-	-	-	-	-	-	Schistosity undulates and varies at this location.
14	62	204	1	_____	_____	____	Ft	200.0	-	I	O	IV	-	-	Exposure of back fault
18	68	120	1	_____	_____	____	Jt	5.0	-	O	O	V	15.0	Dry	Opening along joint
22(a)	58	091	1	_____	_____	____	Jt	3.0	2	O	O	V	0.2	Dry	Jointing
22(b)	45	185	1	_____	_____	____	Jt	2.0	1	O	O	V	1.0	Dry	Jointing
22(c)	80	031	1	_____	_____	____	Jt	0.5	0.5	A	A	VIII	1.0	Dry	Joint set being released from face by toppling mechanism
23	64	182	1	_____	_____	____	Ft	8.0	-	O	O	IV	-	-	Exposed fault plane in face
24(a)	65	100	1	_____	_____	____	Jt	6.0	-	O	A	V	-	-	Joint forming western defect to wedge failure
24(b)	62	201	1	_____	_____	____	Jt	8.0	-	O	O	V	-	-	Joint forming eastern defect to wedge failure
25	78	346	2	_____	_____	____	Jt	7.0	-	O	O	V	-	-	Toppling failure occuring along this joint orientation
26(a)	75	200	1	_____	_____	____	Jt	3.0	2	O	O	VII	1.0	Dry	Jointing
26(b)	80	120	1	_____	_____	____	Jt	3.0	3	O	O	VII	-	-	Jointing
26(c)	26	250	1	_____	_____	____	Fo	-	-	-	-	-	-	-	Schistosity
27(a)	85	212	1	_____	_____	____	Jt	0.3	0.5	A	A	VIII	-	-	Jointing
27(b)	85	139	1	_____	_____	____	Jt	2.0	0.5	A	I	VIII	-	-	Jointing
28	60	072	1	_____	_____	____	Ft	10.0	-	O	O				
30	35	267	1	_____	_____	____	Ft	15.0	-	O	O	VII	10.0	Dry	Normal movement on fault
31	65	108	1	_____	_____	____	Jt	6.0	-	O	O	I	-	-	Western defect of wedge failure
32	63	189	1	_____	_____	____	Jt	30.0	-	O	O	IV	-	-	Eastern defect to wedge failure
33(a)	44	308	3	_____	_____	____	Jt	3.0	1	O	O	V	-	-	Joint exposed face
33(b)	83	211	3	_____	_____	____	Jt	2.0	3	O	O	V	-	-	Joint exposed face
34(a)	42	292	3	_____	_____	____	Jt	3.0	1	O	O	IV	-	-	Joint exposed face
34(b)	58	228	3	_____	_____	____	Jt	2.0	3	O	O	II	-	-	Joint exposed face
35(a)	64	288	3	_____	_____	____	Jt	2.0	1	O	O	I	-	-	Joint exposed face
35(b)	87	200	3	_____	_____	____	Jt	2.0	4	O	O	V	-	-	Joint exposed face
36	58	200	2	_____	_____	____	Ft	30.0	-	O	O	V	-	-	Forms exposed face in berm
37(a)	45	178	2	_____	_____	____	Jt	10.0	2	O	O	IV	-	-	Controlling defect to small plane failure
37(b)	74	278	2	_____	_____	____	Jt	1.0	0.5	A	A	VIII	1.0	Dry	Jointing
37(c)	45	065	2	_____	_____	____	Jt	5.0	1.5	O	I	VIII	-	-	Jointing
38(a)	38	302	2	_____	_____	____	Ft	20.0	-	O	O	IV	10.0	Dry	Fault showing reverse movement
38(b)	58	247	2	_____	_____	____	Ft	10.0	3.0	O	A	IV	5.0	Dry	
38(c)	53	240	2	_____	_____	____	Ft	10.0	3	O	A	IV	-	Dry	
39(a)	76	218	2	_____	_____	____	Jt	1.0	0.3	I	I	II	-	-	Jointing
39(b)	74	134	2	_____	_____	____	Jt	1.0	0.5	-	-	IV	-	-	Jointing
40	34	333	2	_____	_____	____	Ft	20.0	-	O	O	VII	-	-	Normal movement on fault
41(a)	56	308	2	_____	_____	____	Ft	15.0	-	O	O	I	-	-	
41(b)	44	246	2	_____	_____	____	Ft	13+	-	O	O	VII	5.0	0	
42(a)	64	028	2	_____	_____	____	Jt	2.0	1	A	A	VII	-	-	Jointing
42(b)	78	268	2	_____	_____	____	Jt	3.0	2	A	O	II	-	-	Jointing
43(a)	85	216	2	_____	_____	____	Jt	4.0	1	O	O	IV	-	-	
43(b)	87	091	2	_____	_____	____	Jt	1.0	0.5	A	O	IV	-	-	
43(c)	72	115	2	_____	_____	____	Jt	1.0	1.5	O	O	VII	-	-	

44(a)	75	186	2			Jt	2.0	2	O	A	VII	0.0	0	
44(b)	44	285	2			Jt	1.0	0.5	A	O	VII	0.3	0	
44(c)	84	173	2			Jt	2.0	2	O	O	IV	0.2	0	
45(a)	78	080	1			Jt	0.5	1	A	O	II	0.2	0	
45(b)	78	194	1			Jt	1.0	2	O	O	V	0.2	0	
46(a)	84	072	1			Jt	0.3	0.75	A	I	VII	0.0	0	
46(b)	55	307	1			Jt	0.3	1	A	I	I	0.3	0	
47	58	208	1			Jt	10.0	1	O	I	IV	-	-	Eastern defect to wedge failure
48	72	237	1			Jt	2.0	1	A	I	VIII	0.0	0	
49(a)	68	243	1			Jt	-	-	-	-	I	-	-	
49(b)	58	180	1			Jt	-	-	-	-	IV	-	-	
49(c)	58	117	1			Jt	-	-	-	-	I	-	-	
50(a)	88	037	1			Jt	1.0	0.5	I	I	VII	-	-	
50(b)	78	138	1			Jt	-	-	-	-	II	-	-	
51	64	194	1			Ft	-	-	-	-	-	-	-	1.5m high scarp
52	73	188	3			Ft	-	-	-	-	IV	-	-	Back Fault
61(a)	84	003	2			Jt	0.5	0.5	A	I	II	0.4	0	
61(b)	84	236	2			Jt	1.0	0.5	A	A	II	0.8	0	
61(c)	67	254	2			Jt	0.5	1	A	A	VIII	0.2	0	
62	39	271	2			Ft	12.0	-	O	O	IV	25.0	0	Exposed fault plane in face with failed material below (sample taken)
*62														
63(a)	90	196	3			Jt	0.5	1	I	O	VIII	0.5	0	
63(b)	46	285	3			Jt	4.0	3	O	O	IV	0.3	0	
64	63	188	2			Jt	-	-	-	-	II	5.0		
71(a)	56	258	1			Jt	4.0	1	O	A	IV	1.0	0	
71(b)	83	146	1			Jt	2.0	3	A	O	IV	1.0	0	
72(a)	65	262	1			Jt	2.0	3	O	I	II	0.2	0	
72(b)	44	329	1			Jt	4.0	2	I	O	V	0.5	0	
72(c)	90	213	1			Jt	1.5	0.5	A	I	II	-	-	
73(a)	73	218	1			Ft	2.0	1.5	I	I	VII	0.5	0	
73(b)	16	111	1			Fo	-	-	-	-	-	-	-	
75	62	201	1			Jt	10.0	2	O	O	IV	-	-	
76	58	100	1			Ft	See Map	-	O	O	VII	5.0	0	
78	11	226	1			Fo	-	-	-	-	-	-	-	
80	49	102	1			Ft	See Map	-	O	O	VI	15.0	-	
81	73	167	1			Ft	See Map	-	O	O	IV	-	Seepage	
82	50	060	1			Ft	See Map	-	O	O	VII	30.0	-	
83	46	100	1			Fo	-	-	-	-	-	-	-	
85	90	200	4			Jt	30.0	3	O	O	IV	-	-	
86	90	200	4			Jt	20.0	3	O	O	IV	20.0	0	
87	42	092	4			Ft	See Map	-	O	O	VI	-	-	
88	45	095	5			Ft	See Map	-	O	O	IX	130.0		
89	70	200	4			Jt	See Map	-	O	O	IV	-	-	
91	14	240	4			Ft	-	-	-	-	-	-	-	
92	46	107	5			Fo	-	-	-	-	-	-	-	
93(a)	73	194	5			Jt	5.0	0.75	A	I	IV	0.0	0	
93(b)	67	176	5			Jt	1.5	0.3	I	I	VII	0.2	0	
93(c)	90	230	5			Jt	2.0	2	0	I	IV	-	-	
93(d)	14	094	5			Fo	-	-	-	-	-	-	-	
94(a)	24	091	5			Fo	-	-	-	-	-	-	-	
94(b)	58	175	5			Jt	3.0	2	I	O	IV	0.5	0	
94(c)	41	250	5			Jt	1.5	1.5	I	I	I	0.0	0	
95	41	258	4			Ft	See Map	-	-	-	VI	5.0	-	
96	43	068	4			Ft	-	-	-	-	VI	3.0	0	
97	16	242	4			Fo	-	-	-	-	-	-	-	
100	39	094	4			Ft	See Map	-	O	A	V	5.0	0	
101(a)	87	066	2			Jt	2.0	0.5	I	I	II	0.5	0	
101(b)	80	038	2			Jt	2.0	1	I	I	VII	0.0	0	
101(c)	44	310	2			Jt	4.0	5	I	I	VII	0.0	0	
101(d)	09	286	2			Fo	-	-	-	-	-	-	-	
102(a)	38	080	4			Jt	5.0	1.5	O	O	V	1.0	0	
102(b)	82	196	4			Jt	10.0	3	A	O	IV	30.0	0	
103(a)	87	161	4			Jt	3.0	2	I	A	II	0.0	0	
103(b)	37	296	4			Jt	2.0	0.5	A	I	II	0.0	0	
103(c)	57	087	4			Jt	1.0	1	A	I	VII	0.2	0	
103(d)	08	224	4			Fo	-	-	-	-	-	-	-	
104	42	083	4			Ft	See Map	-	O	O	VI	10.0	Seepage	
105	21	122	4			Ft	See Map	-	O	O	VI	30.0		
106(a)	33	298	4			Ft	See Map	-	O	O	VII	-	-	
106(b)	50	267	4			Ft	See Map	-	O	A	VII	-	-	
107(a)	46	256	4			Jt	1.0	1	I	I	-	0.2	0	
107(b)	86	189	5			Jt	1.0	0.3	I	I	VII	0.0	0	
108(a)	72	072	5			Ft	See Map	-	O	O	V	30.0	Seepage	
108(b)	50	089	5			Ft	-	-	-	-	-	-	-	
109	82	220	5			Jt	15.0	-	A	O	II	-	-	
110(a)	44	251	5			Jt	1.5	0.5	O	I	I	0.1	0	
110(b)	64	166	5			Jt	2.0	1	O	O	IV	-	-	
110(c)	25	110	5			Fo	-	-	-	-	-	-	-	
111	49	079	4			Ft	See Map	-	-	-	-	10.0	-	
112	70	050	4			Ft	See Map	-	-	-	-	-	-	
113	22	318	4			Ft	See Map	-	O	O	V	20.0	Lots of Seepage	

114(a)	38	310	4				Ft	See Map	-	O	O	VIII	-	Seepage	
114(b)	48	308	4				Ft	See Map	-	O	O	VIII	25.0	Seepage	
115(a)	70	098	4				Jt								
115(b)	44	120	4				Jt								
116(a)	22	250	4				Fo	-	-	-	-	-	-	-	
116(b)	68	110	4				Jt	2.0	0.5	I	I	IV	-	-	
116(c)	40	305	4				Jt	0.5	0.5	A	A	VII	0.0	0	
117(b)	36	292	5				Jt	5.0	1.5	I	I	V	0.0	0	
117(c)	75	032	5				Jt	1.0	2	I	I	VII	0.0	0	
118	48	074	5				Ft	-	-	O	O	-	0.5	Moist	
119	17	100	5				Fo	-	-	-	-	-	-	-	
120	11	335	4				Ft								
129	39	305	4				Ft	See Map	-	O	O	VII	10.0	Dripping Seepage	
130	35	120	4				Ft	See Map	-	-	-	-	-	-	
131	14	315	4				Ft	See Map	-	O	O	IX	-	-	10-20cm overhang
132(a)	78	130	4				Jt	3.0	3	I	I	IV	-	-	
132(b)	85	024	4				Jt	5.0	3	O	O	I	-	-	
136(a)	88	189	5				Jt	2.0	2	A	O	II	-	-	
136(b)	42	275	5				Jt	2.0	2	O	I	-	-	-	
138	26	300	4				Ft	See Map	-	O	O	IX	20.0	0	Low Angle Fault
139	31	315	5				Ft	See Map	-	O	O	IX	10.0	0	Low Angle Fault
141	52	302	4				Ft	See Map	-	O	A	V	2.0	Seepage	Splay off Fault 140
143	42	275	4				Ft	See Map	-	O	A	VIII	2.0	-	
145	67	062	4				Ft	See Map	-	O	O	VIII	3.0	0	Offsets faults 144, & 146
147	40	286	4				Ft	See Map	-	O	A	IV	15.0	-	
148	45	120	4				Ft	-	-	O	O	-	-	-	
149	48	285	4				Ft	See Map	-	O	O	VI	30.0	0	Reverse Fault
150	11	320	4				Ft	See Map	-	O	O	V	2.0	0	Foliation shear
151	47	098	4				Ft	See Map	-	O	O	VI	10.0	0	
152(a)	11	250	4				Fo	-	-	-	-	-	-	-	
152(b)	58	105	4				Jt	3.0	1.5	A	O	IV	0.2	0	
152(c)	52	290	4				Jt	3.0	1.5	O	A	IV	0.2	0	
152(d)	55	170	4				Jt	4.0	3	O	O	IV	-	-	
153(a)	10	120	4				Fo	-	-	-	-	-	-	-	
153(b)	90	231	4				Jt	10.0	4	O	O	IV	2.0	0	
154	88	190	4				Jt	See Map	-	O	O	IV	40.0	-	
156	88	224	4				Jt	-	-	-	-	IV	-	-	
157	90	182	4				Jt	-	-	-	-	IV	-	-	
159(a)	22	110	4				Fo	-	-	-	-	-	-	-	
159(b)	58	193	4				Jt	4.0	3	O	A	VII	-	-	
160(a)	88	164	4				Jt	2.0	2	O	O	VIII	-	-	
160(b)	75	090	4				Jt	2.0	1.5	I	O	VIII	-	-	
161(a)	24	110	2				Fo	-	-	-	-	-	-	-	
161(b)	50	251	2				Jt	3.0	0.5	O	I	VIII	-	-	
161(c)	89	189	2				Jt	2.0	1	-	-	II	0.0	0	
162	48	265	4				Ft	See Map	-	A	O	VII	2.5	0	
163	48	100	4				Ft	See Map	-	O	O	V	125.0	0	
164	41	169	4				Ft	See Map	-	O	O	VII	5.0	0	
165(a)	13	125	4				Fo	-	-	-	-	-	-	-	
165(b)	86	031	4				Jt	0.5	1	A	A	II	-	-	
171(a)	25	095	4				Fo	-	-	-	-	-	-	-	
171(b)	84	190	4				Jt	2.0	1	I	I	IV	-	-	
176(a)	21	125	4				Fo	-	-	-	-	-	-	-	
176(b)	44	280	4				Jt	5.0	1	O	I	IV	-	-	
176(c)	32	200	4				Jt	3.0	1.5	I	O	V	-	-	
177(a)	52	079	2				Ft	See Map	-	-	-	-	-	-	
177(b)	54	091	2				Ft	See Map	-	-	-	-	-	-	
178(a)	21	150	2				Fo	-	-	-	-	-	-	-	
178(b)	49	100	2				Jt	5.0	1.5	A	I	VIII	-	-	
178(c)	49	156	2				Jt	2.0	0.5	I	A	VIII	0.0	0	
182(a)	17	105	4				Fo	-	-	-	-	-	-	-	
182(b)	54	110	4				Jt	-	-	-	-	VII	-	-	
182(c)	78	214	4				Jt	-	-	-	-	-	-	-	
184	42	323	4				Ft	See Map	-	-	-	-	-	-	
185(a)	19	075	4				Fo	-	-	-	-	-	-	-	
185(b)	75	010	4				Jt	5.0	1	O	O	II	-	-	
185(c)	74	115	4				Jt	-	-	-	-	-	-	-	
186	42	323	4				Ft	See Map	-	-	-	-	-	-	
187	38	125	4				Fo	-	-	-	-	-	-	-	
188	60	062	4				Ft	See Map	-	O	O	V	2.0	0	
189	87	064	4				Ft	See Map	-	O	O	II	2.0	Seepage	
190	58	060	4				Ft	See Map	-	O	O	VIII	2.0	0	
191(a)	16	160	4				Fo	-	-	-	-	-	-	-	
192	33	084	4				Fo	-	-	-	-	-	-	-	
193	60	297	4				Ft	-	-	-	-	-	0.5	0	
194	36	269	4				Ft	-	-	O	O	IX	50.0	0	
195	22	248	4				Fo	-	-	-	-	-	-	-	
196	12	252	4				Fo	-	-	-	-	-	-	-	
197	29	220	4				Fo	-	-	-	-	-	-	-	
198	55	095	1				Ft								
199	65	195	1				Ft								
200	20	265	1				Ft								

B5 RH28 Prism Monitoring

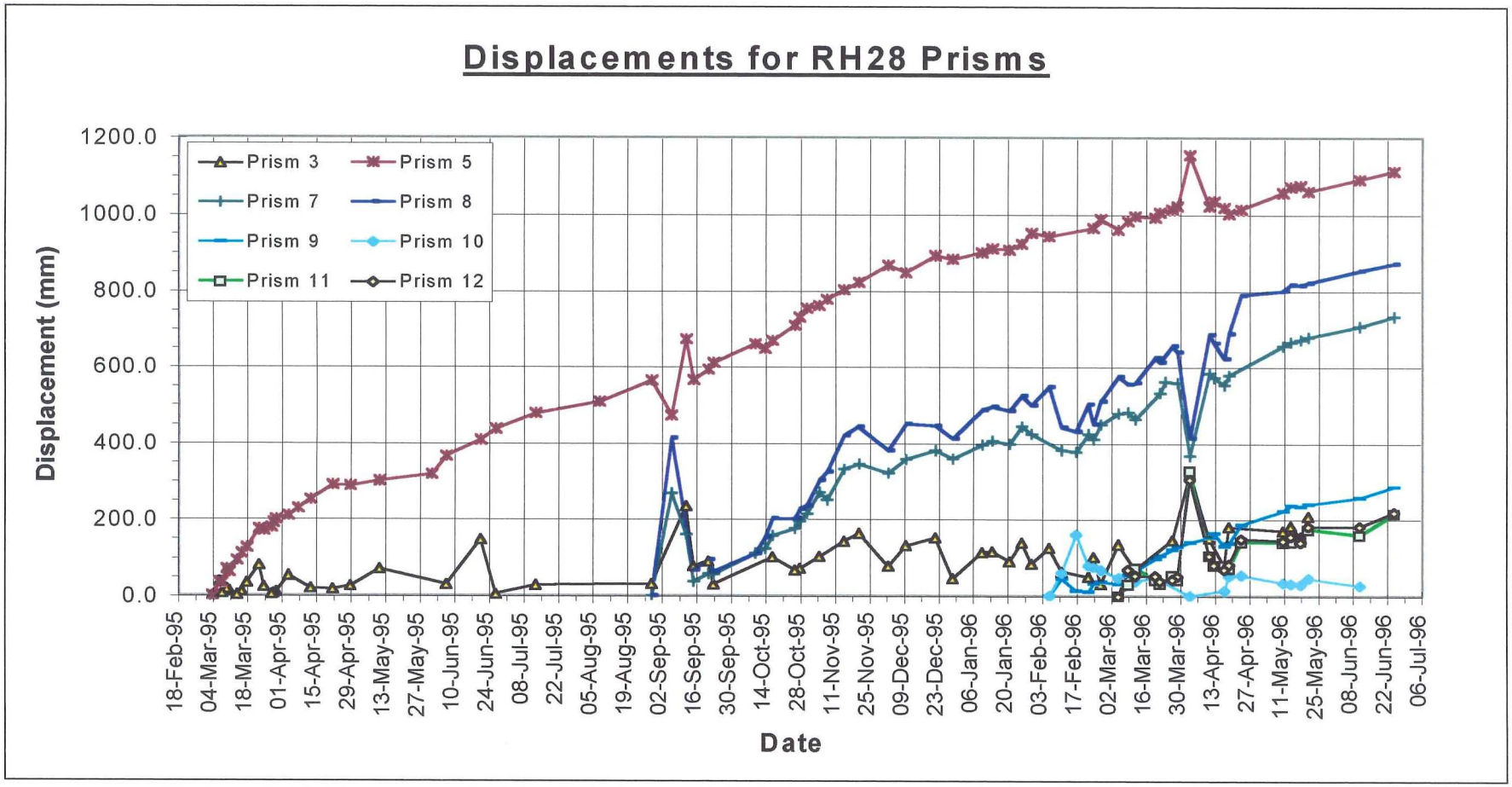

FigureB5-1: Displacements of RH28 prisms

B6 RH28 Crack Pin Monitoring

Date Time	Pin 28A	Pin 28B	Pin 28C	Pin 28D	Pin 28E	Pin 28F	Pin 28G	Pin 28H	Pin 28I	Pin 28J	Pin 28K	Pin 28L	Pin 28M	Pin 28N	Pin 28O	Pin 28P	Pin 28Q
Initial reading	*605*	*1,039*	*1,077*	*730*	*958*	*827*	*636*	*391*	*645*	*649*	*695*	*221*	*717*	*689*	*582*	*737*	*761*
22/04/96	605	1,039	1,077														
24/04/96	606	1,041	1,078														
27/04/96	607	1,044	1,080														
30/04/96	607	1,045	1,081	730	958	827	636	391		649	695			689	582	737	761
1/05/96	607	1,047	1,082	730	958	827	637	391	645	650	695	221	717	690	582	738	761
14/05/96	608	1,057	1,089	732	960	830	635	391	642	652	699			689	582	741	762
18/05/96	608	1,059	1,091	731	960	830	635	392	648	653	699	223	718	690	582	742	762
21/05/96	609	1,060	1,090	732	960	831	635	391	649	653	699	224	717	690	584	742	762
25/05/96	609	1,060	1,092	731	959	831	635	392	648	653	700	224	714	689	582	742	762
28/05/96	609	1,061	1,093	731	959	834	635	392	648	653	699	225	719	690	583	743	762
6/06/96	609	1,060	1,093	730	959	833	635	391	648	653	693	225	718	689	582	744	762
8/06/96	608	1,061	1,093	730	959	833	634	392	648	653	698	225	719	689	582	743	762
30/07/96	609	1,070	1,105	729	960	836	633	391	650	653	695	225	718	687	581	746	762
9/08/96	611	1,070	1,103	731	962	837	633	392		654	696	225	717	689	581		

APPENDIX C: LABORATORY DATA

C1 Sample Descriptions and Locations

Table C1-1: Sample Descriptions and Locations

Sample(s)	Tests Conducted	Description	Notes	Easting	Northing	mRL
FG1	Ring Shear, XRD	Unweathered, moist , very soft, plastic, whitish grey massive, silty clay; containing schist breccia fragments with some kaolinite?	Slip 27 Fault	70185mE	15250mN	365mRL
FG2	Ring Shear, XRD	Unweathered, wet , very soft, plastic, bluish grey massive, silty clay; containing schist breccia fragments.	Bottom Fault (RH28)	70125mE	15350mN	420mRL
FG3	Ring Shear, XRD	Unweathered, wet , soft, plastic, bluish grey massive, clayey silt; containing schist breccia fragments.	Bag Farm Fault (RH28)	70050mE	15375mN	440mRL
FG4	Ring Shear, XRD	Unweathered, wet , soft, plastic, grey massive, clayey silt;; containing schist breccia fragments.	RH33 Failure Plane	70075mE	15070mN	360mRL
FG5	Ring Shear, XRD	Unweathered, wet , soft, plastic, bluish grey massive, clayey silt;; containing schist breccia fragments.	Battery Creek Fault	69950mE	15300mN	385mRL
FG6	Ring Shear	Unweathered, wet , firm-soft, plastic, grey massive, clayey silt;; containing schist breccia fragments.	RH27 Obs. 95	70230mE	15220mN	375mRL
FG10	XRD	Unweathered, wet , firm, plastic, bluish grey massive, clayey silt;; containing schist breccia fragments.	Failure RH35	70170mE	15255mN	355mRL
c/PLT 1 - c/PLT7	Point load on core samples	see Results Sheet Appendix C3	see Results Sheet Appendix C3	Appendix C3	Appendix C3	Appendix C3
i/PLT8 - i/PLT11	Point load on irregular lumps samples	see Results Sheet Appendix C3	see Results Sheet Appendix C3	Appendix C3	Appendix C3	Appendix C3
AP UCS1 - AP UCS9	Uniaxial compressive strength testing	see Table 2-3 of Chapter 2	Hole No. DDG 33	69919mE	15374mN	430mRL
AP UCS11 - AP UCS12	Uniaxial compressive strength testing	see Table 2-3 of Chapter 2	Hole No. DDG 34	69973mE	15248mN	335mRL
AP UCS13 - AP UCS15	Uniaxial compressive strength testing	see Table 2-3 of Chapter 2	Hole No. DDG 31	70137mE	13581mN	576mRL
AP UCS16 - AP UCS19	Uniaxial compressive strength testing	see Table 2-3 of Chapter 2	Hole No. DDG 35	70122mE	13058mN	548mRL

C2 Uniaxial Compressive Strength Testing

Uniaxial compressive strength (UCS) testing was undertaken according to the ISRM suggested methods (Brown, 1981). Core samples were initially diamond sawed and then ground so that the ends of the specimen were flat to 0.02mm and so that the ends did not depart from perpendicularity to the core axis by more than 0.05mm in 50mm.

Testing was undertaken in the University of Canterbury Civil Engineering department using concrete testing equipment (Figure C2-1). PQ core (83mm diameter) and HQ core (61mm diameter) were both tested at a stress rate of approximately 0.1 MPa.

The uniaxial compressive strength of the core sample is calculated by dividing the maximum load carried by the specimen by the original cross-sectional area of the core. Photographic records of each of the core samples were taken both before and after testing and these are presented on the following pages.

Figure C2-1: The Department of Civil Engineering's, concrete testing machine used for uniaxial compressive strength testing in this study.

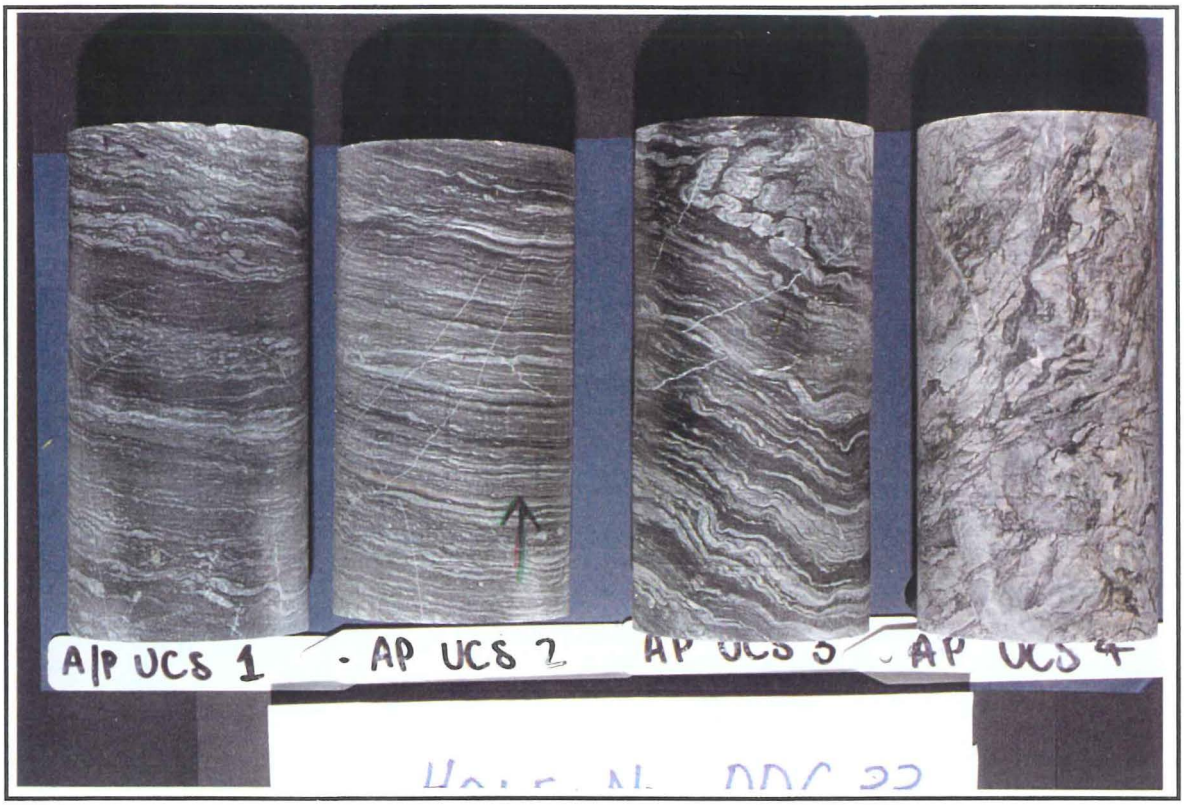

Figure C2-2: Core samples AP UCS 1, AP UCS 2, AP UCS 3, and AP UCS 4 prior to UCS testing. Hole No. DDG33 (69919mE, 15374mN). Core size is PQ (83mm diameter).

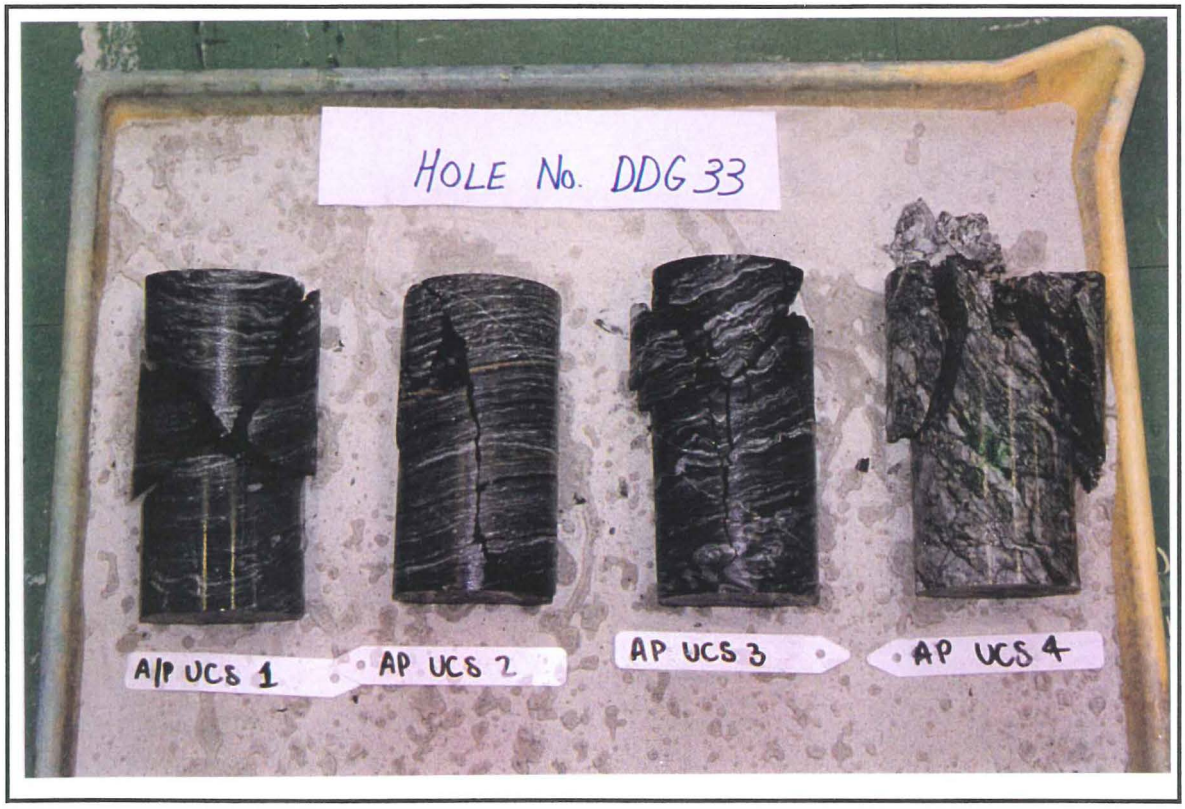

Figure C2-3: Core samples AP UCS 1 (50.9 MPa), AP UCS 2 (35.3MPa) , AP UCS 3 (20.4MPa), and AP UCS 4 (17.4MPa) after UCS testing. Hole No. DDG33 (69919mE, 15374mN). Core size is PQ (83mm diameter).

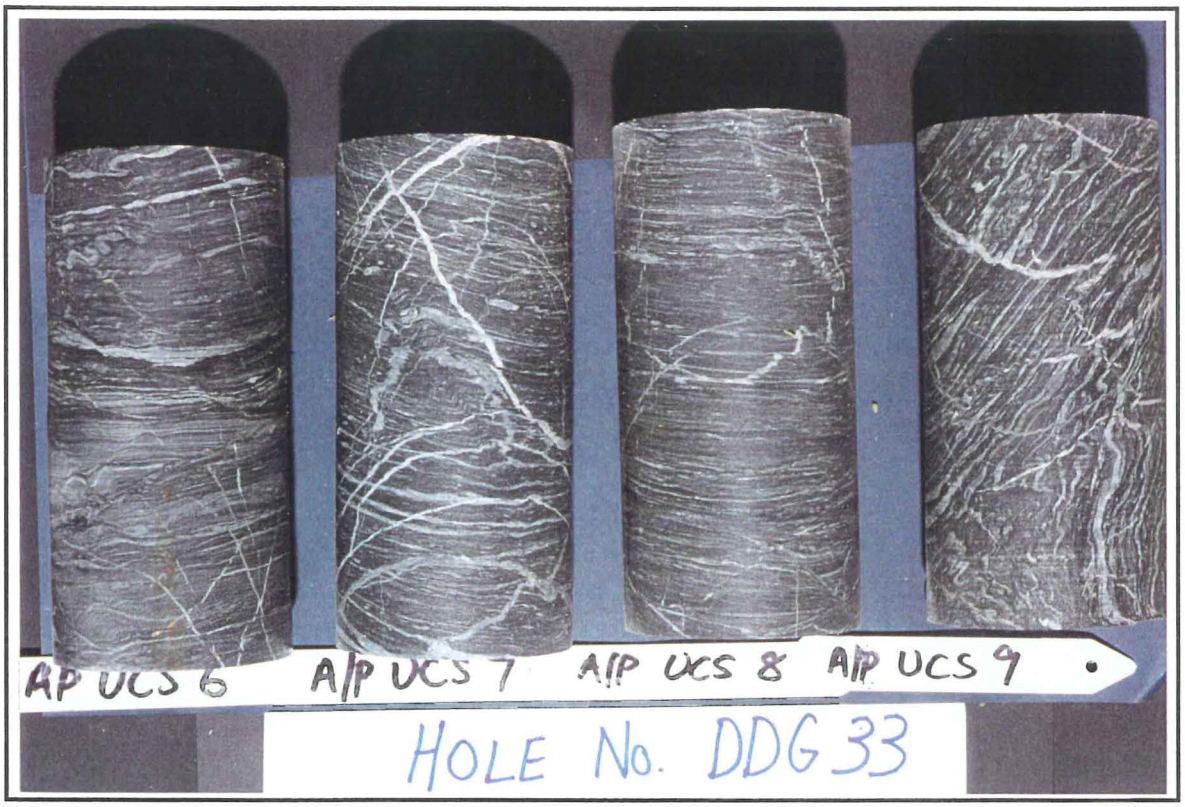

Figure C2-4: Core samples AP UCS 6, AP UCS 7, AP UCS 8, and APUCS 9 prior to UCS testing. Hole No. DDG33 (69919mE, 15374mN). Core size is PQ (83mm diameter).

Figure C2-5: Core samples AP UCS 6 (8.7 MPa), AP UCS 7 (34.5 MPa), AP UCS 8 (29.5 MPa), and AP UCS 9 (4.8 MPa)after UCS testing. Hole No. DDG33 (69919mE, 15374mN). Core size is PQ (83mm diameter).

Figure C2-6: Core samples AP UCS 10 and AP UCS 11 prior to UCS testing. Hole No. DDG34 (69973.9mE, 15248.5mN). Core size is PQ (83mm diameter).

Figure C2-7: Figure C2-6: Core samples AP UCS 11 (15.6 MPa) and AP UCS 12 (29.5 MPa) after UCS testing. Hole No. DDG34 (69973.9mE, 15248.5mN). Core size is PQ (83mm diameter).

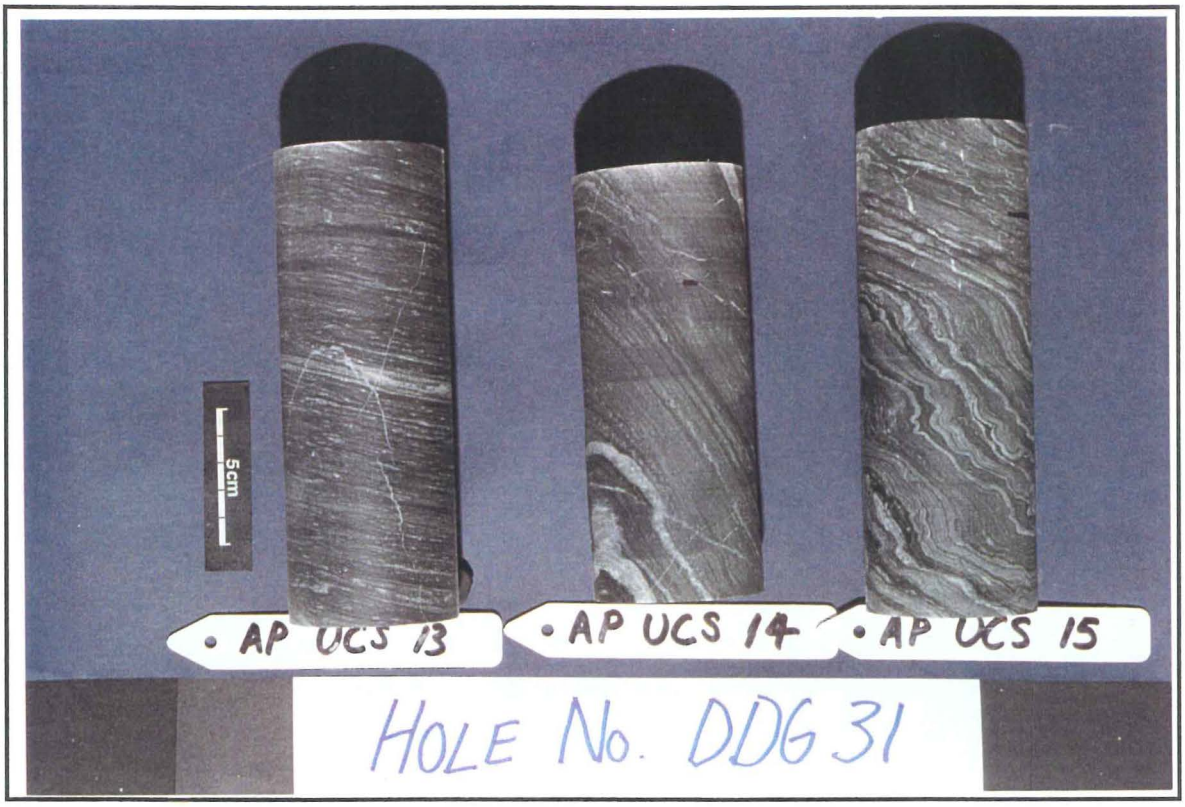

Figure C2-8: Core samples AP UCS 13, AP UCS 14 and AP UCS 15 prior to UCS testing. Hole No. DDG31 (70137mE, 13581.7mN). Core size is HQ (61mm diameter).

Figure C2-9: Core samples AP UCS 13 (61.2 MPa), AP UCS 14 (18.1 MPa) and AP UCS 15 (10.0 MPa) after UCS testing. Hole No. DDG31 (70137mE, 13581.7mN). Core size is HQ (61mm diameter).

Figure C2-10: Core samples AP UCS 16, AP UCS 17, AP UCS 18 and AP UCS 19 prior to UCS testing. Hole No. DDG35 (70122.6mE, 13581.7mN). Core size is HQ (61mm diameter).

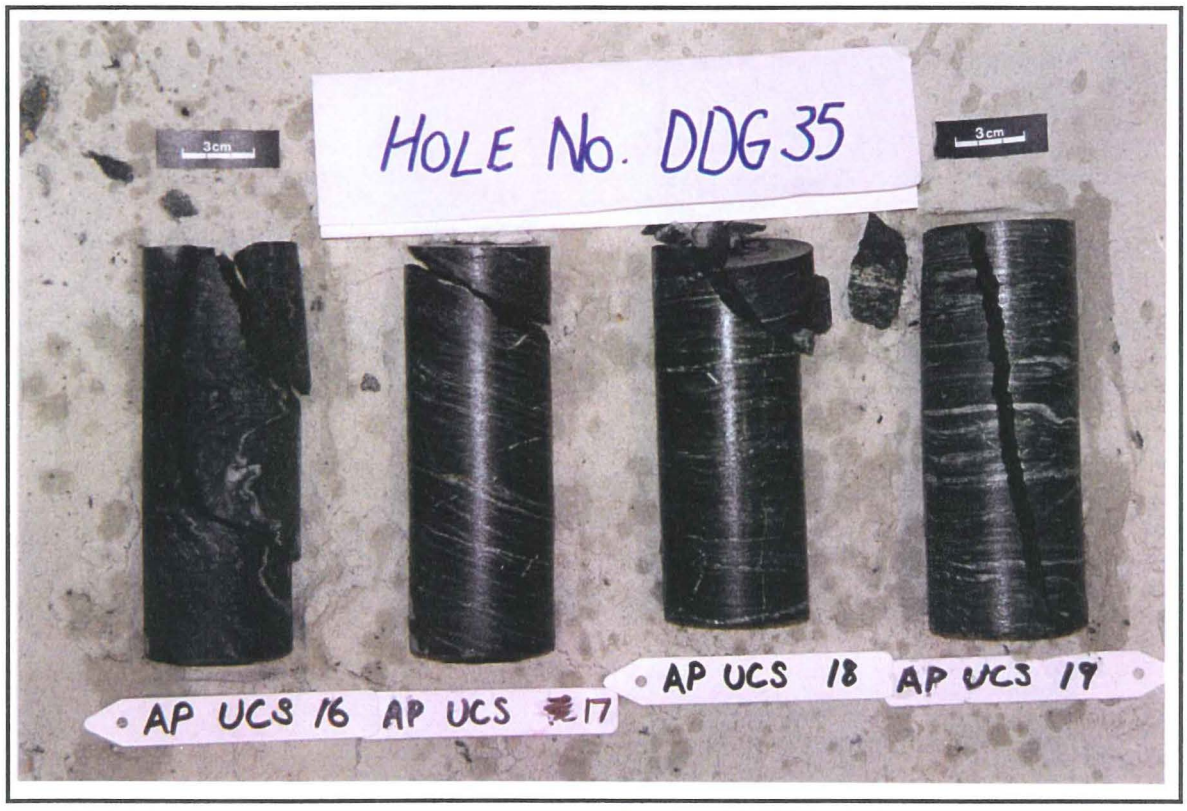

Figure C2-11: Core samples AP UCS 16 (12.7MPa), AP UCS 17 (21.1 MPa), AP UCS 18 (13.6 MPa) and AP UCS 19 (20.5 MPa) after UCS testing. Hole No. DDG35 (70122.6mE, 13581.7mN). Core size is HQ (61mm diameter)

C3 Point Load Testing

Point load testing was carried out in accordance with the ISRM "Suggested method for determining point load strength" (1995).

Specimens were tested both axially (force applied ⊥ to schistosity) and diametrically (force applied // to schistosity). For diametrical testing specimens with a length/diameter ratio greater than one are suitable for testing. Axial testing requires that the length to diameter ratio lies between 0.3 and 1.0. While for the irregular lump test, lumps of size 50±35mm are suitable for testing. Through a hydraulic system the load is steadily increased through the platens such that failure occurs within 10 - 60 seconds.

Calculations

The uncorrected point load strength index (I_s) is calculated as

$$I_s = \frac{P}{D_e^2}$$

where P = the force at which the sample breaks and D_e is the "equivalent core diameter" and is given by

$D_e^2 = D^2$ for diametrical tests

$= 4A\pi$ for axial, block and lump tests:

and

A = WD = minimum cross sectional area of a plane through the platen contact points.

The size-corrected point load strength $I_{s(50)}$ is calculated by applying a "size correction factor F" where

$$I_{s(50)} = F \times I_s$$

The size correction factor can be obtained from the expression

$$F = \left(\frac{D_e}{50}\right)^{0.45}$$

Point load results are presented in the tables on the following pages.

Table C2-1: Point load test results for sample c/PLT 1 (core pieces)

Hole No. = DDG33 *Depth range* = 0.00-10.60m

Rock Description = Unweathered, moderately strong to stong, grey semi-pelitic schist with some limonite staining on broken surfaces

Sample	Box No.	Test Type	W (mm)	D (mm)	P (kN)	De^2 (mm^2)	De (mm)	Is	F	$I_{s(50)}$ (MPa)	UCS (MPa)
1	1	axial	83	68	15.0	7186	85	2.09	1.27	2.65	55.6
2	2	axial	83	65	12.0	6869	83	1.75	1.26	2.19	46.1
3	2	axial	83	70	11.0	7398	86	1.49	1.28	1.90	39.9
4	2	axial	83	58	11.0	6129	78	1.79	1.22	2.20	46.1
5	~~2~~	~~axial~~	~~83~~	~~60~~	~~16.0~~	~~6341~~	~~80~~	~~2.52~~	~~1.23~~	~~3.11~~	65.3
~~6~~	~~2~~	~~axial~~	~~83~~	~~51~~	~~14.5~~	~~5390~~	~~73~~	~~2.69~~	~~1.19~~	~~3.20~~	67.2
~~7~~	~~3~~	~~axial~~	~~83~~	~~61~~	~~2.5~~	~~6446~~	~~80~~	~~0.39~~	~~1.24~~	~~0.48~~	10.1
~~8~~	~~3~~	~~axial~~	~~83~~	~~52~~	~~1.0~~	~~5495~~	~~74~~	~~0.18~~	~~1.19~~	~~0.22~~	4.6
~~9~~	4	axial	83	70	15.5	7398	86	2.10	1.28	2.67	56.2
10	5	axial	83	54	3.0	5707	76	0.53	1.20	0.63	13.3
11	2	Diametrical	108	83	1.5	6889	83	0.22	1.26	0.27	5.7
~~12~~	~~2~~	~~Diametrical~~	~~125~~	83	~~2.0~~	6889	~~83~~	~~0.29~~	~~1.26~~	~~0.36~~	7.7
~~13~~	~~3~~	~~Diametrical~~	~~110~~	83	~~6.5~~	6889	~~83~~	~~0.94~~	~~1.26~~	~~1.19~~	24.9
14	4	Diametrical	105	83	1.5	6889	83	0.22	1.26	0.27	5.7
15	4	Diametrical	94	83	1.5	6889	83	0.22	1.26	0.27	5.7
16	5	Diametrical	130	83	1.0	6889	83	0.15	1.26	0.18	3.8
~~17~~	~~5~~	~~Diametrical~~	~~128~~	83	~~0.5~~	6889	~~83~~	~~0.07~~	~~1.26~~	~~0.09~~	1.9
~~18~~	~~6~~	~~Diametrical~~	~~104~~	83	~~1.0~~	6889	~~83~~	~~0.15~~	~~1.26~~	~~0.18~~	3.8
19	6	Diametrical	94	83	1.0	6889	83	0.15	1.26	0.18	3.8
20	6	Diametrical	106	83	1.0	6889	83	0.15	1.26	0.18	3.8

	$I_{s(50)}$	UCS
Average of axial tests (MPa) =	2.04	42.8
Average of diametrical tests (MPa)=	0.23	4.8
Anisotophy Index =	9.0	9.0

Table C2-2: Point load test results for sample c/PLT 2 (core pieces) -

Hole No. = DDG34 *Depth range* = 7.61-14.59m

scription = Unweathered, moderately strong to moderately weak, whitish grey psammitic schist containing quartz veins up to 3mm in thickness

Box No.	Test Type	W (mm)	D (mm)	P (kN)	De^2 (mm^2)	De (mm)	Is	F	$I_{s(50)}$ (MPa)	UCS (MPa)
2	axial	83	65	2.0	6869	83	0.29	1.26	0.37	7.7
~~2~~	~~axial~~	~~83~~	~~73~~	~~18.5~~	~~7715~~	~~88~~	~~2.40~~	~~1.29~~	~~3.09~~	64.9
~~2~~	~~axial~~	~~83~~	~~77~~	~~12.0~~	~~8137~~	~~90~~	~~1.47~~	~~1.30~~	~~1.92~~	40.4
~~2~~	~~axial~~	~~83~~	~~60~~	~~0.3~~	~~6341~~	~~80~~	~~0.04~~	~~1.23~~	~~0.05~~	1.0
2	axial	83	69	0.5	7292	85	0.07	1.27	0.09	1.8
~~4~~	~~axial~~	~~83~~	~~77~~	~~0.3~~	~~8137~~	~~90~~	~~0.03~~	~~1.30~~	~~0.04~~	0.8
4	axial	83	66	1.0	6975	84	0.14	1.26	0.18	3.8
4	axial	83	70	1.0	7398	86	0.14	1.28	0.17	3.6
4	axial	83	53	1.0	5601	75	0.18	1.20	0.21	4.5
4	axial	83	77	1.0	8137	90	0.12	1.30	0.16	3.4
~~2~~	~~Diametrical~~	~~91~~	~~83~~	~~0.2~~	~~6889~~	~~83~~	~~0.03~~	~~1.26~~	~~0.04~~	0.8
~~2~~	~~Diametrical~~	~~112~~	~~83~~	~~1.3~~	~~6889~~	~~83~~	~~0.18~~	~~1.26~~	~~0.23~~	4.8
~~2~~	~~Diametrical~~	~~148~~	~~83~~	~~1.8~~	~~6889~~	~~83~~	~~0.25~~	~~1.26~~	~~0.32~~	6.7
~~3~~	~~Diametrical~~	~~124~~	~~83~~	~~0.1~~	~~6889~~	~~83~~	~~0.01~~	~~1.26~~	~~0.02~~	0.4
4	Diametrical	125	83	1.0	6889	83	0.15	1.26	0.18	3.8
4	Diametrical	133	83	1.0	6889	83	0.15	1.26	0.18	3.8
4	Diametrical	123	83	1.0	6889	83	0.15	1.26	0.18	3.8
5	Diametrical	111	83	1.0	6889	83	0.15	1.26	0.18	3.8
5	Diametrical	112	83	0.5	6889	83	0.07	1.26	0.09	1.9
5	Diametrical	105	83	0.5	6889	83	0.07	1.26	0.09	1.9

	$I_{s(50)}$	UCS
Average of axial tests (MPa) =	0.20	4.1
Average of diametrical tests (MPa)=	0.15	3.2
Anisotophy Index =	1.3	1.3

Table C2-3: Point load test results for sample c/PLT3 (core pieces)

Hole No. = DDG35 *Depth range* = 66.70 - 78.90m

Rock Description = Unweathered, strong to moderately strong, whitish grey, semi-pelitic schist

Sample	Box No.	Test Type	W (mm)	D (mm)	P (kN)	De^2 (mm^2)	De (mm)	Is	F	$I_{s(50)}$ (MPa)	UCS (MPa)
1	20	axial	61	54	7.5	4194	65	1.79	1.12	2.01	42.2
2	20	axial	61	44	8.0	3417	58	2.34	1.07	2.51	52.7
~~3~~	~~20~~	~~axial~~	~~61~~	~~48~~	~~12.0~~	~~3728~~	~~61~~	~~3.22~~	~~1.09~~	~~3.52~~	74.0
4	21	axial	61	45	2.0	3495	59	0.57	1.08	0.62	13.0
~~5~~	~~21~~	~~axial~~	~~61~~	~~54~~	~~15.5~~	~~4194~~	~~65~~	~~3.70~~	~~1.12~~	~~4.15~~	87.2
~~6~~	~~21~~	~~axial~~	~~61~~	~~58~~	~~1.0~~	~~4505~~	~~67~~	~~0.22~~	~~1.14~~	~~0.25~~	5.3
7	22	axial	61	49	5.0	3806	62	1.31	1.10	1.44	30.3
~~8~~	~~23~~	~~axial~~	~~61~~	~~57~~	~~1.0~~	~~4427~~	~~67~~	~~0.23~~	~~1.14~~	~~0.26~~	5.4
9	23	axial	61	61	2.0	4738	69	0.42	1.15	0.49	10.2
10	23	axial	61	57	2.0	4427	67	0.45	1.14	0.51	10.8
11	20	Diametrical	81	61	1.0	3721	61	0.27	1.09	0.29	6.2
12	20	Diametrical	68	61	1.0	3721	61	0.27	1.09	0.29	6.2
13	20	Diametrical	63	61	1.0	3721	61	0.27	1.09	0.29	6.2
14	20	Diametrical	91	61	1.0	3721	61	0.27	1.09	0.29	6.2
~~15~~	~~21~~	~~Diametrical~~	~~58~~	~~61~~	~~0.5~~	~~3721~~	~~61~~	~~0.13~~	~~1.09~~	~~0.15~~	3.1
16	21	Diametrical	63	61	1.0	3721	61	0.27	1.09	0.29	6.2
~~17~~	~~22~~	~~Diametrical~~	~~65~~	~~61~~	~~0.5~~	~~3721~~	~~61~~	~~0.13~~	~~1.09~~	~~0.15~~	3.1
18	22	Diametrical	70	61	1.0	3721	61	0.27	1.09	0.29	6.2
~~19~~	~~23~~	~~Diametrical~~	~~84~~	~~61~~	~~1.5~~	~~3721~~	~~61~~	~~0.40~~	~~1.09~~	~~0.44~~	9.3
~~20~~	~~23~~	~~Diametrical~~	~~76~~	~~61~~	~~13.0~~	~~3721~~	~~61~~	~~3.49~~	~~1.09~~	~~3.82~~	80.2

	$I_{s(50)}$	UCS
Average of axial tests (MPa) =	1.26	26.5
Average of diametrical tests (MPa)=	0.29	6.2
Anisotophy Index =	4.3	4.3

Table C2-4: Point load test results for sample c/PLT 4 (core pieces)

Hole No. = DDG31 *Depth range* = 67.40 - 76.00m

Rock Description = Unweathered, moderately strong, whitish grey, semi pelitic schist containing cubic pyrite crystals up to 4mm in diameter

Sample	Box No.	Test Type	W (mm)	D (mm)	P (kN)	De^2 (mm^2)	De (mm)	Is	F	$I_{s(50)}$ (MPa)	UCS (MPa)
~~1~~	~~22~~	~~axial~~	~~61~~	~~52~~	~~8.0~~	~~4039~~	~~64~~	~~1.98~~	~~1.11~~	~~2.21~~	~~46.3~~
2	22	axial	61	49	6.0	3806	62	1.58	1.10	1.73	~~36.4~~
3	22	axial	61	60	2.5	4660	68	0.54	1.15	0.62	~~13.0~~
4	23	axial	61	62	8.5	4815	69	1.77	1.16	2.05	~~43.0~~
~~5~~	~~23~~	~~axial~~	~~61~~	~~53~~	~~1.5~~	~~4116~~	~~64~~	~~0.36~~	~~1.12~~	~~0.41~~	~~8.6~~
6	23	axial	61	59	8.0	4582	68	1.75	1.15	2.00	~~42.0~~
~~7~~	~~24~~	~~axial~~	~~61~~	~~56~~	~~10.0~~	~~4349~~	~~66~~	~~2.30~~	~~1.13~~	~~2.60~~	~~54.7~~
8	25	axial	61	49	7.0	3806	62	1.84	1.10	2.02	~~42.5~~
9	25	axial	61	65	9.5	5048	71	1.88	1.17	2.20	~~46.3~~
~~10~~	~~25~~	~~axial~~	~~61~~	~~72~~	~~1.5~~	~~5592~~	~~75~~	~~0.27~~	~~1.20~~	~~0.32~~	~~6.8~~
~~11~~	~~22~~	~~Diametrical~~	~~75~~	~~61~~	~~1.0~~	~~3721~~	~~61~~	~~0.27~~	~~1.09~~	~~0.29~~	~~6.2~~
12	22	Diametrical	55	61	1.0	3721	61	0.27	1.09	0.29	~~6.2~~
13	22	Diametrical	76	61	0.8	3721	61	0.20	1.09	0.22	~~4.6~~
14	22	Diametrical	97	61	0.8	3721	61	0.20	1.09	0.22	~~4.6~~
~~15~~	~~23~~	~~Diametrical~~	~~77~~	~~61~~	~~12.5~~	~~3721~~	~~61~~	~~3.36~~	~~1.09~~	~~3.67~~	~~77.1~~
16	23	Diametrical	92	61	1.0	3721	61	0.27	1.09	0.29	~~6.2~~
17	24	Diametrical	92	61	1.0	3721	61	0.27	1.09	0.29	~~6.2~~
18	25	Diametrical	83	61	1.0	3721	61	0.27	1.09	0.29	~~6.2~~
~~19~~	~~25~~	~~Diametrical~~	~~111~~	~~61~~	~~0.5~~	~~3721~~	~~61~~	~~0.13~~	~~1.09~~	~~0.15~~	~~3.1~~
~~20~~	~~25~~	~~Diametrical~~	~~57~~	~~61~~	~~0.3~~	~~3721~~	~~61~~	~~0.07~~	~~1.09~~	~~0.07~~	~~1.5~~

	$I_{s(50)}$	UCS
Average of axial tests (MPa) =	1.77	37.2
Average of diametrical tests (MPa)=	0.27	5.7
Anisotophy Index =	6.57	6.6

Table C2-5: Point load test results for sample c/PLT 5 (core pieces)

Hole No. = DDH127 *Depth range* = 15.30 - 24.30m

Rock Description = Unweathered to slightly weathered, moderately strong to moderately weak whitish-grey psammitic schist; contains some orange stuff concordant to foliation

Sample	Box No.	Test Type	W (mm)	D (mm)	P (kN)	De^2 (mm^2)	De (mm)	Is	F	$I_{s(50)}$ (MPa)	UCS (MPa)
1	4	axial	61	57	3.0	4427	67	0.68	1.14	0.77	16.2
~~2~~	~~4~~	~~axial~~	~~61~~	~~82~~	~~9.5~~	~~6369~~	~~80~~	~~1.49~~	~~1.23~~	~~1.84~~	38.7
~~3~~	~~4~~	~~axial~~	~~61~~	~~62~~	~~11.0~~	~~4815~~	~~69~~	~~2.28~~	~~1.16~~	~~2.65~~	55.6
4	4	axial	61	53	2.5	4116	64	0.61	1.12	0.68	14.3
~~5~~	~~4~~	~~axial~~	~~61~~	~~48~~	~~1.0~~	~~3728~~	~~61~~	~~0.27~~	~~1.09~~	~~0.29~~	6.2
6	4	axial	61	63	7.0	4893	70	1.43	1.16	1.66	34.9
7	4	axial	61	65	7.0	5048	71	1.39	1.17	1.62	34.1
8	5	axial	61	57	3.5	4427	67	0.79	1.14	0.90	18.9
~~9~~	~~6~~	~~axial~~	~~61~~	~~50~~	~~1.5~~	~~3883~~	~~62~~	~~0.39~~	~~1.10~~	~~0.43~~	9.0
10	6	axial	61	56	2.5	4349	66	0.57	1.13	0.65	13.7
~~11~~	~~4~~	~~Diametrical~~	~~80~~	~~61~~	~~0.2~~	~~3721~~	~~61~~	~~0.05~~	~~1.09~~	~~0.06~~	1.2
12	4	Diametrical	78	61	1.0	3721	61	0.27	1.09	0.29	6.2
13	5	Diametrical	86	61	1.0	3721	61	0.27	1.09	0.29	6.2
14	5	Diametrical	80	61	0.8	3721	61	0.20	1.09	0.22	4.6
15	6	Diametrical	74	61	1.0	3721	61	0.27	1.09	0.29	6.2
~~16~~	~~6~~	~~Diametrical~~	~~96~~	~~61~~	~~1.0~~	~~3721~~	~~61~~	~~0.27~~	~~1.09~~	~~0.29~~	6.2

	$I_{s(50)}$	UCS
Average of axial tests (MPa) =	1.05	22.0
Average of diametrical tests (MPa)=	0.28	5.8
Anisotophy Index =	3.8	3.8

Table C2-6: Point load test results for sample c/PLT 6 (core pieces)

Hole No. = RCD2919 *Depth range* = 246.00 - 255.00m

Rock Description = Unweathered, moderately strong dark grey semi pelitic schist.

Sample	Box No.	Test Type	W (mm)	D (mm)	P (kN)	De^2 (mm^2)	De (mm)	Is	F	$I_{s(50)}$ (MPa)	UCS (MPa)
1	1	axial	61	54	1.0	4194	65	0.24	1.12	0.27	5.6
~~2~~	~~1~~	~~axial~~	61	~~49~~	~~11.0~~	~~3806~~	~~62~~	~~2.89~~	~~1.10~~	~~3.18~~	66.7
3	1	axial	~~61~~	68	6.5	5281	73	1.23	1.18	1.46	30.6
4	1	axial	61	61	1.5	4738	69	0.32	1.15	0.37	7.7
~~5~~	~~2~~	~~axial~~	~~61~~	~~72~~	~~0.2~~	~~5592~~	~~75~~	~~0.04~~	~~1.20~~	~~0.04~~	0.9
6	2	axial	61	53	7.0	4116	64	1.70	1.12	1.90	40.0
~~7~~	~~3~~	~~axial~~	~~61~~	~~49~~	~~9.0~~	~~3806~~	~~62~~	~~2.36~~	~~1.10~~	~~2.60~~	54.6
8	3	axial	61	68	8.0	5281	73	1.51	1.18	1.79	37.6
9	3	axial	61	55	7.0	4272	65	1.64	1.13	1.85	38.8
~~10~~	~~3~~	~~axial~~	~~61~~	~~52~~	~~0.5~~	~~4039~~	~~64~~	~~0.12~~	~~1.11~~	~~0.14~~	2.9

	$I_{s(50)}$	UCS
Average of axial tests (MPa) =	1.27	26.7

Table C2-7: Point load test results for sample c/PLT 7 (core pieces)

Hole No. = RCD2919 *Depth range* = 246.00 - 255.00m

Rock Description = Unweathered, strong, dark greenish grey, semi psammitic schist

Sample	Box No.	Test Type	W (mm)	D (mm)	P (kN)	De^2 (mm^2)	De (mm)	Is	F	$I_{s(50)}$ (MPa)	UCS (MPa)
1	1	axial	61	65	15.0	5048	71	2.97	1.17	3.48	73.1
~~2~~	~~2~~	~~axial~~	~~61~~	~~64~~	~~7.0~~	~~4971~~	~~71~~	~~1.41~~	~~1.17~~	~~1.64~~	34.5
~~3~~	~~2~~	~~axial~~	~~61~~	~~78~~	~~2.0~~	~~6058~~	~~78~~	~~0.33~~	~~1.22~~	~~0.40~~	8.5
~~4~~	~~2~~	~~axial~~	~~61~~	~~72~~	~~19.0~~	~~5592~~	~~75~~	~~3.40~~	~~1.20~~	~~4.07~~	85.5
5	3	axial	61	88	16.5	6835	83	2.41	1.25	3.03	63.6
6	3	axial	61	50	13.5	3883	62	3.48	1.10	3.84	80.6
~~7~~	~~3~~	~~axial~~	~~61~~	~~65~~	~~22.0~~	~~5048~~	~~71~~	~~4.36~~	~~1.17~~	~~5.10~~	107.2
8	4	axial	61	72	8.5	5592	75	1.52	1.20	1.82	38.3
9	4	axial	61	56	13.5	4349	66	3.10	1.13	3.52	73.8
10	4	axial	61	67	14.0	5204	72	2.69	1.18	3.17	66.6

	$I_{s(50)}$	UCS
Average of axial tests (MPa) =	3.14	66.0

Table C2-8: Point load test results for sample i/PLT 8 (irregular lumps)

Location= Round Hill Pit Floor (340mRL)

Rock Description= Unweathered, strong, dark greyish-black, cataclasite schist; containing quartz veins

Sample No.	*Orientation of Platens to Foliation*	*W (mm)*	*D (mm)*	*L (mm)*	*P (kN)*	*D_e^2 (mm^2)*	*De (mm)*	*Is*	*F*	*Is_{50}*	*UCS (MPa)*
1	Perpendicular	83	76	55	29.0	8096	90	3.58	1.30	4.67	98.0
2	Perpendicular	80	78	54	10.0	7904	89	1.27	1.30	1.64	34.4
3	Perpendicular	97	88	64	10.5	10811	104	0.97	1.39	1.35	28.4
4	Perpendicular	78	73	53	13.0	7223	85	1.80	1.27	2.29	48.0
5	Perpendicular	75	71	54	8.5	6828	83	1.24	1.25	1.56	32.8
6	Perpendicular	101	77	64	16.0	9890	99	1.62	1.36	2.20	46.3
7	Perpendicular	106	76	57	14.0	10306	102	1.36	1.38	1.87	39.2
8	Perpendicular	102	86	65	17.5	11245	106	1.56	1.40	2.18	45.8
9	Perpendicular	93	85	52	22.5	10015	100	2.25	1.37	3.07	64.5
10	Perpendicular	95	58	54	11.0	6965	83	1.58	1.26	1.99	41.8
11	Perpendicular	81	73	52	11.0	7563	87	1.45	1.28	1.87	39.2
12	Perpendicular	94	62	56	11.5	7373	86	1.56	1.28	1.99	41.8
13	Perpendicular	92	73	54	23.0	8469	92	2.72	1.32	3.57	75.0
14	Perpendicular	81	62	65	14.5	6328	80	2.29	1.23	2.82	59.3
15	Parallel	81	71	80	6.5	7349	86	0.88	1.27	1.13	23.7
16	Parallel	73	66	85	1.5	6106	78	0.25	1.22	0.30	6.3
17	Parallel	93	62	90	1.0	7322	86	0.14	1.27	0.17	3.7
18	Parallel	58	55	71	8.0	4059	64	1.97	1.12	2.20	46.2
19	Parallel	73	68	92	6.5	6330	80	1.03	1.23	1.27	26.6
20	Parallel	85	79	67	3.0	8546	92	0.35	1.32	0.46	9.7
21	Parallel	69	63	62	1.0	5527	74	0.18	1.20	0.22	4.5
22	Parallel	89	61	85	1.0	6896	83	0.15	1.26	0.18	3.8
23	Parallel	88	85	70	2.0	9530	98	0.21	1.35	0.28	6.0
24	Parallel	95	70	83	1.0	8538	92	0.12	1.32	0.15	3.2
25	Parallel	105	64	80	8.5	8648	93	0.98	1.32	1.30	27.3
26	Parallel	93	54	92	1.5	6447	80	0.23	1.24	0.29	6.0
27	Parallel	91	63	77	3.0	7310	85	0.41	1.27	0.52	11.0
28	Parallel	78	76	74	7.0	7531	87	0.93	1.28	1.19	25.0

Table C2-9: Point load test results for sample i/PLT9 (irregular lumps)

Highly weathered, moderately strong, dark blackish-grey, oxide stained semi-psammitic schist

Sample No.	*Description*	*W (mm)*	*D (mm)*	*L (mm)*	*P (kN)*	*D_e^2 (mm^2)*	*De (mm)*	*Is*	*F*	*Is_{50}*	*UCS (MPa)*
1	Perpendicular	84	83	60	2.0	8930.43	94.50	0.22	1.33	0.30	6.3
~~2~~	~~Perpendicular~~	~~83~~	~~65~~	~~70~~	~~4~~	~~6926.98~~	~~83.23~~	~~0.58~~	~~1.26~~	~~0.73~~	15.3
3	Perpendicular	76	48	59	1	4629.08	68.04	0.22	1.15	0.25	5.2
4	Perpendicular	77	73	52	1.5	7186.93	84.78	0.21	1.27	0.26	5.6
5	Perpendicular	76	75	51	2	7290.80	85.39	0.27	1.27	0.35	7.3
6	Perpendicular	92	78	51	3	9142.07	95.61	0.33	1.34	0.44	9.2
~~7~~	~~Perpendicular~~	~~84~~	~~71~~	~~66~~	~~4~~	~~7566.23~~	~~86.98~~	~~0.53~~	~~1.28~~	~~0.68~~	14.2
8	Perpendicular	97	62	60	2	7592.17	87.13	0.26	1.28	0.34	7.1
~~9~~	~~Perpendicular~~	~~90~~	~~53~~	~~52~~	~~1~~	~~6060.54~~	~~77.85~~	~~0.17~~	~~1.22~~	~~0.20~~	4.2
~~10~~	~~Perpendicular~~	~~95~~	~~63~~	~~50~~	~~1~~	~~7574.12~~	~~87.03~~	~~0.13~~	~~1.28~~	~~0.17~~	3.6
11	Perpendicular	85	55	71	1.5	5902.45	76.83	0.25	1.21	0.31	6.5
~~12~~	~~Perpendicular~~	~~74~~	~~72~~	~~51~~	~~1~~	~~6813.15~~	~~82.54~~	~~0.15~~	~~1.25~~	~~0.18~~	3.9
13	Perpendicular	87	66	63	1.5	7337.50	85.66	0.20	1.27	0.26	5.5
14	Perpendicular	69	52	51	1	4577.44	67.66	0.22	1.15	0.25	5.3
15	Perpendicular	91	71	50	2	8209.66	90.61	0.24	1.31	0.32	6.7
~~16~~	~~Perpendicular~~	~~80~~	~~67~~	~~51~~	~~1~~	~~6820.18~~	~~82.58~~	~~0.15~~	~~1.25~~	~~0.18~~	3.9
~~17~~	~~Perpendicular~~	~~70~~	~~67~~	~~50~~	~~1~~	~~5951.73~~	~~77.15~~	~~0.17~~	~~1.22~~	~~0.20~~	4.3
~~18~~	~~Perpendicular~~	~~97~~	~~79~~	~~50~~	~~10~~	~~9722.50~~	~~98.60~~	~~1.03~~	~~1.36~~	~~1.40~~	29.3
~~19~~	~~Perpendicular~~	~~72~~	~~66~~	~~61~~	~~5~~	~~6028.96~~	~~77.65~~	~~0.83~~	~~1.22~~	~~1.01~~	21.2
20	Perpendicular	83	62	50	1.5	6581.34	81.13	0.23	1.24	0.28	6.0
21	Perpendicular	73	57	52	2	5330.70	73.01	0.38	1.19	0.44	9.3
22	Perpendicular	68	51	56	1	4373.21	66.13	0.23	1.13	0.26	5.4
23	Perpendicular	62	58	61	1.5	4536.97	67.36	0.33	1.14	0.38	7.9
24	Perpendicular	78	65	51	1.3	6442.35	80.26	0.20	1.24	0.25	5.2
25	Perpendicular	98	58	60	1.5	7257.26	85.19	0.21	1.27	0.26	5.5
26	Perpendicular	83	58	61	1.5	6166.82	78.53	0.24	1.23	0.30	6.3
~~27~~	~~Perpendicular~~	~~80~~	~~60~~	~~51~~	~~2.5~~	~~6132.67~~	~~78.31~~	~~0.41~~	~~1.22~~	~~0.50~~	10.5

Table C2-10: Point load test results for sample i/PLT10 (irregular lumps)

Rock Description = Unweathered, strong, dark whitish-grey, graphitic bearing pelitic schist

Sample No.	*Description*	*W (mm)*	*D (mm)*	*L (mm)*	*P (kN)*	*D_e^2 (mm^2)*	*De (mm)*	*Is*	*F*	*Is_{50}*	*UCS (MPa)*
1	Perpendicular	90	75	69	16.0	8562	93	1.87	1.32	2.47	51.8
~~2~~	~~Perpendicular~~	~~89~~	~~71~~	~~71~~	~~7.0~~	~~8053~~	~~90~~	~~0.87~~	~~1.30~~	~~1.13~~	23.8
3	Perpendicular	88	76	72	17.0	8580	93	1.98	1.32	2.61	54.9
~~4~~	~~Perpendicular~~	~~96~~	~~79~~	~~84~~	~~24.0~~	~~9688~~	~~98~~	~~2.48~~	~~1.36~~	~~3.36~~	70.6
5	Perpendicular	102	70	51	11.0	9189	96	1.20	1.34	1.60	33.7
6	Perpendicular	103	64	60	10.5	8377	92	1.25	1.31	1.65	34.6
~~7~~	~~Perpendicular~~	~~98~~	~~65~~	~~59~~	~~2.5~~	~~8140~~	~~90~~	~~0.31~~	~~1.30~~	~~0.40~~	8.4
8	Perpendicular	87	88	52	19.0	9737	99	1.95	1.36	2.65	55.6
9	Perpendicular	107	71	59	10.0	9698	98	1.03	1.36	1.40	29.4
10	Perpendicular	88	83	60	17.5	9264	96	1.89	1.34	2.54	53.3
~~11~~	~~Perpendicular~~	~~71~~	~~63~~	~~51~~	~~1.5~~	~~5736~~	~~76~~	~~0.26~~	~~1.21~~	~~0.32~~	6.6
12	Perpendicular	92	82	61	14.0	9599	98	1.46	1.35	1.97	41.5
~~13~~	~~Perpendicular~~	~~75~~	~~56~~	~~51~~	~~21.0~~	~~5362~~	~~73~~	~~3.92~~	~~1.19~~	~~4.65~~	97.6
14	Perpendicular	73	69	51	7.0	6398	80	1.09	1.24	1.35	28.4
~~15~~	~~Perpendicular~~	~~68~~	~~58~~	~~59~~	~~3.5~~	~~5068~~	~~71~~	~~0.69~~	~~1.17~~	~~0.81~~	17.0
16	Perpendicular	72	57	50	11.0	5244	72	2.10	1.18	2.48	52.0
17	Perpendicular	65	53	64	8.0	4384	66	1.82	1.13	2.07	43.5
~~18~~	~~Perpendicular~~	~~83~~	~~63~~	~~59~~	~~16.0~~	~~6639~~	~~81~~	~~2.41~~	~~1.25~~	~~3.00~~	63.0
19	Perpendicular	102	79	59	19.5	10232	101	1.91	1.37	2.62	55.0
20	Perpendicular	87	83	53	18.5	9216	96	2.01	1.34	2.69	56.5
21	Perpendicular	79	77	50	12.0	7745	88	1.55	1.29	2.00	42.0
~~22~~	~~Perpendicular~~	~~85~~	~~73~~	~~58~~	~~19.0~~	~~7900~~	~~89~~	~~2.40~~	~~1.30~~	~~3.12~~	65.4
23	Perpendicular	82	66	50	10.0	6891	83	1.45	1.26	1.82	38.3
24	Perpendicular	86	74	66	15.0	8103	90	1.85	1.30	2.41	50.6
25	Perpendicular	99	89	64	13.0	11219	106	1.16	1.40	1.62	34.1

26	Perpendicular	92	90	71	11.5	10542	103	1.09	1.38	1.51	31.7
~~27~~	~~Perpendicular~~	~~110~~	~~88~~	~~71~~	~~24.0~~	~~12325~~	~~111~~	~~1.95~~	~~1.43~~	~~2.79~~	58.6
~~28~~	~~Perpendicular~~	~~87~~	~~72~~	~~54~~	~~31.0~~	~~7976~~	~~89~~	~~3.89~~	~~1.30~~	~~5.05~~	106.0
~~29~~	~~Perpendicular~~	~~99~~	~~79~~	~~57~~	~~20.0~~	~~9958~~	~~100~~	~~2.01~~	~~1.36~~	~~2.74~~	57.6
30	Perpendicular	100	105	62	15.0	13369	116	1.12	1.46	1.64	34.4
31	Perpendicular	92	82	45	8.5	9576	98	0.89	1.35	1.20	25.2
32	Perpendicular	94	74	42	9.0	8878	94	1.01	1.33	1.35	28.3
~~33~~	~~Perpendicular~~	~~91~~	~~76~~	~~63~~	~~4.0~~	~~8836~~	~~94~~	~~0.45~~	~~1.33~~	~~0.60~~	12.6
~~34~~	~~Perpendicular~~	~~100~~	~~96~~	~~60~~	~~10.0~~	~~12263~~	~~111~~	~~0.82~~	~~1.43~~	~~1.17~~	24.5
35	Perpendicular	91	57	71	8.0	6603	81	1.21	1.24	1.51	31.7
~~36~~	~~Perpendicular~~	~~101~~	~~54~~	~~53~~	~~1.5~~	~~6987~~	~~84~~	~~0.21~~	~~1.26~~	~~0.27~~	5.7
37	Perpendicular	80	66	50	11.0	6700	82	1.64	1.25	2.05	43.0

Table C2-11: Point load test results for sample i/PLT 11 (irregular lumps).

	Rock Description =	*Highly weathered, moderately strong, oxide stained semi-pelite to pelitic schist*									
Sample No.	*Orientation of Platens to Foliation*	*W(mm)*	*D (mm)*	*L (mm)*	*P (kN)*	*D_e^2 (mm^2)*	*De (mm)*	*Is*	*F*	*Is_{50}*	*UCS (MPa)*
1	Perpendicular	95	82	67	3.0	9918.54	99.59	0.30	1.36	0.4	8.7
2	Perpendicular	83	54	48	4.0	5692.47	75.45	0.70	1.20	0.8	17.8
3	Perpendicular	101	80	51	6.5	10304.88	101.51	0.63	1.38	0.9	18.2
~~4~~	~~Perpendicular~~	~~81~~	~~70~~	~~55~~	~~0.5~~	~~7204.31~~	~~84.88~~	~~0.07~~	~~1.27~~	~~0.1~~	1.8
5	Perpendicular	103	70	60	4.2	9228.45	96.06	0.46	1.34	0.6	12.8
~~6~~	~~Perpendicular~~	~~106~~	~~59~~	~~57~~	~~0.6~~	~~7984.02~~	~~89.35~~	~~0.08~~	~~1.30~~	~~0.1~~	2.0
7	Perpendicular	81	47	46	5.2	4766.65	69.04	1.09	1.16	1.3	26.5
8	Perpendicular	131	85	60	4.9	14108.82	118.78	0.35	1.48	0.5	10.8
9	Perpendicular	99	89	58	5.5	11173.44	105.70	0.49	1.40	0.7	14.5
~~10~~	~~Perpendicular~~	~~88~~	~~80~~	~~65~~	~~10.2~~	~~9004.87~~	~~94.89~~	~~1.13~~	~~1.33~~	~~1.5~~	31.7
~~11~~	~~Perpendicular~~	~~84~~	~~56~~	~~51~~	~~6.8~~	~~6069.80~~	~~77.91~~	~~1.12~~	~~1.22~~	~~1.4~~	28.7
12	Perpendicular	78	50	53	2.0	4981.63	70.58	0.40	1.17	0.5	9.8

13	Perpendicular	104	54	50	0.5	7152.41	84.57	0.07	1.27	0.1	1.9
14	Perpendicular	98	87	60	4.5	10888.36	104.35	0.41	1.39	0.6	12.1
15	Perpendicular	103	93	57	13.5	12192.87	110.42	1.11	1.43	1.6	33.2
16	Perpendicular	134	84	60	5.5	14331.35	119.71	0.38	1.48	0.6	11.9
17	Perpendicular	78	64	32	8.0	6315.45	79.47	1.27	1.23	1.6	32.8
18	Perpendicular	107	64	48	3.5	8679.22	93.16	0.40	1.32	0.5	11.2
19	Perpendicular	103	76	50	9.0	9939.97	99.70	0.91	1.36	1.2	25.9
20	Perpendicular	86	63	72	1.3	6834.91	82.67	0.19	1.25	0.2	5.0
21	Perpendicular	107	103	63	7.8	14026.75	118.43	0.56	1.47	0.8	17.2
22	Perpendicular	114	80	47	1.5	11574.31	107.58	0.13	1.41	0.2	3.8
23	Perpendicular	120	86	42	6.0	13159.48	114.71	0.46	1.45	0.7	13.9
24	Perpendicular	133	97	60	1.2	16409.29	128.10	0.07	1.53	0.1	2.3
25	Perpendicular	108	85	75	5.2	11658.45	107.97	0.45	1.41	0.6	13.2
26	Parallel	98	61	67	0.3	7675.72	87.61	0.03	1.29	0.0	0.9
27	Parallel	71	50	59	0.1	4546.44	67.43	0.02	1.14	0.0	0.5
28	Parallel	65	51	50	0.1	4267.99	65.33	0.02	1.13	0.0	0.6
29	Parallel	93	64	62	0.2	7646.27	87.44	0.02	1.29	0.0	0.5
30	Parallel	85	68	51	0.5	7415.71	86.11	0.06	1.28	0.1	1.6
31	Parallel	78	55	50	0.2	5519.05	74.29	0.03	1.20	0.0	0.7
32	Parallel	78	67	52	0.1	6663.23	81.63	0.01	1.25	0.0	0.2
33	Parallel	55	53	51	0.1	3748.24	61.22	0.01	1.10	0.0	0.3
34	Parallel	77	50	52	0.1	4922.49	70.16	0.01	1.16	0.0	0.3
35	Parallel	70	50	55	0.3	4464.61	66.82	0.06	1.14	0.1	1.3
36	Parallel	82	52	56	0.2	5383.66	73.37	0.04	1.19	0.0	0.9
37	Parallel	88	64	56	0.2	7131.17	84.45	0.02	1.27	0.0	0.6
38	Parallel	89	56	58	0.2	6340.58	79.63	0.03	1.23	0.0	0.8
39	Parallel	65	61	60	0.1	5050.97	71.07	0.02	1.17	0.0	0.5
40	Parallel	59	57	50	0.1	4296.00	65.54	0.02	1.13	0.0	0.6
41	Parallel	78	52	70	0.1	5127.45	71.61	0.02	1.18	0.0	0.5
42	Parallel	73	64	59	0.1	5954.80	77.17	0.02	1.22	0.0	0.4
43	Parallel	80	65	61	0.2	6648.35	81.54	0.02	1.25	0.0	0.6
44	Parallel	75	57	51	0.1	5413.30	73.58	0.02	1.19	0.0	0.5

C4 Ring Shear Testing

Ring shear testing was performed on the University of Canterbury, Department of Geological Sciences' Bromhead Ring Shear (WF25850). Preparation of samples followed BS1377:Part 7:1990 with material passing a 1.18mm sieve being retained for testing. Testing on the material was carried out at moisture contents slightly above their plastic limit. Remoulded samples are then kneaded into a lower annular ring and levelled off to the top of the mould. The upper ring is then replaced with a load hanger and a dial gauge is lowered to take an initial reading. The water bath is then filled around the sample to prevent it from drying out. A weight is placed on the hanger arm, with the specimen in the mould is being allowed to consolidate, and the total time for consolidation recorded. A shear plane is then formed by rotating the lower annular ring, 1-5 rotations within a period of approximately two minutes, whilst the upper ring is held in a fixed position by two load cells. The sample is then allowed to further consolidate so that any excess pore pressures generated during the formation of the shear plane previous step may dissipate.

The normal stress acting on the sample is calculated as follows:

$$\sigma_n = \frac{M_T + (M_w \times 10) \times g}{A \times 1000}$$

where M_T = torque arm mass = 1.143kg

M_W = Mass of hanging weight = 4-20kg in this study.

g = gravitational constant = 9.81 m/s^2

A = sample area = 4.006×10^{-3} m^2

C5 X-ray Diffraction (XRD) Analysis

Samples were wet sieved through a 4ϕ sieve with the material passing then placed in a 1000ml pipette with 20ml of Calgon (sodium hexametaphosphate) added to prevent any flocculation of the clay particles. The pipette was then plunged for 20 seconds with a sample taken from 10cm depth after a period of 8hours, thus representing the 9ϕ clay fraction of the sample (NZS4402:1986). Samples were then mounted on a glass slide and allowed to dry for XRD testing. Samples were analysed using a Phillips PW1729/PW1710 x-ray diffractometer. Mounts were irradiated with a Cu-anode ($Cu_{k\alpha}$ wavelength 1.5418 A°) at 50kV/40mA.

Clay analysis of the samples involved 3 scans per sample.

1. Air dried (dried at room temperature).
2. Glycolated (12 hours at 60°C in a saturated ethylene-glycol environment).
3. Fired (1 hour at 550°C).

The so called Braggs Law equation ($n\lambda = 2d\sin\theta$) gives the relationship where n=1 for first-order diffraction peaks, 2 for second order peaks etc., between: the x-ray wavelength used, λ; the atomic layer spacing between the diffracting planes, d; and half the angle between the incident x-rays and the diffracted x-rays, θ.

The XRD plots obtained are presented on the following pages with the peaks and the associated mineral identification tabulated.

XRD FG1 - Failure RH27 (Slip 27 Fault)

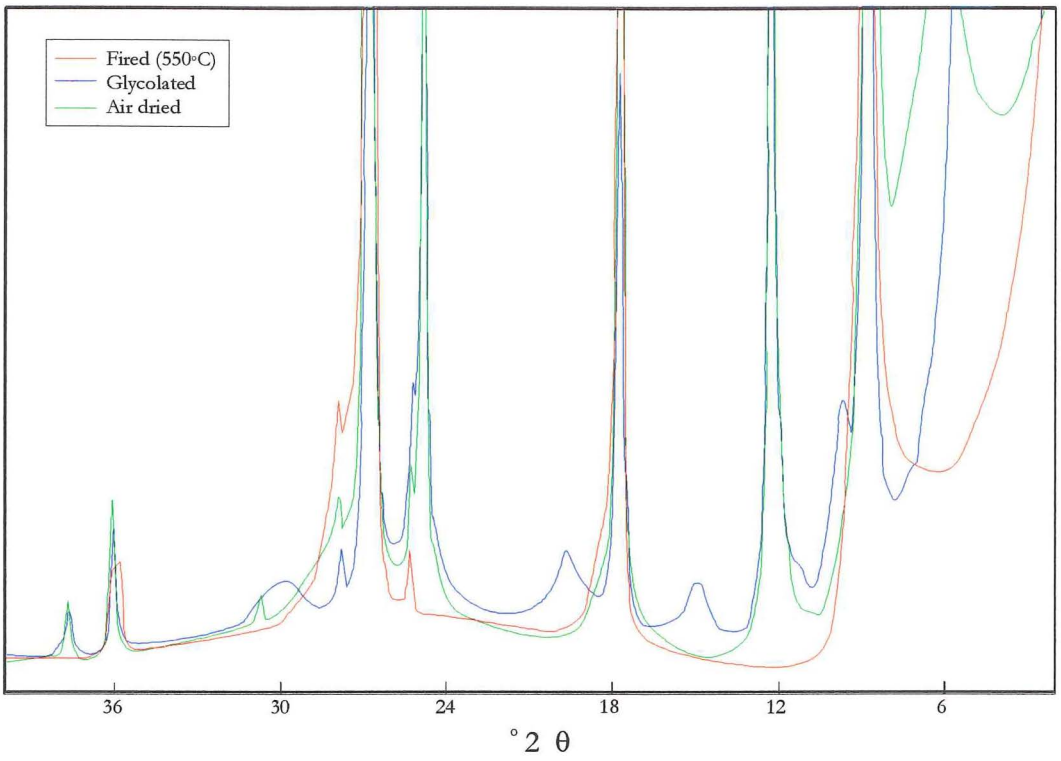

Air Dried		Glycolated		Fired (550°C)		Mineral
°2θ	d A°	°2θ	d A°	°2θ	d A°	
≈6.2	≈ 14.25	≈4.2	≈ 21.04	*Disappears*		Swelling Chlorite/Smectite + Chlorite
8.8	10.05	8.9	9.93	8.9	9.94	Muscovite
Masked		≈9.7	9.12	*Disappears?*		Swelling Chlorite/Smectite
12.4	7.14	12.4	7.14	*Disappears*		Kaolinite + Chlorite (Non-swelling)
Masked		15.0	5.91	*Disappears?*		Swelling Chlorite/Smectite
17.8	4.98	17.8	4.98	17.9	4.96	Muscovite
Masked		≈19.8	4.48	*Disappears?*		Swelling Chlorite/Smectite
24.9	3.58	24.9	3.58	*Disappears*		Kaolinite
25.3	3.52	25.3	3.52	25.4	3.51	Chlorite (Non-swelling)
26.9	3.31	26.9	3.31	26.9	3.31	Muscovite
28.0	3.19	27.9	3.20	28.0	3.19	Muscovite
30.8	2.90	≈30.8	2.90	*Disappears*		Kaolinite
36.1	2.49	36.1	2.49	36.0	2.49	Muscovite
37.7	2.39	37.7	2.39	*Disappears*		Kaolinite

XRD Sample FG2 - Failure RH28 (Bottom Fault)

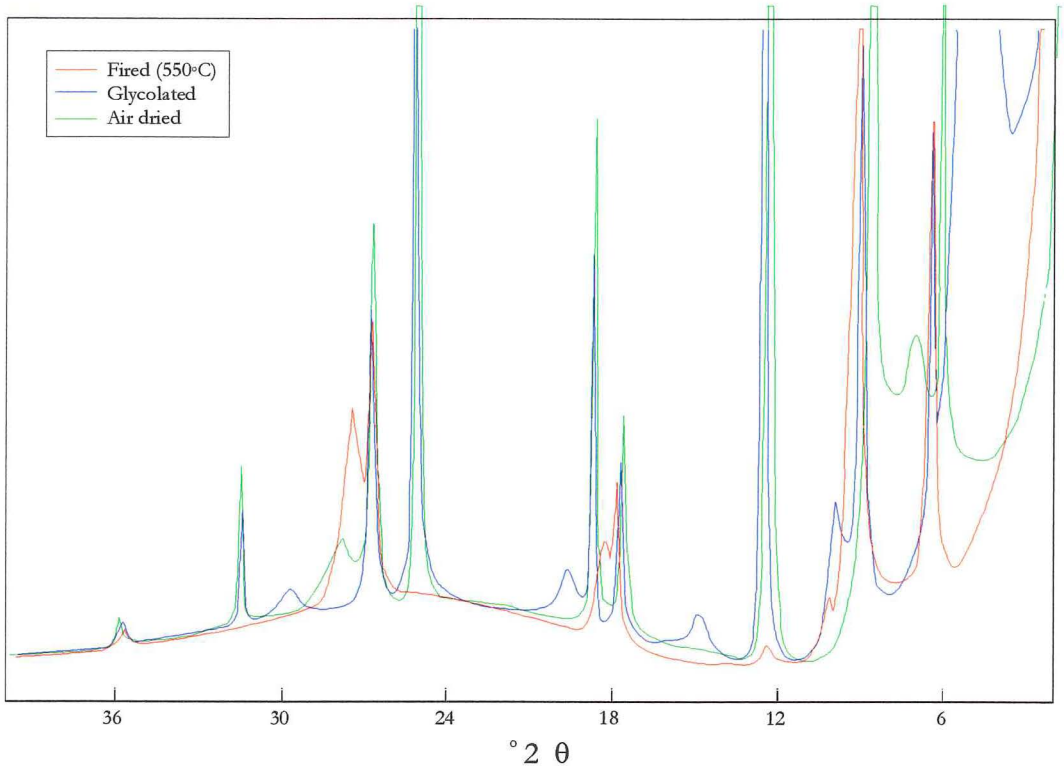

Air Dried		Glycolated		Fired (550°C)		Mineral
°2θ	d A°	°2θ	d A°	°2θ	d A°	
6.3	14.03	≈4.6	≈19.21	Disappears		Swelling Chlorite + Chlorite
≈7.2	12.28	6.2	14.25	6.2	14.25	Smectite
8.9	9.94	8.9	9.94	8.9	9.94	Muscovite
Masked		9.8	9.03	Disappears		Swelling Chlorite/Smectite
Masked		Masked		12.2	7.25	Chlorite (Non-swelling)
12.6	7.03	12.5	7.08	Disappears		Kaolinite
Masked		≈14.9	5.95	Disappears		Swelling Chlorite/Smectite
17.8	4.98	17.8	4.98	17.8	4.98	Muscovite
Masked		Masked		≈18.2	≈ 4.87	Chlorite (Non-swelling)
18.9	4.70	18.8	4.72	Masked?		Chlorite (Non-swelling)
Masked		19.7	4.51	Disappears		Swelling Chlorite/Smectite
25.3	3.52	25.2	3.53	Disappears		Kaolinite
26.9	3.31	26.9	3.31	26.9	3.31	Muscovite
≈28.0	3.19	Masked		27.6	3.23	Quartz
31.7	2.82	31.7	2.82	Disappears		Kaolinite
36.1	2.49	36.0	2.49	36.0	2.49	Muscovite

XRD FG3 - Failure RH28 (Bag Farm Fault)

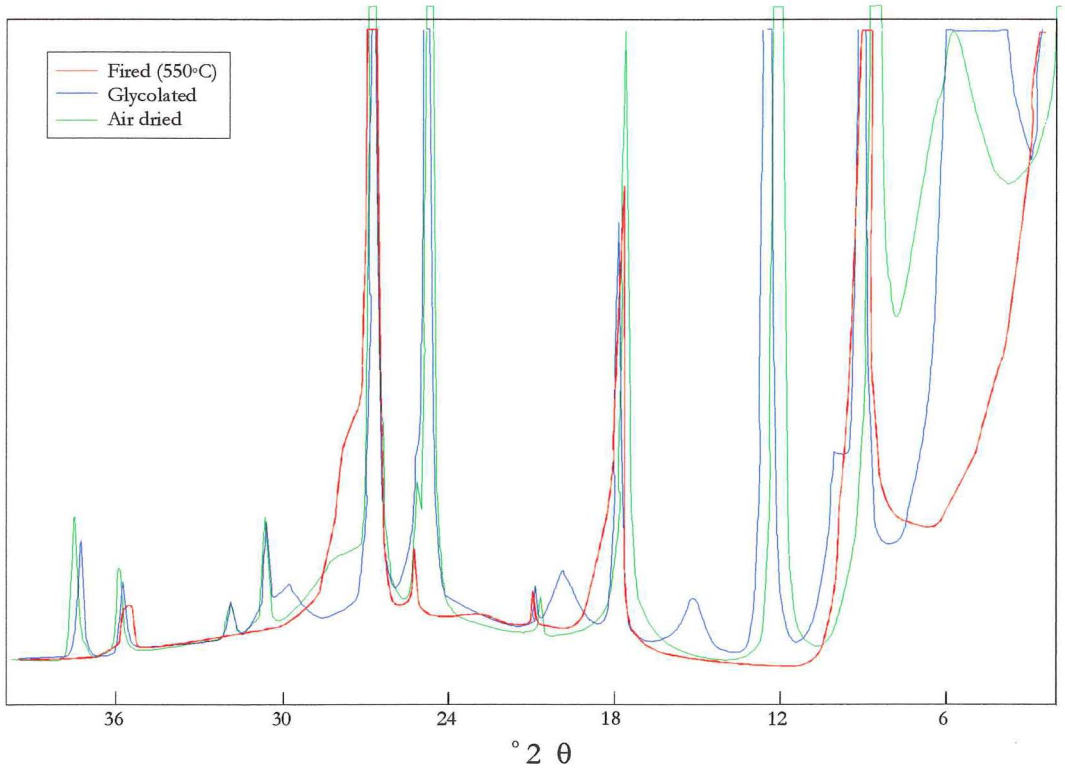

Air Dried		Glycolated		Fired (550°C)		Mineral
°2θ	d A°	*°2θ*	d A°	°2 θ	*d A°*	
6.0	14.73	*≈4.6*	≈ 19.21	Disappears		Swelling Chlorite/Smectite
8.8	10.05	*8.9*	9.94	*8.8*	10.05	Muscovite
Masked		*≈9.6*	9.21	Disappears?		Swelling Chlorite/Smectite
12.4	7.14	*12.4*	7.14	Disappears		Kaolinite + Chlorite (Non-swelling)
Masked		*≈15.0*	≈ 5.91	Disappears		Swelling Chlorite/Smectite
17.9	4.96	*17.8*	4.98	*17.8*	4.98	Muscovite
Masked		*≈19.8*	≈ 4.48	Disappears		Swelling Chlorite/Smectite
20.9	4.25	*20.8*	4.27	*20.9*	4.25	Quartz
24.9	3.58	*24.9*	3.58	Disappears		Kaolinite
25.3	3.52	Masked		*25.3*	3.52	Chlorite (Non-swelling)
27.0	3.30	*26.9*	3.31	*26.8*	3.33	Muscovite + Quartz
30.9	2.89	*30.9*	2.89	Disappears		Kaolinite
32.1	2.79	*32.2*	2.78	Disappears		Kaolinite
36.1	2.49	*36.1*	2.49	*≈36.0*	2.49	Muscovite
37.7	2.39	*37.7*	2.39	*Disappears*		Kaolinite

XRD FG4 - Failure RH33 (Basal Fault)

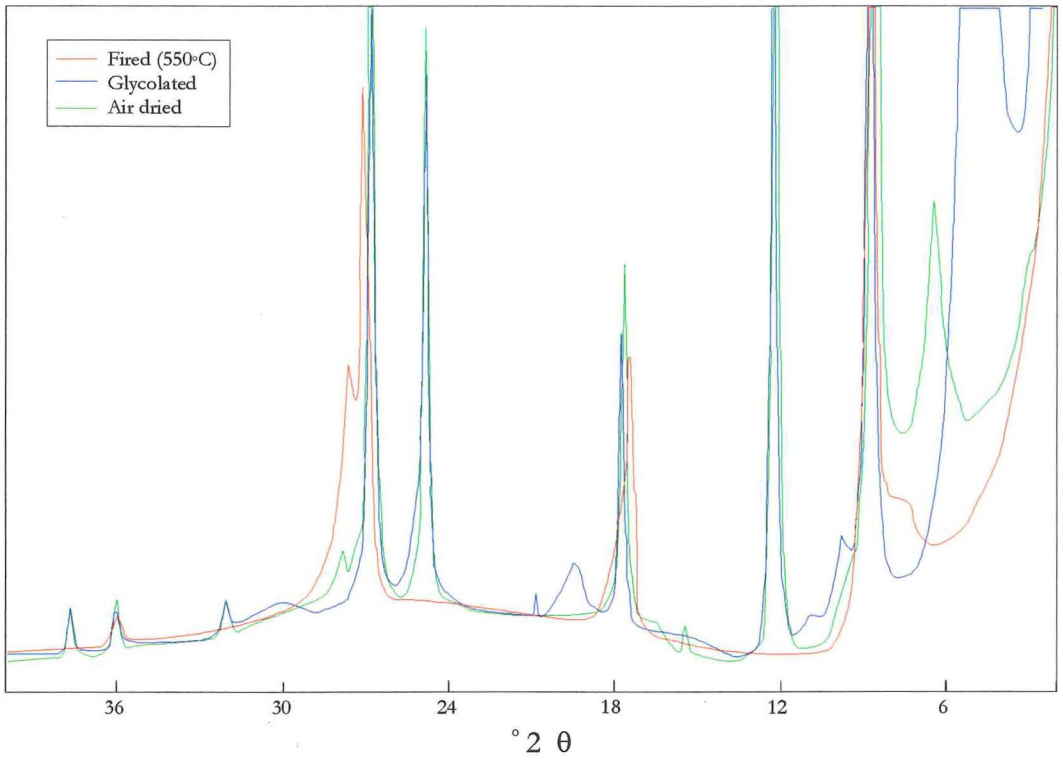

Air Dried		Glycolated		Fired (550°C)		Mineral
°2 θ	*d A°*	°2 θ	*d A°*	°2 θ	*d A°*	
6.5	*13.59*	4.9	*18.03*	*Disappears*		Swelling Chlorite/Smectite
8.8	*10.05*	8.8	*10.05*	8.9	*9.94*	Muscovite
Masked		≈ 9.8	*9.03*	*Disappears*		Swelling Chlorite/ Smectite
12.3	*7.20*	12.3	*7.20*	*Disappears*		Kaolinite
15.5	*5.72*	*Masked*		*Disappears*		Swelling Chlorite/Smectite
17.7	*5.01*	17.8	*4.98*	17.8	*4.98*	Muscovite
Masked		≈ 19.5	*≈4.55*	*Disappears*		Swelling Chlorite/Smectite
Masked		20.8	*4.27*	*Masked*		Quartz
24.9	*3.58*	24.9	*3.58*	*Disappears*		Kaolinite
26.8	*3.33*	26.9	*3.31*	26.9	*3.31*	Muscovite
≈ 27.8	*≈3.20*	≈ 27.8	*≈3.20*	27.5	*3.24*	Quartz
32.1	*2.79*	32.1	*2.79*	*Disappears*		Kaolinite
36.0	*2.49*	36.0	*2.49*	36.0	*2.49*	Muscovite
37.7	*2.39*	37.7	*2.39*	*Disappears*		Kaolinite

XRD Sample FG5 - Round Hill (Battery Creek Fault)

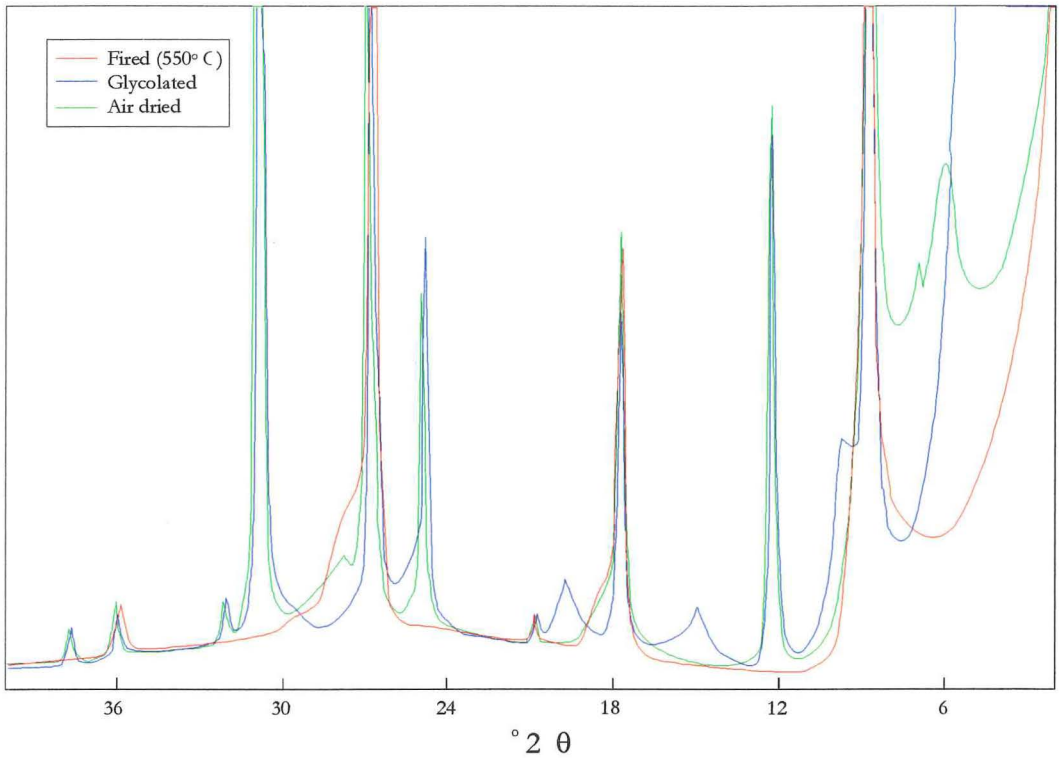

Air Dried		Glycolated		Fired (550°C)		Mineral
°2 θ	*d A°*	°2 θ	*d A°*	°2 θ	*d A°*	
6.1	*14.48*	≈(4.1)	*≈(21.55)*	*Disappears*		Swelling Chlorite/
7.0	*12.6*					Smectite
8.9	*9.94*	8.9	*9.94*	8.9	*9.94*	Muscovite
Masked		9.7	*9.12*	*Disappears*		Swelling Chlorite/Smectite
12.4	*7.13*	12.4	*7.13*	*Disappears*		Kaolinite
Masked		15.1	*5.87*	*Disappears*		Swelling Chlorite/Smectite
17.8	*4.98*	17.8	*4.98*	17.8	*4.98*	Muscovite
Masked		19.8	*4.48*	*Disappears*		Swelling Chlorite/Smectite
20.9	*4.25*	20.8	*4.27*	20.8	*4.27*	Quartz
24.9	*3.58*	24.9	*3.58*	*Disappears*		Kaolinite
26.9	*3.31*	26.9	*3.31*	26.9	*3.31*	Muscovite + Quartz
30.9	*2.89*	30.8	*2.90*	*Disappears*		Kaolinite?
32.2	*2.78*	32.2	*2.78*	*Disappears*		Kaolinite?
36.1	*2.49*	36.1	*2.49*	35.9	*2.50*	Muscovite
37.8	*2.38*	37.7	*2.39*	*Disappears*		Kaolinite

XRD Sample FG10 - Failure RH35

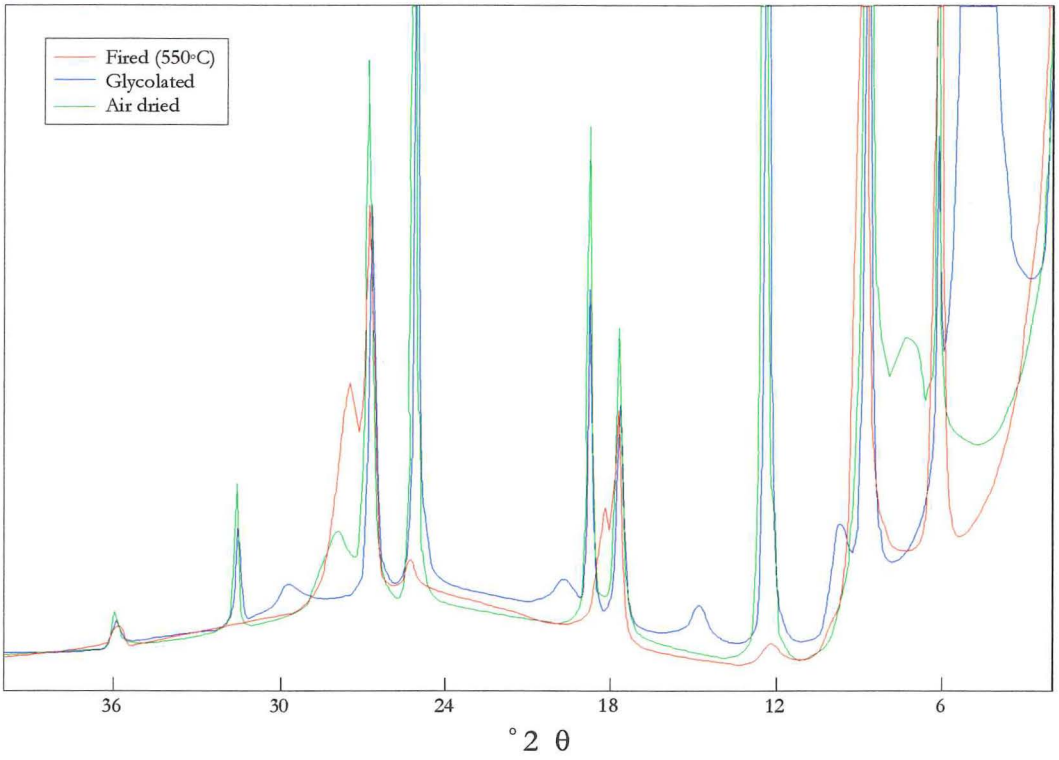

Air Dried		Glycolated		Fired (550°C)		Mineral
°2θ	d A°	°2θ	d A°	°2θ	d A°	
6.2	14.25	*6.2*	14.25	*6.2*	14.25	Chlorite (Non-swelling)
≈7.3	≈ 12.11	*≈4.8*	≈ 18.41	*Disappears*		Swelling Chlorite/Smectite
8.8	10.05	*8.8*	10.05	*8.9*	9.94	Muscovite
Masked		*≈9.7*	≈ 9.12	*Disappears?*		Swelling Chlorite/Smectite
12.6	7.03	*12.4*	7.14	*≈12.3*	≈ 7.20	Kaolinite + Chlorite (Non-swelling)
Masked		*≈14.9*	5.95	*Disappears?*		Swelling Chlorite/Smectite
17.7	5.01	*17.7*	5.01	*17.8*	4.98	Muscovite
18.8	4.72	*18.8*	4.72	*≈18.4*	4.82	Chlorite (Non-swelling)
25.3	3.52	*25.1*	3.55	*Disappears*		Kaolinite
26.9	3.31	*26.7*	3.34	*26.9*	3.31	Muscovite
≈28.1	≈ 3.19	*Masked*		*27.5*	*3.24*	Quartz
31.7	2.82	*31.6*	2.83	*Disappears*		Kaolinite
36.1	2.49	*36.0*	2.49	*35.9*	2.50	Muscovite

APPENDIX D: STEREOGRAPHIC PROJECTION TECHNIQUES

D1 The Fisher Distribution

The Fisher method for contouring was used throughout this thesis as opposed to the generally accepted Schmidt method. Under the Fisher method each pole is assigned a normal influence (or Fisher Distribution), rather than a point value as in the Schmidt method. The real advantage of the Fisher method over the Scmidt method is that it smooths density plots for sparse data sets (Hoek and Diederichs, 1989).

For a more detailed description on the mathematics behind the Fisher distribution the reader is referred to Cheeney (1982).

D2 Determination of Counting Circle Size

The size of the counting circle used in contour plots was calculated in accordance with the method outlined by Kamb (1959) where.

For a given area A, expressed as its fraction of the area of the hemisphere, the distribution of n values for random samples of size N is binomial, and for a population without preferred orientation we find

$$\frac{\sigma}{E} = \sqrt{\frac{(1-A)}{NA}}$$

where E = NA

Setting $\sigma/E = 1/3$, we compute for a given fabric with N points the appropriate area A of the counter to be used in preparing the density diagram.

D3 Calculation of Terzaghi Weighting Function

The geometric weighting function in Dips is calculated as follows (Hoek and Diederichs, 1989):

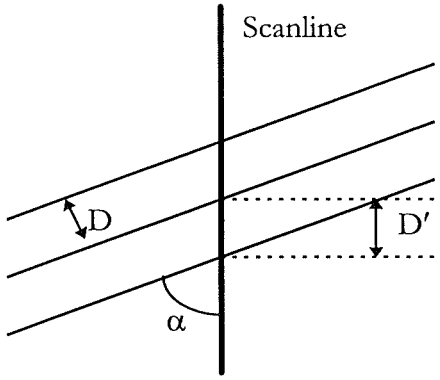

α		Minimum angle between plane and traverse
D′		Apparent spacing along traverse
D	= D′sin α = D′ 1/W	True spacing of discontinuity set
R′	= 1/D′	Apparent density of joint population
R	= 1/D = 1/D′ sin α = D′cosec α	True density of joint population
W	= (1) cosec α	Weighting applied to individual pole before density calculation.

Since the weighting function tends to infinity as α approaches 0°, a maximum weighting must be set to prevent unreasonable results. This maximum limit corresponds to a minimum angle, before the weighting function is applied. For the interpretation of structural domains in the minimum α angle before the weighting function was applied was set to 15°.

APPENDIX E: STRUCTURAL DOMAIN STEREOPLOTS

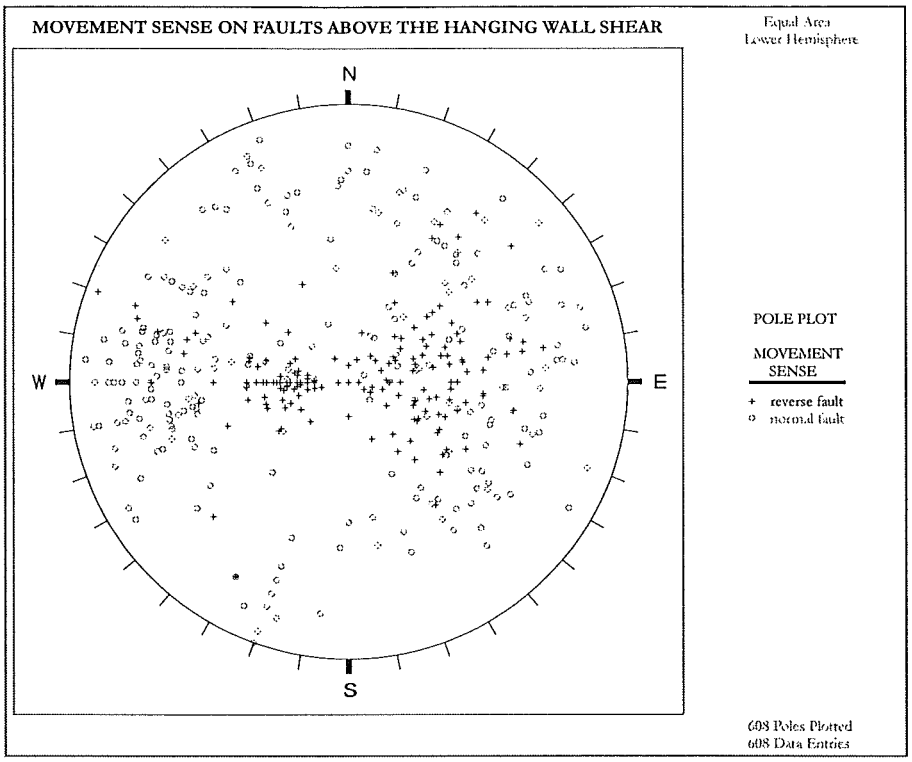

Figure E-1: Pole plot of movement sense for faults above Hanging Wall Shear

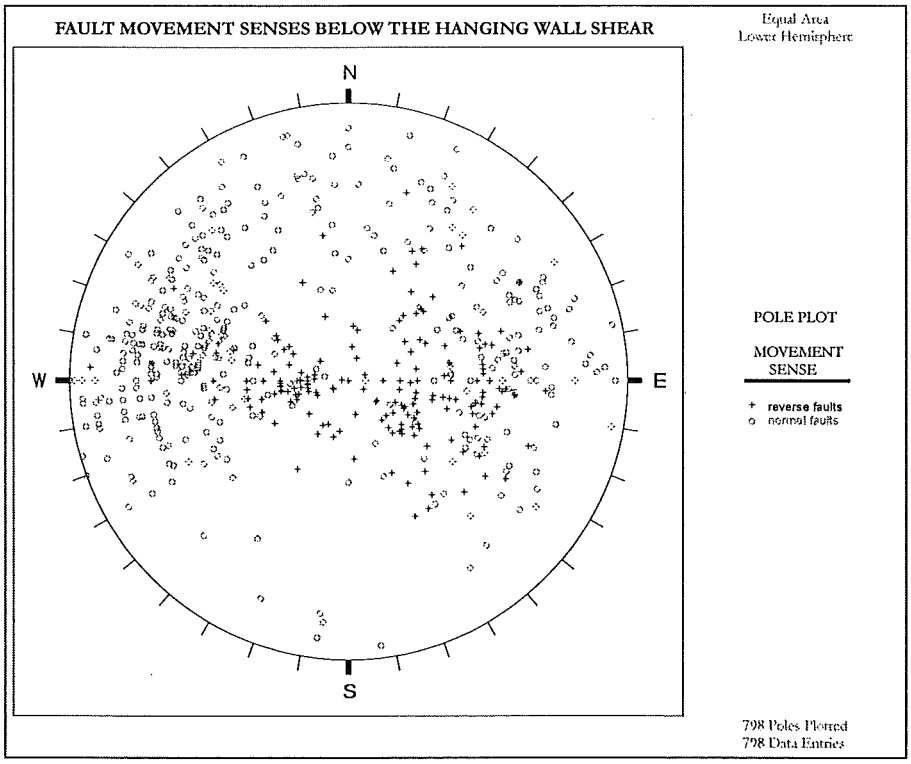

Figure E-2: Pole plot of movement sense for faults below Hanging Wall Shear.

APPENDIX F: PIT SLOPE FAILURE DATABASE AND MODELS

F1 Pit Slope Failure Types

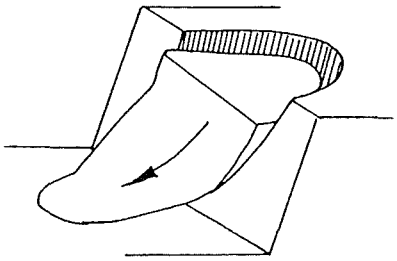

a. Circular failure in overburden soil, waste rock or heavily fractured rock with no identifiable structural pattern.

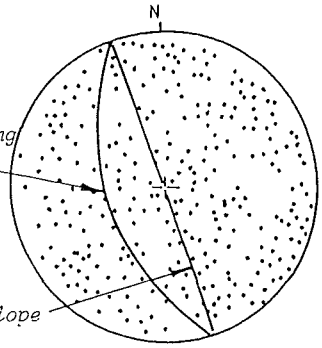

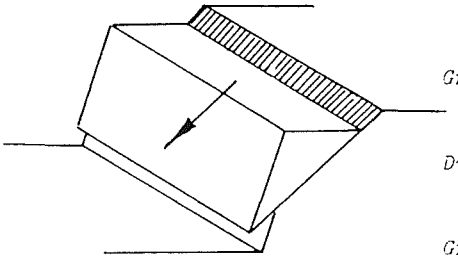

b. Plane failure in rock with highly ordered structure such as slate.

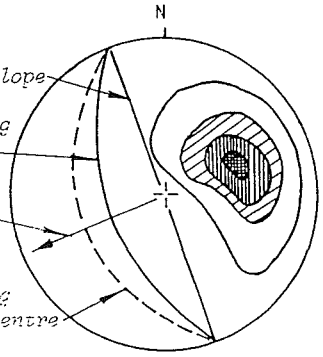

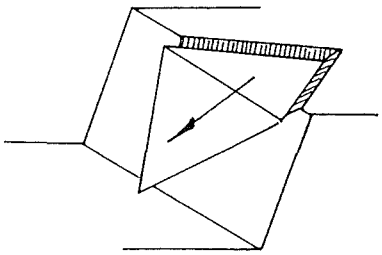

c. Wedge failure on two intersecting discontinuities.

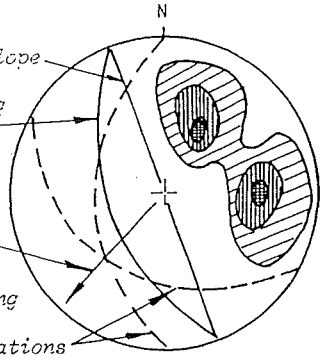

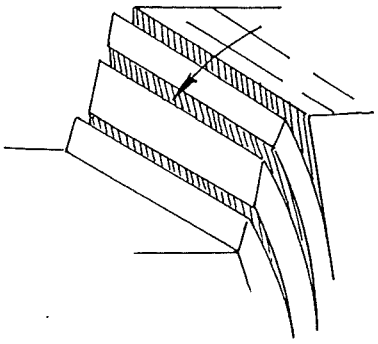

d. Toppling failure in hard rock which can form columnar structure separated by steeply dipping discontinuities.

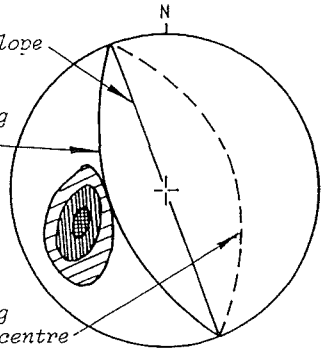

(After Hoek and Bray, 1981)

F2 Pit Slope Failure Terminology

NAME	DEFINITION
Crown	Practically undisplaced material adjacent to highest parts of main scarp
Main scarp	Steep surface on undisturbed ground at upper edge of landslide caused by movement of displaced material (*13*, stippled area) away from undisturbed ground; it is visible part of surface of rupture (*10*)
Top	Highest point of contact between displaced material (*13*) and main scarp (*2*)
Head	Upper parts of landslide along contact between displaced material and main scarp (*2*)
Minor scarp	Steep surface on displaced material of landslide produced by differential movements within displaced material
Main body	Part of displaced material of landslide that overlies surface of rupture between main scarp (*2*) and toe of surface of rupture (*11*)
Foot	Portion of landslide that has moved beyond toe of surface of rupture (*11*) and overlies original ground surface (*20*)
Tip	Point on toe (9) farthest from top (3) of landslide
Toe	Lower, usually curved margin of displaced material of a landslide, most distant from main scarp (*2*)
Surface of rupture	Surface that forms (or that has formed) lower boundary of displaced material (*13*) below original ground surface (*20*); mechanical idealization of surface of rupture is called *slip surface* in Chapter 13
Toe of surface of rupture	Intersection (usually buried) between lower part of surface of rupture (*10*) of a landslide and original ground surface (*20*)
Surface of separation	Part of original ground surface (*20*) now overlain by foot (*7*) of landslide
Displaced material	Material displaced from its original position on slope by movement in landslide; forms both depleted mass (*17*) and accumulation (*18*); it is stippled in Figure 3-4
Zone of depletion	Area of landslide within which displaced material (*13*) lies below original ground surface (*20*)
Zone of accumulation	Area of landslide within which displaced material lies above original ground surface (*20*)
Depletion	Volume bounded by main scarp (*2*), depleted mass (*17*), and original ground surface (*20*)
Depleted mass	Volume of displaced material that overlies surface of rupture (*10*) but underlies original ground surface (*20*)
Accumulation	Volume of displaced material (*13*) that lies above original ground surface (*20*)
Flank	Undisplaced material adjacent to sides of surface of rupture; compass directions are preferable in describing flanks, but if left and right are used, they refer to flanks as viewed from crown
Original ground surface	Surface of slope that existed before landslide took place

F3 Classification of Landslide Movement Rates

Table F3: Suggested method for describing the rate of movement of a landslide (International Union of Geological Sciences Working Group on Landslides, Table 1, 1995)

Velocity Class.	Description of Velocity	Velocity Limits
7	Extremely rapid	>5m/sec
6	Very rapid	3m/min - 5m/sec
5	Rapid	1.8m/hour - 3m/min
4	Moderate	13m/month - 1.8m/hour
3	Slow	1.6m/year - 13m/month
2	Very slow	16mm/year - 1.6m/year
1	Extremely slow	<16mm/year

F4 Standard Recording Sheet for Pit Slope Failures

PIT SLOPE FAILURE REPORT FOR MACRAES GOLD MINE

Pit Affected: _____ **Failure No. (Name):** _____

Report Compiled By: _____

Mapped By: _____

Location: _____ *easting to* _____ *easting*

_____ *northing to* _____ *northing*

Bench Levels Affected: _____ *R.L. to* _____ *R.L.*

Timing Details: *First indications of failure* _____ *date* _____ *hours*

Timing of main failure _____ *date* _____ *hours*

Pit Slope Details: (prior to failure)

Berm Height = _____ metres

Bench Width = _____ metres

Berm Angle = _____ °

Slope Dip Direction = _____ °

Overall Slope Angle = _____ °

Antecedent Conditions Contributing to Pit Slope Failure (*attach records*):

_____

_____

_____

_____

_____

_____

_____

_____

_____

_____

FAILURE DESCRIPTION

Failure Type: ☐ Planar ☐ Wedge ☐ Circular ☐ Toppling ☐ Other

comments: _____

_____

_____

Movement Rate: *Initial Movement* = _____

Subsequent Movement = _____

Failure Dimensions: *Crest Width* = _____ metres

Crest Length = _____ metres

Depth = _____ metres

Height = _____ metres

Failure Volume: ≈ _____ m^3

Failure Material: i) ☐ oxidised ☐ unoxidised

ii) ☐ waste ☐ mineralised

comments: _____

_____

_____

Engineering Geological Description of Failure Material: _____

_____

_____

_____

_____

_____

_____

GEOTECHNICAL DETAILS OF DISCONTINUITIES CONTROLLING SLOPE FAILURE

CONTROLLING DEFECT INFORMATION												
Obs. No. (Name)	*Type*	*Dip*	*Dip Direction*	*Length (m)*	*Weathering*	*Persistence*	*Termination*		*Roughness*	*Aperture Width*	*Water*	*Comments*
							left	*right*				

DESCRIPTION OF APERTURE MATERIAL								
Obs. No. (Name)	*Type*	*Thickness (cm)*	*Weathering Term*	*Colour*	*Water Content Term*	*Strength Term*	*Toughness*	*Comments*

ATTACHMENTS

Maps and Cross sections Attached ☐

Stereoplots Attached ☐

Photos Attached ☐

Movement Records Attached ☐

Other Records ☐

give details: _____

_____

_____

IMPLICATIONS OF FAILURE TO MINING OPERATIONS

_____

_____

_____

_____

_____

_____

_____

_____

_____

_____

_____

_____

_____

_____

Failure Description Summary- Macraes Pit Slope Failure Database

Failure Date	Failure Name	Failure Type	Failure Orientation	Hanging Wall Position	Volume	Easting	Northing	m R.L.	Berm Angle	Slope Angle	Slope Trend
18/06/96	RH36	Wedge	47/141	Below	100	69840	15295	360	60		141
29/05/96	IM3	Planar	20/210	Above	500	69960	14000	360	70	48	215
15/05/96	RH34	Planar	40/300	Transects	100	70165	15180	355	52		295
15/05/96	RH35	Planar	48/240	Transects	50	70170	15255	355	54		218
3/05/96	RH33	Planar	13/300	Below	325	70075	15070	360	60		325
29/04/96	RH32	Wedge	46/132	Below	100	69825	15310	400	63		125
9/03/96	IM2	Wedge	41/169	Above		69790	14010	550	48		180
16/02/96	RH30	Planar	60/100	Below	100	69875	15145	375	70		066
16/02/96	RH31	Toppling	90/182	Transects	500	70000	15310	390	68	180	54
21/07/95	RH29										
14/02/95	RH28	Complex	02/181	Above							
7/12/94	RH27	Wedge	37/240	Above	3000	70190	15235	370	70	43	222
27/07/94	RH26	Wedge	39/021					450			
17/12/93	RH25	Wedge	43/018					445			
19/10/93	RH23	Wedge						445			
17/10/93	RH22	Planar	45/315			70120	14940	430		50	293
13/10/93	RH21	Planar	57/100					405	70		270

Failure Date	Failure Name	Failure Type	Failure Orientation	Hanging Wall Position	Volume	Easting	Northing	m R.L.	Berm Angle	Slope Angle	Slope Trend.
16/06/93	RH20	Planar	59/213					455	50		270
12/03/93	RH18										
21/02/92	RH10	Planar	35/265	Above		70040	15200	460			260
21/01/92	RH8	Wedge	46/262			69618	15277	458	45		300
20/11/91	RH6	Wedge	49/225		90	69989		470	60		
11/11/91	RH5	Complex	59/213		225			460			
20/09/91	SP1 (Failure 3)	Planar	35/095	Above	840	69640	14480	532			105
16/04/91	RH2	Wedge	39/358	Below	700	69833	14976	470	60	50	000
	RH19							440			
	RH14										
	RH24	Toppling	75/180					430			000

F6 Back Analysis Models and Plots

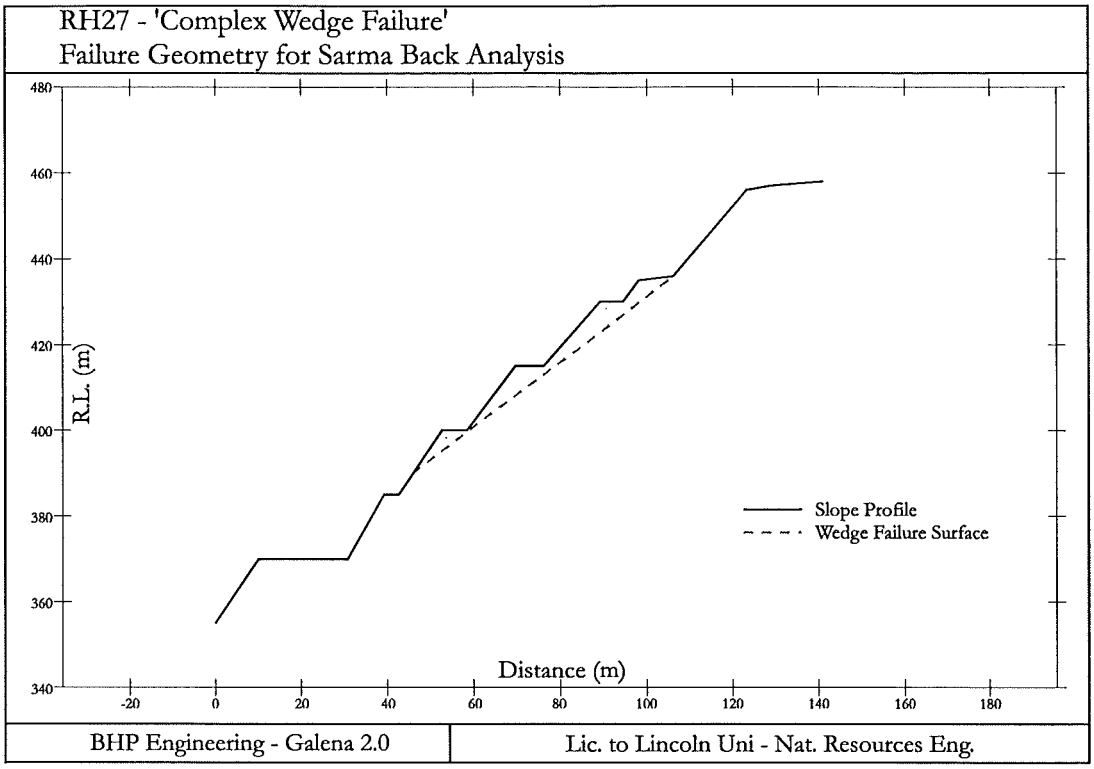

Figure F6-1: RH27 failure geometry for back analysis.

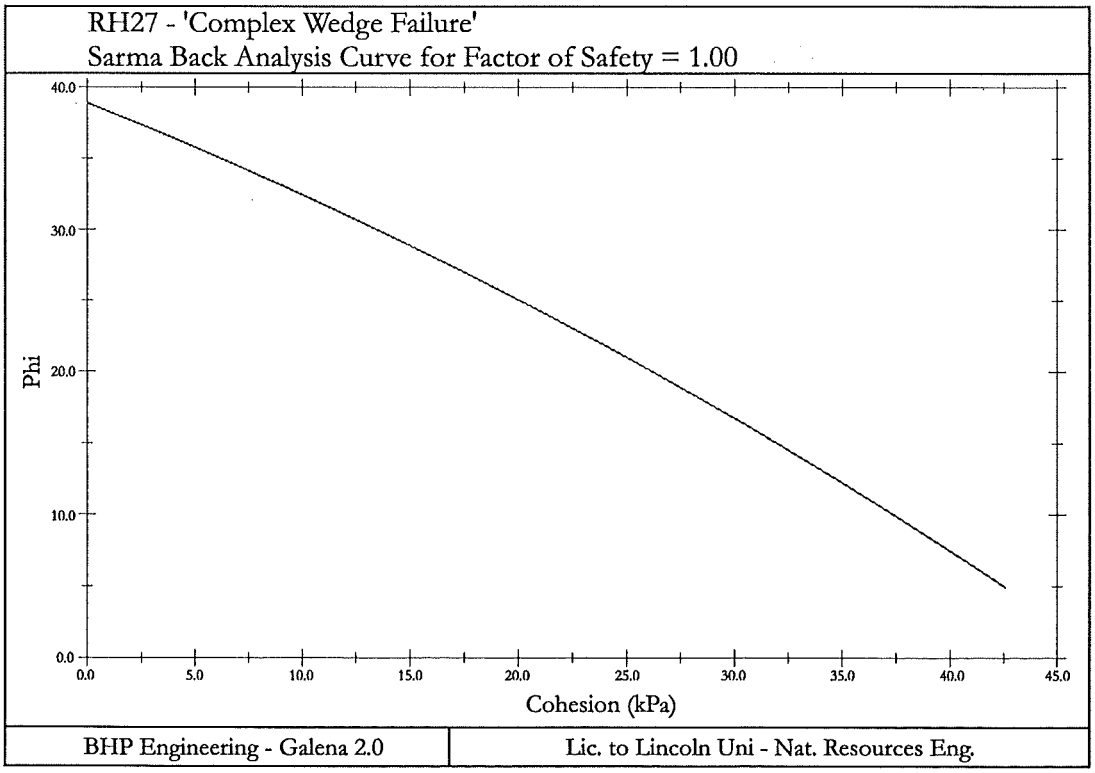

Figure F6-2: RH27 back analysis curve.

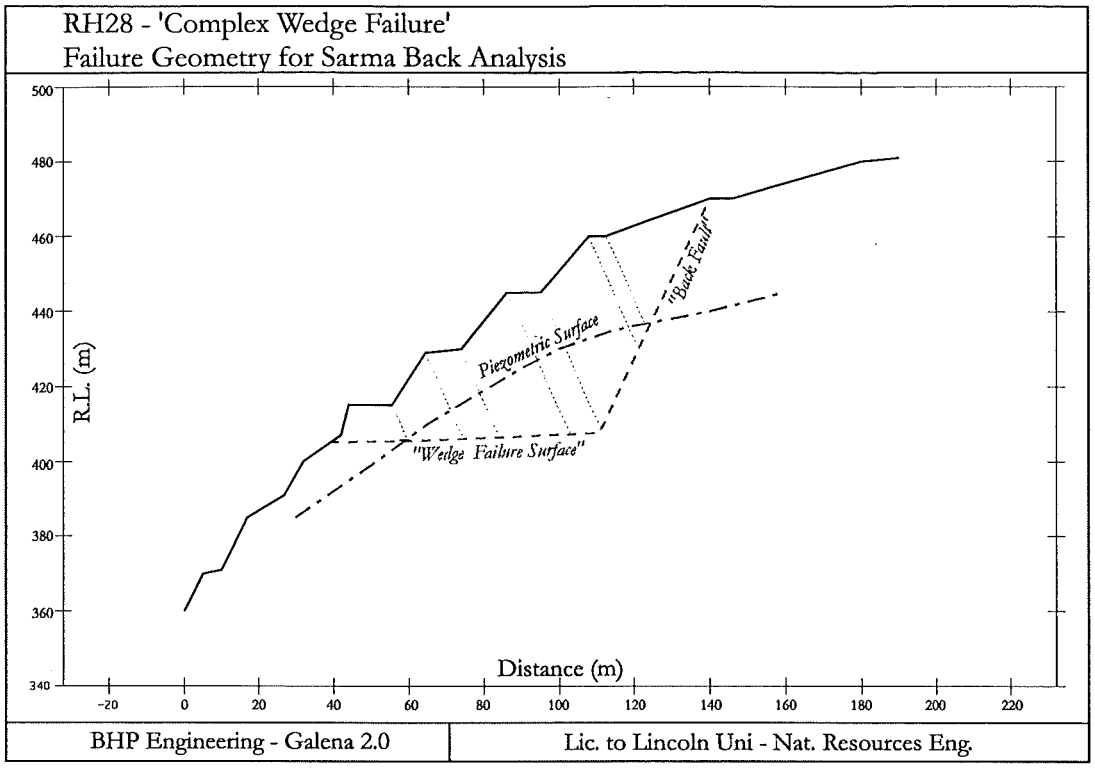

Figure F6-3: RH28 failure geometry for back analysis.

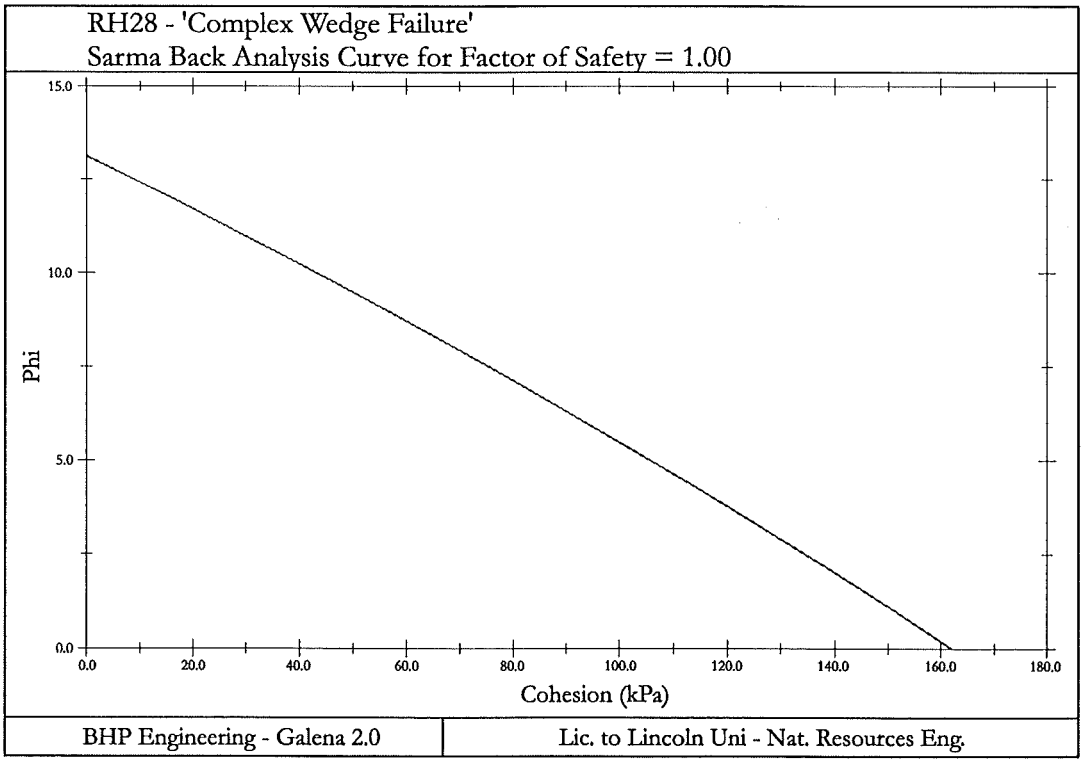

Figure F6-4: RH28 back analysis curve.

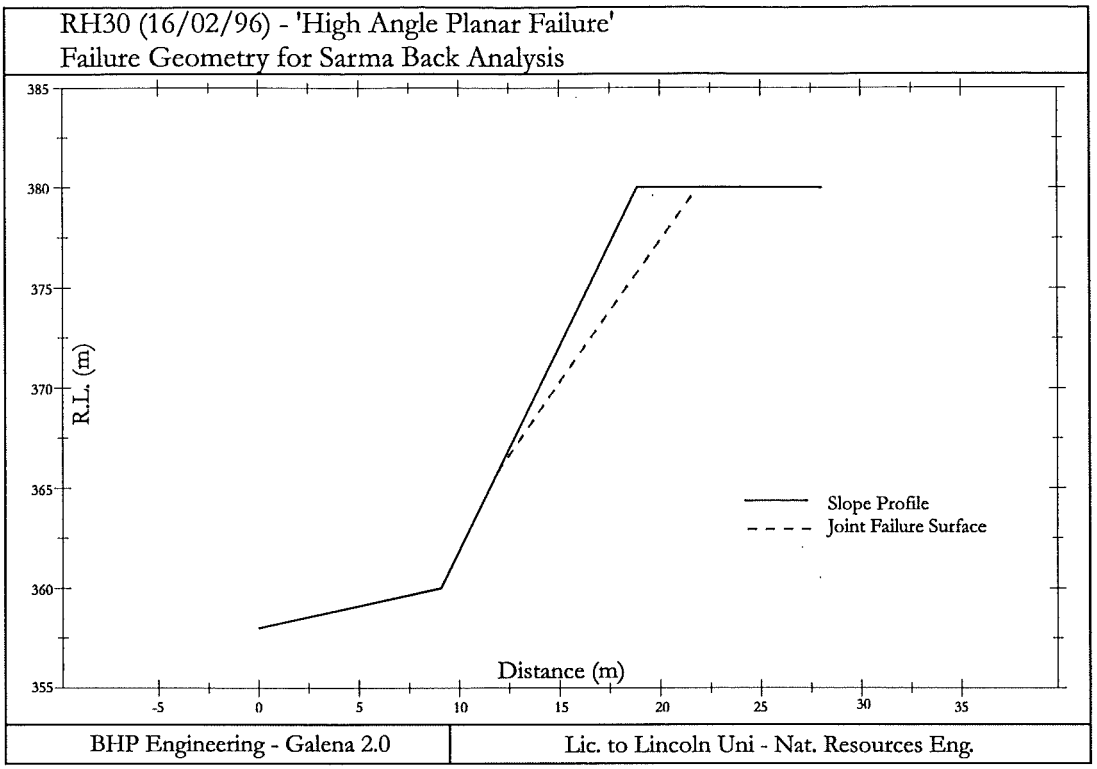

Figure F6-5: RH30 failure geometry for back analysis.

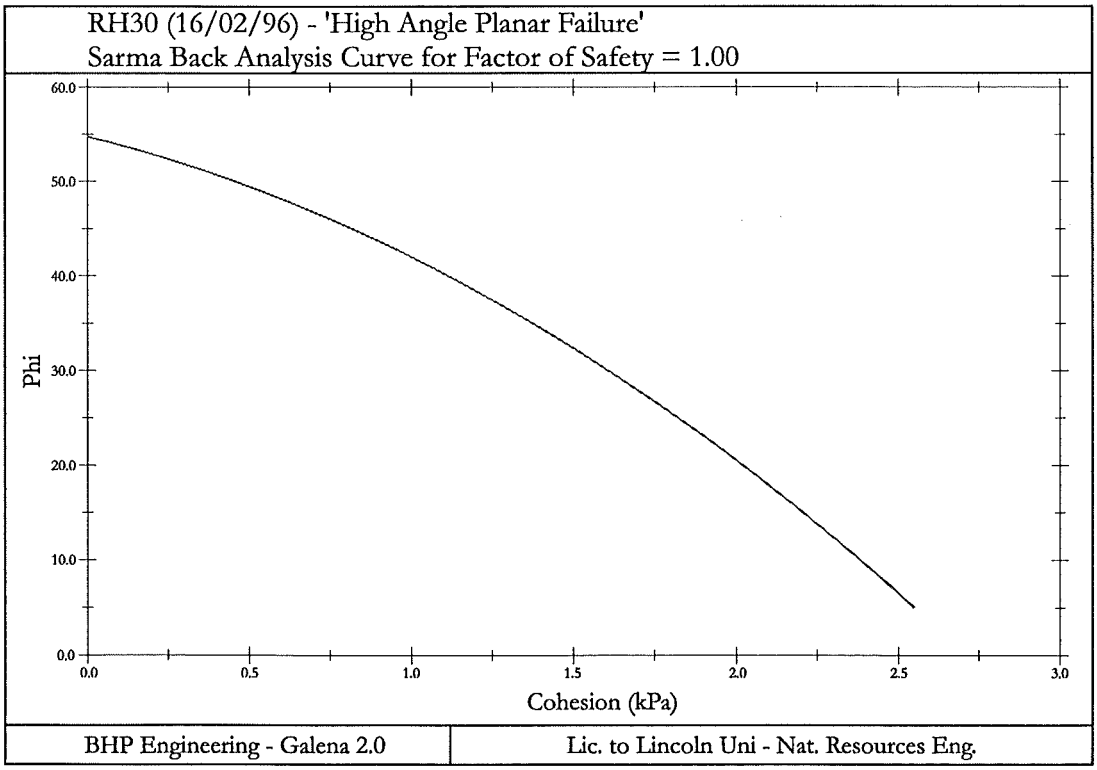

Figure F6-6: RH30 back analysis curve.

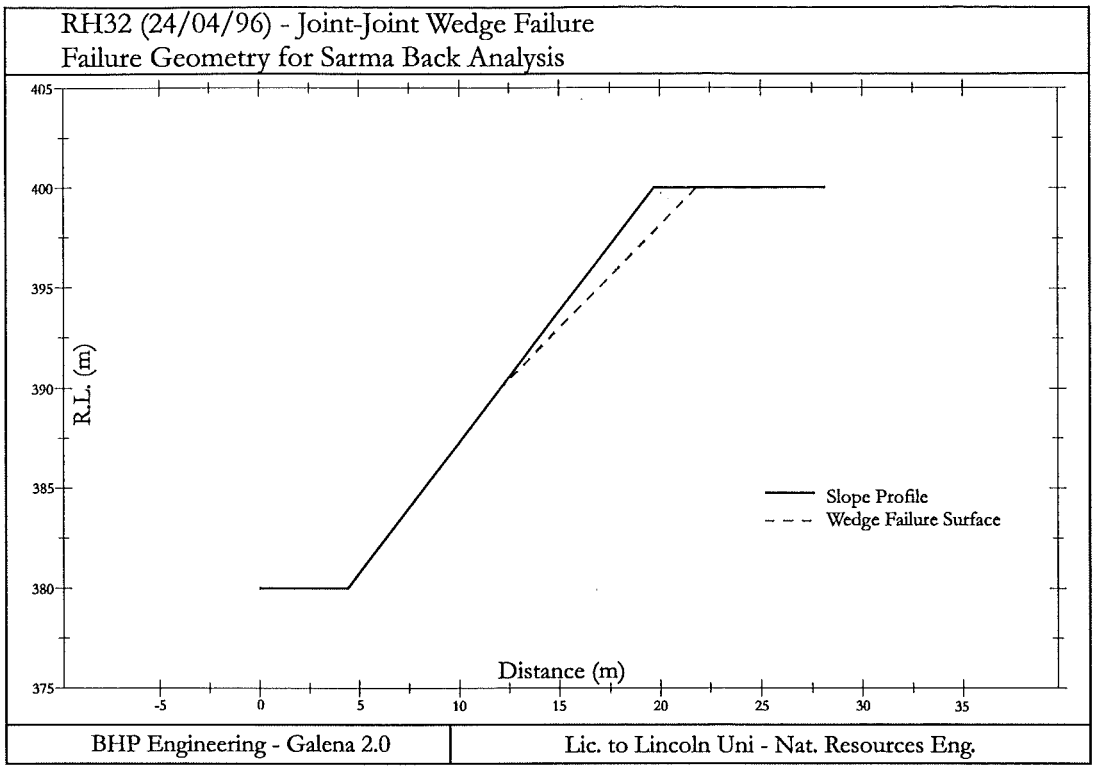

Figure F6-7: RH32 failure geometry for back analysis.

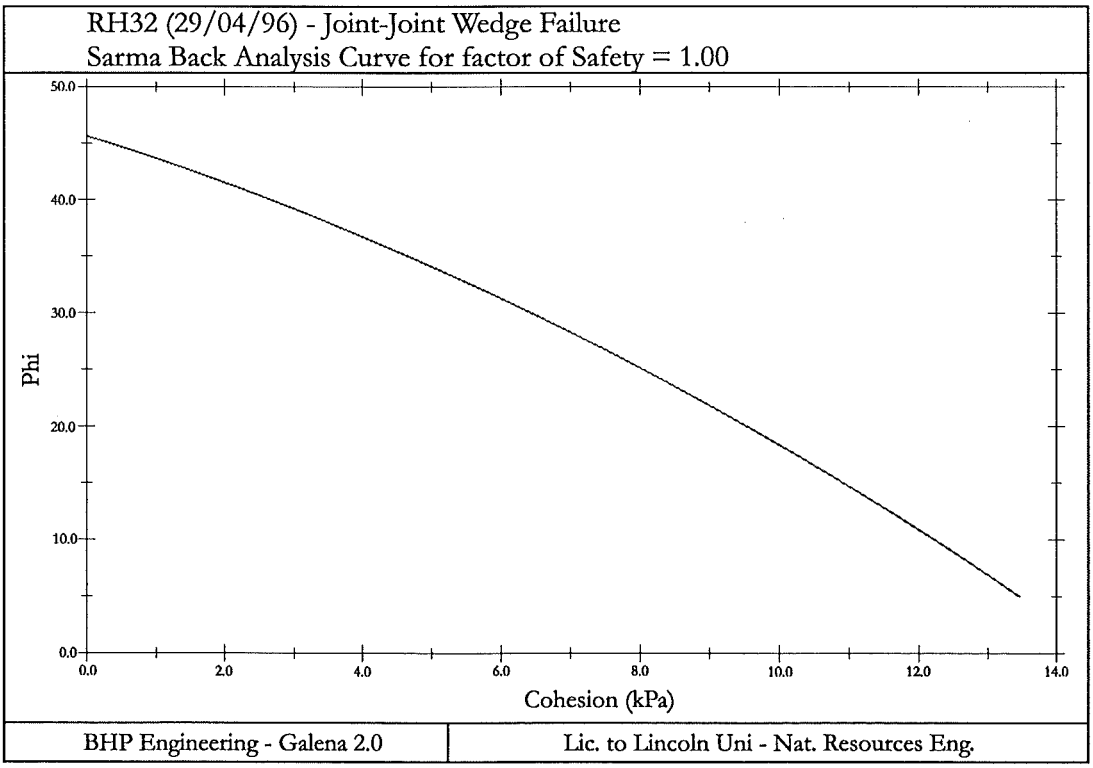

Figure F6-8: RH32 back analysis curve.

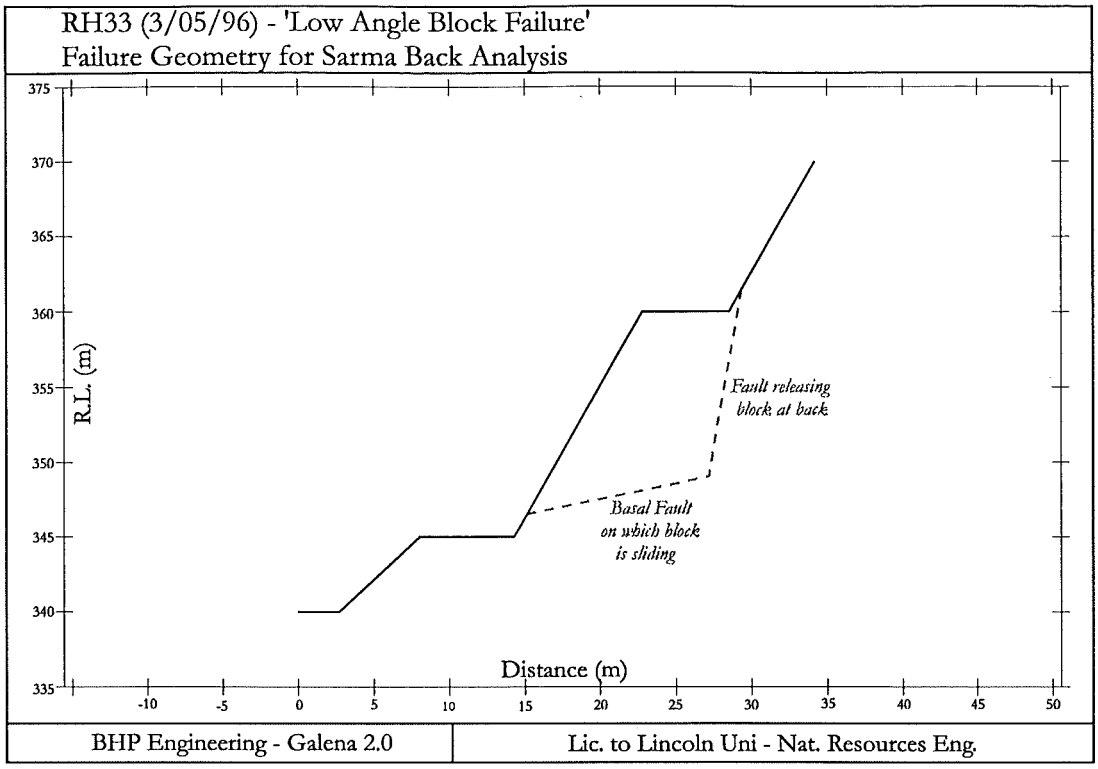

Figure F6-9: RH33 failure geometry for back analysis.

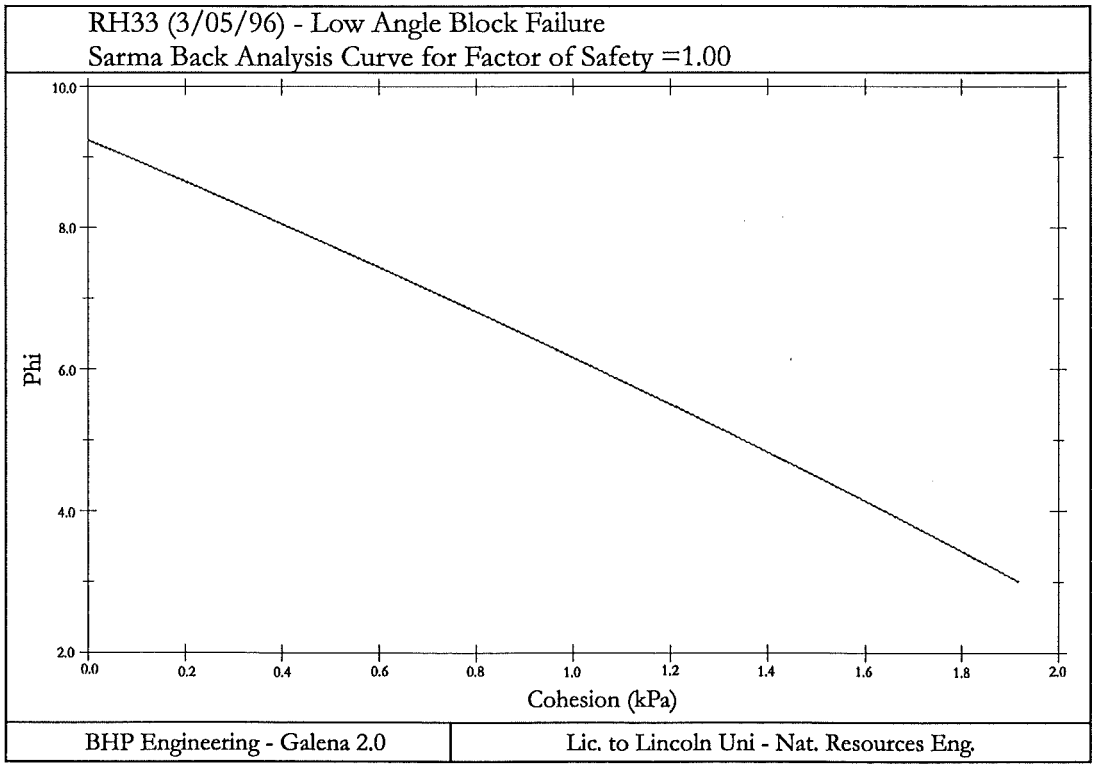

Figure F6-10: RH33 back analysis curve.

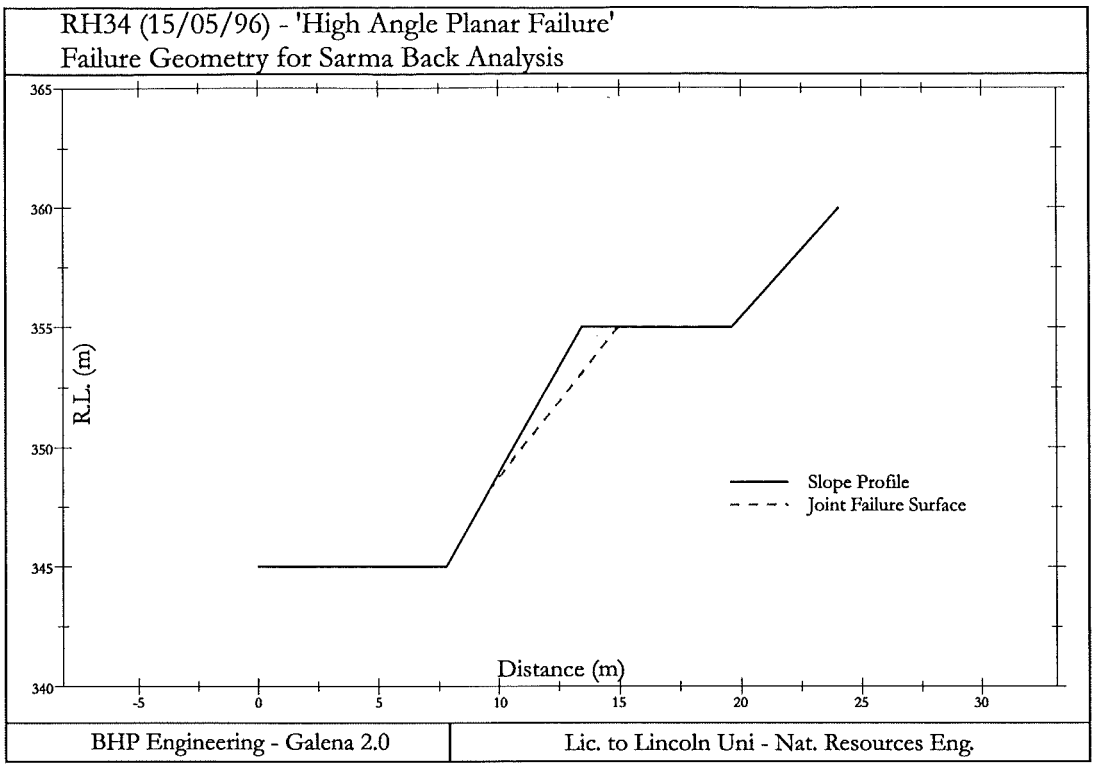

Figure F6-11: RH34 failure geometry for back analysis.

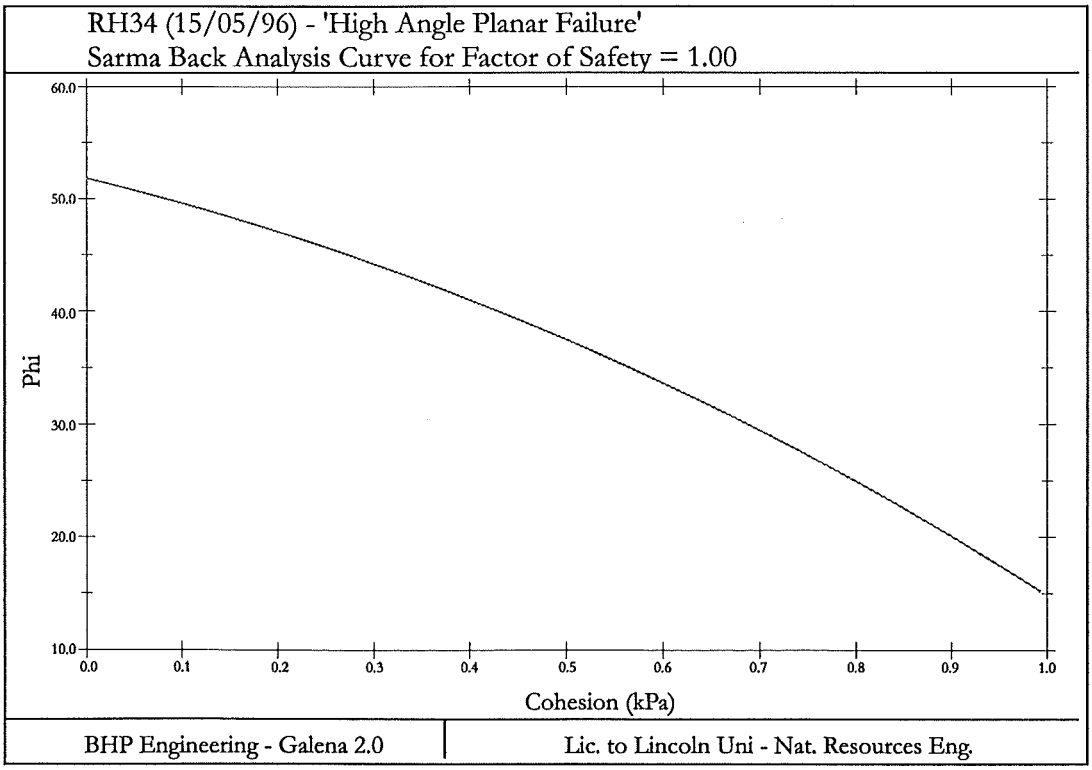

Figure F6-12: RH34 back analysis curve.

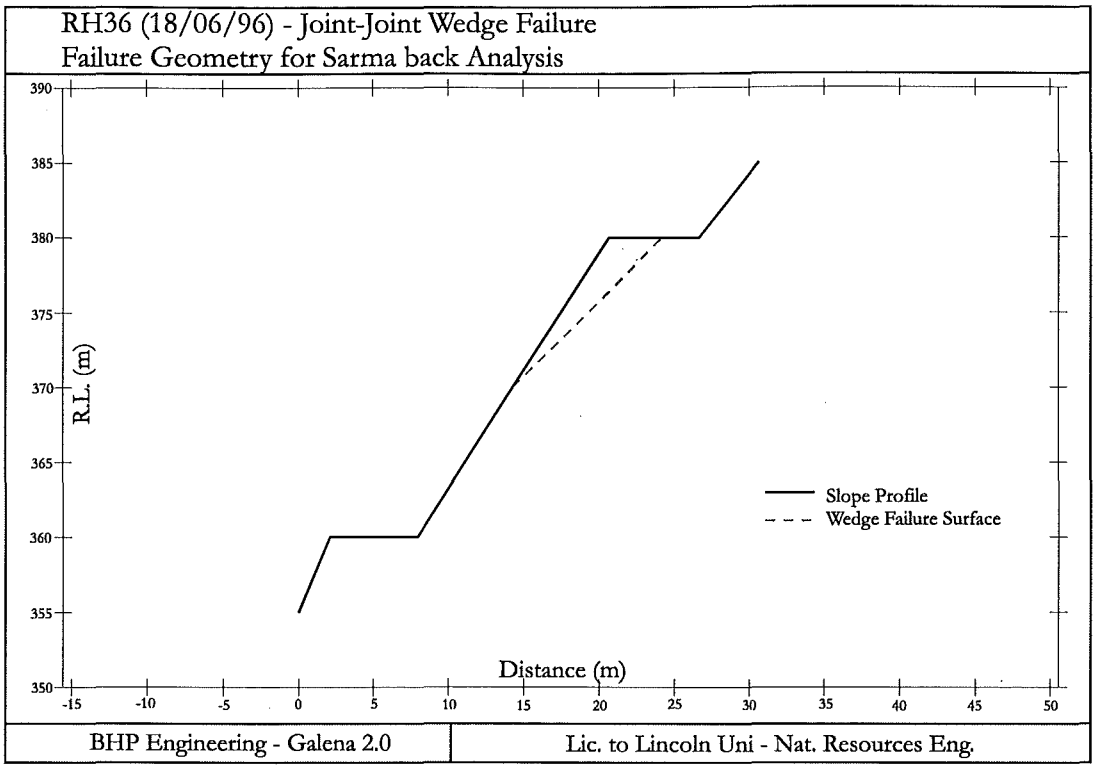

Figure F6-13: RH36 failure geometry for back analysis.

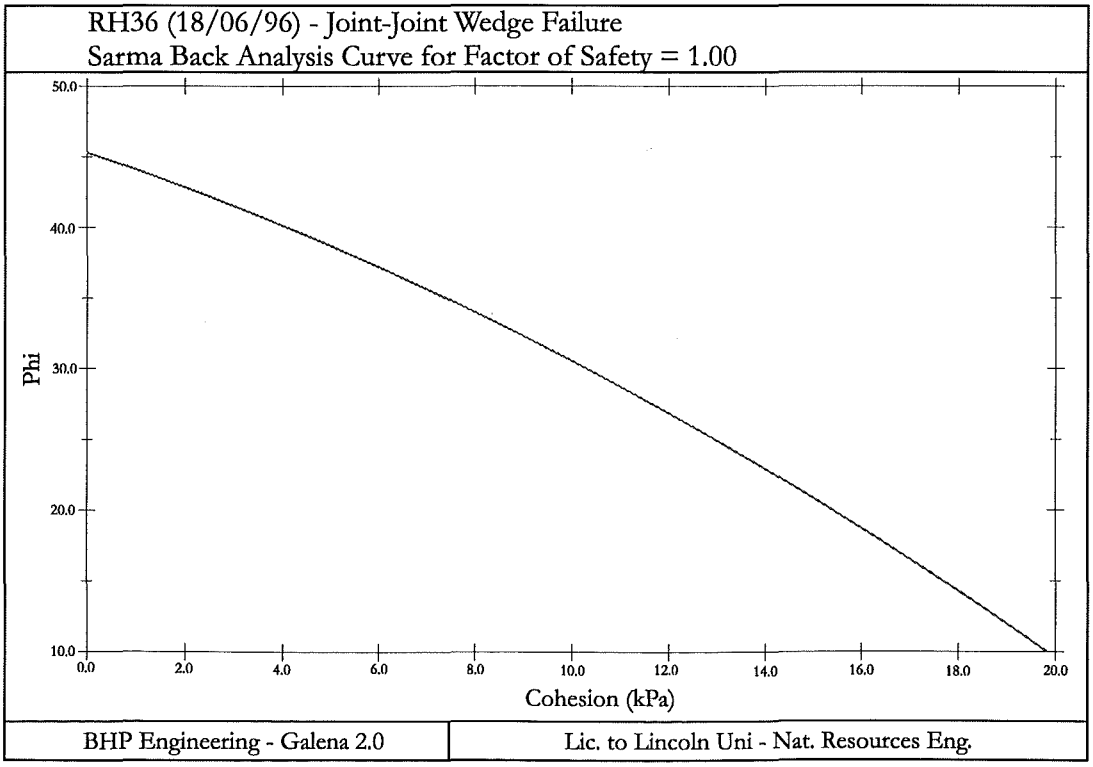

Figure F6-14: RH36 back analysis curve.

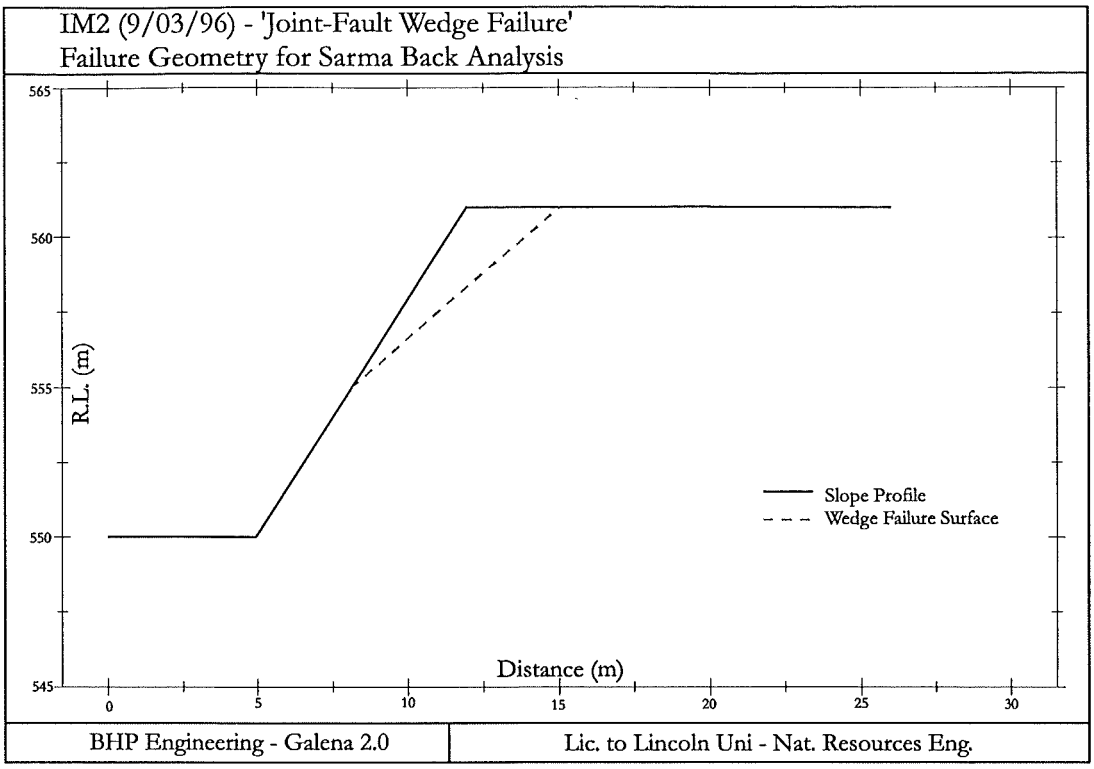

Figure F6-15: IM2 failure geometry for back analysis.

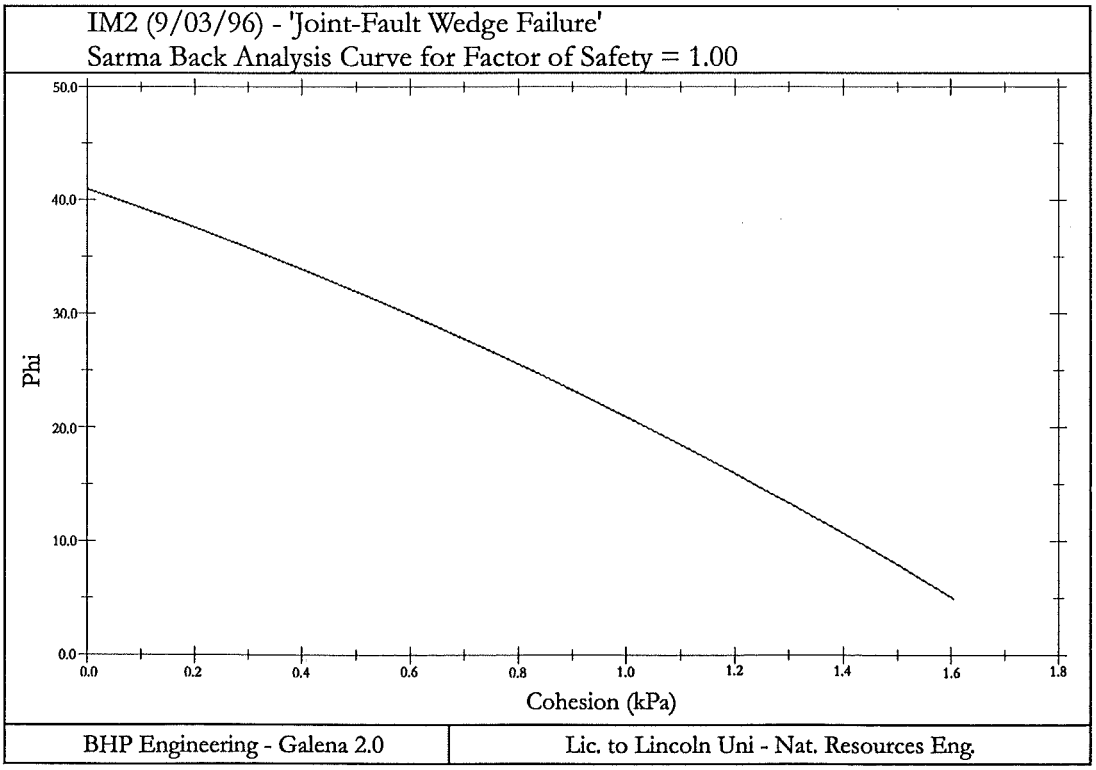

Figure F6-16: IM2 back analysis curve.

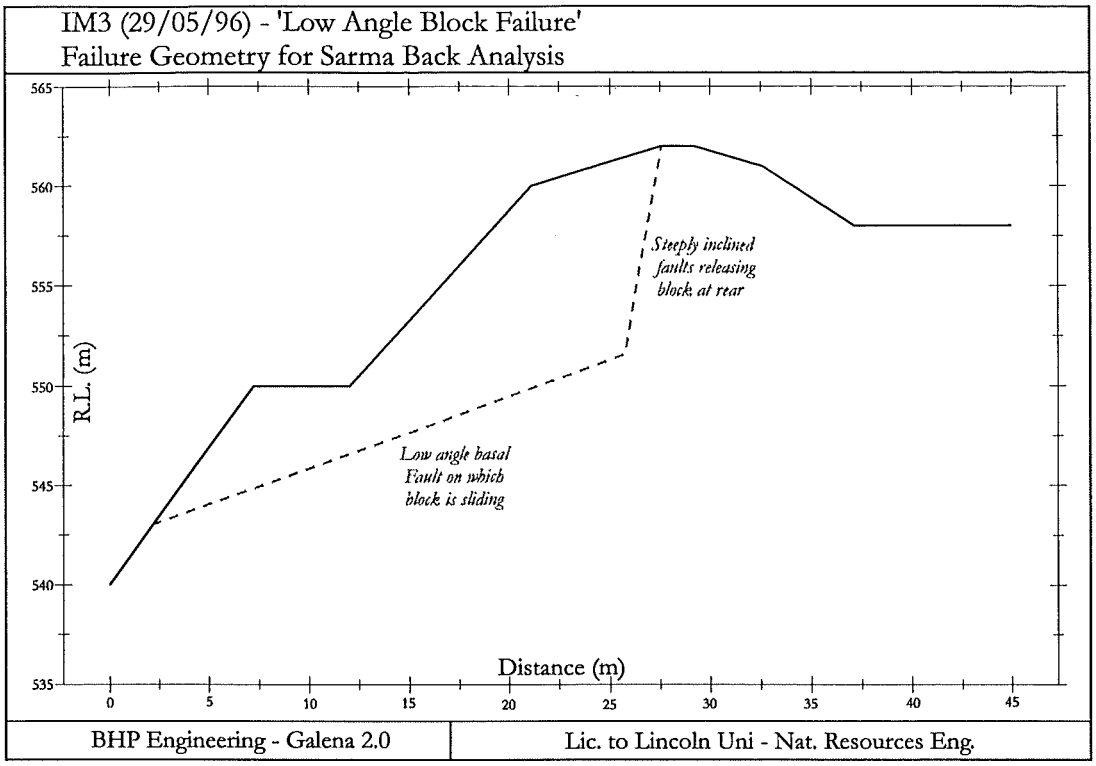

Figure F6-17: IM3 failure geometry for back analysis.

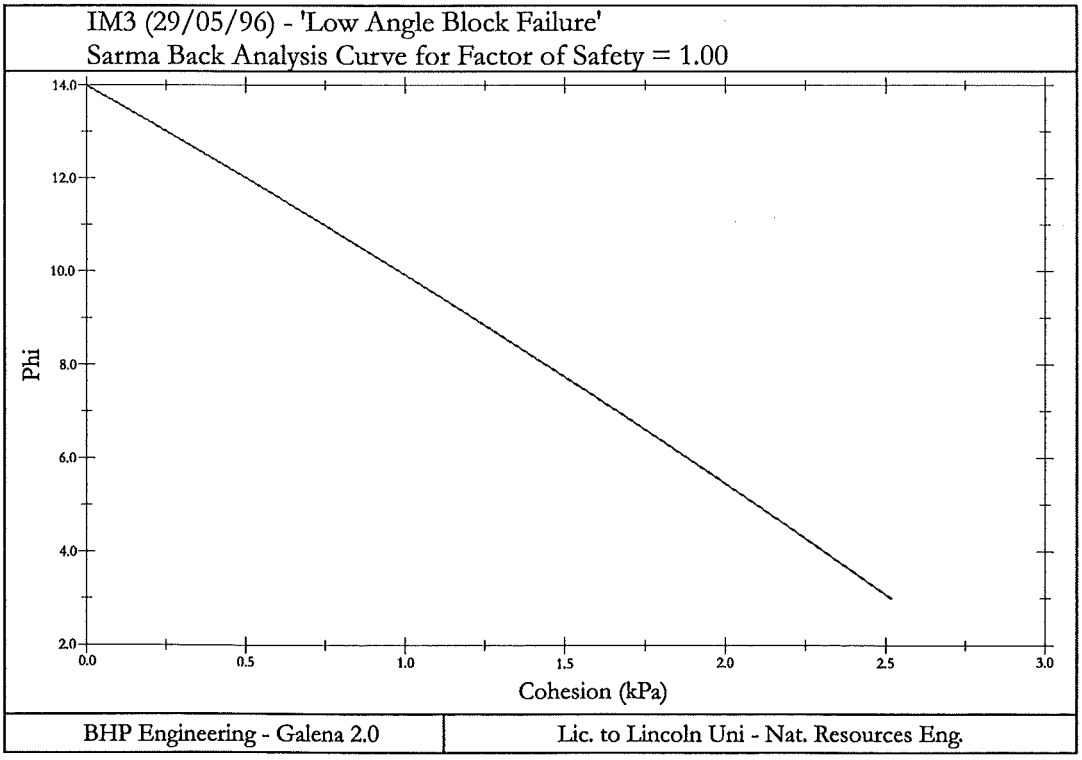

Figure F6-18: IM3 back analysis curve

TAILPIECE: Going off!. Production blast Innes Mills Pit.